UNIVERSIDADE NOVA DE LISBOA

Faculdade de Ciências e Tecnologia

THERMODYNAMIC AND KINETIC MODELLING OF THE REDOX PROPERTIES OF TETRAHAEM CYTOCHROMES c_3

MARIA TERESA NUNES MANGAS CATARINO

Dissertação apresentada para obtenção do grau de Doutor em Bioquímica, especialidade Bioquímica-Física, pela Universidade Nova de Lisboa, Faculdade de Ciências e Tecnologia.

Lisboa 1998

Agradecimentos

Em primeiro lugar quero agradecer ao Prof. António Xavier, meu orientador ao longo destes anos, pelo interesse e empenhamento sempre demonstrados em relação ao meu trabalho. Admiro particularmente a sua intuição científica e a disponibilidade que consegue encontrar, apesar da grande responsabilidade que a direcção do Instituto acarreta. As discussões que tivemos, por vezes acaloradas, serviram sempre para levantar questões pertinentes ou esclarecer dúvidas. A sua capacidade para encontrar alternativas inteligentes, mesmo nas situações em que parecia não existir alternativa possível, foi fundamental para o desenvolvimento e conclusão deste trabalho.

Ao Prof. Massimo Coletta devo a minha 'iniciação' no campo da cinética. Durante os estágios realizados no seu laboratório em Roma tive os primeiros contactos com a técnica de 'stopped-flow', que permitiram o posterior desenvolvimento desta técnica no nosso laboratório. As experiências que realizamos em conjunto constituem grande parte do trabalho experimental apresentado nesta tese. A sua colaboração foi fundamental para o desenvolvimento do modelo termodinâmico A/B, bem como do modelo cinético. Agradeço muito especialmente a sua amizade e a forma como a Carmen, o Andrea, o Matteo e o Jacopo me têm sempre recebido ao longo destes anos, quer em Roma quer em Panicale.

Ao Prof. David Turner agradeço o desenvolvimento do modelo termodinâmico dos cinco centros aqui apresentado. Os conhecimentos que me tem transmitido contribuiram substancialmente para uma melhor compreensão dos problemas associados à modelização termodinâmica e cinética do citocromo $\underline{c_3}$. Agradeço a sua sugestão para a aplicação da teoria de Marcus aos factores sigma do modelo cinético. O apoio fornecido durante a construção dos programas em FORTRAN foi também fundamental. Devo-lhe ainda, a revisão do manuscrito em língua inglesa. Esse processo, no início certamente moroso, acabou por ser classificado como 'moving commas around', pelo que lhe devo também os progressos que fiz no domínio língua inglesa escrita. Por último, agradeço todas as discussões que tivemos durante os jantares no 'Restaurant at the End of the Universe'.

Ao Prof. Jean LeGall agradeço os conselhos relativos a aspectos da microbiologia das bactérias sulfato-redutoras e ainda os presentes de biomassa ou de proteína purificada.

À Isabel Pacheco agradeço a purificação das proteínas utilizadas neste trabalho. A sua capacidade de trabalho e eficiência, tanto no domínio das técnicas de purificação como na gestão do laboratório, contribuem em larga escala para que o trabalho de todo o grupo decorra da melhor forma. Agradeço ainda a amizade resultante de longos anos de convívio e de festas de aniversário comuns.

Ao Eng. Pedro Fernandes, representante da Hi-Tech Scientific em Portugal, agradeço todo o empenho demonstrado na resolução do problema da anaerobicidade do aparelho de 'stopped-flow'. Durante quase dois anos o Pedro foi uma presença constante no nosso laboratório. Juntos, de chave de fendas em punho, desmontámos e montámos o aparelho inúmeras vezes, testando diferentes tipos de vedantes, ora vermelhos, ora pretos... Quando por fim tomamos a decisão de colocar o aparelho dentro de uma câmara anaeróbica, as soluções encontradas e parte das peças necessárias à instalação, foram resultado do nosso esforço conjunto.

À Prof. Helena Santos agradeço ter-me facultado o acesso aos seus resultados das titulações redox do citocromo $\underline{c_3}$ de $\underline{D.\ gigas}$ seguidas por NMR a zero graus centígrados. A análise desses dados é parte integrante da sua tese de doutoramento e constituiu o ponto de partida para o desenvolvimento do modelo termodinâmico A/B. Agradeço ainda as suas opiniões relativamente aos modelos termodinâmicos e ao modelo proposto para o envolvimento do citocromo $\underline{c_3}$ em processos de transdução de energia.

Ao Ricardo Louro agradeço a utilização dos resultados de titulações redox do citocromo c_3 de D. gigas seguidas por NMR à temperatura ambiente. De um modo especial gostaria de salientar a disponibilidade e a paciência com que o Ricardo me tem ouvido ao longo destes anos de trabalho em conjunto. A ajuda prestada durante a realização de experiências de 'stopped-flow' na câmara anaeróbica, a pesquisa bibliográfica, os 'Serviços Informáticos ON-LINE' e, acima de tudo, as numerosas discussões acerca dos modelos, contribuíram decisivamente para o êxito deste trabalho. O convívio diário resultou numa amizade sólida que tem sido o suporte do bom ambiente que se vive no grupo.

Ao Carlos Salgueiro agradeço a utilização dos resultados de titulações redox do citocromo c_3 de D. vulgaris seguidas por NMR. Agradeço de uma forma especial as 'discussões inesperadas'. Quando tudo parecia óbvio, o Carlos, quase pedindo desculpa, soube sempre levantar a questão certa no momento exacto. As discussões assim despoletadas serviram invariavelmente para atingir um melhor conhecimento do sistema. A amizade e o espírito de entre-ajuda existentes entre nós foram muito importantes durante a fase de redacção da tese.

Ao Prof. P. L. Dutton agradeço a prontidão com que respondeu aos meus pedidos de esclarecimento. Agradeço também o interesse com que tem seguido o meu trabalho, desde que, há alguns anos atrás, visitou o nosso laboratório. Nessa altura, o envio de um 'pré-print' do seu artigo sobre transferência electrónica em sistemas biológicos, publicado na revista Nature, deixou-me muito sensibilizada.

Ao meu irmão agradeço o arranjo gráfico da capa.

Aos colegas da secção de Bioquímica da FCT/UNL, Prof. Isabel Moura, Prof. Teresa Moura, Prof. Helena Santos, Prof. Isabel Coutinho e Dr. Carlos Salgueiro, agradeço o trabalho suplementar que tiveram durante a minha dispensa de serviço docente.

À Maria Manuel e à Maria José, secretárias do Departamento de Química da FCT, agradeço a forma como, com eficiência e amizade, têm tratado dos assuntos relativos ao Departamento e ao serviço docente ao longo destes anos. À Ermelinda agradeço todo o apoio às aulas de laboratório. Todos contribuiram para uma maior dedicação à investigação nos intervalos dos períodos lectivos.

Aos colegas do ITQB agradeço a amizade, o espírito de entre-ajuda e todas as discussões que tivemos sobre os temas mais diversos.

Aos funcionários das oficinas, serviços administrativos, centro de apoio informático e secretárias do ITQB agradeço todo o apoio prestado.

Às colegas e amigas, Isabel Coutinho, Teresa Moura, Anjos Macedo e Margarida Martinez, agradeço o incentivo e apoio psicológico que foi fundamental nos períodos mais críticos.

Aos meus pais, ao Sérgio, e à Cristina, agradeço a amizade, o interesse e o respeito com que sempre encararam o meu trabalho. Agradeço de um modo especial todo o apoio que, nesta última fase, permitiu a conclusão da escrita dentro do prazo. O facto de nunca terem deixado de acreditar nas minhas capacidades foi muito importante nos momentos de maior desânimo.

Por último, quero agradecer ao João Sebastião a curiosidade que sempre manifestou em relação ao 'trabalho da mãe'. A compreensão com que, nesta fase final, tem aceitado as minhas ausências ao fim de semana foi um factor determinante para a conclusão do trabalho. A sua vontade de aprender, o seu sentido da responsabilidade e os rápidos progressos que tem feito na escola, têm sido motivo de muita alegria durante este último ano.

RESUMO

O trabalho apresentado nesta dissertação descreve e modeliza as propriedades termodinâmicas e cinéticas de citocromos c_3 tetrahémicos, isolados a partir de bactérias pertencentes ao género *Desulfovibrio*.

O capítulo I consta de uma breve introdução geral na qual são referidas algumas características das bactérias sulfato-redutoras, dando especial ênfase aos aspectos relacionados com o metabolismo bioenergético. Neste capítulo, são ainda abordados aspectos gerais do papel fisiológico do citocromo c_3, assim como da sua estrutura e das suas propriedades termodinâmicas e cinéticas. Este capítulo termina com a descrição da organização e conteúdo da dissertação.

Os capítulos II e III versam as propriedades termodinâmicas e cinéticas do citocromo c_3, respectivamente. Estes capítulos são auto-suficientes, cada um incluindo uma introdução onde se definem os objectivos do presente estudo e se faz uma revisão da literatura sobre o assunto, bem como uma secção de materiais e métodos, contendo a descrição das técnicas utilizadas no desenvolvimento do trabalho experimental. Nestes capítulos são apresentados e discutidos os modelos matemáticos utilizados na simulação dos resultados experimentais, assim como os valores dos parâmetros que melhor descrevem as propriedades do sistema em cada caso. No final de cada capítulo são apresentadas perspectivas futuras, quer ao nível do desenvolvimento experimental quer ao nível da modelização.

No capítulo IV encontram-se resumidas as principais conclusões retiradas deste trabalho. Na secção relativa aos estudos cinéticos foi ainda incluída uma discussão acerca do tipo de informação que se pode retirar de experiências de fluxo interrompido semelhantes às realizadas, consoante as propriedades do sistema. São ainda discutidos alguns resultados da literatura à luz do modelo cinético desenvolvido nesta tese. Este capítulo termina com a integração das propriedades termodinâmicas e cinéticas ao nível de um modelo proposto para o envolvimento do citocromo c_3 nos processos de transdução de energia que ocorrem nas bactérias sulfato-redutoras.

Características gerais do citocromo c_3

Os citocromos c_3 tetrahámicos são proteínas relativamente pequenas, com cerca de 120 resíduos de aminoácidos e massa molecular entre 13 e 15 kD. Esta proteína é produzida em grandes quantidades pelas bactérias redutoras de sulfato, encontrando-se localizada no espaço periplasmático da célula, onde se pensa que funcione como cofactor da enzima hidrogenase, participando no metabolismo bioenergético. Os quatro hemos encontram-se covalentemente ligados à proteína através de ligações tioéter com resíduos de cisteína, sendo a coordenação axial do ferro feita sempre por duas histidinas. Apesar do pequeno grau de homologia encontrado para as sequências de aminoácidos dos citocromos c_3 isolados a partir de diferentes estirpes, o arranjo espacial dos quatro hemos é conservado. Os quatro hemos apresentam potenciais redox distintos e bastante negativos (entre -100 e -500 mV), tendo sido demonstrada a existência de potenciais de interacção entre eles. Além disso, os valores dos potenciais redox dependem do pH, apresentando o chamado efeito 'redox-Bohr'. Do ponto de vista cinético há que referir que os processos de transferência electrónica intramolecular são mais rápidos do que os processos de transferência electrónica intermolecular, quer entre diferentes moléculas de citocromo c_3, quer envolvendo dadores ou aceitadores exógenos de electrões. Desta forma, independentemente do hemo através do qual se dá a entrada dos electrões na proteína, a distribuição electrónica dentro da molécula é feita de acordo com os potenciais relativos dos vários centros. Por esta razão, o citocromo c_3 é um sistema termodinamicamente controlado. A redução do citocromo c_3 por agentes redutores exógenos, ou por outras proteínas envolvidas em processos de transferência electrónica, apresenta características bifásicas na maior parte dos casos, tendo as constantes de velocidade de segunda ordem valores compreendidos entre 10^6 - 10^7 $M^{-1}s^{-1}$. Os processos de oxidação apresentam constantes de velocidade inferiores, com valores da ordem de 10^4 - 10^5 $M^{-1}s^{-1}$.

Propriedades termodinâmicas

Apresentam-se os modelos termodinâmicos desenvolvidos até ao presente para a descrição dos processos de oxidação-redução em que o citocromo c_3 se encontra envolvido. Os modelos mais simples consideram o processo de redução global como o resultado da redução de quatro centros redox independentes ('modelo individual'), ou como quatro passos consecutivos de um electrão ('modelo sequencial'). O significado físico dos parâmetros obtidos em cada caso é discutido, assim como as limitações inerentes a cada um dos modelos.

O primeiro modelo que inclui interacções entre os hemos foi proposto em 1984 (Santos, H., Moura, J.J.G., Moura, I., LeGall, J. and Xavier, A.V. (1984), *Eur. J. Biochem. 141*, 283-296). De acordo com este modelo a distribuição dos electrões entre os quatro centros redox dá origem a 16 microestados que se relacionam entre si através de 32 equações de Nernst. Contudo, ficou demonstrado nesse trabalho, que é possível descrever as propriedades do sistema, nomeadamente os desvios químicos dos grupos metilo dos hemos em diferentes estados de oxidação, utilizando apenas dez parâmetros: os potenciais redox dos quatro centros definidos para a forma reduzida e seis potenciais de interacção definidos entre os hemos dois a dois. A determinação destes parâmetros para dois valores de pH mostrou que os potenciais microscopicos dos hemos dependem do pH e que o mesmo parecia acontecer com os valores das interacções hemo-hemo, ficando demonstrada a existência de interacções hemo-protão.

A este modelo seguiu-se o 'modelo A/B' que, para explicar a dependência dos potenciais e das interacções com o pH, propõe a existência de uma alteração conformacional da proteína associada ao processo de protonação (Coletta, M., Catarino, T., LeGall, J. and Xavier, A.V. (1991), *Eur. J. Biochem. 202*, 1101-1106). O modelo ácido/base (A/B) foi o primeiro modelo a incluir simultaneamente o pH e o potencial da solução como variáveis do sistema. Devido à introdução do equilíbrio ácido/base, o número total de microestados aumenta para 32, pois cada um dos 16 microestados anteriores se pode encontrar protonado ou desprotonado. Segundo o modelo A/B, cada conformação é caracterizada pelos quatro potenciais microscópicos dos hemos e por seis potenciais de interacção hemo-hemo, com a constante de equilíbrio ácido/base definida para o estado de referência, o número total de parâmetros necessários para descrever o sistema eleva-se para 21. Através da comparação entre os resultados experimentais anteriormente obtidos (Santos, H., Moura, J.J.G., Moura, I., LeGall, J. and Xavier, A.V. (1984), *Eur. J. Biochem. 141*, 283-296) e curvas simuladas de acordo com o formalismo matemático do modelo A/B, determinaram-se os parâmetros por aproximações sucessivas, tendo como ponto de partida os valores dos parâmetros anteriormente determinados. Foram ainda utilizadas titulações espectrofotométricas para definir a escala absoluta de potencial, impossível de obter apartir dos dados de ressonância magnética nuclear. Como resultado da aplicação do modelo A/B obtiveram-se potenciais e interacções hemo-hemo diferentes para as conformações protonada e desprotonada. Curiosamente, apenas as interacções envolvendo o hemo IV (definido de acordo com a ordem de ligação à cadeia polipeptídica) pareciam ser dependentes do pH, o que foi interpretado como sendo o resultado de uma alteração conformacional significativa envolvendo as relações estruturais entre o hemo IV e os restantes hemos. Mais tarde, foi demonstrado que quer devido ao elevado

número de parâmetros, quer à forma como esses parâmetros foram definidos, no modelo A/B as interacções hemo-hemo englobam as interacções hemo-protão. Este problema, e o facto de o potencial do hemo IV se encontrar relativamente separado dos potenciais dos outros hemos, aumenta a imprecisão dos parâmetros determinados para o citocromo c_3 de *Desulfovibrio gigas* com o modelo A/B. No entanto, é importante referir que, apesar de envolver um número de parâmetros superior ao necessário, o modelo A/B permitiu antever o acoplamento entre o processo de redução e a protonação da molécula que ocorre a pH fisiológico.

Posteriormente, com o desenvolvimento do modelo dos cinco centros (Turner, D.L., Salgueiro, C.A., Catarino, T., LeGall, J. and Xavier, A.V. (1996), *Eur. J. Biochem. 241*, 723-731), demonstrou-se que era possível simular todo o conjunto de resultados experimentais com potenciais de interacção hemo-hemo independentes do pH. O novo modelo parte de um pressuposto diferente pois, em vez assumir *a priori* a existência de alterações conformacionais da proteína, considera apenas a existência de cinco centros, quatro centros redox e um centro ácido/base, que, interactuando entre si, condicionam mutuamente as respectivas propriedades. Os parâmetros deste modelo são os potenciais redox dos quatro hemos, o pK_a do centro ácido/base para o estado de referência e, ainda, as interacções dos centros dois a dois. Mais concretamente: seis interacções hemo-hemo e quatro interacções hemo-protão. Apesar do número de microestados envolvidos nos equilíbrios redox e ácido/base continuar a ser 32, este modelo necessita de apenas 15 parâmetros para descrever o sistema. Os parâmetros que caracterizam as propriedades termodinâmicas dos citocromos c_3 isolados a partir de *D. gigas* e de *D. vulgaris* foram determinados a partir do ajuste de curvas simuladas de acordo com o modelo dos cinco centros aos resultados experimentais obtidos em titulações redox seguidas quer por ressonância magnética nuclear quer por espectroscopia de visível, utilizando o método de Marquardt. Demonstra-se que o modelo dos cinco centros consegue simular as propriedades termodinâmicas do citocromo c_3, incluindo a dependência com o pH dos desvios químicos dos grupos metilo dos hemos, com menor número de parâmetros. Por essa razão, os valores dos parâmetros encontram-se mais bem definidos do que no modelo anterior e o seu significado físico é mais evidente. Como não foi necessário introduzir interacções dos centros três a três para explicar os resultados experimentais, não existe evidência para alterações conformacionais significativas associadas quer ao processo de redução quer ao processo de protonação. No entanto, o aparecimento de uma cooperatividade positiva entre dois centros com carga do mesmo tipo (os hemos I e II no citocromo c_3 de *D. vulgaris* e os hemos II e III no citocromo c_3 de *D. gigas*) não pode ser explicada por efeitos electrostáticos entre os hemos,

propondo-se que resulte de pequenos movimentos de resíduos carregados, associados ao processo de oxidação-redução.

A aplicação do modelo dos cinco centros a citocromos c_3 isolados a partir de organismos diferentes mostra que, apesar de apresentarem parâmetros termodinâmicos diferentes, em ambos se observa uma cooperatividade positiva entre dois dos hemos e cooperatividades positivas entre os hemos e um centro ionisável. No entanto, e apesar da conservação do arranjo espacial dos hemos, a cooperatividade positiva não se estabelece sempre entre o mesmo par de hemos. Assim, parece não existir uma correlação óbvia entre a arquitectura dos centros e a rede de cooperatividades estabelecida entre eles. Contudo, qualquer destas proteínas tem a capacidade de acoplar a transferência de electrões com a transferência de protões, característica que lhes confere as propriedades termodinâmicas necessárias para efectuar transdução de energia, se o controlo cinético dos vários passos do ciclo energético o permitir.

Propriedades cinéticas

Utilizando a técnica de 'fluxo interrompido' acoplada à espectroscopia de visível, estudou-se a cinética de reacções de transferência electrónica envolvendo o citocromo c_3 isolado a partir de *D. gigas* e diferentes dadores e aceitadores de electrões. A análise dos resultados obtidos foi feita com um modelo cinético especificamente desenvolvido para este sistema.

A primeira hipótese restritiva introduzida na modelização está relacionada com a utilização de um mecanismo cinético puramente colisional, ou seja, no qual são ignorados os passos de formação e dissociação do complexo entre os parceiros redox, por não serem passos limitantes. Mesmo assumindo um mecanismo colisional o esquema cinético é muito complexo, pois envolve todas as reacções de transferência electrónica possíveis entre o dador/aceitador de electrões e os 32 microestados do citocromo c_3. No entanto, como a transferência electrónica intramolecular é mais rápida do que a transferência electrónica intermolecular, o equilíbrio entre os microestados que pertencem ao mesmo estado redox é muito rápido e o esquema cinético reduz-se a quatro passos consecutivos de um electrão. Se, ao longo do processo redox, as constantes de velocidade dos hemos individuais forem afectadas apenas pela variação da energia livre padrão (ΔG^0) para o processo de transferência electrónica, demonstra-se que as constantes de velocidade macroscópicas que caracterizam as transições entre os estados redox se podem relacionar com as constantes de velocidade dos

hemos, através dos parâmetros termodinâmicos do sistema. De acordo com a teoria de Marcus, se a energia de reorganização (λ) for muito superior ao valor do ΔG^0 para a transferência electrónica, as constantes de velocidade dos hemos ao longo do processo redox podem ser relacionadas entre si através de factores (factores σ_{ij}) que dependem unicamente dos potenciais de interacção hemo-hemo. De modo análogo, as constantes de velocidade da forma desprotonada podem ser relacionadas com as constantes de velocidade da forma protonada através de factores σ_{iH} que dependem exclusivamente das interacções 'redox-Bohr'. A abordagem colisional em conjunto com a aproximação dos factores σ permitiu reduzir o número de parâmetros do modelo para apenas quatro constantes de velocidade, uma para cada hemo, no estado de referência.

A aplicação do modelo cinético, aos resultados obtidos nas experiências de redução do citocromo c_3 com ditionito de sódio, mostrou que é impossível definir as quatro constantes de velocidade porque alguns hemos se encontram termodinamicamente acoplados. É importante sublinhar que esta limitação não é consequência da fraca resolução da espectroscopia de visível nem do modelo cinético utilizado, mas sim das propriedades intrínsecas do sistema, nomeadamente da existência de rápido equilíbrio intramolecular. Os resultados experimentais foram por isso simulados utilizado um modelo com apenas dois parâmetros: a constante de velocidade do hemo IV, que se encontra bem definida porque este hemo tem um potencial redox relativamente separado dos potenciais redox dos outros hemos, e constantes de velocidade iguais para os restantes hemos. A aplicação do modelo cinético a experiências com ditionito de sódio, realizadas a diferentes valores de pH, demonstram a validade da utilização dos factores σ relativos à protonação, pois a dependência da velocidade com o pH pode ser explicada pelo efeito das interacções hemo-protão nas constantes de velocidade dos hemos individuais. Estas interacções determinam que as constantes de velocidade sejam superiores na forma protonada e, ainda, que a constante de velocidade do hemo I seja a mais afectada, porque este hemo tem o maior potencial de interacção com o protão. Por outro lado, o hemo IV apresenta o menor potencial de interacção com o protão, sendo a sua constante de velocidade a menos afectada pelo pH. A pH fisiológico, este efeito dá origem a uma aceleração do processo global de redução, pois esta inicia-se pelo hemo IV na forma desprotonada, terminando com a redução do hemo I na forma protonada, devido à alteração dos valores de pK_a ao longo do processo. Desta forma, as cooperatividades termodinâmicas responsáveis pela transferência concertada de dois electrões são assistidas cinéticamente pelo aumento das constantes de velocidade devido à protonação. Pensa-se que esta aceleração do

processo de redução, acoplada à protonação da molécula, possa contribuir para o controlo cinético do ciclo de transdução de energia.

Apresentam-se também os resultados de estudos cinéticos envolvendo o citocromo c_3 de *D. gigas* e flavodoxina isolada a partir do mesmo organismo. A flavodoxina é uma proteína com 16 kD que contém um cofactor flavina mononucleotídeo (FMN). Devido à sua localização citoplasmática não se espera que ocorra transferência electrónica entre a flavodoxina e o citocromo c_3 *in vivo*. No entanto, a homologia recentemente encontrada entre o domínio N-terminal da subunidade 28 kD da hidrogenase periplásmica e a flavodoxina, além da homologia existente entre os quatro domínios do citocromo hexadecahémico membranar e o citocromo c_3, conferem relevância fisiológica a destes estudos. Com o objectivo de comparar o comportamento do grupo prostético da flavodoxina quando isolado e quando inserido na proteína, realizaram-se também estudos de transferência electrónica entre o citocromo c_3 e FMN.

A análise qualitativa dos resultados obtidos foi feita utilizando também um modelo cinético com apenas dois parâmetros: a constante de velocidade para o hemo IV e a constante de velocidade para o hemo I. Tal como tinha sido anteriormente observado para a reacção com ditionito de sódio, a constante de velocidade do hemo IV é sempre superior às constantes de velocidade dos restantes hemos. Concluiu-se que do ponto de vista cinético o hemo IV tem um comportamento distinto dos outros hemos, sendo responsável pela fase rápida observada nas curvas da variação da fracção de redução com o tempo. A simulação por computador da evolução temporal das fracções de redução dos hemos individuais mostra ainda que, devido às cooperatividades do sistema e à rápida permuta intramolecular, o hemo IV contribui para a redução dos outros hemos, funcionando como a principal porta de entrada de electrões na molécula do citocromo c_3. É interessante referir que este hemo fica rodeado por uma série de resíduos de lisina que se pensa estarem envolvidas no reconhecimento do parceiro fisiológico.

ABSTRACT

The work presented in this thesis concerns the description and modelling of the thermodynamic and kinetic properties of tetrahaem cytochromes c_3 isolated from different *Desulfovibrio* spp.. Sulfate-reducing bacteria produce tetrahaem cytochrome c_3 in large quantities. This small (13 - 15 kD) protein is located in the periplasmic space of the cells, where it has been proposed to work as a cofactor of the enzyme hydrogenase. The four haems in cytochrome c_3 are covalently bound to the protein through thioether linkages with cysteinyl residues and all display bis-histidinyl axial coordination. Although the degree of homology between the amino acid sequence of cytochromes c_3 isolated from different organisms is low, the architecture of the haem core, is strictly conserved.

The modelling of the thermodynamic properties of this protein has to take into account the fact that the four haems display different, interacting, and pH dependent redox potentials. Various approaches are described and discussed in this thesis, giving special emphasis to models which include both haem-haem and haem-proton interactions. To explain the pH dependence of the NMR resonances, the acid/base (A/B) model was developed under the assumption that the protein could undergo a proton-linked conformational change, each conformation being characterised by a different set of microscopic redox potentials and haem-haem interacting potentials. The model of five interacting centres, developed later, demonstrated that it is not necessary to make any structural assumptions and that the experimental data can be simulated using fewer parameters, which are therefore better defined. According to this model, the thermodynamic properties of cytochrome c_3 can be described by the intrinsic microscopic parameters of one acid/base and four redox centres plus the two-site interactions established between the five centres, namely, six haem-haem interactions plus four haem-proton interactions. Application of this model to NMR and visible redox titrations enabled the accurate determination of the complete set of microscopic parameters that characterise the thermodynamic behaviour of cytochromes c_3 isolated from *D. gigas* and *D. vulgaris*.

It is apparent from the values of the thermodynamic parameters that these cytochromes are able to perform a concerted two-electron step, which is coupled to the simultaneous uptake or release of protons, depending on the direction of the electron flow. These properties allow cytochrome c_3 to work as an energy transducing system. However, since kinetic control of the electron and proton transfer steps is essential to achieve energy transduction, the kinetic

properties of cytochrome c_3 isolated from *D. gigas* are described and analysed in the second half of this thesis, making use of a specially developed kinetic model.

Due to the existence of fast intramolecular electron equilibration within the cytochrome c_3 molecule, the very complex kinetic scheme can be reduced to four consecutive steps of one electron. It is shown that, under certain circumstances, it is possible to relate the macroscopic rate constants of these steps to the electron transfer rate constants of the individual haems, through the complete set of microscopic thermodynamic parameters. It is stressed that it is impossible to define the rate constants of thermodynamically coupled haems and that this limitation is not a consequence of the low resolution of the visible spectrum nor of the kinetic model used, but derives from the intrinsic properties of the system, particularly from the fast intramolecular electron exchange.

The kinetics of reduction of cytochrome c_3 by sodium dithionite were studied by stopped-flow techniques coupled to visible spectroscopy at different pH values. In this work, it is demonstrated that the pH dependence of the rate constants can be explained by the change in the driving force induced by the existence of haem-proton interacting potentials (redox-Bohr interactions), according to Marcus theory. The main conclusion of the pH dependence studies is that, because of the transition from the deprotonated to the protonated form that is associated with the reduction process at physiological pH, there is an acceleration of the electron transfer which may provide the means for the kinetic control of the energy transducing cycle.

Stopped-flow kinetic studies involving cytochrome c_3 and flavodoxin isolated from *D. gigas*, or cytochrome c_3 and FMN, both in the presence and in the absence of sodium dithionite, are also presented.

The general conclusion of these kinetic studies, when using negatively charged redox agents, is that haem IV, which is surrounded by several lysine residues in most cytochromes c_3, shows a distinct kinetic behaviour when compared to the other three haems. This haem is responsible for the fast phase of the kinetic traces and, because of the interplay of the cooperativities of the system, after attaining a certain percentage of reduction starts draining electrons to the other haems. Haem IV therefore works as the main gateway for electrons in the molecule.

SYMBOLS AND ABBREVIATIONS

A/B	acid/base
ADP	adenosine diphosphate
AMP	adenosine monophosphate
APS	adenylylsulfate
ATCC	American Type Culture Collection, Rockville, Md., USA
ATP	adenosine triphosphate
C+G	cytosine plus guanine
c_3	tetrahaem cytochrome c_3
cys	cysteine
cyt	cytochrome
D.	*Desulfovibrio*
Ddc_3	tetrahaem cytochrome c_3 from *Desulfovibrio desulfuricans*
Dgc_3	tetrahaem cytochrome c_3 from *Desulfovibrio gigas*
Dmbc_3	tetrahaem cytochrome c_3 from *Desulfomicrobium baculatum* (*)
5DRFH$^{\bullet}$	5-deazariboflavin semiquinone
Dsm.	*Desulfomicrobium*
Dvc_3	tetrahaem cytochrome c_3 from *Desulfovibrio vulgaris*
E	solution potential (V)
E^0	midpoint redox potential (V)
EPR	electron paramagnetic resonance
F	Faraday constant (= 96500 C mol^{-1})
fd I	ferredoxin I
fl	flavodoxin
FMN	flavin mononucleotide
FTIR	Fourier transform infra-red
hase	hydrogenase
his	histidine
lys	lysine

(*) *Desulfomicrobium baculatum* strain Norway 4 had been formerly classified as *Desulfovibrio desulfuricans* strain Norway 4 and was recently reclassified as *Desulfomicrobium norvegicum*.

MeV	methyl viologen
MW	molecular weight
NAD^+	nicotinamide adenine dinucleotide (oxidised form)
NADH	nicotinamide adenine dinucleotide (reduced form)
$NADP^+$	nicotinamide adenine dinucleotide phosphate (oxidised form)
NADPH	nicotinamide adenine dinucleotide phosphate (reduced form)
NCIMB	The National Collections of Industrial and Marine Bacteria, Torry Research Station, Aberdeen, Scotland, UK.
NMR	nuclear magnetic resonance
OD	optical density
ox	oxidised
$PDQ^{+\bullet}$	reduced propylene diquat
PP_i	inorganic pyrophosphate
R	gas constant (= 8.314 J mol^{-1} K^{-1})
red	reduced
rmsd	root mean square deviation
RNA	ribonucleic acid
spp.	species
sq	semiquinone
T	temperature (K)
tris	tris-(hydroxymethyl)-aminomethane
UV	ultra-violet
ΔG^0	standard free energy change (J mol^{-1})
ε	molar absorption coefficient ($M^{-1}cm^{-1}$)
λ	reorganisation energy for electron transfer
λ	wavelength (nm)

CONTENTS

Chapter I : INTRODUCTION

Chapter II: THERMODYNAMIC PROPERTIES

Chapter III: KINETIC PROPERTIES

I INTRODUCTION

I INTRODUCTION

I.1 General characteristics and activities of sulfate-reducing bacteria

Sulfate-reducing bacteria are a very heterogeneous group of anaerobic prokaryotes which share the common ability of using sulfate or sulfur as terminal acceptor for the electrons that result from the oxidation of both organic and inorganic compounds in their bioenergetic processes. Work in recent years has demonstrated that there is an enormous diversity of morphological and metabolic characteristics among these bacteria, which could be the result of an early evolutionary divergence. This diversity enables sulfate-reducing bacteria to live in many different environments and increases their economic interest and their importance as objects of scientific investigation. Since sulfate-reducers play an important role in contamination of petroleum products and in anaerobic corrosion of iron and steel, these organisms are of great economic interest in many industrial sectors. Their environmental impact is also very important in highly polluted ecosystems.

These bacteria were difficult to grow and manipulate in the laboratory but newly developed experimental techniques are leading to the discovery of a great variety of metabolic processes and are revealing a diversity of microbial forms not previously apparent in this group of organisms. Moreover, significant advances in the understanding of their bioenergetics, genetics and molecular biology are leading to an increase in their environmental and industrial importance.

The early taxonomic organisation of sulfate-reducing bacteria was very simple. According to Postgate and Campbell (Campbell and Postgate, 1965 and Postgate and Campbell, 1966) only two genera were considered on the basis of morphological characteristics, the ability to form spores, the C+G content and the presence of certain pigments. These genera were *Desulfovibrio* and *Desulfotomaculum*. Although most of the organisms responsible for dissimilatory sulfate reduction still fit into these two categories, it was demonstrated later that sulfate-reducers are much more diverse than previously recognised and at least 14 new genera with different morphological and metabolic capabilities are presently recognised (Widdel and Hansen 1991 ; Singleton, 1993). Antigenic studies and comparison of 16S ribosomal RNA sequences indeed support the idea that sulfate-reducing bacteria are very diversified.

I.2 Considerations about the bioenergetic metabolism of sulfate-reducing bacteria

Sulfate-reducing bacteria extract the energy necessary for their growth from the anaerobic respiration of sulfate. In this process, sulfate is used as the terminal acceptor for the electrons and protons that result from the oxidation of foodstuffs. Note that, since sulfate reduction is being used for bioenergetic purposes and not for the incorporation of sulfur into biological compounds, sulfate respiration is a dissimilatory rather than an assimilatory process.

It will be mentioned below that it would be impossible for the bacteria to grow on lactate and sulfate in the absence of oxidative phosphorylation coupled to the overall process of sulfate reduction. This is because the ATP obtained by substrate level phosphorylation in the process of lactate oxidation is completely consumed in the activation of sulfate. Also, the finding that some sulfate-reducing bacteria can grow chemolithotrophically on H_2 plus sulfate as the sole energy source clearly established that the reduction of sulfate to sulfide is coupled to ATP phosphorylation (Badziong et al., 1978 ; Badziong and Thauer, 1978).

I.2.1 Electron donors

Most of the substrates used by sulfate-reducing bacteria as carbon and energy sources are low-molecular-weight compounds which are typical fermentation products that result from the anaerobic bacterial degradation of carbohydrates, proteins and other components of dead biomass (Widdel, 1988). The number of compounds which are known to be metabolised by these bacteria increased enormously during the past two decades and now amounts to over 125. Also, great progress has been made in the knowledge of the pathways and the enzymes that are used in the degradation of the substrates by sulfate-reducing bacteria (Hansen, 1994).

Examples of electron donors used by sulfate-reducing bacteria are hydrogen, ethanol, lactate, pyruvate and malate (Widdel, 1988 ; Singleton, 1993 ; Woordouw, 1995). However, many other organic compounds, including crude oil components (Rueter et al., 1994) and metallic iron, (Odom, 1993) can serve as electron donors for sulfate reduction.

It has been proposed that sulfate-reducers can be organised in two major metabolic groups (Widdel 1988): one carries out incomplete oxidation of lactate or other organic substrates to acetate and CO_2, whereas the other is capable of completely oxidising a variety of compounds, including acetate, fatty acids and aromatic compounds, to CO_2. Apparently the members of the first group do not have an operating enzymatic mechanism to oxidise the

acetate unit (acetyl coenzyme A). Although some of them can utilise alcohols and aldehydes of low molecular weight (Turner et al., 1987 ; Widdel, 1988 ; Hensgens et al., 1993 ; Barata et al., 1993 ; Hansen, 1994) they are nutritionally less versatile than those of the second group. The complete oxidisers are able to use most of the electron donors utilised by the incomplete oxidisers and also other substrates which have not been observed so far to be used by the members of the first group. Such compounds, besides acetate, include branched fatty acids, acetone, phenyl-substituted organic acids, phenolic compounds and indole. Most complete oxidisers grow significantly more slowly than incomplete oxidisers (Widdel 1988).

Chemolithotrophic growth of *Desulfovibrio* spp. in the presence of SO_4^{2-} with H_2 as the sole energy source was reported and explained by Badziong and Thauer, 1978. Under these conditions, acetate and CO_2 are required as the carbon source (Badziong et al., 1979). Some sulfate-reducers have the ability to grow autotrophically using CO_2 as the sole carbon source (Brysch et al., 1987). Hydrogen is oxidised by periplasmic hydrogenases and a proton gradient results from this process because hydrogen oxidation and sulfate reduction occur in different cellular compartments (Badziong and Thauer, 1980). Since in energetic terms 2 moles of ATP are necessary for the activation of sulfate (see below) the net synthesis of 1 mole of ATP per mole of SO_4^{2-} reduced requires the phosphorylation of 3 moles of ATP as the result of the proton gradient (cf. Figure I.1).

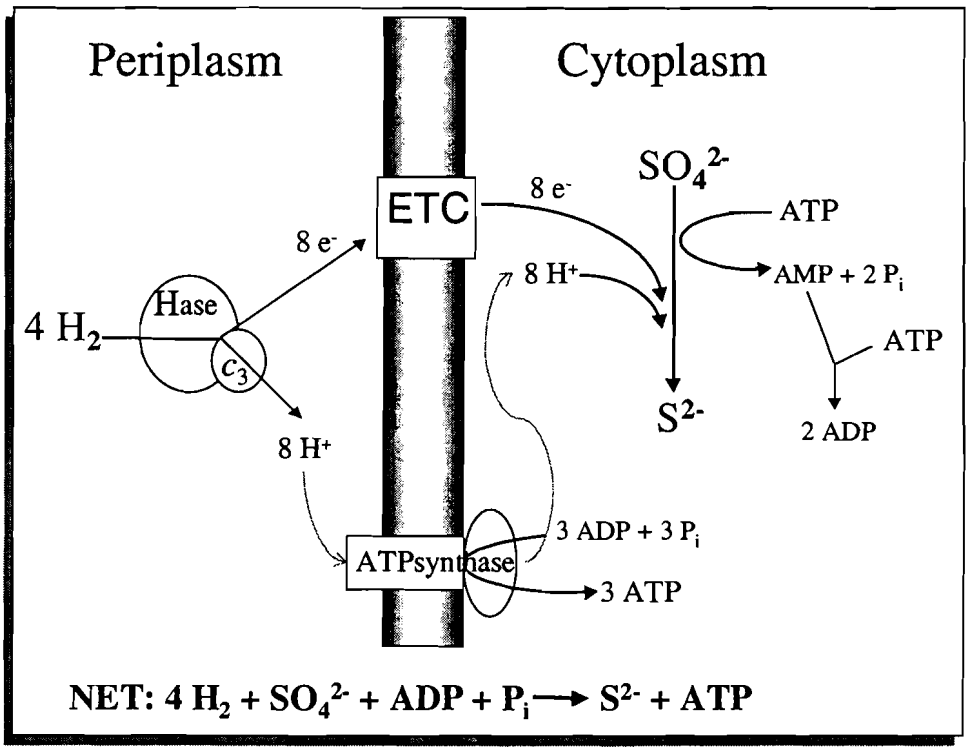

Figure I.1. Bioenergetic processes occurring in sulfate-reducing bacteria growing on hydrogen and sulfate. Hydrogen oxidation and sulfate reduction take place in different cellular compartments, generating a proton gradient. c_3: tetrahaem cytochrome c_3 ; ETC: electron transfer complex ; Hase: periplasmic hydrogenase.

When lactate and pyruvate are used as electron donors their oxidation is incomplete because CO_2 and acetate result from this process. Lactate is first oxidised to pyruvate by an NAD(P) independent membrane bound lactate dehydrogenase that is not well characterised (Hansen, 1993). Subsequently, pyruvate is oxidised to acetate and CO_2 via acetyl coenzyme A and acetylphosphate intermediates. In this process, 1 mole of ATP is produced by substrate level phosphorylation (Figure I.2). Since 2 electrons and 2 protons are released in each oxidation step and 8 electrons are required for the reduction of sulfate to sulfide, two moles of lactate are oxidised per mole of sulfate. The overall balance shows that there is no net production of ATP in this process, unless proton-driven ATP synthesis occurs in addition to substrate level phosphorylation. However, the mechanism for the generation of the proton gradient is not obvious because production and consumption of electrons and protons take place in the same cellular compartment. Odom and Peck, 1981 proposed the hydrogen cycling hypothesis to explain the formation of the proton gradient under these conditions (see below).

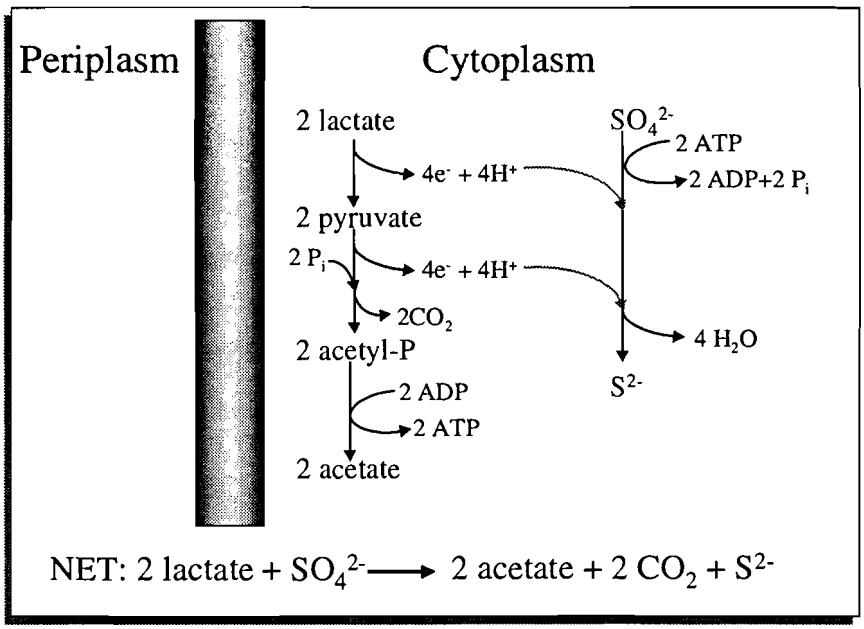

Figure I.2. Oxidation of lactate to acetate and CO_2 is coupled to sulfate reduction. Since the 2 ATP formed by substrate level phosphorylation in the conversion of 2 acetylphosphate (acetyl-P) into 2 acetate are consumed in the activation of sulfate, there is no net production of ATP, unless proton-driven ATP synthesis occurs in addition to the processes represented in the picture.

It should be noted that, if pyruvate only is used as electron donor, the ATP formed by substrate level phosphorylation is sufficient to sustain growth. However, oxidation of pyruvate is similarly thought to be coupled to proton translocation (Peck 1993). In some organisms, pyruvate can support growth in the absence of sulfate. The mechanism is not clearly established, but it probably involves the pyruvate phosphoroclastic system because acetate, CO_2 and hydrogen are often produced as the result of the metabolic activity of these

organisms (Peck, 1993).

Some strains can grow on malate and sulfate, possibly oxidising malate to pyruvate and CO_2 (Postgate, 1984 ; Hansen, 1993). In the absence of sulfate, *Desulfovibrio gigas* converts 3 mol of malate into 2 mol of succinate plus 1 mol of acetate (Chen et al., 1995). Acetate is formed from decarboxylation of pyruvate and succinate results from the reduction of fumarate, which works as the electron acceptor in the absence of sulfate. These authors observed NADH-linked fumarate reductase activity, supporting the involvement of pyridine nucleotides in the electron pathway toward the reduction of sulfate or fumarate.

I.2.2 Hydrogen cycling hypothesis

To explain the bioenergetics of growth when lactate is used as electron donor, Odom and Peck, 1981 proposed a mechanism known as the hydrogen cycling. According to this hypothesis, the electrons produced by oxidation of lactate and pyruvate cannot be used directly for sulfate reduction. Instead, they combine to form hydrogen in a reaction catalysed by cytoplasmic hydrogenase. Then, hydrogen diffuses to the periplasmic space where it is decomposed again into electrons and protons by a periplasmic hydrogenase (Figure I.3).

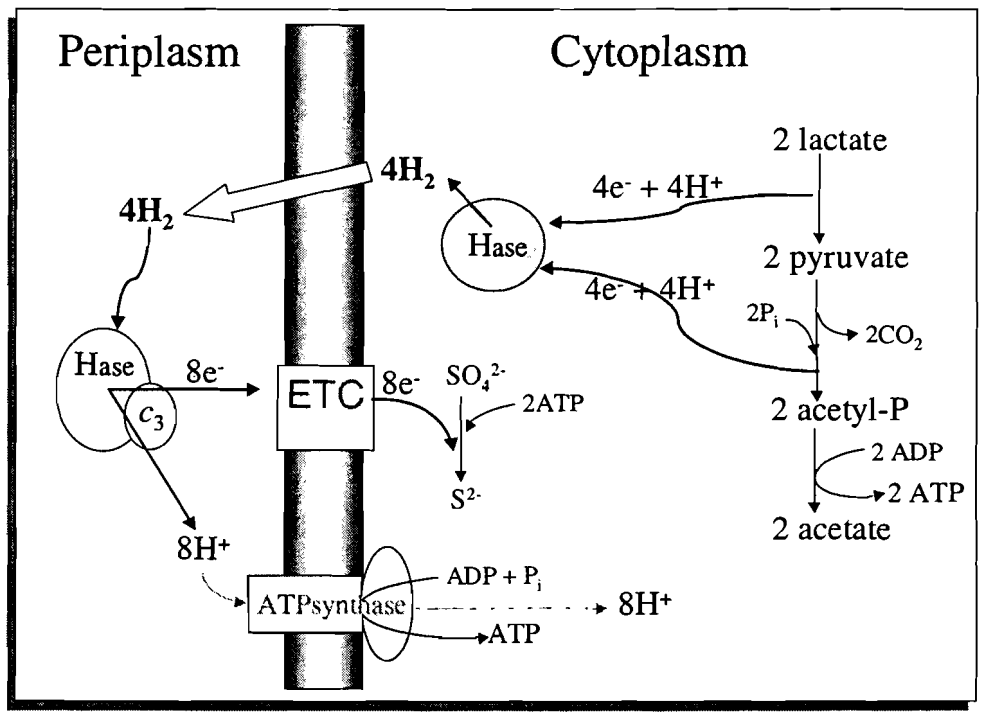

Figure I.3. Hydrogen cycling hypothesis. The electrons and protons produced by the oxidation of lactate in the cytoplasm combine to form hydrogen in a reaction catalysed by the cytoplasmic hydrogenase (dark Hase). Hydrogen diffuses to the periplasmic space where it is re-oxidised back to electrons and protons in a reaction catalysed by the periplasmic hydrogenase (light Hase). This process generates a proton gradient that is utilised by ATPsynthase to phosphorylate ATP. c_3: tetrahaem cytochrome c_3 ; ETC: electron transfer complex.

The protons produced in the periplasm from the oxidation of molecular hydrogen contribute to the proton gradient used by the ATPsynthase to generate ATP. The electrons that result from the same reaction are transported across the membrane, through a transmembrane electron transfer complex, to be used in the cytoplasm for sulfate reduction. The hydrogen cycling hypothesis requires the presence of both cytoplasmic and periplasmic hydrogenases in *Desulfovibrio* spp. Since only the periplasmic hydrogenases are present in all sulfate-reducers belonging to this genus, there might be alternative mechanisms for the generation of the coupled proton gradient, for instance involving the membrane bound lactate dehydrogenase or the membrane-bound NADH or NADPH dehydrogenases (Hansen, 1994 ; Woordouw, 1995).

Note that the mechanism proposed by Badziong and Thauer, 1980 to explain the bioenergetics of growth in the presence of sulfate with hydrogen as sole energy source (cf. Figure I.1), corresponds to the second half of the mechanism of hydrogen cycling. However, since external hydrogen is being utilised, only the periplasmic hydrogenases are necessary for this bioenergetic mechanism.

Independently of the general validity of the hydrogen cycling model, an important question concerns the involvement of pyridine nucleotides in linking substrate oxidation to sulfate reduction. Recent work has shown a role for NADH and NADPH as redox carriers in the degradation of certain substrates (Hansen, 1994 ; Chen et al., 1995 ; Fareleira et al., 1997). If NADH is reoxidised by the final electron acceptor via H_2, an efficient removal of the hydrogen gas could change the unfavourable transfer of reducing equivalents from NADH to H^+ into a thermodynamically favourable process (Fareleira et al., 1997). Moreover, an alternative mechanism could be envisaged for the production of hydrogen in the cytoplasm in those organisms that lack the cytoplasmic hydrogenase.

I.2.3 Electron acceptors

The electrons and protons resulting from the oxidative processes mentioned above are used to reduce sulfate to sulfide via an electron transport system. Interestingly, many electron transfer proteins of sulfate-reducing bacteria are soluble and cytoplasmic, which raises some questions about the mechanism of oxidative phosphorylation coupled to electron transfer (see below).

Reduction of sulfate to sulfide takes place in several steps (Figure I.4).

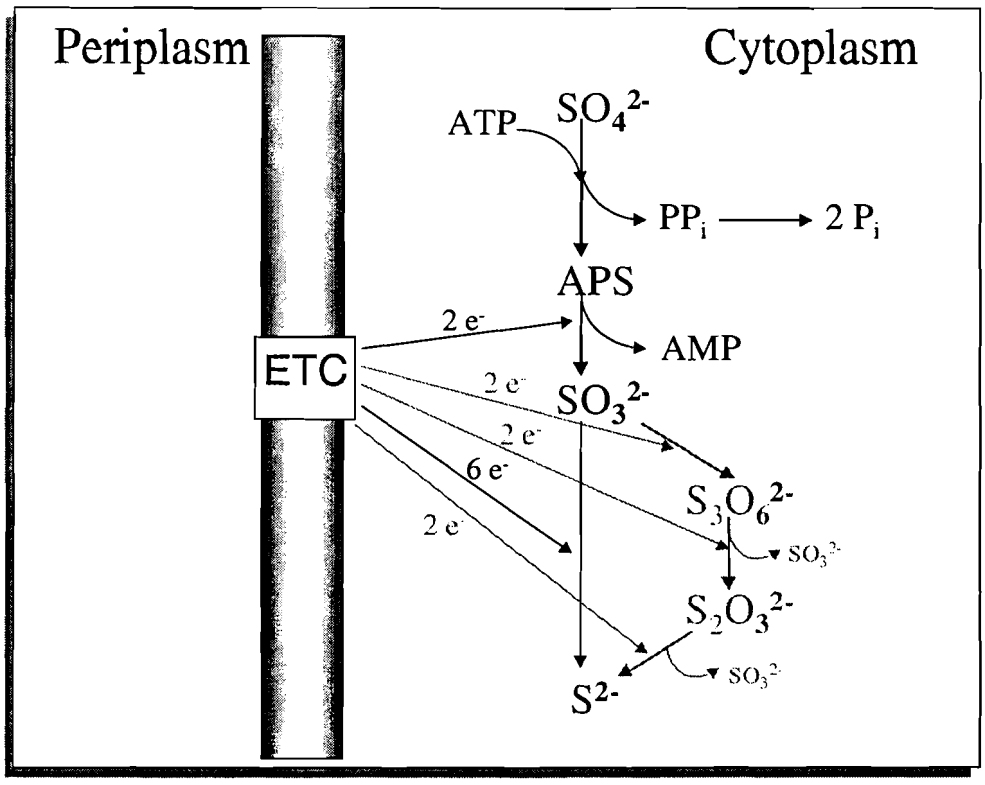

Figure I.4. Steps involved in dissimilatory sulfate reduction. The activation of sulfate (SO_4^{2-}) by ATP results in adenylylsulfate (APS) formation. APS is reduced to sulfite (SO_3^{2-}) and AMP is released. The reduction of sulfite to sulfide (S^{2-}) is either a 6-electron step (dark reaction) or involves trithionate ($S_3O_6^{2-}$) and thiosulfate ($S_2O_3^{2-}$) as intermediates. The reactions of the trithionate pathway are shown in grey. ETC: electron transfer complex.

The first step is thermodynamically unfavourable, requiring activation by ATP. This reaction is catalysed by ATP sulfurylase and generates adenylylsulfate (APS) and inorganic pyrophosphate (PP_i). Further hydrolysis of PP_i drives the reaction forward. Since both phosphoanhydride bonds of ATP are hydrolysed in this process, this is energetically equivalent to the consumption of two moles of ATP. It has also been suggested that, in some species of the genus *Desulfotomaculum*, PP_i could be used for ATP production via phosphorylation of acetate to form acetylphosphate (Liu and Peck, 1981 ; Liu et al., 1982).

The second step in the process of sulfate reduction is the reduction of APS to bisulfite, a reaction catalysed by APS reductase, which is a soluble, cytoplasmic enzyme, containing non-haem iron and flavin centres.

Finally, there is the reduction of bisulfite to sulfide. This reaction is catalysed by dissimilatory bisulfite reductase, which is a high-molecular-weight heterooligomer containing iron-sulfur clusters and sirohaem. Depending on the spectral characteristics, four different enzymes have been described so far: desulfoviridin, desulforubidin, desulfofuscidin and P582 (LeGall and Fauque, 1988 ; Pereira et al., 1998). There is still some discussion about the mechanism of

reduction of bisulfite to sulfide. Two major mechanisms have been proposed: the trithionate pathway (see reactions in grey in Figure I.4) and direct reduction of sulfite to sulfide involving six electrons in a single step. The main arguments for and against the trithionate pathway are discussed by LeGall and Fauque, 1988. This question is not resolved but physiologically it seems likely that a single enzyme catalyses the overall reaction with formation of relatively stable intermediates. However, it is also possible that the absence of free intermediates is limited to *Desulfovibrio* species, whereas an active trithionate pathway is operative in *Desulfotomaculum* (LeGall and Fauque, 1988).

It is worth mentioning that sulfate-reducing bacteria can use electron acceptors other than sulfate. One example is the process of fumarate respiration mentioned above, in which the electrons from the oxidation of malate and pyruvate are transferred to fumarate, generating succinate (Chen et al., 1995).

Some organisms can reduce nitrate or nitrite to ammonia (Mitchell, et al., 1986 ; Seitz and Cypionka, 1986 ; Dalsgaard and Bak, 1994).

Under microaerophilic conditions, some *Desulfovibrio* spp. can even use oxygen as an electron acceptor (Dilling and Cypionka, 1990 ; Chen et al., 1993a,b). Apparently, the ATP produced in this process can be used for cell maintenance but not for growth.

Sulfate-reducers can use Fe(III) (Coleman et al., 1993) and heavy metals such as Cr(VI) (Fude et al., 1994 ; Lovley and Phillips, 1994) and U(VI) (Lovley et al., 1993) as electron acceptors contributing to their reduction and immobilisation. It is thought that cytochrome c_3 works as the metal reductase in some of these cases (Lovley et al., 1993 ; Lovley and Phillips, 1994).

As mentioned above, *D. vulgaris* can grow on pyruvate in the absence of sulfate, producing acetate, CO_2 and stoichiometric amounts of hydrogen (Postgate, 1952). Protons are used as electron acceptors in this system. Interestingly, growth in lactate in the absence of sulfate is negligible or absent, unless H_2-utilising methanogenic bacteria are also present (Bryant et al., 1977). These bacteria contribute to the lowering of the hydrogen pressure in the media, thus facilitating growth of the sulfate-reducers. Under these circumstances, all reducing equivalents generated from oxidation of lactate to acetate and CO_2 appear as methane. In this case, the energy for growth in lactate is provided by substrate level phosphorylation, because no ATP is consumed in the activation of the electron acceptor in the absence of sulfate.

I.3 Tetrahaem cytochrome c_3

Tetrahaem cytochrome c_3 is one of the proteins involved in the bioenergetic metabolism of sulfate-reducing bacteria. It is produced in large quantities by these organisms and it is probably the best characterised multi-haem cytochrome.

The name 'cytochrome c_3' has been given to many multihaem *c*-type cytochromes isolated from sulfate-reducers which have approximately 25 aminoacid residues per haem and display bis-histidinyl axial coordination of the haems. In this work, cytochrome c_3 refers to the tetrahaem protein only. This cytochrome was first isolated in 1954 (Postgate,1954 and Ishimoto et al., 1954) from two *Desulfovibrio vulgaris* strains and was the first cytochrome discovered in an anaerobic, non-photosynthetic organism. It is a soluble protein with a molecular weight of ca. 15 000 and is present in all species of *Desulfovibrio*. All sequenced cytochromes c_3 have a typical N-terminal signal peptide that indicates a periplasmic localisation. The four haems have bis-histidinyl axial coordination and exhibit different and low redox potentials. They are also low spin in both oxidation states. Cytochromes c_3 isolated from different organisms can have very different aminoacid compositions and, consequently, the isoelectric points and the distribution of charges on the protein can vary appreciably from one molecule to another. Interestingly, the architecture of the haem core as well as the general folding of the protein are highly conserved, despite the low sequence homology observed between most of these molecules (Coutinho and Xavier, 1994).

I.3.1 Physiological role

Since the presence of cytochrome c_3 is necessary for the reduction *in vitro* of low molecular weight electron transfer proteins such as ferredoxin, flavodoxin and rubredoxin by hydrogen in the presence of hydrogenase, this cytochrome has been proposed as a coupling factor for the enzyme hydrogenase (Bell et al., 1978). Computer modelling studies indeed suggested that cytochrome c_3 may specifically dock with flavodoxin (Stewart et al., 1988), ferredoxin (Cambillau et al., 1988) and rubredoxin (Stewart et al., 1989). However, localisation of the cytochrome in the periplasmic space would preclude their direct interaction *in vivo* because the small redox proteins are localised in the cytoplasm. This compartmentalisation of the redox proteins raises some questions about the physiological relevance of these complexes. A transmembrane localisation of cytochrome c_3 would resolve this enigma but it is highly improbable given the distribution of hydrophobic residues in this protein (LeGall and Fauque,

1988). However, studies with artificial liposomes modified with cytochrome c_3 showed that the electron transport rate across the membrane was very much accelerated and coupled to rapid proton influx in the presence of the cytochrome (Tabushi et al., 1984). These authors suggested that a cytochrome c_3 dimer could form an electron-channel across the membrane of the liposome. Peck, 1993 also proposed that a cytochrome c_3 dimer could mediate the transmembrane electron transfer between hydrogen oxidation in the periplasm and APS reduction in the cytoplasm. Furthermore, the homology between tetrahaem cytochrome c_3 and the hexadecahaem cytochrome c_3, which was proposed to be part of a transmembrane electron transfer complex (Rossi et al., 1993), may provide some physiological relevance for the studies of complex formation between tetrahaem cytochrome c_3 and the small cytoplasmic redox proteins.

It has been shown recently that, in the presence of cytochrome c_3, the periplasmic hydrogenase maintains the maximum hydrogen uptake activity at physiological pH, whereas in the absence of the cytochrome this activity decreases to ca. 40% (Louro et al., 1997a). According to the hydrogen cycling hypothesis, the reaction of hydrogen oxidation that takes place in the periplasm is crucial for the bioenergetic metabolism of sulfate-reducers, because it is the only energy production step for cells growing with hydrogen as sole energy source. Louro et al., 1997a proposed that cytochrome c_3 coupled to hydrogenase performs energy transduction, acidifying the protons produced in the reaction of hydrogen oxidation at the expense of electronic energy, in the absence of a membrane confinement. The role played by cytochrome c_3 in this mechanism is fundamental: its peculiar thermodynamic properties make it capable of accepting both electrons and protons from hydrogenase, thus favouring the reaction of hydrogen oxidation and, by giving electrons and protons to different acceptors, this cytochrome conserves and increases the charge separation achieved by hydrogenase.

I.3.2 Structure

The structures of several cytochromes c_3 have been solved by X-ray crystallography: cytochrome c_3 from *Desulfovibrio vulgaris* (Dvc_3) strain Hildenborough (Matias et al., 1993), Dvc_3 strain Miyazaki (Higuchi et al., 1984), cytochrome c_3 from *Desulfovibrio gigas* (Dgc_3) (Matias et al., 1996), cytochrome c_3 from *Desulfovibrio desulfuricans* (Ddc_3) strain ATCC 27774 (Morais et al., 1995) and cytochrome c_3 from *Desulfomicrobium baculatum* (Dmbc_3) strain Norway, formerly *Desulfovibrio desulfuricans* Norway, (Czjzek et al., 1994). Up to

now, only the oxidised form of the cytochrome has been accessible to crystallographic studies because this protein is readily oxidised in the presence of small amounts of oxygen. Recently, the structure in solution of the reduced form of Dvc_3 Hildenborough has been solved by NMR techniques (Messias et al., 1998) opening interesting new perspectives for studies of structure-function correlation.

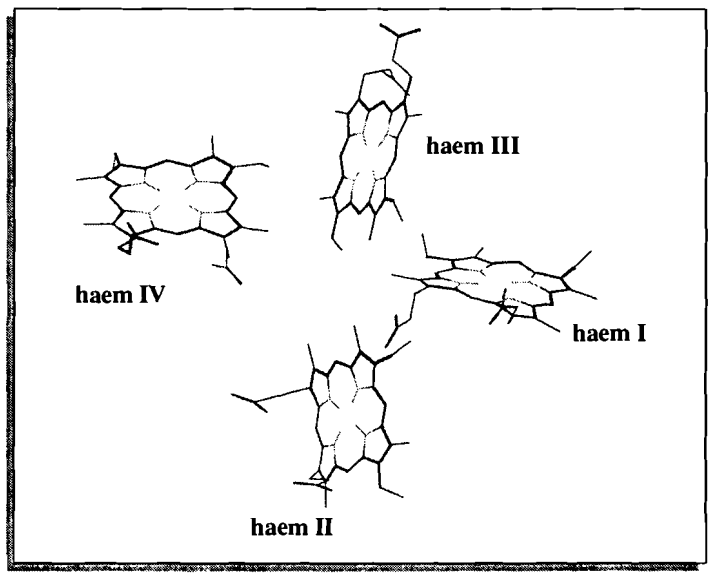

Figure I.5. Haem core of cytochrome c_3 from *Desulfovibrio gigas*. The haems are numbered according to the order of attachment to the polypeptide chain. Picture taken from the X-ray structure determined by Matias et al., 1996.

In all structures, the four haems are ligated to the apoprotein through sequence segments of the type Cys-X-X-(X-X)-Cys-His in which the cysteine residues are covalently bound through thioether linkages to the vinyl sidechains of the porphyrin ring and the histidine is the fifth axial ligand of the iron. The sixth axial histidine ligand to the iron is provided by a different region of the polypeptide chain. As stated above, the haem core is highly conserved: all cytochromes c_3 display similar iron to iron distances and the same relative orientations of the haem planes. The haem core of cytochrome c_3 from *D. gigas* is shown in Figure I.5. All the haems are well exposed to the solvent, which is easily understood given the small number of aminoacid residues of this protein. Structural invariants other than the haem ligations include the conservation of a threonine close to haem IV, a glycine close to haem II and a phenylalanine close to haems I and III. Depending on the sequence alignment chosen, a few other residues may be regarded as conserved. The conserved phenylalanine was thought to play an important role in the electron transfer process but site-directed mutagenesis of this residue in Dvc_3 has shown that fast intramolecular electron transfer is still observed and that the thermodynamic properties, namely the positive cooperativity observed between haems I and II, are maintained in the mutant protein (Saraiva et al.,1996). Many cytochromes c_3 also

present a segment with a high content of lysine residues close to haem IV in the C-terminal region. This highly positively charged region has been postulated as the docking site for the physiological redox partners (Stewart et al., 1988).

Sequence alignments were proposed assuming that all cytochromes have a similar haem core and postulating sequence insertions and deletions in order to maximise the homologies between the various segments (Kissinger, 1989 ; Moore and Pettigrew, 1990 ; Palma et al., 1994 ; Magro et al., 1997). The lowest homology (ca. 25%) is found between the cytochromes from *Dsm. baculatum* and *D.vulgaris*.

I.3.3 Thermodynamic properties

The thermodynamic properties of cytochrome c_3 are very complex and, since their modelling is one of the main objectives of this thesis (cf. chapter II), only the general properties are mentioned here. As stated above, the four haems in cytochrome c_3 have different environments, thus displaying different redox potentials. Moreover, since the distances between them are small, the redox potential of each of the four haems is affected by the redox state of the neighbouring haems. This effect is accounted for by the definition of haem-haem interacting potentials (Santos et al., 1984a). Only negative cooperativities would be expected if the interactions were simply of an electrostatic nature. However, at least two of the haems show positive cooperativity between them, in all cytochromes c_3 studied so far (Louro et al., 1997b). This positive cooperativity probably arises from a localised conformational change linked to the redox process. In addition to that, the redox potentials of the haems depend upon the protonation state of an ionisable residue, thus displaying a redox-Bohr effect. It was demonstrated (Turner et al., 1994, 1996) that the pH-dependence of the redox potentials of the haems can be accounted for by the definition of four haem-proton interacting potentials. Since all these interacting potentials correspond to positive cooperativities, they can be explained by simple electrostatics.

It should be noted that, although the structure of the haem core is strictly conserved, the order of reduction of the four haems is not the same for all cytochromes c_3 (Coutinho and Xavier, 1994 ; Pereira et al., 1998), nor is the positive cooperativity always observed between the same pair of haems. However, for all cases studied up to now, the interplay between all haem-haem and haem-proton cooperativities results in a concerted two-electron step which is coupled to the uptake or release of protons, depending on the direction of the electron flow

(Louro et al., 1997b). These thermodynamic properties give cytochrome c_3 the ability to work as an energy transducing system (Louro et al., 1996a), but kinetic control of the various steps is essential to avoid unproductive pathways.

I.3.4 Kinetic properties

Cytochrome c_3 has four redox centres and, therefore, both intramolecular and intermolecular electron transfer processes must be considered for the analysis of the kinetic properties of this molecule. NMR studies have shown that the first order rate constant for the intramolecular electron exchange is higher than 10^5 s^{-1} (Santos et al., 1984a). Since this process is faster than the bimolecular electron exchange with the redox partners or artificial reducing agents, the system is under thermodynamic control. Therefore, independently of the electron entrance gate, the electrons are distributed inside the molecule according to the relative redox potentials of the haems. Thus, the correct modelling of the kinetic properties of cytochrome c_3 has to rely on an accurate thermodynamic description of the system.

The reduction of cytochrome c_3 by redox proteins or exogenous electron donors usually exhibits a biphasic kinetic profile. Most of the second order rate constants determined for the reduction process from stopped-flow studies with sodium dithionite or with redox proteins are of the order of 10^6-10^7 $M^{-1}s^{-1}$ (Favaudon et al., 1978; Tabushi et al., 1983; Capeillère-Blandin et al., 1986; Catarino et al., 1991). The second order rate constants for the oxidation of reduced cytochrome c_3 by molecular oxygen or by oxidised flavodoxin are smaller, having values of the order of 10^4-10^5 $M^{-1}s^{-1}$ (Capeillère-Blandin et al., 1986; De Francesco et al., 1994). It is apparent from the values of the rate constants reported in the literature that factors such as the pH and the ionic strength affect the electron transfer rates and also the relative amplitudes of the fast and slow phases. These rate constants are also strongly dependent on the formal charge of the reducing agent.

I.4 Thesis plan

Apart from the general introduction and the concluding remarks, this thesis is divided into two main chapters, one dealing with the thermodynamic and the other with the kinetic properties of cytochrome c_3. Both aspects are fundamental to the global understanding of the function of this cytochrome. While thermodynamic studies give information about what might occur in

the system, kinetic studies are essential to define what happens in practice. Since strategies for the modelling of both thermodynamic and kinetic properties are presented and discussed in this thesis, it may represent an important contribution for a more comprehensive approach to the study of cytochrome c_3 and to the understanding of its role in the bioenergetic mechanisms of sulfate-reducing bacteria. Moreover, since the thermodynamic and kinetic models developed are general, they can be applied to the study of other systems. Indeed, care has been taken in the presentation of the models in order to make it sufficiently explicit to facilitate the eventual application to other systems. The definition of the parameters of each model is explained and discussed, as well as their physical significance, whenever possible.

The two chapters are self-contained, each including a detailed introduction to the subject, with a brief review of the literature and a materials and methods section where the more relevant procedures of my contribution to the experimental work are described. However, to simplify the organisation and avoid repetitions, all the references are grouped at the end of the thesis.

The models which have been used up to now for the analysis of the thermodynamic properties of cytochrome c_3 are presented and discussed in chapter II. After a brief introduction to the first model, including haem-haem interactions (Santos et al., 1984a), the A/B model (Coletta et al., 1991), which was the first model to include both pH and solution potential as variables, and the model of five interacting centres (Turner et al., 1996) are thoroughly explained and compared in sections I.3.2. and I.3.3, respectively. Section I.3.2 is a revised version of the article published by Coletta et al., 1991, in which some discrepancies related to the visible titration data are discussed and a new interpretation of the parameters obtained for the protonated and deprotonated forms of Dgc_3 is made, according to our present knowledge of the system. Section I.3.3 is based on the article published by Turner et al., 1996, but also includes the application of the model to new Dgc_3 data. The peculiarities of the thermodynamic properties of cytochrome c_3, which were revealed by the analysis of the parameters obtained from the application of the models to the experimental data, are described and discussed in the end of chapter II. Future modelling strategies are also proposed.

Chapter III is concerned with the kinetic properties of cytochrome c_3. In the introduction to this chapter, besides defining the objective of our studies, previously published work in the field is discussed. The materials and methods section of this chapter includes the experimental procedures used in the stopped-flow studies with Dgc_3 presented in this work, as well as the description and analysis of the results of anaerobicity tests developed in our laboratory in

order to probe the anaerobic capacities of the sample-handling-unit of the stopped-flow apparatus. The model proposed in this thesis for the analysis of intermolecular electron transfer data of systems in fast intramolecular electron exchange is presented in section III.3. Section III.4 includes the results obtained in stopped-flow studies of the reduction of Dgc_3 by sodium dithionite. The data presented in this section have been published in 1991 (Catarino et al., 1991) but were re-analysed for this thesis, using a new kinetic model with a smaller number of parameters, together with the new thermodynamic parameters. Section III.5 includes the results of stopped-flow studies of the interaction between Dgc_3 and FMN or flavodoxin isolated from *D. gigas*. The data presented in this section have not been published previously. A detailed analysis and discussion of the results is presented, together with future perspectives concerning both data acquisition and analysis.

The general conclusions of the thermodynamic and kinetic chapters are stressed again in the concluding remarks. An extended discussion about the information which can be extracted from the kind of kinetic studies presented in this work is also included. Some apparent discrepancies found in the literature concerning stopped-flow data of cytochromes c_3 isolated from other *Desulfovibrio* spp. are interpreted in the light of the kinetic model developed in this work. Finally, the model proposed by Louro et al., 1997a,b for the physiological role of cytochrome c_3 in the bioenergetic metabolism of sulfate-reducing bacteria is discussed in the light of the information obtained from the kinetic studies.

II THERMODYNAMIC PROPERTIES

II. THERMODYNAMIC PROPERTIES

II.1 Introduction

Cytochrome c_3 is a small monomeric protein with four haem groups. The four haems have bis-histidinyl axial coordination and display very low redox potentials, in the range from –100 mV to –400 mV. Different redox potentials are expected for different haems because each haem is situated in a different environment inside the protein and factors such as solvent exposure and the character of the aminoacid side chains around the haems control their redox potentials (Stellwagen, 1978 ; Bertini et al., 1997 ; Gunner et al., 1997 ; Mauk and Moore, 1997 ; Zhou, 1997). According to the crystal structures (Higuchi et al., 1984 ; Matias et al., 1993 ; Czjzek et al., 1994 ; Morais et al., 1995 ; Matias et al., 1996) distances from about 11 to 18 Å separate the irons of the four haems. These short distances allow the development of electrostatic interactions between the redox centres. Indeed, NMR studies have shown that the four haems display different redox potentials and that, during an oxidation/reduction process, interactions among the different haems occur, thus changing the values of redox potentials depending on the haems which are oxidised (Santos et al., 1984a ; Fan et al., 1990a ; Turner et al., 1994 and 1996 ; Park et al., 1996). Moreover, the redox potentials exhibit a redox-Bohr effect (Papa et al., 1979 ; Louro et al., 1996a) since their values are pH dependent (Moura et al., 1982 ; Santos et al., 1984a). Thus, modelling the thermodynamic properties of such a complex system has to take into account all the cooperativities established between the four redox centres and an acid/base group.

Since four electrons can be exchanged by this molecule, five redox stages are defined at the macroscopic level. Starting from the fully reduced state, which is named here as stage zero, four successive one-electron steps convert the molecule into the fully oxidised form, which corresponds to stage IV (see scheme I).

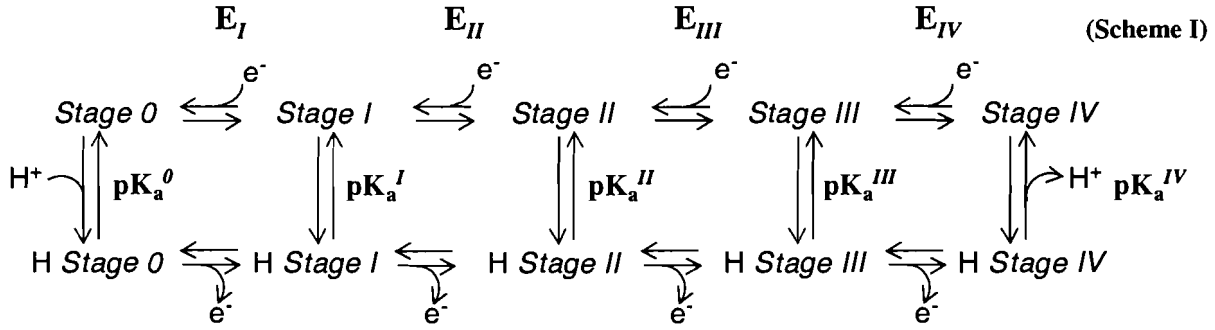

The relative populations of the five stages at equilibrium for any solution potential are defined by four macroscopic redox potentials (E_I, E_{II}, E_{III} and E_{IV}) according to the Nernst equation.

Since, independently of the redox centres, the ionisable group can be either protonated or deprotonated, a parallel acid/base equilibrium is established for each of the five oxidation stages. Five macroscopic pK_a values (pK_a^0, pK_a^I, pK_a^{II}, pK_a^{III} and pK_a^{IV}) one for each stage, determine the relative populations of protonated and deprotonated forms for any solution pH.

Scheme I represents the macroscopic stages and the relationships between them, but gives no information about the individual haems. The general scheme for the equilibrium distribution of electrons in a molecule with four redox centres and one ionisable group is presented in Figure II.1. The redox equilibria involve 16 microstates (Palmer and Olson, 1980) for each protonation state, giving a total of 32 microstates. Since any one of the four haems can lose the electron in the first oxidation step, there are four different possibilities leading to four microstates in stage I. In the second oxidation step, each of the four microstates of stage I can lose one out of the three transferable electrons that are still on the molecule. Thus, there are twelve routes leading to the six microstates that belong to stage II. Another twelve routes lead to the four microstates of stage III and, finally, four routes end in the single microstate of stage IV. Note that, according to the nomenclature used in this work, the number of oxidised haems of a microstate is equal to the number of the oxidation stage it belongs to.

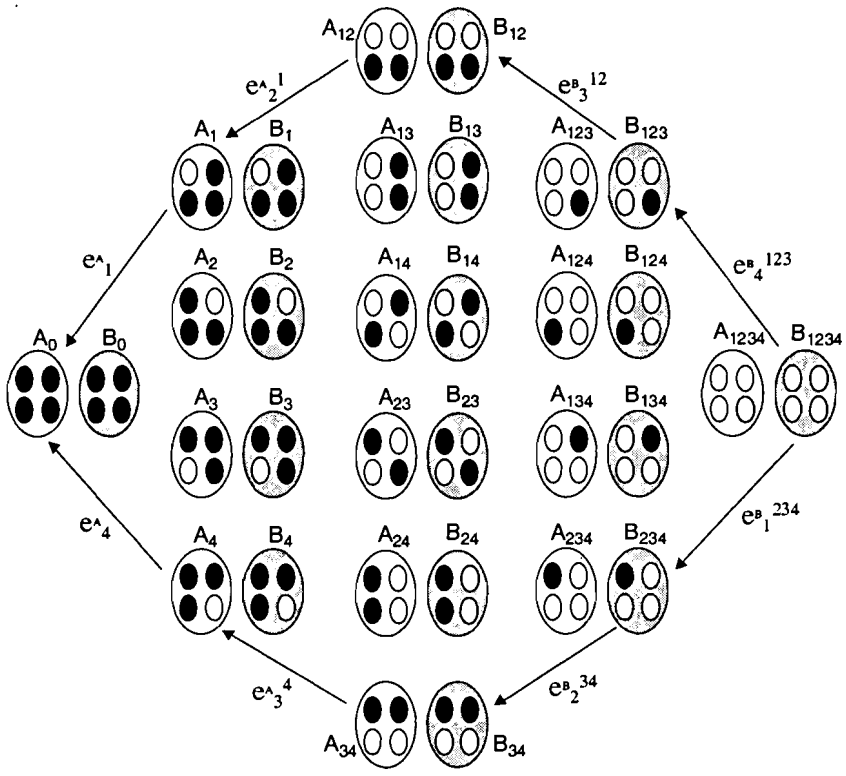

Figure II.1. General scheme for the electronic distribution in a molecule with four redox centres and one ionisable centre. The nomenclature used for the microstates is the following: 'A' stands for all protonated species and 'B' for the deprotonated ones (shaded), the numbers in subscript indicate the haems which are oxidised in each microstate. The reduction potentials defined between protonated species are represented by e^A and those defined between deprotonated species by e^B, in both cases the letters are followed by the number of the haem which is being reduced (subscript) and the number of the haems which remain oxidised (superscript).

The microscopic parameters of the system are the redox potentials and pK_a values that define the relative populations of all 32 microstates for any pH and any solution potential. For each protonation state, four microscopic redox potentials (e_i with i=1-4) characterise the four equilibria between stages 0 and I, twelve redox potentials (e_i^j, with i,j=1-4 and $j \neq i$,) characterise the twelve equilibria between stages I and II, another twelve potentials (e_i^{jk} with i,j,k=1-4 and $k \neq j \neq i$) define the twelve equilibria between stages II and III and, finally, four potentials (e_i^{jkl} with i,j,k,l=1-4 and $l \neq k \neq j \neq i$) characterise the four equilibria between stages III and IV. According to this notation, the subscript indicates the haem which is being oxidised in a certain step whereas the superscript indicates the haems which are already oxidised in the starting microstate. In addition to the 32 redox potentials for each protonation state, there are 16 pK_a values that define 16 acid/base equilibria between protonated and deprotonated microstates.

It can be shown that the parameters mentioned above are not all independent. They can be defined by linear combinations of a smaller number of independent parameters, for which we shall use, the intrinsic microscopic parameters of the five centres plus interaction terms defined between the individual centres. The microscopic redox potential of haem i when haem j is already oxidised can be expressed as $e_i^j=e_i+I_{ij}$ if the change in the microscopic redox potential of haem i caused by the oxidation of haem j is expressed as haem-haem interaction I_{ij}. Because of microreversibility, I_{ij} is equal to I_{ji}, the change in the microscopic redox potential of haem j caused by the oxidation of haem i, and therefore $e_j^i=e_j+I_{ij}$. Since this also applies to the interactions between the haems and the ionisable centre, each microscopic redox potential of the deprotonated molecule can be expressed as the sum of the equivalent microscopic potential of the protonated molecule plus the haem-proton interaction term I_{iH}, $e_i^B=e_i^A+I_{iH}$. Application of microreversibility also shows that only one pK_a is independent, out of the 16 pK_a values that define the acid/base equilibria between the 32 microstates. The number of microscopic parameters is further reduced by assuming that the interactions are additive.

Note that the minimum number of independent parameters of the model corresponds to the situation in which there are no interactions between the five centres. Under these circumstances, the five intrinsic parameters of the centres, which are the four microscopic redox potentials of the individual haems plus the pK_a of the ionisable centre, are sufficient to describe the system. Conversely, the maximum number of independent parameters corresponds to the situation when all possible interactions are effective, i.e. there are interactions between the centres two by two, three by three, four by four and five by five. If this is the case, the number of parameters necessary to describe the properties of the system is

32, as will be discussed in section II.3.3. It is interesting to note that the need for three-site and higher order interactions, is equivalent to the situation of non additive two-site interactions which might be caused by major conformational changes in the protein molecule during the oxidation process and/or upon deprotonation.

Microscopic parameters are only accessible from experimental techniques that are able to probe each individual centre during the redox process. Although both NMR and EPR spectroscopies have been used extensively for this purpose, the thermodynamic parameters which can be obtained in each case are different. From NMR studies of systems in fast intramolecular and slow intermolecular electron exchange (Santos et al, 1984a), such as Dgc_3 and Dvc_3, it is possible to determine the intrinsic microscopic parameters of the redox and acid/base centres and define two-site interactions between them, if a complementary technique is used to fix the absolute redox potential scale. The thermodynamic properties of Dgc_3 (Coletta et al., 1991 and Louro et al., 1998b) and Dvc_3 Hildenborough (Turner et al., 1994 and 1996) were characterised by NMR spectroscopy coupled to visible redox titrations, whereas those from Dvc_3 Miyazaki were studied by Fan et al., 1990a and Park et al., 1996 using NMR coupled to electrochemical techniques and UV-visible potentiometric titrations. The different models which have been used for the determination of microscopic parameters from NMR data of cytochromes c_3 in slow intermolecular electron exchange will be discussed in detail in this chapter.

The information which can be obtained from NMR studies of systems in fast intermolecular electron exchange is more limited since it does not allow the accurate determination of haem-haem interactions (Coutinho, 1993), and the same is true for EPR studies (Moura et al., 1988). For a system in fast intermolecular electron exchange in the NMR time scale, it is possible to obtain the oxidised fraction of the individual haems as a function of the solution potential, if an independent method is used to measure the solution potential (Coutinho, 1993). However, deconvolution of these curves to obtain the microscopic redox potentials and interactions is very difficult because the system is undefined and the accurate determination of microscopic redox potentials is restricted to those haems which display no interactions. Note that the existence of interactions among haems with close redox potentials causes distortion of the experimental curves relative to a simple Nernst curve and the midpoint potentials calculated from 50% oxidised fraction do not correspond to the 'true' microscopic redox potentials of the haems. The 'apparent microscopic' redox potentials of Dmbc_3 strain Norway were determined by Coutinho, 1993 from the curves of the oxidised fraction of the individual

haems, assuming a non-interacting model. Redox titrations monitored by NMR at pH 7.8 and 9.0 showed that the microscopic redox potentials are not pH dependent in this pH range.

As stated above, the information which can be obtained from EPR studies is similar, with the difference that the solution potential of each sample is measured at room temperature in the presence of redox mediators during an EPR titration. Therefore, no additional information is necessary to construct the curves of oxidised fraction as a function of the solution potential. However, since the sample has to be frozen before the EPR spectrum is taken, the temperature at which the sample is equilibrated and the solution potential measured does not correspond to the temperature at which the spectrum is recorded. Although in some cases the similarity between redox titrations monitored by EPR at low temperature and by UV-visible spectroscopy at room temperature indicates that the redox equilibria are only weakly affected by the freezing process (Gayda et al., 1988), there is also reference in the literature to non-negligible temperature effects (Porras and Palmer, 1982).

Several authors determined the redox potentials of the haems for different cytochromes c_3 by redox potentiometry coupled to EPR spectroscopy. For most of the cases, a non-interacting model was used to fit the data (see discussion about the 'individual model' below). Dgc_3 was studied by Xavier et al., 1979, Dvc_3 Hildenborough by Der Vartanian et al., 1978, Dvc_3 Miyazaki by Gayda, et al., 1987, Dmbc_3 Norway 4 by Cammack et al., 1984 and Gayda, et al., 1985, Dmbc_3 ATCC 9974 by Moura, et al., 1988 and Ddc_3 ATCC 27774 by Morais et al., 1995. However, some attempts have been made to determine intrinsic microscopic potentials and haem-haem interactions by Gayda et al., 1988 (Dmbc_3 Norway 4) Benosman et al., 1989 (Dvc_3 Miyazaki) and Campos, 1994 (Dvc_3 Hildenborough and Dgc_3).

Since many studies have been published on the characterisation of the thermodynamic properties of cytochromes c_3 by electrochemical methods, this overview of the literature would not be complete without reference to them. Electrochemical techniques such as cyclic voltammetry, differential pulse polarography and differential pulse voltammetry have been extensively applied to the determination of redox potentials of Dgc_3 (Nivière et al., 1988), Dvc_3 Hildenborough (Bruschi et al., 1984 and Moreno et al., 1991), Dvc_3 Miyazaki F (Sokol et al., 1980 and Park et al., 1996), Dmbc_3 Norway (Bianco and Haladjian, 1981) and Dmbc_3 ATCC 9974 (Moreno et al., 1991). Other references can be found in a review by Bianco and Haladjian, 1994.

To have a better understanding of the physical meaning of the redox potentials determined by the various experimental techniques, it is important to note that two types of model have been

used for the analysis of electrochemical data or potentiometric titrations monitored by UV-visible spectroscopy; they will be referred to here as the 'sequential model' and the 'individual model'. Since these experimental techniques give information about the global redox state of the protein, it is impossible to obtain accurate microscopic information on the individual centres and the data are usually fitted with four parameters for each pH value. However, depending on the model used to fit the data, the four redox potentials have different meanings, which is not always pointed out by the authors.

The 'sequential model' describes cytochrome c_3 as a unit, giving or accepting one electron at a time. This model consists of four consecutive reversible redox steps and the four parameters are the four macroscopic redox potentials defined in the beginning of this chapter. Note that these potentials do not correspond to the potentials of the individual centres and, although they refer to four consecutive steps, they do not necessarily appear in decreasing order, the occurrence of inversions being indicative of strong positive cooperativity in the system. The equation for the calculation of the global oxidised fraction as a function of the four macroscopic redox potentials and the solution potential is given in appendix A. The mathematical expressions for the simulation of electrochemical data according to the 'sequential model' were derived by Niki et al., 1984. It is important to stress that this model makes no assumptions about interactions.

The 'individual model'considers four independent redox centres, each one being characterised by an intrinsic redox potential. According to this model, the oxidation of the four centres is not sequential but parallel. In this case the four parameters of the model correspond to the four microscopic redox potentials of the centres, as defined in this chapter, for the particular case of non-interacting centres. Since the redox processes are assumed to be independent, from the mathematical point of view, this model consists simply of the sum of four Nernst equations, one for each redox centre (see appendix B). The equations for the simulation of electrochemical data were derived by Bianco and Haladjian, 1981. Note that this model is not compatible with inversions of the redox potentials and, therefore, cannot describe titration curves displaying positive cooperativity. However, it is usually impossible to demonstrate unequivocally the presence of redox interactions on the basis of UV-visible or electrochemical data and examples of the application of both models can be found in the literature. Therefore, it is important to know in each case to which kind of redox potentials the authors are referring. The application of the two models to electrochemical data was discussed by Wang et al., 1991 together with the determination of the two sets of parameters for cytochrome c_3 from *Desulfovibrio desulfuricans* NCIMB 8372.

The 'sequential model' is general and, although the values of the cooperativities of the system are not defined, the macroscopic redox potentials include information about them. The problem of this approach is that, since the macroscopic potentials do not correspond to the potentials of the individual centres, these remain unknown. On the other hand, the 'individual model' deals with the redox potentials of the individual centres but, since this model is valid only in the absence of interactions, the physical significance of the parameters may be distorted. If there are non-negligible redox interactions in the system, the redox potentials determined are not the intrinsic microscopic redox potentials of the centres but correspond to the midpoint of the Nernst curves that best fit the data of the individual centres. Since these parameters include contributions from different factors they will be referred to as 'apparent microscopic' potentials of the individual centres.

Note that, if the separation between the redox potentials of the individual centres is higher than 120 mV, the ambiguity in the physical significance of the parameters disappears. Although interactions may still exist between the redox centres, their determination is impossible because the titration of each group is well separated from the others. Under these circumstances the definition of interactions becomes inappropriate and so does the definition of intrinsic redox potentials. Also, the macroscopic redox potentials of the steps become equal to the apparent microscopic potentials of the centres.

The different models which have been used for the analysis of the NMR data of cytochromes c_3 in fast intramolecular and slow intermolecular electron exchange will be described in this chapter, with special emphasis for the models that integrate redox and acid/base properties. Modelling of the thermodynamic data is necessary to provide a solid basis for the understanding of the complex network of cooperativities operative in this molecule which, in turn, makes it possible to formulate hypothesis about the role of these cooperativities in the energy transducing mechanism of sulfate reducing bacteria.

If the microscopic thermodynamic parameters are correctly attributed to the haems in the crystal structure, the information provided by these parameters can be used to establish structure-function relationships. The assignment of the haem methyl resonances of the NMR spectrum to the haems in the structure allowed the correlation between oxidation order and order of attachment of the four haems to the polypeptide chain to be established. These results are presented in Table II.1 for several cytochromes c_3 isolated from different sources.

Table II.1. Assignment of the oxidation order at pH 8.0 to the haems in the structure. Roman numbers indicate the order of attachment of the haems to the polypeptide chain. At some pH values the oxidation order of haems II and I for Dvc_3 and Ddc_3 and haems I and IV for Dmbc_3 is reversed. Shaded areas indicate the haems displaying positive cooperativity between them in each case. (*) The assignment proposed by Coletta et al., 1991 for Dgc_3 was wrong because at that time it was a commonly held view that the correspondence between the oxidation order and the haems in the structure was the same for all cytochromes c_3. Besides, it was based on a wrong assignment reported by Fan et al., 1990a.

oxidation order	**Dgc_3**	**Dvc_3** Hildenborough	**Dvc_3** Miyazaki	**Ddc_3** ATCC 27774	**Dmbc_3** Norway
1	I	III	III	II	II
2	II	II	II	I	I
3	III	I	I	IV	IV
4	IV	IV	IV	III	III
reference	Piçarra-Pereira et al., 1993*	Salgueiro et al., 1992	Park et al., 1996	Louro et al., 1996b	Coutinho et al., 1993 and 1995 ; Coutinho and Xavier, 1994

It is interesting to note that, although the architecture of the four haems is maintained in all cytochromes c_3 isolated so far, there is no correlation between oxidation order and the position that each haem occupies in the sequence. Moreover, the haems which display positive cooperativity between them are not the same haems for all cytochrome c_3 molecules.

The development of models is fundamental to a better understanding of these complex redox systems. When the available information is integrated in the framework of a model, it is possible to make predictions about the behaviour of the system under different conditions, even those which are not experimentally accessible. Moreover, models facilitate the comparison between the thermodynamic properties of different cytochromes c_3, allowing structure-function relationships to be established. The interpretation of the results of the thermodynamic model for the particular case of Dvc_3, led to the proposal of a new mechanism for energy transduction involving cytochrome c_3 and the periplasmic hydrogenase (Louro et al., 1997a) which will be discussed in section IV.3.

Although the thermodynamic characterisation of different cytochromes c_3 led to different parameters in each case, the global result in terms of the electron transfer mechanism is the same. All cytochromes c_3 studied up to now have the capacity of performing a concerted two-electron step, which is coupled to the simultaneous transfer of protons (Coletta et al., 1991 ; Turner et al., 1994 and 1996 ; Louro et al., 1997b ; Salgueiro et al., 1997b ; Louro et al., 1998b,c).

II.2 Materials and Methods

As discussed above, the determination of the thermodynamic parameters of cytochrome c_3 can be made by different experimental techniques. However, only NMR experiments can provide the information necessary for the complete description of the system. With this powerful spectroscopic tool, it is possible to obtain information about each separate haem while the reduction or the oxidation process takes place (Moura et al., 1982, Santos et al., 1984a). However, since it is impractical to measure the redox potential inside the NMR tube, only relative redox potentials can be determined from a redox titration monitored by NMR. In this work, redox titrations monitored by UV-visible spectroscopy were used as a complementary technique to obtain the absolute values for the thermodynamic parameters.

The detailed experimental technique used for the NMR experiments can be found in Santos et al., 1984b, Salgueiro et al., 1992, Turner et al., 1996. It is important to note that, since the NMR samples are not buffered and because the redox reactions are coupled to acid/base reactions in cytochrome c_3, the pH of the sample changes along the oxidation process. Therefore, in order to have a correct evaluation of this parameter, the pH of the NMR samples at intermediate oxidation levels was measured inside an anaerobic chamber to avoid reoxidation.

Only the redox titrations monitored by visible spectroscopy will be described in detail in this section because the development of this technique in our laboratory was my particular contribution, at the experimental level, to the determination of the thermodynamic parameters of Dgc_3 and Dvc_3.

II.2.1 Potentiometric titrations coupled to visible spectroscopy

The experimental technique used for the potentiometric titrations is that described by Dutton, 1978. The redox potential of the solution is measured after each addition of the reducing or oxidising agent and, simultaneously, the redox state of the protein centres is monitored by the visible spectrum. Rapid and complete equilibration between the redox centres inside the protein and the platinum electrode is, therefore, essential (Wilson, 1978). If the solution potential measured does not correspond to the visible spectrum recorded at the same time, the titration curve will appear distorted and the redox potentials determined from it are not reliable. Since observation of hysteresis between titration curves performed in the oxidative

and in the reductive direction is indicative of non-equilibrium conditions, it is good practice to perform the titration in both senses until identical results are obtained.

Stability, both of the redox potential measurement and the visible spectrum, can only be obtained under strict anaerobic conditions, especially for proteins with very negative redox potentials which are readily oxidised by molecular oxygen, such as cytochrome c_3. Also, efficient stirring of the protein solution inside the spectrophotometer cell has to be maintained, but care has to be taken in order to avoid disturbing the optical density measurements.

The time response of the electrodes used for the measurement of the solution potential is another important feature. The measuring electrode is usually a platinum electrode and the reference most commonly used is either a standard calomel or a silver | silver chloride electrode. If the electrodes are in good working order the time response is fast and the values obtained in the calibration against saturated quinhydrone solutions at two different pH values are practically identical (Bühler and Baumann, 1982). However, contamination of the diaphragm of the reference electrode may occur as a result of the reaction between dissolved silver chloride and reducing agents or solutions containing sulphides, particularly when sodium dithionite is used as the reducing agent. This must be avoided, together with other poisoning problems caused by adsorption of grease or proteins on to the measuring electrode, because they can lead to a sluggish response of the electrodes or even to measuring errors of up to 60 mV (Bühler and Galster, 1980). An electrode that is not in good working condition not only takes a long time to give a stable measurement but also gives significantly different values for the calibration at different pH values. Therefore, it is good practice to perform the calibration with saturated quinhydrone solutions at different pH values, for instance at pH 7 and 4.

Unlike many small inorganic and organic redox molecules, proteins usually do not equilibrate easily with the measuring platinum electrode and it is necessary to perform the titrations in the presence of redox mediators (Dutton, 1978 ; Wilson, 1978). Figure II.2 shows the comparison between two redox titrations of *D.gigas* cytochrome c_3 performed in the presence and absence of redox mediators. Both titrations were done in the oxidative sense. The upper part of the two curves coincide, but, as the cytochrome becomes more oxidised, the curve without mediators drops sharply while that with mediators displays a more accentuated shoulder. What happens in the steeper part of the curve without mediators is that, as the oxidising agent is added, the cytochrome is readily oxidised and the absorbance decreases. However, since there is no

communication between the redox centre and the electrode, the value of the solution potential measured at the electrode hardly changes.

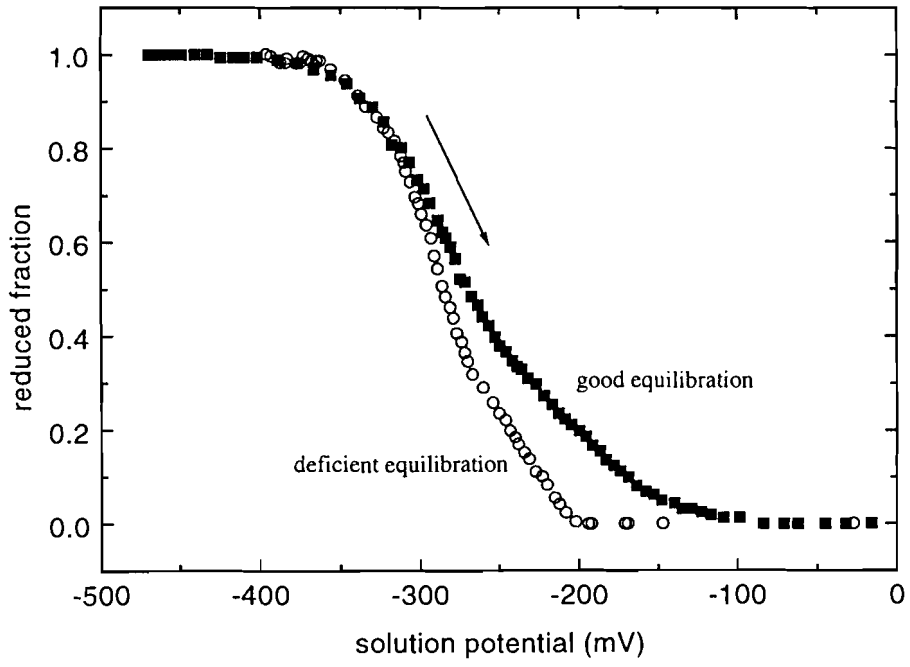

Figure II.2. Effect of deficient equilibration between the protein and the measuring electrode in an oxidative redox titration. Comparison between two redox titrations of Dgc_3 performed at pH 7.2 in the presence (filled squares) and in the absence (open circles) of redox mediators.

It should be noted that, for a titration performed in the reductive sense, the same phenomenon leads to a displacement of the curve without mediators to the other side of the equilibrium curve, generating the hysteresis referred to above.

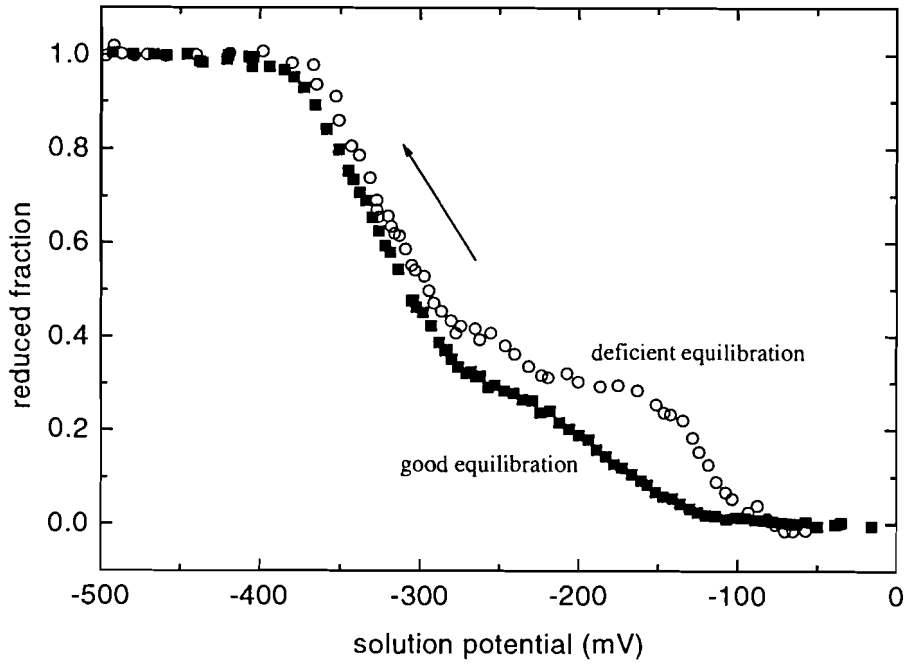

Figure II.3. Effect of deficient equilibration between the protein and the measuring electrode in a reductive redox titration. Comparison between two redox titrations of Dgc_3 performed at pH 9.6.

This is apparent from Figure II.3, where a reductive titration performed at equilibrium is compared with another titration in which the communication between the redox centres and the electrode was deficient. In the beginning of the titration, the addition of reducing agent results in the reduction of the first haem and consequent increase of the absorbance but, since there is no equilibrium between the redox centres and the electrode, the solution potential measured hardly changes and the titration curve shows an initial steep increase of the reduced fraction.

The result of these experiments indicates that, although the haems with more negative redox potentials equilibrate reasonably well with the electrode, the haem with the higher redox potential does not, and good equilibration is achieved only in the presence of redox mediators. It is interesting to note that this observation is in agreement with what would be expected from structural considerations, since the haem which unequivocally needs mediators is haem IV, one of the least exposed to the solvent (Matias et al., 1996).

II.2.1.1 Redox mediators

Redox mediators are small organic or inorganic redox agents which work as shuttles between the electrode and the redox centres inside the protein, facilitating the equilibration of electrons between the various species in solution and the electrode surface. These molecules must be chemically stable and react effectively and reversibly both with the electrode and with the biological redox component. It is important to confirm that the mediators used in a titration are not complexing or otherwise interacting with the biological components so as to affect their electrochemical behaviour. It is common practice to perform titrations for a wide range of different concentrations of the redox mediators, in order to detect any interference from them, and also to choose the appropriate concentration to be used in the experiment. The higher the concentration of mediators, the more efficient is the equilibration with the electrode, but care must be taken in order to avoid spectroscopic interference. Thus, similar concentrations of mediators and biological sample are usually used in a titration.

Some of the organic molecules used as redox mediators are not soluble in water. Aqueous solutions may be prepared by dissolving the powder in a few microliters of an organic solvent which is miscible with water. After complete dissolution, water is added to the desired volume. Since some of the compounds tend to degrade with time, the solutions of the mediators should be freshly prepared at least once a week.

Most of the molecules used as redox mediators are dyes which have different colours in the oxidised and in the reduced forms. During a redox titration, the changes of the visible spectra of the mediators are superimposed on the change of the visible spectrum of the biological compound. The spectral interference can be significant if high concentrations of mediators which have peaks close to the wavelength at which the absorbance is being measured are used. The appropriate concentration of mediators is therefore, a compromise between the quantity necessary to ensure good equilibration with the electrode and the optical interference caused. Whenever possible, the use of mediators with peaks around the working wavelength should be avoided, but, since it is practically impossible to eliminate all spectral interference, the absorbance measurements have to be corrected for the contribution of the mediators. Usually, a control redox titration is performed with the mixture of mediators in the absence of the biological sample. For each value of the solution potential, the absorbance measured in the titration of the mediators is subtracted from the absorbance measured in the titration of the biological sample in the presence of the mediators. For direct subtraction, the concentration of redox mediators must be exactly the same in both titrations.

Although equivalent, the method used in this work is simpler and less time consuming. This method takes advantage of the presence of two isosbestic points near the α-peak of the spectra of cytochrome c_3. Since, by definition, the absorbance of the cytochrome does not change at the isosbestic points, any change of absorbance observed at these wavelengths is due to the redox mediators. Moreover, it can be shown that the absorbance of the mixture of mediators at the α-peak, can be approximated for any value of the solution potential by the average of the absorbances at the isosbestic points (Figure II.4). Therefore, if the absorbance is measured simultaneously at the α-peak and at the proximal isosbestic points, a single titration is sufficient for obtaining all the necessary information to construct titration curves corrected for spectral interference from the redox mediators.

The choice of the mediators to be used in a potentiometric titration is made on the basis of their midpoint redox potentials. The entire range of solution potentials of a particular titration has to be covered by mediators whose midpoint redox potentials are not more than 60 mV apart. Since the midpoint redox potentials of most of the mediators commonly used are pH dependent (Clark, 1972 ; Prince et al., 1981), the pH values at which the redox titrations are going to be performed also have to be taken into account for the correct choice of mediators. The pH dependence of the midpoint redox potentials of the mediators used in the present

work, which span the potential range from zero to –500 mV, is shown in Figure II.5. This graphical representation was constructed from the information included in Clark, 1972.

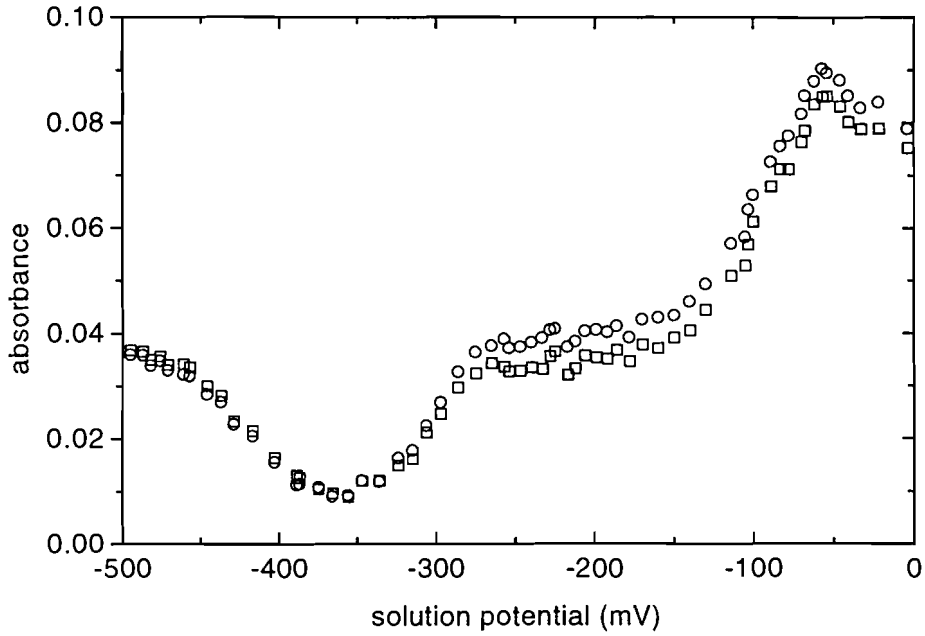

Figure II.4. Correction of the absorbance for the optical interference of the redox mediators. Comparison between the absorbance measured at the wavelength of the α-peak (squares: A_{552nm}), and the average of the absorbances at the isosbestic points (circles: $(A_{542nm}+A_{560nm})/2$) in a redox titration of the following mixture of mediators: methylene blue, indigo tetrasulfonate, indigo trisulfonate, indigo disulfonate, 2-hydroxy-1,4-naphthoquinone, anthraquinone-2,7-disulfonate, anthraquinone-2-sulfonate, safranine T, neutral red, diquat and methyl viologen, all at 3 μM and triquat at 0.75 μM concentration. Buffer: 50 mM tris/HCl pH 8.0.

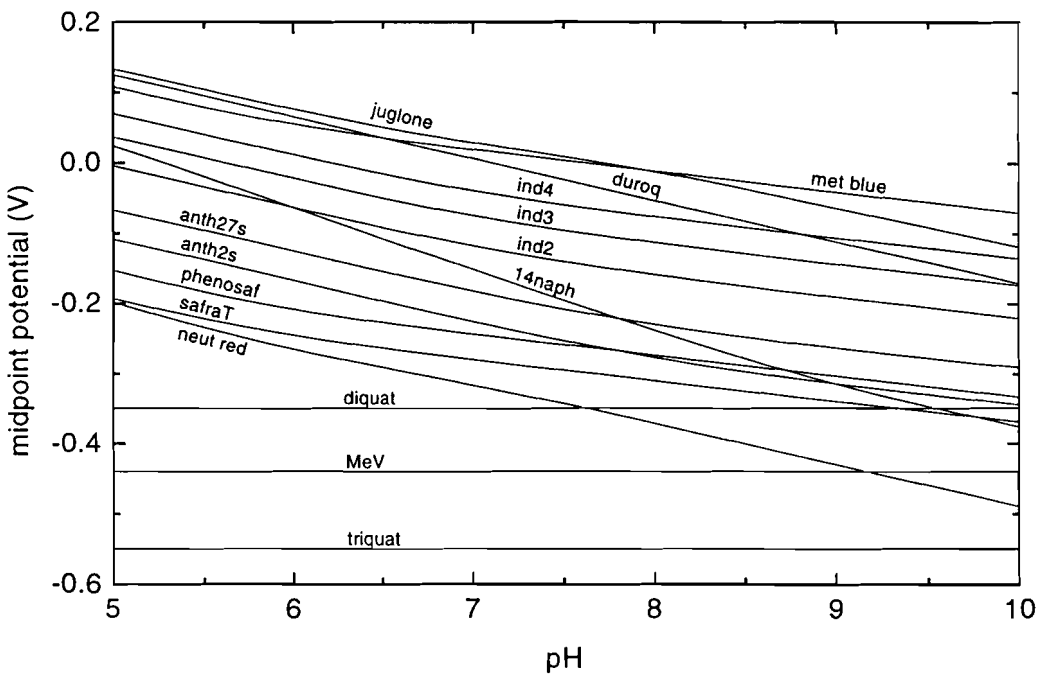

Figure II.5. Midpoint potentials of some redox mediators as a function of the pH. (met blue) methylene blue, (duroq) duroquinone, (ind4) indigo tetrasulfonate, (ind3) indigo trisulfonate, (ind2) indigo disulfonate, (14naph) 2-hydroxy-1,4-naphthoquinone, (anth27s) anthraquinone-2,7-disulfonate, (anth2s) anthraquinone-2-sulfonate, (phenosaf) phenosafranine, (safraT) safranine T, (neut red) neutral red, (MeV) methyl viologen. The curves were calculated using equations and parameters reported by Clark, 1972.

To increase confidence in the results, it is important to repeat the titrations using mediators of different chemical structures and various combinations of different redox mediators. As noted above, a wide range of concentrations should also be tested. The same results should be obtained each time, not only with respect to the macroscopic redox potentials determined but also with regard to the shape of the titration curve and its overall absorbance change.

II.2.1.2 Experimental apparatus

The experimental apparatus used for the visible redox titrations is represented in Figure II.6.

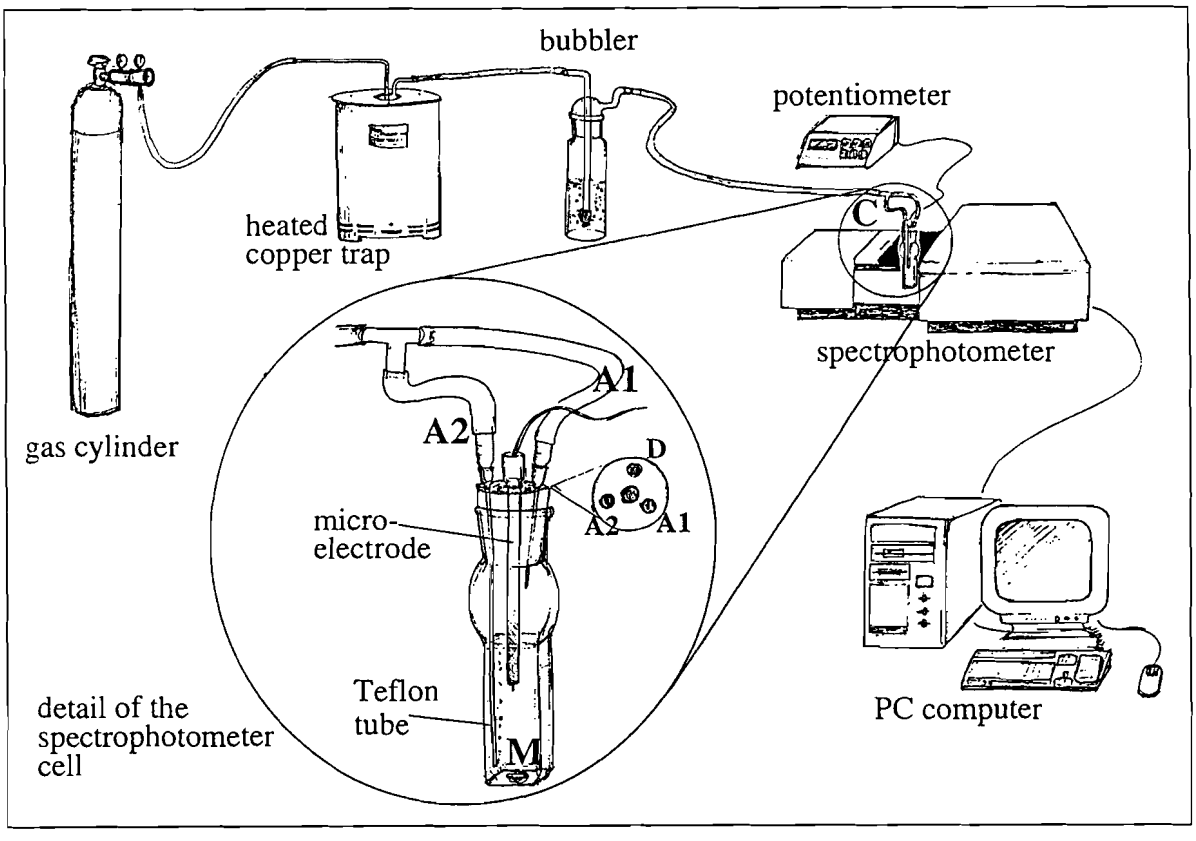

Figure II.6. Experimental apparatus used for the visible redox titrations. A continuous argon flow through the spectrophotometer cell was used to run the visible redox titrations under anaerobic conditions. The gas coming from the cylinder passed through a heated copper trap in order to remove traces of oxygen and then through a bubbler, containing sodium dithionite prepared in NaOH 0.1M, to moisten the gas and reduce sample evaporation during the titration. The redox potential of the solution inside the spectrophotometer cell (C) was measured by a combined microelectrode connected to a potentiometer. The spectra of the protein solution were recorded by a UV-visible spectrophotometer connected to a PC computer to store the data. A detail of the spectrophotometer cell is shown. A1 and A2 are argon entries and D is the argon outlet. Connected to A2 there is a Teflon tube that goes to the bottom of the cell. Care had to be taken in order to avoid interference with the optical path. The gas pressure was regulated such that with both taps opened it flowed only through A1. Dithionite additions were made through D using a 1µl syringe with a needle long enough to reach the solution level. After each dithionite addition, A1 was closed and the gas was forced through A2, bubbling through the solution to achieve fast homogenisation. Continuous magnetic stirring (M) was also used.

The titrations were performed in a quartz cuvette with stirring. The system was kept anaerobic by flushing the cuvette continuously either with argon (grade N46 from Air Liquide) or with nitrogen (grade U from Air Liquide) previously passed through a copper catalyst to remove any residual oxygen and through a bubbler containing an alkaline solution of sodium dithionite. The bubbler was used to maintain a high level of humidity in the gas in order to prevent the evaporation of the sample. The addition of the oxidising or reducing agent to the protein sample was made in steps. At each step, after allowing one or two minutes for equilibration, the solution potential was measured and the visible spectrum recorded. The combined Platinum | Ag /AgCl electrode used to measure the solution potential was calibrated against saturated quinhydrone solutions at pH 4.0 and 7.0 before each experiment. If the difference between the two calibrations was within 7 mV, the mean value was taken, otherwise the electrode was replaced.

II.2.1.2.1 Oxidative titrations of cytochrome c_3 from *Desulfovibrio gigas*.

To start the redox titration from the fully reduced state, a few microliters of a concentrated sodium dithionite solution were added to the ca. 2 μM cytochrome solution. The sample was subsequently oxidised in steps by bubbling nitrogen (grade U from Air Liquide) which contained ca. 5 ppm of oxygen. For each step, the solution potential was measured with a combined Platinum | Ag / AgCl electrode (Ingold) and the visible spectrum was recorded in a Shimadzu UV-260 spectrophotometer with a spectral slit width of 0.5 nm. The redox titrations of Dgc_3 were performed in 50 mM tris/maleate buffer at pHs 5.6 and 8.5 at room temperature. To assure good equilibration between the redox centres and the electrode used to measure the solution potential, the following redox mediators were added to the protein solution, all at ca. 3 μM final concentration: juglone, duroquinone, indigo tetrasulfonate, indigo trisulfonate, indigo disulfonate, 2-hydroxy-1,4-naphthoquinone, anthraquinone-2,7-disulfonate, anthraquinone-2-sulfonate, phenosafranine, safranine T, neutral red, cobalt sepulchrate (Creaser et al., 1982), diquat and methyl viologen. The pH dependence of the midpoint redox potentials of the mediators is presented in Figure II.5. The pH value was always measured at the beginning and the end of the experiments and remained constant throughout the titrations.

II.2.1.3.1 Reductive titrations of cytochrome c_3 from *Desulfovibrio vulgaris*.

Starting from the ca. 3 μM oxidised protein solution, reduction was accomplished in steps by adding each time a few tenths of a microliter of ca. 10 mM degassed sodium dithionite solution. The redox titrations of D*v*c_3 were performed in 50 mM tris/maleate pH 7.0 and 50 mM tris/HCl pH 8.0 buffers at 24-25 °C. A combined Platinum | Ag / AgCl microelectrode from Microelectrodes, Inc. USA, (MI-800-710MOD) was used to measure the solution potential and the spectra were recorded with a spectral slit width of 0.5 nm in a Shimadzu UV-3100 spectrophotometer connected to a PC computer for acquisition of the data. The following redox mediators were added to the solution, to a final concentration of ca. 1 μM except triquat at ca. 0.25 μM: methylene blue, indigo tetrasulfonate, indigo trisulfonate, indigo disulfonate, 2-hydroxy-1,4-naphthoquinone, anthraquinone-2,7-disulfonate, anthraquinone-2-sulfonate, safranine T, neutral red, diquat, methyl viologen and triquat.

II.2.1.3 Data analysis

Since the four haems in cytochrome c_3 have very similar UV-visible spectra, the absorbance measured at a given solution potential reflects the global reduced fraction but provides no information about the redox state of the individual haems. Therefore, from a simple potentiometric titration monitored by UV-visible spectroscopy it is possible to obtain either the four macroscopic midpoint redox potentials of the tetrahaem cytochrome or the four apparent microscopic potentials of the redox centres (see discussion about 'sequential model vs. 'individual model' in section II.1). However, note that it is impossible to determine the absolute microscopic redox potentials from the macroscopic ones because different combinations of midpoint potentials for the individual haems and haem-haem interactions could produce the same macroscopic titration curve.

The four macroscopic potentials can be determined by fitting the equations of the 'sequential model' derived in Appendix A to the experimental curve of the oxidised or reduced fraction as a function of the solution potential.

As noted above, it is necessary to correct the data for the optical interference of the redox mediators because their contribution to the optical density at the α-peak (λ= 552 nm) is not constant throughout the titration (cf. Figure II.4). The correction was made by taking the absorbance at the two isosbestic points near to the α-peak (λ= 542 nm and λ= 560 nm) and

subtracting the mean value from the absorbance of the α-peak. The normalisation of the absorbance values (A_{552}) to give the global reduced fraction was made according to $(A_{552}-A_{552ox})/(A_{552red}-A_{552ox})$, where A_{552red} and A_{552ox} are the absorbance values of the fully reduced and fully oxidised forms, respectively.

In this work, the visible redox titrations were not used for direct determination of the four macroscopic redox potentials but for the calibration of the microscopic parameters determined from the NMR experiments instead. It is shown in section II.3.3 that the macroscopic redox potential for the fully reduced protein (E_I) is independent of the haem-haem interactions and determines the absolute values for the microscopic redox potentials of the four haems. On the other side of the titration curve, the macroscopic redox potential for the fully oxidised protein (E_{IV}), depends both on the absolute microscopic potentials and on the absolute values for the haem-haem interactions. Thus, from a visible redox titration, it is possible to take the two parameters which are necessary to scale the microscopic redox potentials of the four haems and the six haem-haem interactions, whose relative values are determined from redox titrations monitored by NMR.

For the determination of the thermodynamic parameters of Dvc_3, the differences between the observed chemical shifts and the pH-independent shifts of the methyl groups in the fully reduced protein were fitted to thirteen parameters of the model described in section II.3.3 (three relative microscopic midpoint potentials, five relative haem-haem interactions, four redox-Bohr interacting potentials and the ionisation energy of the fully reduced molecule) on the basis of accurate pH readings and experimental errors for each shift which are proportional to the linewidths. The remaining two calibration parameters, necessary to define the absolute values of the redox potentials and the haem-haem interactions, were subsequently obtained from the fitting of the visible titrations. In the case of Dgc_3, the NMR and the visible titration data were simultaneously fitted to the fifteen parameters of the model (cf. section II.3.3) assuming different weights for the two sets of data. The chemical shifts were weighted by the linewidths and a weight corresponding to an error of ± 5 mV was taken for the visible data. The fittings were made using the Marquardt method.

II.3 Modelling of the thermodynamic properties

II.3.1 Modelling each pH value separately

The full complexity of redox and acid/base equilibria of cytochrome c_3 was described above, but until the work published by Santos et al. in 1984a only very simple models, such as the 'sequential model' and the 'individual model', had been applied to the determination of the thermodynamic parameters of this cytochrome. These authors demonstrated the existence of redox interactions in Dgc_3 and determined their values from the analysis of NMR data on the basis of a model for the electron distribution between the four haems including redox interactions. Since the model developed by Santos et al., 1984a comprised only the 16 microstates of the redox equilibria, four microscopic redox potentials and six haem-haem interacting potentials are necessary to fully characterise the redox behaviour of the system at each pH value.

The haem methyl chemical shifts of molecules in intermediate oxidation stages were used for the first time to measure the differences between the redox potentials of the haems within each stage. It should be noted that, since the solution potential inside the NMR tube was not measured, only relative values of the microscopic redox potentials and interactions could be obtained from the chemical shifts. However, measurements of the intensity of the NMR peaks provided the additional information necessary to define the absolute scale for the haem-haem interactions, thus leaving undefined the absolute scale for the redox potentials only.

Table II.2. Relative microscopic redox potentials and haem-haem interacting potentials of Dgc_3 at pH 7.2 and 9.6 (Santos et al., 1984a). According to the definition adopted by these authors positive interactions correspond to positive cooperativity. Subscripts of e_i indicate oxidation order.

relative redox potentials (mV)	pH 7.2	pH 9.6
$(e_2\text{-}e_1)$	35 ±5	51 ±1
$(e_2\text{-}e_3)$	-1 ±8	-5 ±1
$(e_3\text{-}e_4)$	-25 ±8	-75 ±1
haem-haem interactions (mV)		
I_{12}	19 ±5	14 ±5
I_{13}	-26 ±5	-29 ±5
I_{14}	6 ±1	36 ±4
I_{23}	42 ±4	41 ±3
I_{24}	-24 ±5	-31 ±3
I_{34}	-18 ±3	0 ±1

The complete analysis of the redox properties of Dgc_3 at pH 7.2 and 9.6 led to three relative redox potentials and six haem-haem interacting potentials for each pH value (Table II.2). It is apparent from this table that the midpoint redox potentials of some of the haems, as well as their interacting potentials are pH-dependent. The fact that only the redox interactions involving haem IV are significantly affected by the change in pH will be discussed later (section II.3.2.3).

Using the same model, Fan et al., 1990a determined the absolute values of the microscopic redox potentials and haem-haem interactions of Dvc_3 Miyazaki at a single pH value. These authors used the macroscopic redox potentials previously determined through the combined use of NMR and optically transparent thin-layer electrode absorption spectra (Fan et al., 1990b) to define the absolute scale for the redox potentials. The pH-dependence of these parameters was investigated later by Park et al., 1996. Although an acid/base equilibrium between two conformations had already been proposed for the analysis of the thermodynamic properties of Dgc_3 (Coletta et al., 1991) and a model considering redox and redox-Bohr interactions between four haems and one ionisable centre had been proposed for the analysis of the NMR data of the homologous Dvc_3 Hildenborough (Turner, et al., 1994) these authors made no attempt to integrate the pH as a variable of the system. Therefore, not only is the number of parameters of their model larger than necessary but also it does not allow the calculation of the populations of the microstates at pH values other than those used in the NMR experiments. More importantly, the cooperativities associated with the ionisable centre that are essential for the understanding of the role of cytochrome c_3 in the energy transducing mechanism of sulphate reducing bacteria (Louro et al., 1996a and 1997a,b) are not immediately apparent from this modelling strategy.

II.3.2 The A/B model

The work published by Santos et al., 1984a showed that Dgc_3 displays different thermodynamic properties at pH 7.2 and pH 9.6. Since not only the microscopic redox potentials but also the haem-haem interactions where found to be pH-dependent in this study, a model assuming an acid/base equilibrium between two conformations of the cytochrome molecule was proposed to explain this result (Coletta et al., 1991). This model was the first attempt to integrate the pH as a variable of the system together with the solution potential. According to the A/B model each conformation is characterised by four microscopic redox

potentials and six haem-haem interactions, and since an equilibrium constant is necessary to define the acid/base equilibrium between the two conformations, the number of parameters of the model is 21, independently of the number of pH values. It was showed that (Coletta et al., 1991), these parameters are sufficient to characterise the thermodynamic behaviour of Dgc_3 at any solution potential and at any pH value. However, it will be shown later that this number of parameters can still be reduced to fifteen (cf. section II.3.3).

II.3.2.1 The model

As noted above (section II.1), there are sixteen possible microstates involved in the redox processes of a system comprising four redox centres. If the pH is introduced as an additional variable, each one of these microstates becomes involved in an acid/base equilibrium which increases the number of possible microstates to 32. Note that this number of microstates corresponds to the simplest acid/base equilibrium, i.e. that involving only one proton or n equivalent and independent protons. The thermodynamic model developed for the description of this system must be able to define the population of each of the 32 microstates as a function of the parameters of the model and of the solution potential and pH.

Each of the four haems is characterised by a different set of microscopic redox potentials for the acidic and for the basic conformations. These potentials (e_i^A and e_i^B) are defined for the fully reduced molecule which is taken as the reference state. However, due to homotropic cooperativities between the haems, the oxidation of one haem affects the redox potentials of the other haems and it is necessary to define six haem-haem interactions for the protonated form (I_{ij}^A) and another six for the deprotonated one (I_{ij}^B). According to the adopted definition, a positive value for the parameter I_{ij} corresponds to a positive cooperativity. Thus, the relationship between the redox potential of haem i when all the other haems are reduced (e_i) and the redox potential of the same haem when haem j is already oxidised (e_i^j) is given by $I_{ij} = e_i - e_i^j$. This equation shows that the oxidation of haem j facilitates the oxidation of haem i if I_{ij} is positive, since e_i^j is lower than e_i. The same is true for the reduction pathway, since the reduction of haem j facilitates the reduction of haem i, i.e. e_i is higher than e_i^j. A negative value for I_{ij} corresponds to a negative cooperativity and works in the opposite way: the reduction of haem j decreases the tendency of haem i to be reduced and the oxidation of haem j makes it more difficult to oxidise haem i, as would be expected for a simple electrostatic interaction. Note that according to this model the interaction I_{ij} is equal to the interaction $I_{ji} = e_j - e_j^i$ and is independent of the redox state of the other haems.

The remaining parameter, L_0, is the equilibrium constant for the protonation of the fully reduced molecule given by equation 1,

$$L_0 = \frac{[A_0]}{[B_0][H^+]} \qquad (1)$$

where A_0 is the fully reduced protonated species and B_0 is the fully reduced deprotonated one. Note that the pK_a of the fully reduced cytochrome is equal to the logarithm of L_0.

To characterise the thermodynamic behaviour of cytochrome c_3 it is necessary to express the populations of the 32 microstates in terms of the 21 thermodynamic parameters of the model. The relationships between the 32 microstates are establish by 64 Nernst equations and it is possible to express the population of any microstate relative to the population of a microstate taken as the reference state. The fully reduced deprotonated form (B_0) was chosen for the reference state in this model. If the redox potentials (e_i) are expressed as redox constants (β_i) (equation 2a) on the basis of the Nernst equation and the same kind of transformation is used to express the redox interactions (I_{ij}) as (δ_{ij}) (equation 2b) and the solution potential (E) as X (equation 2c) the mathematical expressions that define the populations of the 32 microstates become very simple and intuitive.

$$\beta_i = \exp\left(\frac{-e_i F}{RT}\right) \qquad (2a)$$

$$\delta_{ij} = \exp\left(\frac{I_{ij} F}{RT}\right) \qquad (2b)$$

$$X = \exp\left(\frac{EF}{RT}\right) \qquad (2c)$$

It follows from the Nernst equation that the population of a deprotonated microstate from stage I with haem i oxidised (B_i) is given by equation 3a. Note that β_i^B is the redox constant for the oxidation of haem i in the deprotonated molecule. Since only one haem is oxidised in stage I, there are no haem-haem interactions involved and the term X appears raised to the power of one.

$$[B_i] = [B_0]\beta_i^B X \qquad (3a)$$

The population of a microstate from stage II with haems i and j oxidised (B_{ij}) is given by

equation (3b) where β_i^B and β_j^B are the redox constants for the oxidation of haems i and j and δ_{ij}^B is the redox interaction between the two oxidised haems for the deprotonated (B) conformation. The term *X* appears raised to the power of two because two redox steps mediate the conversion of B_0 into B_{ij}.

$$[B_{ij}] = [B_0]\beta_i^B \beta_j^B \delta_{ij}^B X^2 \qquad (3b)$$

The extrapolation for equations 3c and 3d that give the populations of a microstate from stage III with haems i,j and k oxidised (B_{ijk}) and of a microstate from stage IV with all haems oxidised (B_{ijkl}), respectively, is straightforward.

$$[B_{ijk}] = [B_0]\beta_i^B \beta_j^B \beta_k^B \delta_{ij}^B \delta_{ik}^B \delta_{jk}^B X^3 \qquad (3c)$$

$$[B_{ijkl}] = [B_0]\beta_i^B \beta_j^B \beta_k^B \beta_l^B \delta_{ij}^B \delta_{ik}^B \delta_{il}^B \delta_{jk}^B \delta_{jl}^B \delta_{kl}^B X^4 \qquad (3d)$$

The populations of the protonated microstates relative to the fully reduced protonated species (A_0) are given by equations analogous to 3a-d. Since the equilibrium constant for the protonation of the fully reduced molecule establishes the relationship between A_0, B_0 and the concentration of protons (equation 1), the populations of the protonated microstates from stages I to IV are obtained from equations 4 a-d , respectively.

$$[A_i] = [B_0]L_0[H^+]\beta_i^A X \qquad (4a)$$

$$[A_{ij}] = [B_0]L_0[H^+]\beta_i^A \beta_j^A \delta_{ij}^A X^2 \qquad (4b)$$

$$[A_{ijk}] = [B_0]L_0[H^+]\beta_i^A \beta_j^A \beta_k^A \delta_{ij}^A \delta_{ik}^A \delta_{jk}^A X^3 \qquad (4c)$$

$$[A_{ijkl}] = [B_0]L_0[H^+]\beta_i^A \beta_j^A \beta_k^A \beta_l^A \delta_{ij}^A \delta_{ik}^A \delta_{il}^A \delta_{jk}^A \delta_{jl}^A \delta_{kl}^A X^4 \qquad (4d)$$

Note that the equilibrium constant for the protonation, L, is not constant throughout the oxidation process. In fact, each pair of A and B microstates has a different protonation constant which depends on the haems which are oxidised in that particular microstate. For instance, the protonation constant for the fully oxidised molecule, L_{ijkl}, that establishes the relation between A_{ijkl} and B_{ijkl} is given by equation 5.

$$L_{ijkl} = L_0 \frac{\beta_i^A \beta_j^A \beta_k^A \beta_l^A \delta_{ij}^A \delta_{ik}^A \delta_{il}^A \delta_{jk}^A \delta_{jl}^A \delta_{kl}^A}{\beta_i^B \beta_j^B \beta_k^B \beta_l^B \delta_{ij}^B \delta_{ik}^B \delta_{il}^B \delta_{jk}^B \delta_{jl}^B \delta_{kl}^B} \qquad (5)$$

It is assumed that the sum of all populations is equal to 1 because the total concentration of cytochrome is constant. Therefore, for a given set of thermodynamic parameters, the normalised populations of the 32 microstates can be calculated from equations 3 and 4 for any solution potential and pH. It will be shown in the next section that the A/B model is well able to describe the thermodynamic properties of cytochrome c_3.

II.3.2.2 Application of the model

The application of the A/B model described above to the simulation of NMR and visible titration data led to a set of parameters that characterise the thermodynamic properties of cytochrome c_3 from *D. gigas*. The model is able to account for the pH dependence of the chemical shifts of the haem methyl groups during a reoxidation process monitored by NMR, and also for the pH dependence of the redox titrations followed by UV-visible spectroscopy.

Because of the fast intramolecular electron exchange (Santos et al., 1984a), the observed chemical shift of a haem methyl group in each stage depends on the ratio between the populations of the microstates which have that particular haem oxidised and the sum of the populations of all microstates of that stage. The observed chemical shift of a methyl group of haem i (δ_i^{stage}) in stages I to IV can be calculated from equations 6a-d, respectively.

$$\delta_i^{I} = \Delta\delta_{iA}\frac{[A_i]}{\sum_{stageI} P_i} + \Delta\delta_{iB}\frac{[B_i]}{\sum_{stageI} P_i} + \delta_i^0 \qquad (6a)$$

$$\delta_i^{II} = \Delta\delta_{iA}\frac{[A_{ij}]+[A_{ik}]+[A_{il}]}{\sum_{stageII} P_{ij}} + \Delta\delta_{iB}\frac{[B_{ij}]+[B_{ik}]+[B_{il}]}{\sum_{stageII} P_{ij}} + \delta_i^0 \qquad (6b)$$

$$\delta_i^{III} = \Delta\delta_{iA}\frac{[A_{ijk}]+[A_{ijl}]+[A_{ikl}]}{\sum_{stageIII} P_{ijk}} + \Delta\delta_{iB}\frac{[B_{ijk}]+[B_{ijl}]+[B_{ikl}]}{\sum_{stageIII} P_{ijk}} + \delta_i^0 \qquad (6c)$$

$$\delta_i^{IV} = \Delta\delta_{iA}\frac{[A_{ijkl}]}{\sum_{stageIV} P_{ijkl}} + \Delta\delta_{iB}\frac{[B_{ijkl}]}{\sum_{stageIV} P_{ijkl}} + \delta_i^0 \qquad (6d)$$

According to the notation adopted here, [A] and [B] refer to the populations of protonated and deprotonated microstates, respectively. For each microstate the subscripts indicate the haems

which are oxidised, their number being equal to the redox stage. The sum $\sum_{stage} P$ refers to the populations of all microstates, protonated and deprotonated, that belong to the stage indicated below the sum. $\Delta\delta_{iA}$ is the difference between the chemical shift of the haem methyl in the fully oxidised acidic form (δ_{iA}^{IV}) and in the reduced form (δ_i^0) and $\Delta\delta_{iB}$ is the equivalent difference for the basic form. It is assumed that the chemical shift of the haem methyl in the fully reduced form (δ_i^0) is pH independent.

Note that the population ratios in equations 6a-d are independent of the solution potential. The term X cancels because the ratios are defined between populations belonging to the same stage. The immediate consequence of this fact is that it is impossible to obtain absolute values for the redox potentials and redox interactions from the chemical shifts alone, i.e., without an independent measurement of the solution potential.

Equations 6 a-d were used to simulate the pH dependence of the chemical shift of one methyl group from each haem in different redox stages. The parameters of the model were obtained from the fitting of the simulated curves to NMR data points (Santos, 1984 and Santos et al., 1984a). To determine the absolute values for the microscopic redox potentials, two redox titrations monitored by UV-visible spectroscopy at pHs 7.2 and 9.6 were compared with two titration curves simulated with the relative microscopic redox potentials and the haem-haem interactions determined by Santos et al., 1984a. It was possible to define the redox potential scale of the simulated titration curve from this comparison and, therefore, obtain absolute values for the microscopic redox potentials.

To simulate the titration curves, the reduced fraction was calculated from the thermodynamic parameters and plotted as a function of the solution potential for each pH value. The reduced fraction is given by the sum of all populations, each one weighted by the number of reduced haems, divided by the sum of all populations multiplied by 4 (equation 7).

$$\text{reduced fraction} = \frac{4\sum_{stage0} P_0 + 3\sum_{stageI} P_i + 2\sum_{stageII} P_{ij} + \sum_{stageIII} P_{ijk}}{4\left(\sum_{stage0} P_0 + \sum_{stageI} P_i + \sum_{stageII} P_{ij} + \sum_{stageIII} P_{ijk} + \sum_{stageIV} P_{ijkl}\right)} \qquad (7)$$

The expression of the reduced fraction as a function of the solution potential, pH and the thermodynamic parameters of the model is given by equation 8, where the capital Ks are condensed parameters (cf. equations 9a-d) defined for the stages indicated as subscripts of the

protonated (superscript A) or deprotonated (superscript B) molecule.

$$F_{red} = \frac{L_0[H^+]\left(4 + 3K_I^A X + 2K_{II}^A X^2 + K_{III}^A X^3\right) + \left(4 + 3K_I^B X + 2K_{II}^B X^2 + K_{III}^B X^3\right)}{4\left(L_0[H^+]\left(1 + K_I^A X + K_{II}^A X^2 + K_{III}^A X^3 + K_{IV}^A X^4\right) + \left(1 + K_I^B X + K_{II}^B X^2 + K_{III}^B X^3 + K_{IV}^B X^4\right)\right)} \quad (8)$$

The definition of the condensed parameters for the basic form is equivalent to that of the acidic one given by equations 9a-d.

$$K_I^A = \sum_i^4 \beta_i^A \quad (9a)$$

$$K_{II}^A = \sum_{ij}^6 \beta_i^A \beta_j^A \delta_{ij}^A \quad (9b)$$

$$K_{III}^A = \sum_{ijk}^4 \beta_i^A \beta_j^A \beta_k^A \delta_{ij}^A \delta_{ik}^A \delta_{jk}^A \quad (9c)$$

$$K_{IV}^A = \beta_i^A \beta_j^A \beta_k^A \beta_l^A \delta_{ij}^A \delta_{ik}^A \delta_{il}^A \delta_{jk}^A \delta_{jl}^A \delta_{kl}^A \quad (9d)$$

The thermodynamic parameters that characterise the cytochrome c_3 isolated from *D. gigas* in the framework of the A/B model are presented in Table II.3.

Table II.3. Thermodynamic parameters for the A/B model. The e_i values are the absolute values for the redox potentials of the haems in mV, defined for the fully reduced molecule. The I_{ij} values are the absolute haem-haem interacting potentials, also in mV. According to our definition, positive I_{ij} correspond to positive cooperativities and negative I_{ij} correspond to negative cooperativities. L_0 is the equilibrium constant for the protonation of the fully reduced molecule. Note that the logarithm of L_0 is equal to the pK_a of the fully reduced state.

Redox potentials (e_i) and haem-haem interactions (I_{ij}) in mV	**A** Acidic conformation	**B** Basic conformation
e_1	-290	-340
e_2	-255	-285
e_3	-255	-280
e_4	-240	-205
I_{12}	+10	+10
I_{13}	-30	-30
I_{14}	-10	+40
I_{23}	+40	+40
I_{24}	-10	-30
I_{34}	-40	-10
$L_0 = 3\times10^8$		

These parameters were obtained from the application of the model to the NMR data reported by Santos et al., 1984a together with visible titration data. The microscopic redox potentials and the haem-haem interacting potentials were determined by grid search, starting from the values determined by Santos et al., 1984a and taking into consideration that, although the parameters for the basic conformation might be similar to those reported in that study for pH 9.6, the parameters for the acid conformation could be reasonably far from those determined for pH 7.2. This is because virtually all cytochrome molecules are in the B form at pH 9.6, whereas both conformations are populated at pH 7.2, as is apparent from the pH dependence of the chemical shifts.

The simulation of the pH dependence of the chemical shifts of four haem methyl groups, one for each haem, in different redox stages, is presented in Figure II.7. It is apparent from this figure that the A/B model is able to describe the general position and pH dependence of the chemical shifts of the haem methyl groups in different stages, which depend on the population ratios determined by the relative redox potentials and haem-haem interactions.

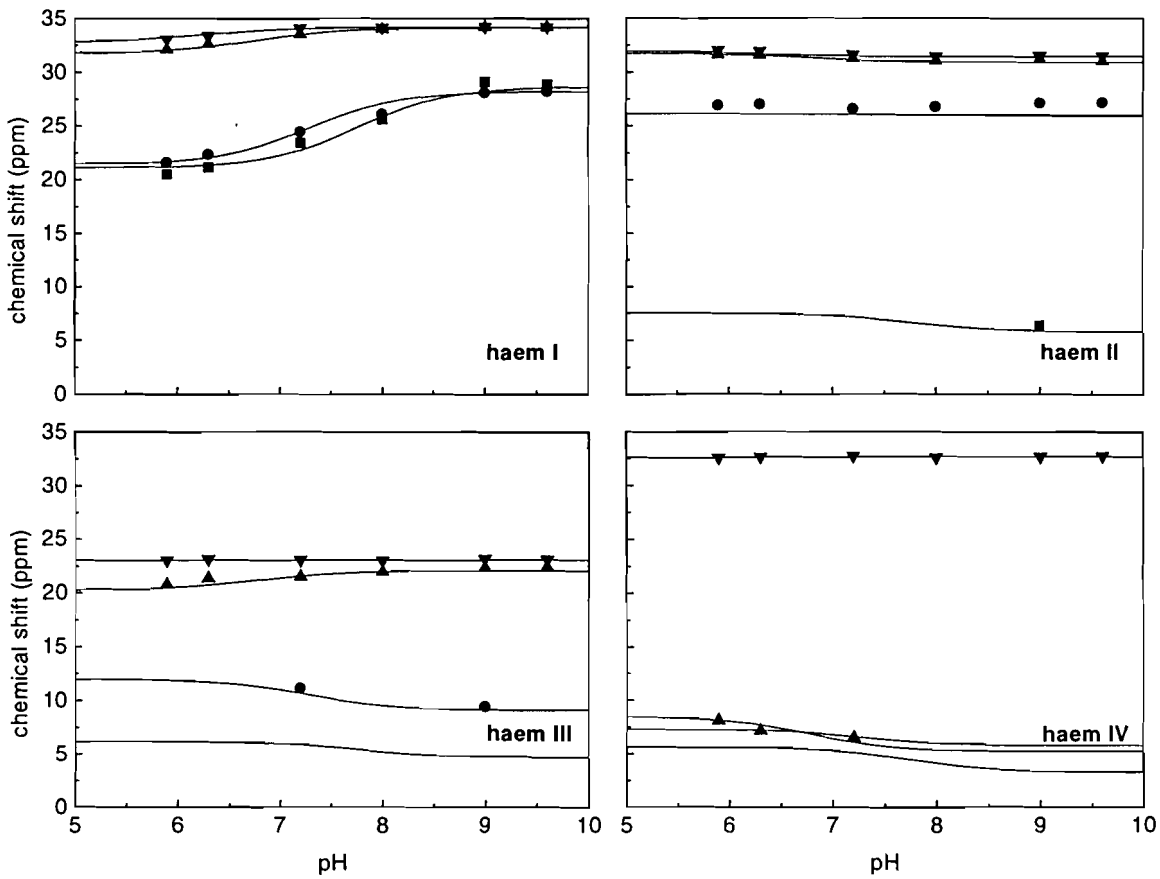

Figure II.7. pH dependence of the ^{1}H NMR chemical shifts of one haem methyl from each of the four haems of Dgc_3 in different oxidation stages. The solid lines correspond to the pH dependence of the chemical shifts calculated according to the A/B model, for the thermodynamic parameters reported in table II.3. NMR data (Santos et al., 1984a) are represented by symbols, each symbol corresponding to a different oxidation stage: (■) stage I; (●) stage II; (▲) stage III; (▼) stage IV. The data points correspond to the following haem methyls: M18^1 for haem I, M18^1 for haem II, M12^1 for haem III and M18^1 for haem IV, according to the assignments reported by Piçarra-Pereira et al., 1993 and Louro et al., 1998a. The NMR data were acquired at 0 °C.

All simulations were made assuming that either a single proton is involved in the acid/base equilibrium or that all protonating groups are equivalent and behave independently. This assumption is supported by the agreement between the simulated curves and the NMR data points in Figure II.7 and also in Figure II.8, where the chemical shifts for stage IV of another two haem methyl groups is plotted as a function of the pH. Note that the pK_a values for the fully oxidised protein (pK_a^{IV}) and for the intermediate redox stages (pK_a^{III}, pK_a^{II} and pK_a^{I}), which are apparent from the pH dependence of the chemical shifts of the different stages in Figures II.7 and II.8, are not independent parameters of the model, but result from the interplay of these parameters according to equation 10.

$$pK_a^{stage} = \log\left(L_0 \frac{K^A_{stage}}{K^B_{stage}} \right) \qquad (10)$$

K^A_{stage} are the condensed parameters of the stages defined by equations 9a-d and K^B_{stage} are the equivalent condensed parameters for the basic form of the cytochrome.

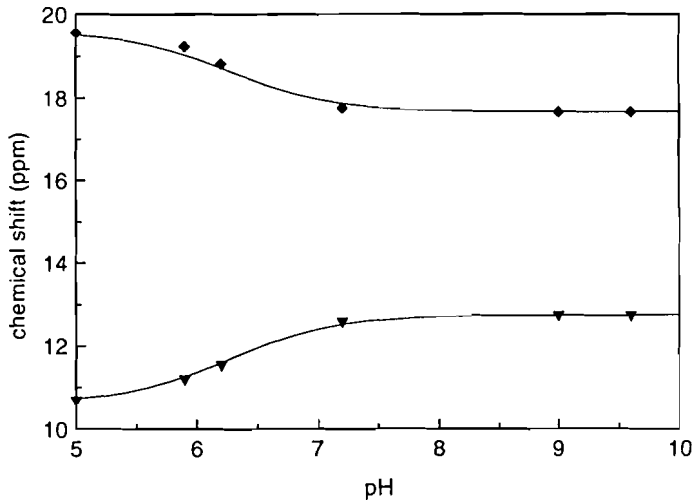

Figure II.8. pH dependence of the chemical shifts of two haem methyls of Dgc_3 in stage IV. The solid lines correspond to the pH dependence calculated using the A/B model, and the NMR data points (Santos, 1984) are from methyls $M2^1$ from haem I (◆) and $M7^1$ from haem I (▼) according to the assignments reported by Louro et al., 1998a.

The comparison between experimental spectrophotometric redox titrations performed at pH 7.2 and 9.6 and theoretical titration curves calculated either from the relative redox potentials and interacting potentials for pHs 7.2 and 9.6 reported by Santos et al., 1984a or from the thermodynamic parameters of the A/B model is shown in Figure II.9.

The shape of the curves calculated from the relative redox potentials is defined because the interacting potentials are absolute, but the reference value for the potential scale is unknown.

The determination of absolute values for the microscopic redox potentials depends upon the definition of this scale, which is obtained from the visible titration curves. It should be noted that, although reasonably good agreement is obtained between the calculated curves, direct comparison of the experimental visible titration data with the calculated curves shows some discrepancies for the lower reduced fractions, which is more noticeable for the curve at pH 9.6.

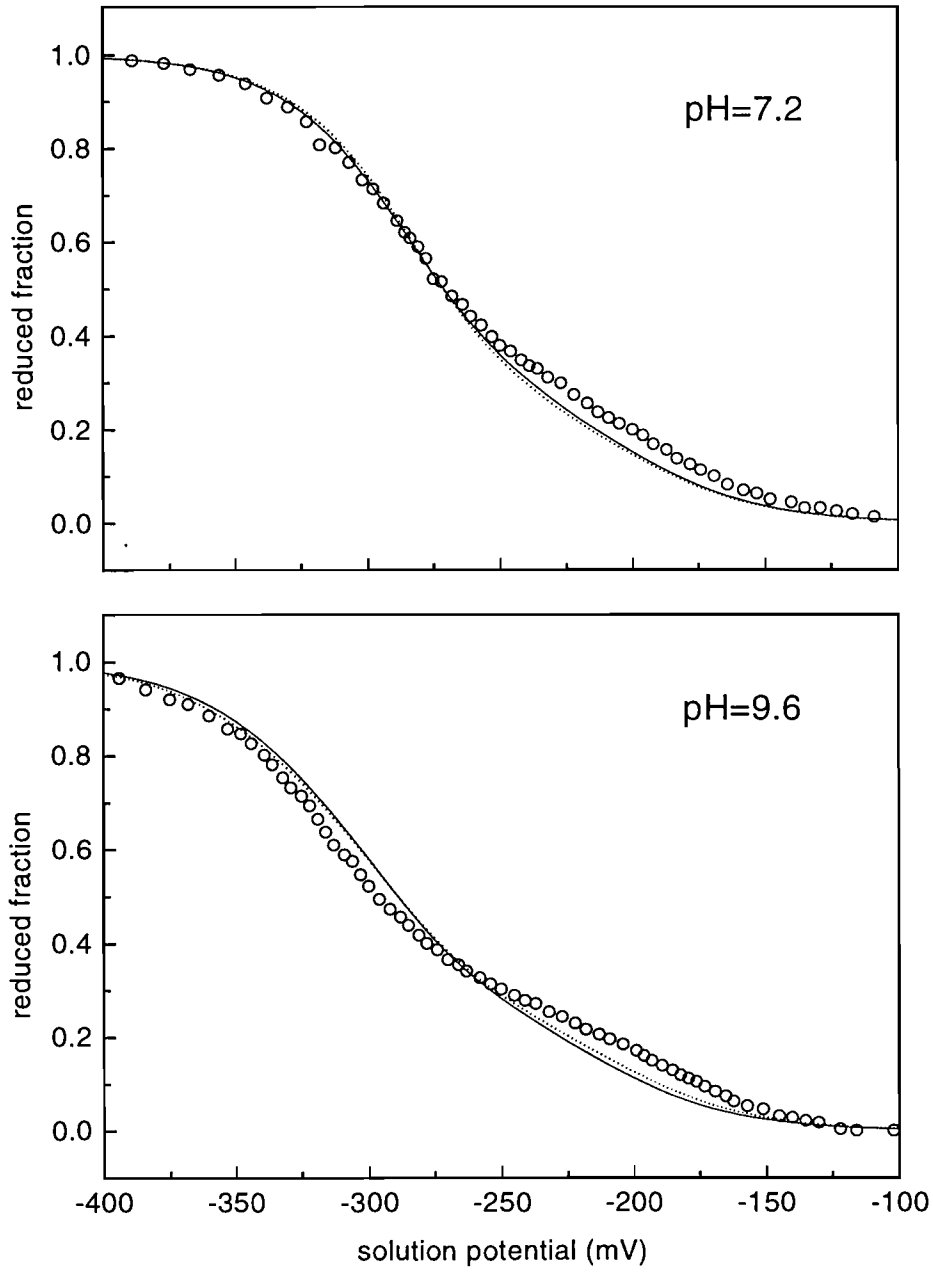

Figure II.9. Comparison between simulated and experimental visible redox titrations of Dgc_3. Experimental data points are represented by circles. Solid line: titration curve calculated from the redox potentials and interactions reported by Santos et al., 1984a after calibration. Dotted line: titration curve calculated using the A/B model with the parameters reported in table II.3. The adjustment between the calculated and the experimental titration curves is poor, especially for percentages of reduction below 25%.

II.3.2.3 Discussion

It is apparent from Figures II.7 and II.8 that the simulation of the pH dependence of the haem methyl chemical shifts, which includes data points at pH values other than 7.2 and 9.6, is good, indicating that the A/B model is a possible approach to the study of the thermodynamic properties of cytochrome c_3. The theoretical curves calculated on the basis of the A/B model are reasonably similar to the titration curves calculated from the relative redox potentials an haem-haem interactions determined by Santos et al., 1984a (cf. Figure II.9). This is because the determination of the thermodynamic parameters for the A/B model was made by a limited grid search around the values previously reported by these authors. However, it is apparent from Figure II.9 that the adjustment between the calculated curves and the experimental visible titrations is very poor, indicating that the theoretical modelling is not yet fully satisfactory for the simulation of all experimental data. Note that since the larger discrepancies between the experimental and the simulated titration curves are observed in the high potential region, they are probably related with the titration of haem IV. Possible explanations for the fact are, inadequacy of the model, poor optimisation of the parameters, or even incompatibility between the NMR and the visible data, which were acquired under different experimental conditions. Whereas the NMR experiments were performed at 0 °C and with mM concentrations of cytochrome, the visible titrations were performed at 25 °C and with μM concentrations of cytochrome.

A recent study of the temperature dependence of the thermodynamic parameters of Dgc_3 (Louro et al., 1998b) showed that the effect of temperature on the absolute values of the redox potentials and haem-haem interacting potentials in the temperature range from 4 to 25 °C is indeed non-negligible. However, it can be shown that the more accentuated shoulder observed around 0.25 reduced fraction in the experimental titration curve obtained at 25 °C is also present in the experimental curve obtained at 4 °C. Therefore, the two experimental titration curves acquired at different temperatures display a similar shape, which is different from the shape of the curve calculated on the basis of the thermodynamic parameters of the A/B model. This indicates that, although there is an effect of the temperature on the thermodynamic parameters, this effect is not responsible for the mismatch observed between the calculated and the experimental titration curves of Figure II.9.

Although the haem methyl chemical shifts depend on the relative values of the haem-haem interacting potentials, they are not sensitive to their absolute values. However, this is not the case for the potentiometric titrations monitored by visible spectroscopy because they are

sensitive to the overall cooperativities of the system. Larger positive cooperativities generate steeper titration curves, whereas larger negative cooperativities decrease the slope of the titration curves relative to the slope of the curve with zero cooperativity (cf. equations 18a-d of section II.3.3). Thus, a good simulation of the NMR data together with an inferior simulation of the visible titration data could be caused by a poor optimisation of the absolute values of the haem-haem interacting potentials, especially those involving haem IV. Santos, 1984, determined the absolute values of these interactions on the basis of measurements of the intensity of the NMR peaks, which are usually less precise than chemical shifts. A different set of values was obtained for pH 7.2 and 9.6 (see Table II.2) which suggested the involvement of a pH linked conformational change, the basis of the A/B model. The application of this model to the same NMR data and to visible redox titrations led to two sets of haem-haem interactions, one for the protonated conformation and another for the deprotonated one, in which only the interactions involving haem IV changed from conformation A to conformation B. At that time this was interpreted as the result of a significant conformational change affecting mostly the relationship between haem IV and the other haems in the molecule (Coletta et al., 1991). However, it will be shown later that it is possible to simulate an extended NMR data set with pH independent haem-haem interactions (cf. section II.3.3) if the redox-Bohr interactions of each haem are more precisely evaluated. In fact, the haem-haem interactions involving haem IV, as well as the absolute value of its redox potential, are not well defined in Dgc_3 because a relatively large gap separates the redox potential of this haem from the redox potentials of the other haems. This indeterminacy led to the different sets of haem-haem interactions which, together with the small NMR data set, the large number of parameters of this model and the fitting by grid search around the previously published redox potentials and interactions, disguised the correlation between the haem redox potentials and their interactions. This discussion also showed that, since the haem-haem interactions are not necessarily pH dependent, it is possible to devise a model free from the assumption of pH-linked conformational changes and with fewer parameters. One immediate consequence is the better definition of the thermodynamic parameters of the system, both in terms of their values and of their physical significance, because a true separation between haem-haem and redox-Bohr interactions is achieved.

It should be noted that, although involving a larger number of parameters than necessary, the A/B model was important in terms of the evolution of the thermodynamic modelling of these complex systems. The mathematical description of the pH dependence of the redox potentials (redox-Bohr effect) had already been applied to monohaem cytochromes (Moore et al., 1980)

but it was the first time that the integration of both pH and solution potential had been attempted in the complex modelling of the thermodynamic properties of a multihaem cytochrome. Moreover, the existence of a coupling between the reduction process and protonation of the molecule and the positive cooperativity associated with the B to A transition upon reduction became apparent from the analysis of the thermodynamic properties of Dgc_3 in the framework of the A/B model (Coletta et al., 1991). This first model was also important for the analysis of the kinetic data with sodium dithionite (Catarino et al., 1991).

II.3.3 Model of five interacting centres

The assumption underlying the previous model was that the protein should undergo a pH-linked change in conformation. Each conformation was characterised by a different set of redox potentials and haem-haem interactions, which means that the pH dependence of the thermodynamic behaviour was necessarily correlated with different conformations of the cytochrome molecule. In this section, it will be shown that it is not necessary to invoke any change in conformation in order to explain the pH dependence of the NMR spectra and also of the visible titration data.

This model involves only two-centre interactions among the four haems and an acid/base centre, so that the pH dependence is attributed solely to the interactions between each of the four haems and the protonating centre. Note that the number of microstates involved in the process is the same as that in the previous model: each of the four haems may be oxidised or reduced, giving 16 microstates, and the acid/base group may be protonated or deprotonated for each of these microstates, leading to a total of 32 possible microstates. However, the number of thermodynamic parameters is reduced from 21 in the A/B model to 15 in the model of five interacting centres: four redox potentials, six haem-haem interactions, four haem-proton interactions (redox-Bohr interactions) and the pK_a of the reference state.

The pH dependence of the paramagnetic NMR shifts of four haem methyl groups, chosen on the basis of being situated far enough from the remaining haems for extrinsic paramagnetic shifts to be negligible, in each of the four oxidation stages is analysed in the framework of the model of five interacting centres. In order to provide a stringent test for the simpler model, the NMR data set has been extended considerably by collecting further data at low temperature and new data at 25 °C. Since the aim of this section is the discussion of the modelling strategy and not the study of the temperature dependence of the thermodynamic parameters, only the

data at 25 °C will be presented here, in order to obtain the thermodynamic parameters of Dgc_3 needed for the analysis of the kinetic data (chapter III). Data from Dvc_3 (Hildenborough) are also presented and analysed to demonstrate the broader applicability of the model to the c_3 family.

II.3.3.1 The model

The thermodynamic properties of a system comprising four haems and an acid/base centre will be determined completely by the standard free energies of each of the 32 microstates, together with the solution potential and the pH. It is convenient to express these energies as sums of other terms which are the intrinsic parameters of the five independent centres plus the parameters corresponding to the interactions defined between the five centres. The numbers of terms of each type are given by the row 1:5:10:10:5:1 from Pascal's triangle in which the first single term is the energy of the reference state. The next group contains five terms that correspond to the energies of the five independent centres and are therefore equivalent to the redox potentials of the four haems plus the pK_a of the acid/base centre, all of them defined for the fully reduced and protonated molecule which has been taken as the reference state. Then there are the energies of the ten possible interactions defined between two centres: six haem-haem plus four haem-proton (redox-Bohr) interacting energies. The second group of ten terms corresponds to the three-site interactions, i.e. four interaction energies involving three haems plus six interacting energies involving two haems and the proton. Note that, out of this second group, the six interacting energies defined between any two haems and the proton are equivalent to the assumption of pH dependent haem-haem interacting potentials considered in the A/B model. Then there are five possible four-centre interaction energies and the last one is the interaction energy between the five centres. Thus, the complete thermodynamic description of the system involves a maximum of 32 energetic parameters, which are constant and independent of the solution potential or pH, but it is impossible to define all 32 parameters on the basis of the present data sets.

It is apparent from Figures II.10 and II.12 (see below), where the chemical shifts of four haem methyl groups from Dgc_3 and from Dvc_3 are represented as a function of the pH, that the five individual energy parameters are insufficient to describe the behaviour observed. The existence of a redox-Bohr effect is obvious from the curves because each redox stage displays a different pK_a, with values increasing from stage IV to stage I. The shifts of the fully

oxidised molecule (stage IV) are only weakly pH dependent, showing that the ionisation of the acid/base centre does not affect the pattern of electron delocalisation significantly. Therefore, the larger differences in chemical shifts observed for the intermediate oxidation stages are, instead, the result of changes in the relative populations of the haems upon protonation or deprotonation of the acid/base centre. Thus, to account for these effects it is necessary to invoke haem-proton interactions.

The effect of haem-haem interactions is not as obvious from the curves as the effect of redox-Bohr interactions. But for instance, the methyl of haem III of Dvc_3 has a smaller paramagnetic shift in stage II than it has in stage I, at neutral and high pH. In order to explain an increase in the reduced fraction of a certain haem while the whole molecule goes up one step in oxidation, it is necessary to introduce haem-haem interacting potentials. Although not as clear as in Dvc_3, a similar situation is observed in Dgc_3 with the methyl from haem I in stages I and II at high pH. Also note that the existence of redox interactions between the haems in Dgc_3 is well known since the work published by Santos et al., 1984a.

Since the qualitative features of the curves in Figures II.10 and II.12 require the introduction of two-site interactions, the interaction terms involving more than two centres will be neglected as a first approach to the problem. Since the energy of the reference state is arbitrary, the 5 energetic terms of the independent centres plus the 10 two-centre interactions lead to a total of 15 parameters.

The energy of each of the 32 microstates relative to the fully reduced and protonated molecule is given by a simple sum of the relevant energetic parameters plus a term $-SFE$ to account for the effect of the solution potential E in oxidation stage S, and a term for the proton chemical potential, $-2.3RT$pH, added for the deprotonated microstates. The energies of the protonated microstates (A), one for each redox stage, are given by equations 11a-d and the energies of the corresponding deprotonated microstates (B) are given by equations 12a-d. The energy of each microstate is represented by a capital G with the haems which are oxidised in that particular microstate indicated as subscripts. Note that the number of subscripts of G is equal to the number of the stage to which that microstate belongs.

Protonated microstates:

Stage I $$G_i^A = g_i - FE \qquad (11a)$$

Stage II $$G_{ij}^A = g_i + g_j + g_{ij} - 2FE \qquad (11b)$$

Stage III $$G^{A}_{ijk} = g_i + g_j + g_k + g_{ij} + g_{ik} + g_{jk} - 3FE \quad (11c)$$

Stage IV $$G^{A}_{ijkl} = g_i + g_j + g_k + g_l + g_{ij} + g_{ik} + g_{il} + g_{jk} + g_{jl} + g_{kl} - 4FE \quad (11d)$$

Deprotonated microstates:

Stage I $$G^{B}_{i} = G^{A}_{i} + g_H + g_{iH} - 2.3RT\,\mathrm{pH} \quad (12a)$$

Stage II $$G^{B}_{ij} = G^{A}_{ij} + g_H + g_{iH} + g_{jH} - 2.3RT\,\mathrm{pH} \quad (12b)$$

Stage III $$G^{B}_{ijk} = G^{A}_{ijk} + g_H + g_{iH} + g_{jH} + g_{kH} - 2.3RT\,\mathrm{pH} \quad (12c)$$

Stage IV $$G^{B}_{ijkl} = G^{A}_{ijkl} + g_H + g_{iH} + g_{jH} + g_{kH} + g_{lH} - 2.3RT\,\mathrm{pH} \quad (12d)$$

In these equations, g_i, g_j, g_k and g_l are the redox energies of the individual haems, which are proportional to the respective redox potentials; g_H is the ionisation energy of the fully reduced protein, which is related to the pK_a of the reference state through $pK_a^{red} = g_H/(2.3RT)$; the energetic parameters that correspond to the two-centre interactions are the haem-haem interacting energies, g_{ij}, g_{ik}, g_{il}, g_{jk}, g_{jl}, g_{kl}, and the redox-Bohr interacting energies g_{iH}, g_{jH}, g_{kH}, g_{lH}. Note that the energetic terms related to the ionising group appear only in the deprotonated microstates because the reference state is protonated. According to the definition adopted in this model, positive cooperativities correspond to negative interacting energies. This is easily understood considering that the addition of negative terms decreases the overall energy of the microstates, which leads to an increase of their relative populations.

After expressing the energies of the 32 microstates in terms of the 15 parameters of the model, the populations of these microstates relative to the fully reduced protonated microstate, $[A_0]$, are obtained from the Boltzmann distribution. For example, the relative population of a protonated microstate from stage III with haems ijk oxidised, $[A_{ijk}]/[A_0]$, and the relative population of the corresponding deprotonated microstate, $[B_{ijk}]/[A_0]$, are given by equations 13a and 13b, respectively.

$$\frac{[A_{ijk}]}{[A_0]} = \exp\left(\frac{-G^{A}_{ijk}}{RT}\right) \quad (13a)$$

$$\frac{[B_{ijk}]}{[A_0]} = \exp\left(\frac{-G^{B}_{ijk}}{RT}\right) \qquad (13b)$$

Since the paramagnetic shifts of each haem methyl in the fully oxidised and in the fully reduced protein are known for the protonated and the deprotonated molecule, the chemical shifts for the intermediate oxidation stages can be calculated from the ratios of the relevant relative populations using equations 6a-d.

Note that the redox-Bohr energies, g_{iH}, and the ionisation energy of the fully reduced molecule, g_H, do not need calibration because the pH was accurately measured inside the NMR tube. The macroscopic pK_as of the stages depend upon the absolute values of the energy terms related to the ionising centre (equations 14a-e), and since these pK_as are apparent from the experimental curves (cf. Figures II. 10 and II.12) the parameters g_H and g_{iH} that result from the fitting of the NMR data are already absolute.

Stage 0 $$K_a^0 = \exp\left(\frac{-g_H}{RT}\right) \qquad (14a)$$

Stage I $$K_a^I = \frac{\sum_{stageI}[A_i]\exp\left[\frac{-(g_H + g_{iH})}{RT}\right]}{\sum_{stageI}[A_i]} \qquad (14b)$$

Stage II $$K_a^{II} = \frac{\sum_{stageII}[A_{ij}]\exp\left[\frac{-(g_H + g_{iH} + g_{jH})}{RT}\right]}{\sum_{stageII}[A_{ij}]} \qquad (14c)$$

Stage III $$K_a^{III} = \frac{\sum_{stageIII}[A_{ijk}]\exp\left[\frac{-(g_H + g_{iH} + g_{jH} + g_{kH})}{RT}\right]}{\sum_{stageIII}[A_{ijk}]} \qquad (14d)$$

Stage IV $$K_a^{IV} = \exp\left[\frac{-(g_H + g_{iH} + g_{jH} + g_{kH} + g_{lH})}{RT}\right] \qquad (14e)$$

However, because it is impossible to measure accurately the solution potential inside the NMR tube in the absence of redox mediators, only relative values of the energies could be

obtained from the NMR data. Redox titrations monitored by UV-visible spectroscopy were used to calibrate both the redox energies and the haem-haem interacting energies through the addition of Δe to all g_i and of ΔI to all g_{ij}. It can be demonstrated that the final adjustment of the absolute values of the reference energies has a purely linear effect on all of the thermodynamic parameters of the model. The effect of Δe and ΔI on the macroscopic redox potentials is particularly interesting because these are the parameters determined from the visible redox titrations. Considering a change in the base value of the microscopic redox energies, Δe, and a change in the base value of the haem-haem interacting energies, ΔI, the energies of the microstates after calibration G', are related to G, the corresponding energies before the calibration, through equations 15a-d.

Stage I $$G_i' = G_i + \Delta e \qquad (15a)$$

Stage II $$G_{ij}' = G_{ij} + 2\Delta e + \Delta I \qquad (15b)$$

Stage III $$G_{ijk}' = G_{ijk} + 3\Delta e + 3\Delta I \qquad (15c)$$

Stage IV $$G_{ijkl}' = G_{ijkl} + 4\Delta e + 6\Delta I \qquad (15d)$$

The superscript indicating the protonation state of the microstate was not included because these equations are valid for both cases. The change in the populations of the microstates is obtained from the application of the Boltzmann equation. Since the term which includes the alteration of the base values is the same for all microstates belonging to the same stage, the change in the sum over all the populations of a stage is given by equations 16a-d. Note that it is because these terms cancel in the population ratios of equations 6a-d that the chemical shifts do not depend on the calibration terms Δe and ΔI, and a complementary experimental technique is needed in order to define the absolute values of the redox thermodynamic parameters.

Stage I $$\sum_{stageI} P_i' = \exp\left(\frac{-\Delta e}{RT}\right) \sum_{stageI} P_i \qquad (16a)$$

Stage II $$\sum_{stageII} P_{ij}' = \exp\left[\frac{-(2\Delta e + \Delta I)}{RT}\right] \sum_{stageII} P_{ij} \qquad (16b)$$

Stage III $$\sum_{stageIII} P'_{ijk} = \exp\left[\frac{-(3\Delta e + 3\Delta I)}{RT}\right] \sum_{stageIII} P_{ijk} \quad (16c)$$

Stage IV $$\sum_{stageIV} P'_{ijkl} = \exp\left[\frac{-(4\Delta e + 6\Delta I)}{RT}\right] \sum_{stageIV} P_{ijkl} \quad (16d)$$

The macroscopic redox potential E_S for the equilibrium between stages S-1 and S is the solution potential E at which $\sum_{stageS-1} P_{S-1}$, the sum over all microstates of stage S-1, is equal to $\sum_{stageS} P_S$, the sum over all microstates of stage S. Therefore, according to the Nernst equation,

$$E_S = E - \frac{RT}{F} \ln \frac{\sum_{stageS} P_S}{\sum_{stageS-1} P_{S-1}} \quad (17)$$

Substitution of equations 16a-d in equation 17 lead to equations 18a-d that express the relationship between the macroscopic redox potentials and the calibration terms, Δe and ΔI.

$$E'_I = E_I + \frac{\Delta e}{F} \quad (18a)$$

$$E'_{II} = E_{II} + \frac{\Delta e + \Delta I}{F} \quad (18b)$$

$$E'_{III} = E_{III} + \frac{\Delta e + 2\Delta I}{F} \quad (18c)$$

$$E'_{IV} = E_{IV} + \frac{\Delta e + 3\Delta I}{F} \quad (18d)$$

The macroscopic redox potential of the first oxidation step, E_I, depends solely on the calibration of the redox energies and, therefore, determines the absolute values for the microscopic redox potentials of the four haems through the value of Δe. The calibration for the haem-haem interactions can be obtained from the macroscopic redox potential of the last oxidation step, E_{IV}, which depends on Δe and on three times ΔI.

Equations 18a-d show that the dependence on Δe is the same for all macroscopic redox potentials, whereas the dependence on ΔI increases from the macroscopic redox potential of the first oxidation step to the last one. As mentioned before, Δe defines the position of the

titration curve relative to the redox potential scale whereas ΔI defines the shape of the titration curve. Positive ΔI values result in broader titration curves, characteristic of systems with negative cooperativities, and negative ΔI values result in steeper titration curves that correspond to higher positive cooperativities.

II.3.3.2 Application of the model

To demonstrate that the model of five interacting centres with 15 parameters can describe the thermodynamic properties of cytochrome c_3 molecules isolated from different sources, the simulation of NMR and visible data from Dvc_3 (Hildenborough) (Turner et al., 1994 and 1996) and Dgc_3 (Louro et al., 1998b) will be shown in this section. Recently, the model has also been applied to Dvc_3 (Miyazaki F) (Salgueiro et al., 1997b). By taking advantage of the simulation of extrinsic shifts (Salgueiro et al., 1997a) it was demonstrated that this simple model is able to simulate the unusual pH dependence of some of the haem methyl chemical shifts of this cytochrome, which Park et al., 1996 were unable to explain. The application of the model to Dmbc_3 and to mutants of Dvc_3 (unpublished results) is also in progress. Moreover, the present model has been extended in order to include an additional ionisable centre for the analysis of the data from cytochrome c_3 isolated from *D. desulfuricans* (ATCC 27774) which showed two distinct ionisation processes (Louro et al., 1998c). In this case a larger number of parameters is necessary to describe the intrinsic properties and the interactions between the six centres, as will be discussed in the section about future developments (section II.3.5).

The fitting of different experimental data sets obtained with Dgc_3 and Dvc_3 Hildenborough to the model results in each case in the determination of 15 energetic parameters that characterise the thermodynamic behaviour of each cytochrome c_3 molecule. Thirteen parameters were obtained from the fitting of the pH dependence of the haem methyl chemical shifts to the model (cf. equations 6a-d) using the Marquardt method on the basis of accurate pH measurements and experimental errors for each shift proportional to the linewidth of the peak (Figures II.10 and II.12). These parameters are the 3 relative redox energies and the ionisation energy of the fully reduced protein plus 5 redox interacting energies and 4 absolute redox-Bohr energies. The two remaining parameters were obtained from redox titrations monitored by UV-visible spectroscopy. For each cytochrome, two redox titrations performed at room temperature, at pH 5.6 and 8.5 for Dgc_3 (Figure II.11) and pH 7.0 and 8.0 for Dvc_3

(Figure II.13), were fitted simultaneously by varying only the two parameters described above, i.e. the calibration term to be added to all microscopic redox potentials, Δe, and the calibration term to be added to all haem-haem interactions, ΔI, with the relative redox potentials and the relative redox interactions kept fixed. The pK_a of the fully reduced protein and the redox-Bohr interactions were also kept fixed at the values obtained by fitting the NMR data. The energetic parameters obtained for Dgc_3 and Dvc_3 are presented in Tables II.4 and II.5, respectively.

The goodness of the fits (cf. Figures II.10-13) indeed shows that the 15 parameters of the model are sufficient to describe the complex thermodynamic behaviour of different cytochrome c_3 molecules. Note that the shape and pH dependence of the visible titration curves provides an additional qualitative test of the parameters obtained from the NMR data since this behaviour is completely determined by the ionisation energy of the centre and its interactions with the four haems, which were fixed by fitting the chemical shifts.

Although much better than that obtained by grid searching with the previous model, the agreement between the model simulations and the visible titration data is not perfect. However, the small deviations observed here are probably more related with experimental deficiencies than with poor optimisation of the parameters or inadequacy of the model. It was noted above (cf. section II.2.1) that a deficient equilibration between the redox centres of the protein and the platinum electrode may affect the shape of the titration curves significantly. Therefore, some of the small deviations observed may be the result of poor equilibration, which is more marked for higher reduced fractions at lower pH values because no additional time could be allowed for equilibration. This is because the reducing agent used, sodium dithionite, is not stable at low pH and so spontaneous reoxidation of the cytochrome becomes a problem.

It should be clear from the discussion of the A/B model and from the quality of the fits in Figures II.10-13 that the model of five interacting centres uses the minimum number of parameters necessary to describe the data and that there is insufficient information to characterise any further parameters. In fact, the effect of introducing three-site interactions has been tested for the data set of Dvc_3 and, since they were poorly defined and yielded no qualitative improvement in the fit, three-site interactions were not considered in the present model.

D. gigas

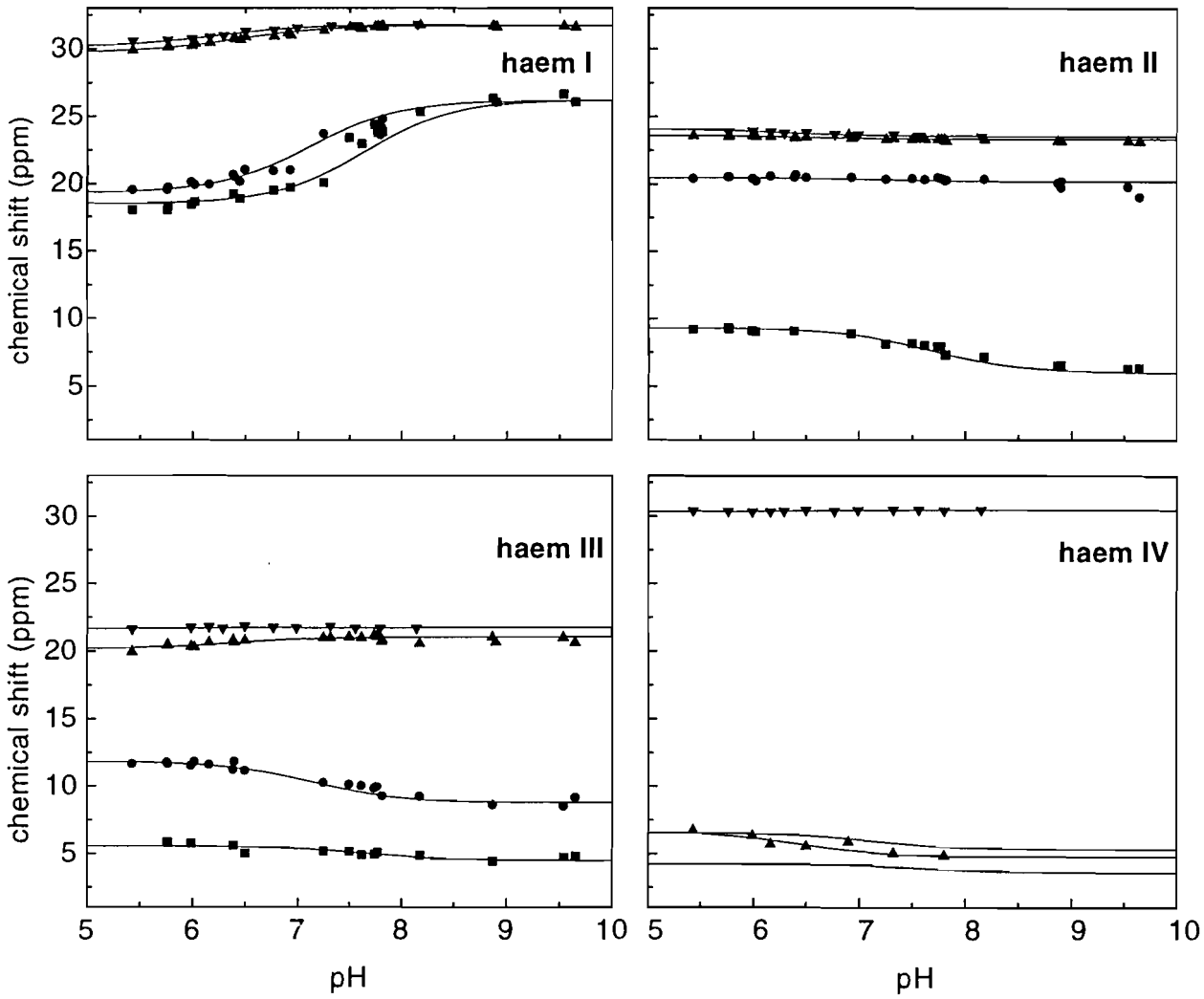

Figure II.10. pH dependence of the ^{1}H NMR chemical shifts of one haem methyl from each of the four haems of Dgc$_3$ in different oxidation stages. The solid lines correspond to the pH dependence of the chemical shifts calculated according to the five interacting centres model, for the thermodynamic parameters presented in table II.4. NMR data (Louro et al., 1998b) are represented by symbols, each symbol corresponding to a different oxidation stage: (■) stage I; (●) stage II; (▲) stage III; (▼) stage IV. The data points correspond to the following haem methyls: M18^1 for haem I, M7^1 for haem II, M12^1 for haem III and M18^1 for haem IV, according to the assignments reported by Piçarra-Pereira et al., 1993 and Louro et al., 1998a. The NMR data were acquired at 25 °C.

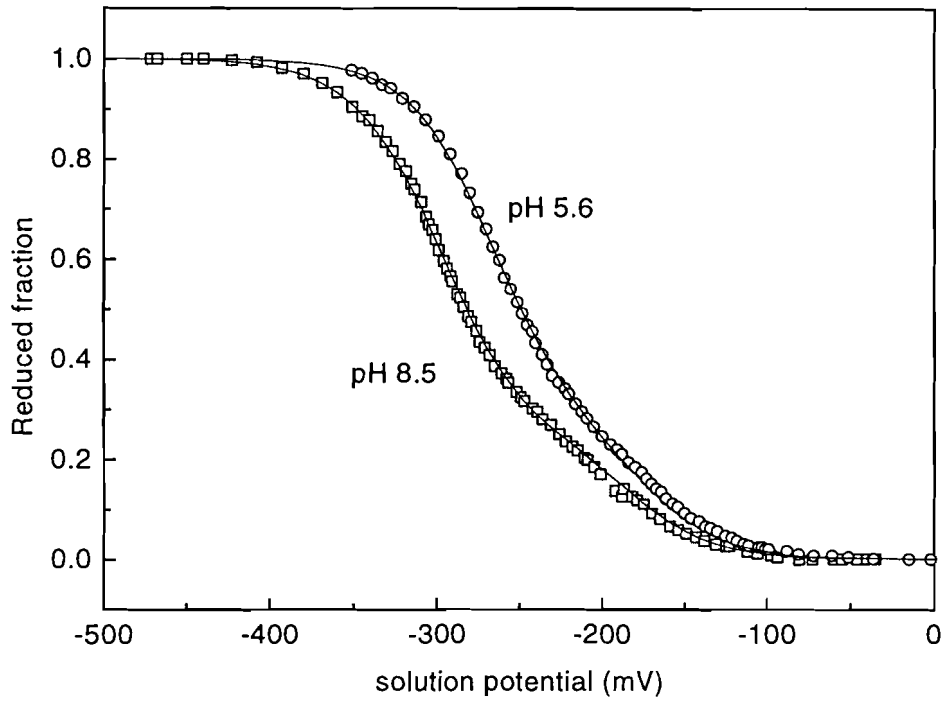

Figure II.11. Visible redox titrations of Dgc$_3$ used for the calibration of the redox potentials and haem-haem interactions. Solid lines: titration curves calculated using the model of five interacting centres with the thermodynamic parameters reported in table II.4. pH 5.6 (circles); pH 8.5 (squares).

Table II.4. Energy parameters for the five interacting centres in Dgc$_3$. The values were obtained by fitting the model described in the text to the NMR (Figure II.10) and the visible data (Figure II.11) simultaneously. Diagonal elements (inside shaded areas) represent the energy (eV) for oxidising haems (i.e. reduction potentials in V) and deprotonating the ionisable centre in the fully reduced molecule. The off-diagonal elements represent the energy of redox interaction (eV) between the oxidised haems and between these and the deprotonated centre. Note that the energy of each oxidised haem is lowered by deprotonation, as expected on electrostatic grounds, and the substantial negative redox interaction between haems II and III represents positive cooperativity. The standard errors are 2 meV for the redox potentials and haem-haem interactions of haems I-III and 6 meV for the redox potential and interactions involving haem IV, 2 meV for the redox-Bohr energies and 4 meV for the ionisation energy. Since the energy terms are in eV it is necessary to multiply these terms by the Faraday constant in order to convert them into Joule before substitution in the equations of the text. The values of the macroscopic pK$_a$s are $pK_a^0 = 8.5$, $pK_a^I = 7.6$, $pK_a^{II} = 7.1$, $pK_a^{III} = 6.4$, $pK_a^{IV} = 6.2$.

	haem I	haem II	haem III	haem IV	proton
haem I	- 0.277	+ 0.000	+ 0.025	- 0.024	- 0.062
haem II		- 0.260	- 0.040	+ 0.035	- 0.033
haem III			- 0.236	+ 0.017	- 0.033
haem IV				- 0.202	- 0.010
proton					+ 0.505

D. vulgaris

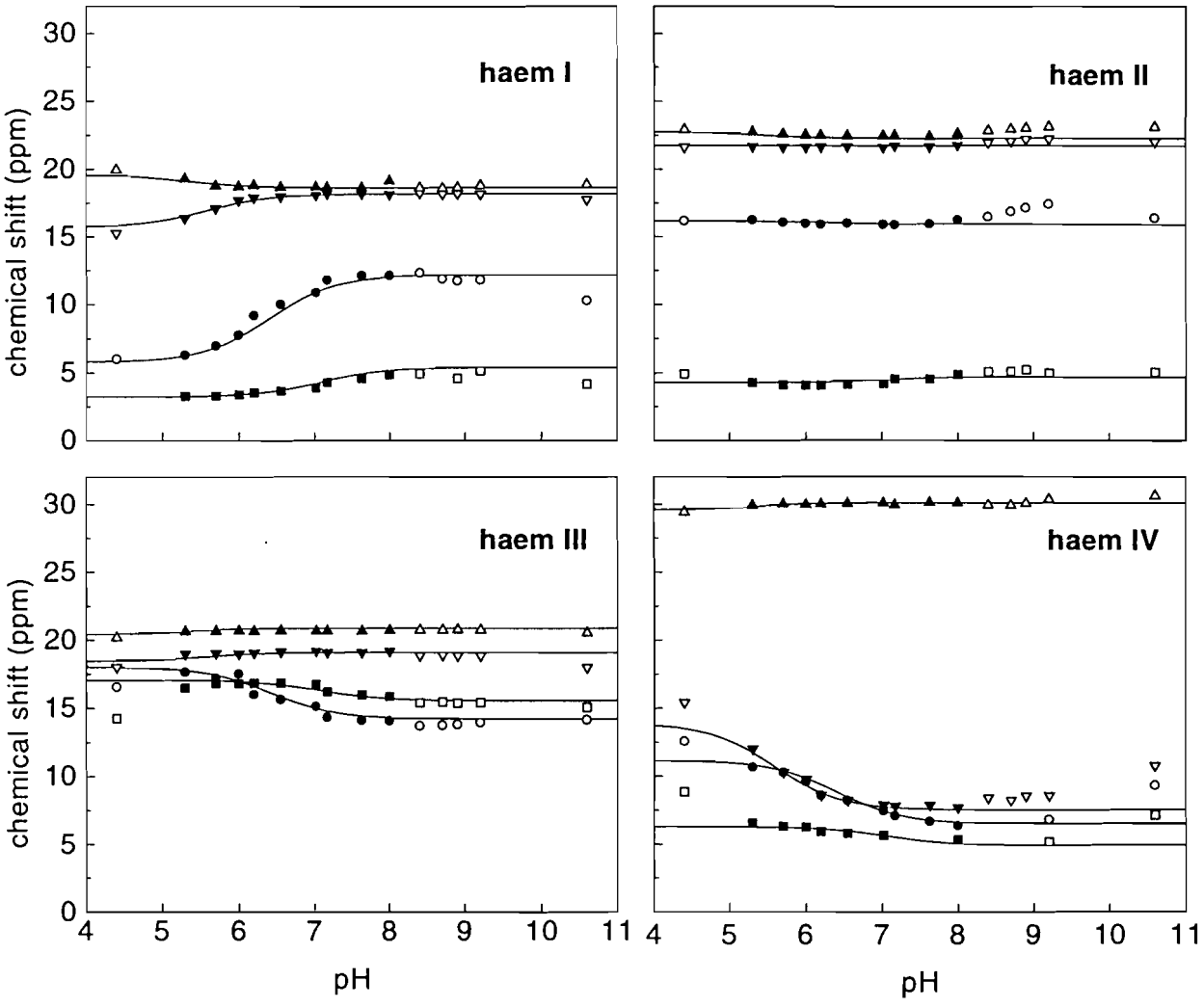

Figure II.12. pH dependence of the ^{1}H NMR chemical shifts of one haem methyl from each of the four haems of Dvc_3 in different oxidation stages. The solid lines correspond to the pH dependence of the chemical shifts calculated according to the five interacting centres model, using the thermodynamic parameters reported in table II.5. The chemical shifts of haem methyls M2^1 (haem I), M18^1 (haem II), M12^1 (haem III) and M18^1 (haem IV) are represented as a function of the pH (Turner et al., 1996), each symbol corresponding to a different oxidation stage: (■) stage I; (●) stage II; (▼) stage III; (▲) stage IV. Open symbols represent data points outside the pH range used for the fitting.

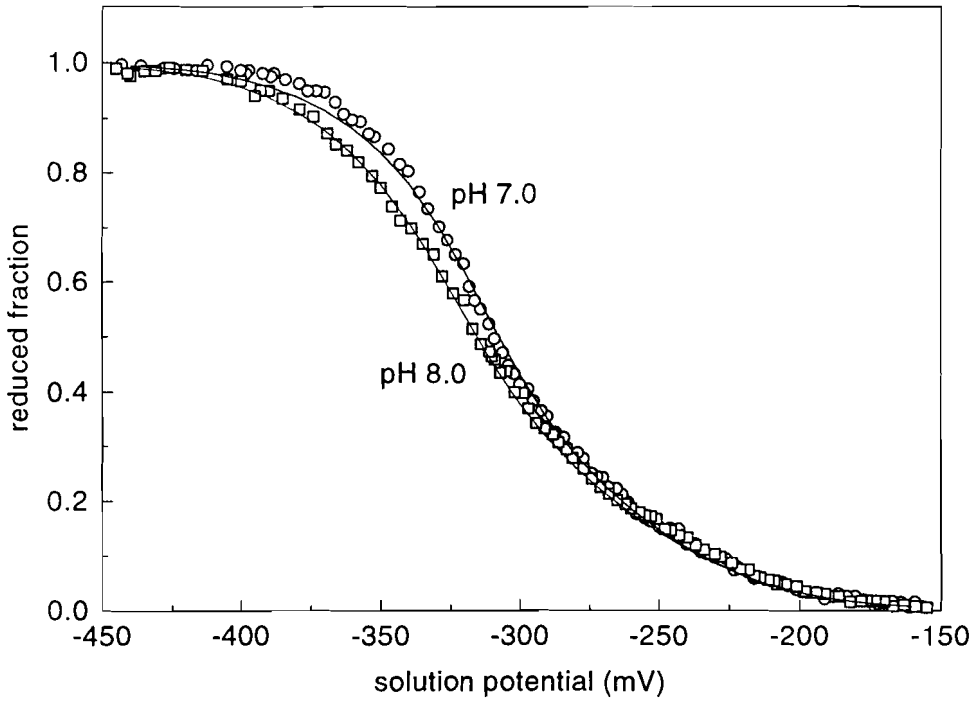

Figure II.13. Visible redox titrations of Dvc_3 used for the calibration of the redox potentials and haem-haem interactions. Solid lines: titration curves calculated using the model of five interacting centres with the thermodynamic parameters reported in table II.5. pH 7.0 (circles); pH 8.0 (squares).

Table II.5. Energy parameters for the five interacting centres in Dvc_3. The values were obtained by fitting the model described in the text to the NMR (Figure II.12) and the visible data (Figure II.13). Diagonal elements (inside shaded areas) represent the energy (eV) for oxidising haems (i.e. reduction potentials in V) and deprotonating the ionisable centre in the fully reduced molecule. The off-diagonal elements represent the energy of redox interaction (eV) between the oxidised haems and between these and the deprotonated centre. Note the positive cooperativity between haems I and II. The standard errors are 5 meV for relative redox potentials and interactions, 5 meV for the absolute reference value for the potentials, and 3 meV for the absolute reference value for the interactions. Since the energy terms are in eV it is necessary to multiply these terms by the Faraday constant in order to convert them into Joule before substitution in the equations of the text. The values of the macroscopic pK_as are $pK_a^0 = 7.4$, $pK_a^I = 7.1$, $pK_a^{II} = 6.4$, $pK_a^{III} = 5.6$, $pK_a^{IV} = 5.3$.

	haem I	haem II	haem III	haem IV	proton
haem I	- 0.245	- 0.043	+ 0.020	- 0.004	- 0.070
haem II		- 0.267	- 0.008	+ 0.008	- 0.030
haem III			- 0.334	+ 0.032	- 0.018
haem IV				- 0.284	- 0.006
proton					+ 0.439

II.3.3.3 Discussion

At least for the case of Dvc_3 there are significant deviations between the observed chemical shifts of the haem methyl groups and the theoretical curves in the regions below pH 5 and above pH 8 (Figure II.12). This is hardly surprising since the protein contains many groups which may ionise at extreme pH values and there must be some electrostatic interactions between such groups and the haems. The important question is whether the parameters obtained from a model which considers a single ionisation process will be significantly distorted by effects which occur at pH values outside the physiological region. In fact, the differences between the parameters obtained by fitting data from the full pH range studied or by restricting the range by excluding the extremes are very small (Turner et al., 1996). Thus, although additional ionisations undoubtedly do occur, the pH dependence of the NMR spectra in the physiological pH range is adequately described by interactions between the haems and a single ionisation process. Note that the number of protons involved in this process is not necessarily equal to one. The interactions observed could be the sum of interactions with more than one ionisable group with microscopic pK_a values such that the macroscopic pK_as observed in the curves are maintained. In fact, pH titrations performed in both the oxidised and reduced form show that two protons are involved in the redox-Bohr effect in Dvc_3 (Louro et al., 1996a).

All of the cooperativities between the ionisable centre and the haems are positive, which is consistent with a purely electrostatic effect. The higher value obtained for the interaction between haem I and the proton indicates that the ionisable centre is most closely associated with haem I, which is consistent with the titration curve observed for the 13^2 CH_2 protons of the propionate group of haem I in Dvc_3 (Miyazaki F) (Park et al., 1996).

Table II.6. Iron-iron distances in nanometers and haem-haem interacting potentials in mV for Dvc_3. Distances determined from the crystal structure of Dvc_3 Hildenborough (Matias et al., 1993) are listed above the diagonal and haem-haem interacting potentials obtained from the fitting of the five interacting centres model to the experimental data (Turner et al., 1996) are listed below the diagonal.

	Haem I	Haem II	Haem III	Haem IV
Haem I		1.24	1.11	1.77
Haem II	- 43		1.60	1.66
Haem III	+ 20	- 8		1.19
Haem IV	- 4	+ 8	+ 32	

For Dvc_3, the haem-haem interaction energies of the haem pairs which have the largest iron-iron distances in the crystal structure (cf. Table II.6) (Matias et al., 1993) are comparable with their standard errors and therefore may not be significant. Also in agreement with the interactions being electrostatic, significant negative cooperativities are found between the haems which have the shorter iron-iron distances with the exception of the large positive cooperativity found between haems I and II. Since positive cooperativities between centres with the same charge cannot be explained by simple electrostatics, this interaction provides evidence for a redox-linked conformational change. Note that, since three-site interactions between three haems or two haems and the proton are not significant, there is no evidence for major conformational changes associated either with electron transfer or with protonation. Therefore, the conformational change responsible for the positive haem-haem cooperativity may simply be the result of a localised movement of charge. The comparison between the crystal structure of the oxidised form of Dvc_3 and the structure in solution of the reduced form determined by NMR showed that there is a localised movement of the backbone of residues 44-47 towards the propionate edge of haem I (Messias et al., 1998). On this basis, these authors proposed that a concerted movement of Lys 45 and Cys 46 could result in the coupled two-proton transfer because these residues are involved in interactions with the two propionates of haem I. Moreover, since Cys 46 is covalently bound to haem II this movement could also be responsible for the positive cooperativity observed between haems I and II in Dvc_3.

The pattern of cooperativities observed in Dgc_3 is different (cf. Table II.7). Although negative cooperativities are still observed between haem pairs I-III and III-IV, some of the closer haem pairs in the structure, the largest negative cooperativity is found between haems II and IV which are separated by the second largest distance. Haems I and II which displayed the positive cooperativity in Dvc_3 do not interact in Dgc_3. The other two haem pairs which are more separated in the crystal structure, I-IV and II-III, display non-negligible positive cooperativities. The most important of these is that observed between haems II and III, which are the middle haems with respect to oxidation order, a similar situation to that of haems I and II in Dvc_3. Note that it is necessary to overcome the negative cooperativity expected on an electrostatic basis to create an observable positive cooperativity between two centres with the same charge. Since this electrostatic interaction depends on the inverse of the square of the distance between the centres, it is easier to obtain positive cooperativities between more separated haems because the negative term is smaller. The structural mechanism that is behind the positive cooperativity between haems II and III in Dgc_3 is not known, but since the

determination of the structure of the reduced form is in progress, the direct comparison of the structures of the oxidised and reduced forms may give some indication about possible mechanisms, similarly to what happened with Dvc_3 (Messias et al., 1998).

Table II.7. Iron-iron distances in nanometers and haem-haem interacting potentials in mV for Dgc_3. Distances determined from the crystal structure of Dgc_3 (Matias et al., 1996) are listed above the diagonal and haem-haem interacting potentials obtained from the fitting of the five interacting centres model to the experimental data (Louro et al., 1998b) are listed below the diagonal.

	Haem I	Haem II	Haem III	Haem IV
Haem I		1.20	1.12	1.80
Haem II	0		1.55	1.67
Haem III	+ 25	- 40		1.20
Haem IV	- 24	+ 35	+ 17	

Other major differences between the interaction patterns in Dgc_3 and Dvc_3 are those involving haem IV. Since the microscopic redox potential of haem IV and the haem-haem interactions with this haem are not as well defined as those of the other haems due to the larger difference in redox potential that separates this haem from the others, these differences might not be as significant as they first seem. The intrinsically poor definition of the thermodynamic parameters of haem IV in Dgc_3 led to the different sets of redox interactions determined for the protonated and deprotonated forms of the cytochrome (Santos et al., 1984a, Coletta et al., 1991). In the present model, the thermodynamic parameters obtained for haem IV indeed show larger standard errors but are statistically meaningful.

All redox-Bohr cooperativities are positive in Dgc_3, as expected for electrostatic interactions between centres with opposite charges. Since the largest one is that with haem I, the ionisable centre is probably situated in the vicinity of this haem, as in Dvc_3. However, the distance correlation with the other haems is not as good as that found in Dvc_3. This is not surprising, taking the spatial anisotropy of the dielectric constant inside the protein molecule into consideration. Since the dielectric constant depends on the character of the aminoacid residues that fill the space between the haems and on the presence of water molecules, this is probably also the cause for the different pattern of interactions observed in Dgc_3 when compared to Dvc_3. In fact, although the spatial arrangement of the four haems is almost equal in these cytochromes, the homology of their aminoacid sequence is very low indeed (Moore and Pettigrew, 1990).

It should be emphasised that, although several of the interaction energies appear reasonable in terms of electrostatic interactions within the crystal structure, the model of five interacting centres from which these values were obtained made no use of any structural information. The model uses the minimum number of parameters necessary to describe the general thermodynamic behaviour of different cytochromes c_3 such as those isolated from *D. gigas* and *D. vulgaris* and fitting these parameters to NMR and visible redox titrations together leads to unique solutions. In contrast with the A/B model, the 15 parameter model presented in this section not only gives an excellent fit to the data but also ensures that each parameter is well defined and is therefore statistically significant.

II.3.4 Conclusions

The analysis of the thermodynamic parameters obtained strengthens the former view of the functional mechanism of Dgc_3 (Coletta et al., 1991) and shows that a similar mechanism is operative in Dvc_3 (Turner et al., 1996). The cytochrome c_3 molecule seems to be designed to accomplish the concerted transfer of two electrons coupled to the uptake or release of protons, depending on the direction of the electron transfer. The calculation of the populations of the microstates during a reduction process shows that the interplay of the cooperativities established between the haems and the ionisable centre results in high positive cooperativity between the second and the third haems to be reduced. Thus, the entry of the first electron in a reduction process, or its exit in an oxidation process, prepares the molecule for a concerted two-electron step. This is apparent from the curves of the pH dependence of the macroscopic redox potentials of Dvc_3 presented in Figure II.14, where it can be seen that E_{II} and E_{III}, the macroscopic redox potentials of the second and third oxidation steps, respectively, are reversed in the physiological pH range. In Dgc_3, the macroscopic redox potentials for the middle reduction steps approach each other but do not cross over. Therefore, the effect is not as striking as in Dvc_3, but the positive cooperativity observed between the middle haems, assisted by the uptake of proton(s), still results in the concerted transfer of two electrons as suggested by Coletta et al., 1991 on the basis of the A/B model. Note that the uptake of proton(s) facilitates reduction, enhancing the global positive cooperativity, because the potentials of the protonated form are less negative than those of the deprotonated one.

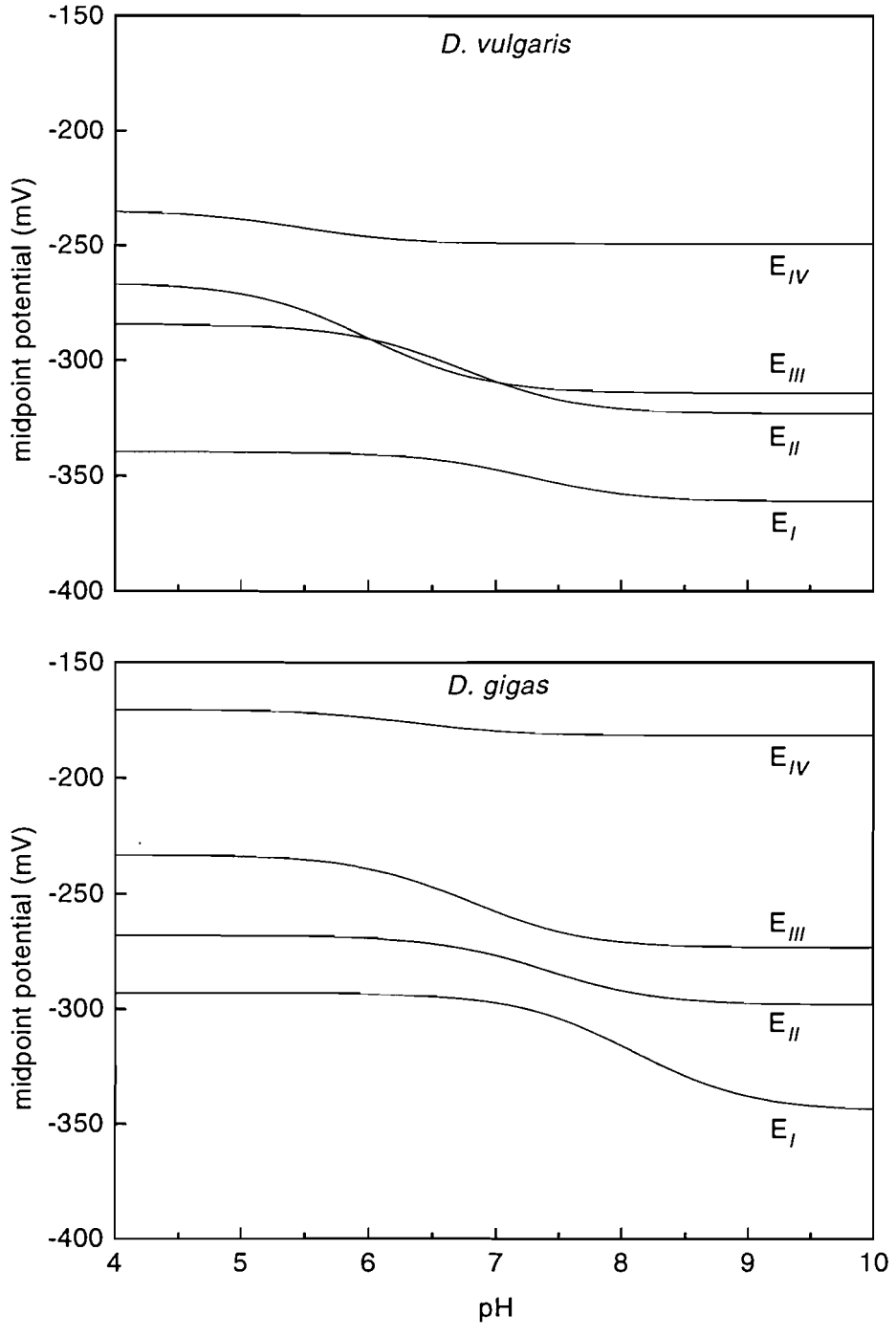

Figure II.14. pH dependence of the macroscopic redox potentials of Dgc_3 and Dvc_3. Curves were calculated using the five interacting centres model with the thermodynamic parameters reported in tables II.4 and II.5, respectively. E_I , E_{II} , E_{III} and E_{IV} refer to the macroscopic midpoint potentials as defined in scheme I of section II.1.

The macroscopic redox potentials for the extreme pH values and the macroscopic pK_as of the five redox stages for Dgc_3 and Dvc_3 are presented in Figure II.15. These values were obtained from the thermodynamic parameters of the five interacting centres model (Tables II.4 and II.5).

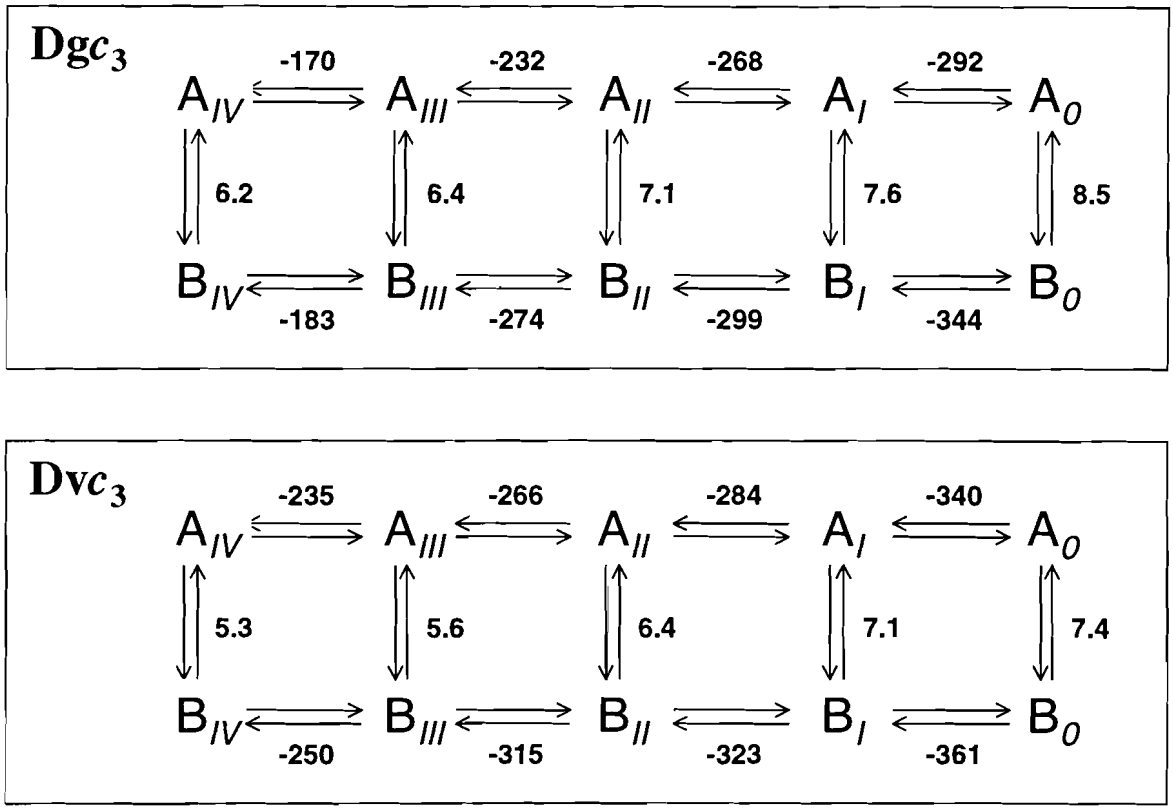

Figure II.15. Macroscopic redox potentials and pK_as for the protonated (A) and deprotonated (B) forms of Dgc_3 and Dvc_3. See scheme I of section II.1 for definition of macroscopic midpoint potentials and macroscopic pK_as. The protonated forms are represented by A and the deprotonated ones by B. Roman numbers refer to the oxidation stages: (*0*) fully reduced form, (*I*) molecules with one haem oxidised, (*II*) molecules with two haems oxidised, (*III*) molecules with three haems oxidised and (*IV*) fully oxidised form. Note that, according to these values, in the physiological pH range, reduction starts in the deprotonated form and ends in the protonated one, thus coupling proton transfer to electron transfer.

It is apparent from the figure that during the reduction process in the physiological pH range the cytochrome molecule not only picks up electrons but also picks up proton(s). The reduction process starts in the oxidised deprotonated molecule because the pK_a of the oxidised form is lower than the optimum pH for the growth of these bacteria, and ends in the fully reduced protonated molecule because the pK_a of the fully reduced form is higher than the pH of the growth medium. It will be shown later (section IV.3) that this result has important implications in the energy transduction processes of these bacteria.

II.3.5 Future developments

It was noted above that potentiometric titrations with Dvc_3 indicate that two protons are involved in the redox-Bohr effect in the physiological pH range (Louro et al., 1996a). Since the model of five interacting centres considers only one ionisable centre, the thermodynamic parameters related to this centre are not microscopic in the sense that they represent the global effect of the two acid/base groups. The extension of the model to include an additional ionisable group requires six additional parameters: the pK_a of the second proton in the reference state, another four redox-Bohr interactions, and the proton-proton interaction defined between the two ionisable groups. However, since the present NMR and visible data set for Dvc_3 and Dgc_3 has insufficient information to discriminate two protons, it is impossible to define the microscopic parameters of each ionisable group. Note that the parameters for the individual acid/base groups cannot be obtained from the present parameters because different combinations of individual parameters can give the macroscopic pH dependence observed in the experimental curves. The pK_a values of the two acid/base groups may be similar, but they do not have to be equal, and the redox-Bohr interactions are probably different, reflecting the different location of the two ionisable groups.

It is interesting to note that, in the case of cytochrome c_3 isolated from *D. desulfuricans* (ATCC 27774), the NMR data show two distinct ionisable centres. A model with an additional acid/base centre was developed to simulate the pH dependence of the haem methyl chemical shifts (Louro et al., 1998c). However, even in this case, the number of parameters of the model had to be reduced because the available data did not include enough information to define all 21 parameters precisely.

A more accurate thermodynamic study could be made if the chemical shifts of more than one methyl group per haem were included in the analysis. The shift of a single methyl group might not be an accurate measure of the fractional oxidation of a haem because the electronic structure could be perturbed by neighbouring charges. However, the total unpaired electron delocalisation is less likely to be affected and inclusion of all four methyl groups should remove this source of uncertainty. Moreover, if the model of five interacting centres with 15 parameters fails to simulate the pH dependence of all 16 methyl groups, the data contain additional information to define further parameters. For instance, the existence of significant three-site interactions would provide direct evidence for conformational changes, either related with electron transfer or with protonation. Alternatively, the model could be extended to include the second ionisable group if the determination of the individual pK_a values and

redox-Bohr interactions became possible. The haem-proton interactions together with the structure in solution could be used for a more precise localisation of the acid/base groups. Note that accurate positioning of these groups would only be possible if the dielectric constants inside the protein were known.

It should be noted that the inclusion of methyl groups other than those pointing to the exterior of the protein molecule requires the calculation of the extrinsic paramagnetic shifts generated by each haem. Dipolar interactions between neighbouring haems cause extrinsic shifts that contribute to the overall chemical shift observed. Therefore, the accurate determination of the fractional populations depends upon the correct estimation of the contribution of extrinsic shifts in each case, as shown by Salgueiro et al., 1997a.

Since only a few crystal structures have been available until now, the structural information about Dgc_3 and Dvc_3 has been limited to a particular conformation of the oxidised form. The use of NMR techniques applied to the resolution of protein structures in solution (Wüthrich, 1986) extends the possibility of structure determination to different experimental conditions, in which the protein may adopt different conformations. Among the cytochromes c_3 mentioned above, the structure in solution of the reduced form of Dvc_3 has been determined (Messias et al., 1998) and those of both oxidised and reduced forms of Dgc_3 are in progress. In the near future, these structures and other structures that may be obtained for intermediate oxidation stages and for different protonation states will allow the development of structural models in which structural and thermodynamic information are combined.

III KINETIC PROPERTIES

III KINETIC PROPERTIES

III.1 Introduction

The kinetic properties of cytochrome c_3 from *D. gigas* are discussed in this chapter and a kinetic model is proposed for the analysis of the electron transfer reactions between this cytochrome and various reducing or oxidising agents. These reactions were followed by stopped-flow techniques coupled to visible spectroscopy and the results obtained are presented and analysed in the framework of a kinetic model which is developed here. It should be noted that the analysis of the kinetic data presented in this thesis is new in the sense that it is the first attempt to provide a sound theoretical basis for the correlation between macroscopic rate constants and the rate constants for electron transfer to the individual haems in cytochrome c_3. This correlation may seem straightforward but it will be shown that it is the subject of several examples of misunderstanding and inaccuracy in the literature. In most cases, simple analysis with exponentials prompted the authors to determine observed rate constants and study their dependence on physical variables such as ionic strength or pH. Although these studies do not provide information about the individual haems, they are important because they give information about the kinetic mechanism: whether or not it involves complex formation, under which conditions, the possible nature of the interactions established between the two redox partners, etc. Depending on the mechanism, it may also be possible to determine the value of the equilibrium binding constant of the complex and the value of the rate constant for the electron transfer reaction within the complex. However, to establish structure-function relationships, it is also necessary to have information about the kinetic behaviour of the individual haems, for which it is essential to determine their individual rate constants. There are examples in the literature in which attempts have been made to correlate the observed rate constants and the rate constants of the haems in cytochromes c_3, but they are not sufficiently well-grounded. Moreover, it will be shown in section III.3. that the expression of the macroscopic rate constants, that correspond to a model of four consecutive steps of one electron, in terms of the individual rate constants is only possible on the basis of a well established thermodynamic description of the system, which was either ignored or not available when most of the kinetic studies were published.

To give an overview of the literature concerning the kinetic properties of cytochromes c_3 isolated from several *Desulfovibrio* spp., a brief reference to the more relevant studies published in the field is made, emphasising the kinetic models used for the analysis of data and the kind of information obtained in each case. A summary table is also presented to

facilitate the comparison between the values of the rate constants determined by different methods for the electron transfer reactions involving cytochromes c_3 from different sources and either inorganic reducing agents or other redox partners.

Table III.1. Summary of the main results obtained in kinetic studies involving cytochromes c_3 isolated from different microorganisms. Abbreviations: (c_3) cytochrome c_3; ($COO^{-\bullet}$) carboxyl radical anion; ($5DRFH^{\bullet}$) 5-deazariboflavin semiquinone; (e^-_{aq}) hydrated electrons; (fd I) ferredoxin I; (fl) flavodoxin; (hase) hydrogenase; ($MeV^{+\bullet}$) reduced methyl viologen; (n.ref.) not referred by the authors; (ox) oxidised; ($PDQ^{+\bullet}$) reduced propylene diquat; (red) reduced; (sq) semiquinone.

Stopped-flow studies with exogenous electron donors/acceptors

Microorganism	Experiment	Rate constants	Observations	Reference
D. vulgaris (Hildenborough)	c_3^{ox} vs. dithionite	$k_{fast}= 6.8\times10^6\ M^{-1}s^{-1}$ $k_{slow}=2.1\times10^6\ M^{-1}s^{-1}$	Biphasic kinetics with 50% fast phase 25 mM borate buffer pH 9.1, 20 °C	Favaudon et al., 1978
D. vulgaris (Hildenborough)	c_3^{ox} vs. dithionite	$k_{fast}= 3.2\times10^6\ M^{-1}s^{-1}$ $k_{slow}=6.3\times10^5\ M^{-1}s^{-1}$	Biphasic kinetics with 72% fast phase 0.1 M phosphate buffer pH 7, 5 °C	Capeillère-Blandin et al., 1986
D. vulgaris (Miyazaki F)	c_3^{ox} vs. dithionite	$k_1=1.9\times10^7\ M^{-1}s^{-1}$ $k_2=1.1\times10^7\ M^{-1}s^{-1}$ $k_3=8.4\times10^6\ M^{-1}s^{-1}$ $k_4=1.5\times10^6\ M^{-1}s^{-1}$	Rate constants for the successive four steps of the reduction of cytochrome c_3 20 mM phosphate buffer pH 7, 21°C	Calculated from Tabushi et al., 1983
D. gigas	c_3^{ox} vs. dithionite	$k_{fast}= 3.6\times10^7\ M^{-1}s^{-1}$ $k_{slow}=1.8\times10^6\ M^{-1}s^{-1}$	Biphasic kinetics with 25% fast phase 0.25 M glycine buffer pH 9.6, 25 °C	Catarino et al., 1991 and section III.4 of this thesis
D. gigas	c_3^{ox} vs. FMN^{red}	$k_{IV}=3.0\times10^7\ M^{-1}s^{-1}$ $k_I= 2.0\times10^6\ M^{-1}s^{-1}$	Rate constants of haems I and IV. 0.25 M glycine buffer pH 9.6, 25 °C	Section III.5 of this thesis
D. desulfuricans (ATCC 27774)	c_3^{ox} vs. dithionite	$k_{fast}=2.5\times10^7\ M^{-1}s^{-1}$ $k_{slow}=1\times10^6\ M^{-1}s^{-1}$	Biphasic kinetics with 54% fast phase 0.1 M tris/maleate buffer pH 8.5, 10 °C	our unpublished results
Dsm. baculatum (Norway 4)	c_3^{ox} vs. dithionite	$k_{fast}=1.0\times10^7\ M^{-1}s^{-1}$ $k_{slow}=6.5\times10^5\ M^{-1}s^{-1}$	Biphasic kinetics with 86% fast phase 0.1 M phosphate buffer pH 7, 5 °C	Capeillère-Blandin et al., 1986
Dsm. baculatum (Norway 4)	c_3^{red} vs. oxygen	$k=3.1\times10^4\ M^{-1}s^{-1}$	0.1 M phosphate buffer pH 7, 5 °C	Capeillère-Blandin et al., 1986

Stopped-flow studies with redox proteins/enzymes				
Microorganism	**Experiment**	**Rate constants (k) and dissociation equilibrium constants (K_d)**	**Observations**	**Reference**
D. vulgaris (Hildenborough)	c_3^{red} vs. fl^{ox}	k_{et}=73.4 s^{-1} K_d=65.9 μM k_{et}=18.5 s^{-1} K_d=54.5 μM	Biphasic kinetics with saturation, 40% fast phase limiting 1st order rate constant and dissociation equilibrium constant for the fast phase limiting 1st order rate constant and dissociation equilibrium constant for the slow phase Low ionic strength; 10 mM phosphate buffer pH 7.5	De Francesco et al., 1994
D. vulgaris (Hildenborough)	c_3^{red} vs. fl^{ox}	k_{fast}=5.3×10^5 $M^{-1}s^{-1}$ k_{slow}=8.5×10^4 $M^{-1}s^{-1}$	Biphasic kinetics without saturation, % fast n.ref. 2nd order rate constants High ionic strength; 10 mM phosphate buffer pH 7.5 with 100 mM KCl	De Francesco et al., 1994
D. vulgaris (Hildenborough)	c_3^{red} vs. fl^{ox}	k_{et}=42 s^{-1} K_d≈8 μM	Monophasic kinetics with saturation, limiting 1st order rate constant and upper limit of dissociation equilibrium constant Low ionic strength; 10 mM MES/KOH buffer pH 6.0	De Francesco et al., 1994
D. vulgaris (Hildenborough)	c_3^{red} vs. fl^{ox}	k_{fast}=5.3×10^5 $M^{-1}s^{-1}$ k_{slow}=1.1×10^5 $M^{-1}s^{-1}$	Biphasic kinetics without saturation, % fast n.ref. 2nd order rate constants High ionic strength; 10 mM MES/KOH buffer pH 6.0 with 100 mM KCl	De Francesco et al., 1994

D. vulgaris (Hildenborough)	c_3^{ox} vs. fd I ^{red}	$k_+=1.4\times10^7\ M^{-1}s^{-1}$ $k_-=140\ s^{-1}$ $k_{max}\geq1000\ s^{-1}$ $K_d=70\ \mu M$	Monophasic reduction of the four haems. 2nd order rate constant for reduction 1st order rate constant for oxidation limiting 1st order rate constant and dissociation equilibrium constant 0.1 M phosphate buffer pH 7, 5 °C	Capeillère-Blandin et al., 1986
D. gigas	c_3^{ox} vs. fl^{red}	$k_{IV}=3.0\times10^9\ M^{-1}s^{-1}$ $k_I=5.0\times10^7\ M^{-1}s^{-1}$	Rate constants of haems I and IV. 0.25 M glycine buffer pH 9.6, 25 °C	Section III.5 of this thesis
D. gigas	c_3^{ox} vs. fl^{sq}	$k_{IV}=2.2\times10^5\ M^{-1}s^{-1}$ $k_I=2.2\times10^4\ M^{-1}s^{-1}$	Rate constants of haems I and IV. 0.25 M glycine buffer pH 9.6, 25 °C	Section III.5 of this thesis
Dsm. baculatum (Norway 4)	c_3^{red} vs. fd I ^{ox}	$k_+=1.5\times10^8\ M^{-1}s^{-1}$ $k_{max}=160\ s^{-1}$ $K_d=1.1\ \mu M$	Monophasic oxidation of one haem per molecule 2nd order rate constant for the oxidation = k_{max}/K_d limiting 1st order rate constant dissociation equilibrium constant 0.1 M phosphate buffer pH 7, 5 °C	Capeillère-Blandin et al., 1986
Dsm. baculatum (Norway 4)	c_3^{ox} vs. fd I ^{red}	$k_+=6.6\times10^7\ M^{-1}s^{-1}$ $k_-=150\ s^{-1}$ $k_{max}\geq1000\ s^{-1}$ $K_d=15\ \mu M$	Monophasic reduction of the four haems. 2nd order rate constant for reduction 1st order rate constant for oxidation limiting 1st order rate constant and dissociation equilibrium constant 0.1 M phosphate buffer pH 7, 5 °C	Capeillère-Blandin et al., 1986
Dsm. baculatum (Norway 4)	c_3^{ox} vs. fd I ^{red}	$k_{max}=780\ s^{-1}$ $K_d=1\ \mu M$	Result of modellisation of data from Capeillère-Blandin et al., 1986, pH 7 ionic strength 100 mM limiting 1st order rate constant for reduction and dissociation equilibrium constant	Bertrand et al., 1994

Flash photolysis studies

Microorganism	Reducing agent	Rate constants	Observations	Reference
D. vulgaris (Hildenborough)	5DRFH$^{\bullet}$	$k=5.7\times10^{8}\ M^{-1}s^{-1}$	2nd order rate constant Low ionic strength; 45-90 mM phosphate buffer pH 7	Akutsu et al., 1992
D. vulgaris (Miyazaki F)	5DRFH$^{\bullet}$	$k=5.3\times10^{8}\ M^{-1}s^{-1}$	2nd order rate constant Low ionic strength; 90 mM phosphate buffer pH 7	Akutsu et al., 1992
D. vulgaris (Hildenborough)	5DRFH$^{\bullet}$	$k_1=10.0\times10^{8}\ M^{-1}s^{-1}$ $k_2=4.2\times10^{8}\ M^{-1}s^{-1}$ $k_3=4.2\times10^{8}\ M^{-1}s^{-1}$ $k_4=4.2\times10^{8}\ M^{-1}s^{-1}$ $k_1=2.6\times10^{8}\ M^{-1}s^{-1}$ $k_2=2.6\times10^{8}\ M^{-1}s^{-1}$ $k_3=2.6\times10^{8}\ M^{-1}s^{-1}$ $k_4=8.8\times10^{8}\ M^{-1}s^{-1}$	Rate constants for the individual haems* phosphate buffer pH 7 Low ionic strength; 90 mM High ionic strength; 500 mM	Akutsu et al., 1992
D. vulgaris (Miyazaki F)	5DRFH$^{\bullet}$	$k_1=8.0\times10^{8}\ M^{-1}s^{-1}$ $k_2=5.2\times10^{8}\ M^{-1}s^{-1}$ $k_3=5.2\times10^{8}\ M^{-1}s^{-1}$ $k_4=5.2\times10^{8}\ M^{-1}s^{-1}$	Rate constants for the individual haems* phosphate buffer pH 7 Low ionic strength; 90 mM	Akutsu et al., 1992
D. vulgaris (Hildenborough)	PDQ$^{+\bullet}$	$k_1=1.6\times10^{8}\ M^{-1}s^{-1}$ $k_2=0.60\times10^{8}\ M^{-1}s^{-1}$ $k_3=0.60\times10^{8}\ M^{-1}s^{-1}$ $k_4=1.6\times10^{8}\ M^{-1}s^{-1}$ $k_1=1.4\times10^{8}\ M^{-1}s^{-1}$ $k_2=1.4\times10^{8}\ M^{-1}s^{-1}$ $k_3=1.4\times10^{8}\ M^{-1}s^{-1}$ $k_4=3.3\times10^{8}\ M^{-1}s^{-1}$	Rate constants for the individual haems* phosphate buffer pH 7 Low ionic strength; 16 mM High ionic strength; 500 mM	Akutsu et al., 1992
D. vulgaris (Miyazaki F)	PDQ$^{+\bullet}$	$k_1=1.1\times10^{8}\ M^{-1}s^{-1}$ $k_2=0.60\times10^{8}\ M^{-1}s^{-1}$ $k_3=0.60\times10^{8}\ M^{-1}s^{-1}$ $k_4=1.9\times10^{8}\ M^{-1}s^{-1}$	Rate constants for the individual haems* phosphate buffer pH 7 Low ionic strength; 16 mM	Akutsu et al., 1992
D. vulgaris (Hildenborough)	MeV$^{+\bullet}$	$k_1=0.86\times10^{8}\ M^{-1}s^{-1}$ $k_2=2.43\times10^{8}\ M^{-1}s^{-1}$	Monophasic traces phosphate buffer pH 7 Low ionic strength;16 mM High ionic strength; 1 M	Akutsu et al., 1992

(*) Haems numbered by order of reduction. The numbering according to the aminoacid sequence is IV, I, II, III. See comment on the text about the determination of the rates for the individual haems in the paper by Akutsu et al., 1992

Pulse radiolysis studies

Microorganism	Reducing agent	Rate constants	Observations	Reference
D. vulgaris (Hildenborough)	e^-_{aq}	$k=2\times10^{10}\ M^{-1}s^{-1}$	Four haems kinetically equivalent towards e^-_{aq} 160 mM formate buffer pH 8.1	Favaudon et al., 1978
D. vulgaris (Hildenborough)	$COO^{-\bullet}$	$k=2.1\times10^{8}\ M^{-1}s^{-1}$	Haems equivalent two by two Nitrous oxide saturated 160 mM formate buffer pH 8.1	Favaudon et al., 1978
D. vulgaris (Hildenborough)	$MeV^{+\bullet}$ radicals	$k=4.5\times10^{8}\ M^{-1}s^{-1}$ $k=12.4\times10^{8}\ M^{-1}s^{-1}$ $k=5.3\times10^{8}\ M^{-1}s^{-1}$ $k=16.0\times10^{8}\ M^{-1}s^{-1}$	The reduction of cyt c_3 by $MeV^{+\bullet}$ radicals is diffusion controlled pH 7.8, I= 5 mM, 20 °C pH 7.8, I= 1 M, 20 °C pH 4.5, I= 50 mM, 20 °C pH 10.8, I= 50 mM, 20 °C	Van Leeuwen et al., 1982

Kinetic studies with the physiological redox partner

Redox proteins	Technique	Rate constants	Observations	Reference
Cytochrome c_3 and hydrogenase from *D. vulgaris* (Miyazaki)	UV-visible spectrophotometry	$k_1 = 0.061\ s^{-1}$ $k_2 = 0.063\ s^{-1}$ $k_3 = 0.039\ s^{-1}$ $k_4 = 0.014\ s^{-1}$	c_3 reduction by H_2 in the presence of hydrogenase 1st order rate constant for the successive reduction steps [c_3]= 2 µM; [hase]= 2 nM 20 mM phosphate buffer pH 7, 20 °C	Yagi 1984
Cytochrome c_3 and hydrogenase from *D. gigas*	Spectrophotometry and cyclic voltammetry	$k=6.5\times10^{7}\ M^{-1}s^{-1}$	$hase^{red}+c_3{}^{ox} \rightleftharpoons hase^{ox}+c_3{}^{red}$ 10 mM tris/HCl buffer pH 7.6	Nivière et al., 1988
Cytochrome c_3 and hydrogenase from *Dsm. baculatum* (Norway 4)	Cyclic voltammetry	$k=3\times10^{7}\ M^{-1}s^{-1}$	$hase^{red}+c_3{}^{ox} \rightleftharpoons hase^{ox}+c_3{}^{red}$ 0.1 M tris/HCl buffer pH 7.6	Haladjian et al., 1987

Akutsu and co-workers studied the reduction kinetics of cytochrome c_3 from *Desulfovibrio vulgaris* by flash photolysis (Akutsu et al, 1992). These authors attempted the determination of rate constants for the individual haems by using different levels of partial reduction of the cytochrome prior to the electron transfer reaction with 5-deazariboflavin (5-DRFH) or propylene diquat (PDQ^{2+}), and studied their dependence on ionic strength (see Table III.1). They found that the dependence of each rate constant on the reduction potential difference between the haem and the reductant could be described by outer sphere electron transfer theory. Cytochromes from both the Miyazaki F and Hildenborough strains were found to be very similar in terms of their reactions with exogenous reductants, as expected from the high homology of their amino acid sequence. The unusual ionic strength dependence observed for the rate constants with the neutral flavin species 5-DRFH, as well as with the methyl viologen radical cation (MeV^{+}) was interpreted as being the result of an effect of the ionic strength on the structure and/or on the haem reduction potentials of the cytochrome.

To determine the rate constants for the individual haems, Akutsu and co-workers assumed that the reducing agent reacts independently with each of the four haems. Since the data could not be fitted by a single rate constant, different models with two rate constants were tested, corresponding to different combinations of haems. These models required the calculation of the oxidised fractions of the individual haems for each of the partially reduced samples. The major problem with this work derives from the calculation of these fractions from macroscopic reduction potentials. Since the four haems have close and interacting redox potentials (Turner et al., 1994 and 1996) these oxidised fractions must be calculated from the microscopic thermodynamic parameters rather than from macroscopic redox potentials. Besides, the assignment of haems 3 and 4 (in order of reduction) to III and II (in the sequence) respectively (Park et al. 1991) was later proved to be wrong (Salgueiro et al. 1992), which compromises part of the structural correlation established.

Tabushi et al., 1983, studied the kinetics of reduction of cytochrome c_3 from *D. vulgaris* (Miyazaki) by sodium dithionite using stopped-flow techniques coupled to UV-visible and circular dichroism spectroscopies. These authors used a model of four consecutive steps of one electron to fit the experimental data and determine four pseudo-first order rate constants. Since the ratios between the rate constants of the four steps were very different from the statistical values of 4:3:2:1 they excluded the possibility of random reduction of haems with equal reactivities. Instead, they proposed a kinetic differentiation of the four haems according to the rate constants determined for the four steps, i.e. one highly reactive haem, two moderate and one very low. In this study non-synchronous phenomena were recorded at some of the

wavelengths and also an unusual intensity change was observed at a wavelength where there should be an isosbestic point (λ= 413 nm). These spectroscopic features were attributed to the formation of an intermediate in the reduction process associated with reduction steps 2 and 3.

Yagi, 1984, studied the kinetics of the enzymatic reduction of Dvc_3 (Miyazaki) by hydrogen in the presence of hydrogenase. The same kinetic model was used to analyse the data and four reduction rate constants were determined. Since the ratios between the rate constants of the four steps for the enzymatic reaction were different from those obtained for the reaction with sodium dithionite, Yagi, 1984 concluded that the kinetic characteristics of the two reduction processes must be different and suggested the involvement of haem-haem interactions during the enzymatic reaction. However, it is not clear from the text to which kind of haem-haem interactions Yagi was referring to.

We shall see in sections III.3 and III.4.1 that the model of four consecutive steps of one electron is adequate for the description of the kinetic properties of cytochromes c_3 for which the intramolecular electron exchange is fast. However, it can be shown that, for the case of haems with equal reactivities, the ratios between the rate constants of the four steps do not follow the statistical values of 4:3:2:1 but are defined instead by the thermodynamic coefficients of equations 14a-d of section III.3. Only a system of four haems with equal reactivities and equal thermodynamic parameters would give the statistical values referred by Tabushi et al. 1983 and Yagi, 1984. Therefore, the conclusion reached by these authors about the kinetic differentiation of the four haems is not necessarily correct. Moreover, as discussed above, the implicit extrapolation from the rate constants of the steps to the rate constants of the haems cannot be made in the simplistic way presented in those articles. It should be noted that Tabushi et al., 1983 never referred to the existence of fast intramolecular electron exchange in their model and they were probably assuming that the four haems were reacting independently and sequentially with the electron donor, without simultaneously exchanging electrons between themselves.

The unusual spectroscopic characteristics found by these authors in the Soret region, which they attributed to the formation of an intermediate with a characteristic absorption spectrum, also deserves comment. The concentration of this intermediate was found to be at a maximum between 25% and 75% reduction. The intermediate is not a true kinetic intermediate in the sense that it is not a transient species observable only by techniques of rapid-kinetics. In fact, similar spectroscopic features were observed in an equilibrium situation for Dvc_3 (Yagi, 1984), Dmbc_3 (Kazanskaya et al., 1996) and Dgc_3 (Schlereth et al., 1993 and our unpublished

results). Results from circular dichroism (Tabushi et al., 1983), EPR (Guigliarelli et al., 1990), FTIR spectroelectrochemistry (Schlereth et al., 1993) and resonance Raman (Kazanskaya et al., 1996) also provided evidence for this intermediate. In their study Kazanskaya et al., 1996 have associated this intermediate with a conformational change triggered by the reduction of haem IV. However, we think that this is not the only possible interpretation and we suggest that these spectroscopic 'abnormalities' may simply derive from haem IV having slightly different spectroscopic characteristics from the other haems.

Capeillère-Blandin et al.,1986 published a detailed study of the kinetic properties of the electron exchange reaction between cytochrome c_3 and ferredoxin isolated from *Desulfomicrobium baculatum* strain Norway 4 (formerly *D. desulfuricans* Norway and recently reclassified as *Desulfomicrobium norvegicum* by Genthner et al., 1997) as well as their individual reactions with sodium dithionite. Stopped-flow techniques coupled to UV-visible spectroscopy under anaerobic conditions were used in this study. The reduction of cytochrome c_3 and ferredoxin II by dithionite are both biphasic whereas the reduction of ferredoxin I by dithionite is monophasic. All rate constants were found to depend on the square root of the dithionite concentration, those for the reduction of cytochrome c_3 being higher than those for the reduction of ferredoxins I and II. The reaction between reduced cytochrome c_3 and oxygen was also studied. The electron transfer reaction between reduced cytochrome c_3 and oxidised ferredoxin I is monophasic with an amplitude corresponding to the oxidation of one haem per molecule. The dependence of the oxidation rate constant on the concentration of ferredoxin is hyperbolic and, consequently, Capeillère-Blandin et al., 1986 proposed a kinetic mechanism involving the formation of an intermediate complex followed by an intramolecular electron exchange leading to the oxidation of the haem of lowest redox potential. The reverse reaction (i.e. mixing the oxidised cytochrome with reduced ferredoxin) was also studied at 5 °C and for small concentrations of ferredoxin I. In this reaction, the four haems are reduced in a monophasic process which is much more rapid than the previous one, with pseudo-first order rate constants near the stopped-flow limit. The dependence of the observed reduction rate constant on the concentration of ferredoxin was found to be linear within the concentration range tested. The interpretation of the results was made taking into consideration the influence of redox potentials, electrostatic interactions and charge distribution on the proteins.

These authors tentatively proposed different models for the interaction between cytochrome c_3 and sodium dithionite or cytochrome c_3 and ferredoxin. In the collisional model proposed for dithionite, the electrons would always enter the molecule through the lowest potential haem

and this would be in fast intramolecular exchange with another two haems. The full reduction of the cytochrome would be limited by slow intramolecular exchange with the fourth haem. The model proposed for ferredoxin involved rapid equilibrium between the two redox partners leading to complex formation. The rate-limiting step would be the electron exchange in either direction within the complex. In this model, a specific interaction between ferredoxin and one of the haems was assumed, with rapid electron distribution between the four redox centres in the cytochrome. The results published by Capeillère-Blandin et al. in 1986 were used some years later by Bertrand et al., 1994 as the basis for a more detailed kinetic model for the electron transfer reaction between Dmbc_3 and ferredoxin I. The ferredoxin was represented in this model by a molecule with one redox centre (with E^0= -375 mV) capable of exchanging one electron, and the complex cytochrome system was simplified to two haems, a high potential haem (E^0= -150 mV) and a low potential haem (with E^0= -330 mV, a redox potential equal to the average of the three most negative potentials). The model included complex formation and dissociation between the two redox partners, electron transfer within the complex *via* a specific haem and also intramolecular electron transfer between the "two" haems. In order to limit the number of adjustable parameters to four it was assumed that all kinetic constants are independent of the redox state of the centres and that the ratios of the rate constants for the direct and reverse electron transfer reactions are fixed by the values of the redox potentials. Simulations were made either considering that the electron transfer takes place through the high potential haem or through the low potential haem. The conclusion drawn from the application of this kinetic model to the available data was that one of the low potential haems interacts specifically with ferredoxin. The authors put forward the hypothesis that haem IV plays this important role.

Although this model might be reasonable for Dmbc_3, the two-haem approximation cannot be used for Dgc_3 and Dvc_3. The closely similar values of the redox potentials of the four haems and the existence of haem-haem cooperativities make it impossible to model these proteins with only "two" haems. Also, since the four haems are well exposed to the solvent, it is probably more reasonable to take into consideration that electron transfer can take place *via* more than one haem simultaneously. This extension increases enormously the number of adjustable parameters, as will be discussed in the kinetic model section III.3.

A kinetic study of the electron transfer process between reduced cytochrome c_3 and flavodoxin isolated from *Desulfovibrio vulgaris* (Hildenborough) was published by De Francesco et al., 1994. Anaerobic stopped-flow techniques were used to study this reaction at two different pH values and two different ionic strengths. Some of the reactions studied by De

Francesco et al., 1994 are similar to reactions presented in this thesis (section III.5). The results of both studies are comparable if the different thermodynamic parameters of the proteins isolated from *D. gigas* and *D. vulgaris* is taken into consideration. However, it should be noted that the analysis of the data which is made in these two works is quite different.

De Francesco et al., 1994, found that four moles of flavodoxin are required to oxidise one mole of fully reduced cytochrome c_3 completely, suggesting that the FMN group in flavodoxin is reduced to the semiquinone state and that no flavin- hydroquinone is formed. A biphasic process is observed at pH 7.5. When fully reduced cytochrome is mixed with oxidised flavodoxin, the amplitude of the initial fast phase amounts to about 40%, and this percentage decreases if partially oxidised cytochrome is used in the reaction. The fast phase of electron transfer occurs when the cytochrome has appreciable populations of three or four reduced haems. Under conditions of low ionic strength at pH 6.0, De Francesco et al., 1994 observed monophasic traces, in contrast with the biphasic traces observed at pH 7.5. However, an increase of the ionic strength results in the appearance of biphasic kinetics at pH 6.0 also.

The dependence of the observed rate constants on the concentration of flavodoxin is non-linear at low ionic strength and for the pH values tested. Such behaviour can be attributed to intermediate complex formation between the reduced cytochrome c_3 and the oxidised flavodoxin. Since this dependence becomes linear at high ionic strength, the authors suggested that electrostatic forces play a major role in stabilising the intermediate complex.

De Francesco et al., 1994 discussed the results obtained in terms of a kinetic model involving an equilibrium between two conformational states for the cytochrome which are dependent both on the pH of the medium and on the level of haem reduction. The authors attributed the biphasic rate of electron transfer observed at pH 7.5 to the conformational equilibrium between the A (protonated) and the B (deprotonated) forms. At pH 6.0, by analogy with Dgc_3, the cytochrome would be largely in the A form, with consequent disappearance of the biphasic character of the kinetic traces. Since the complete thermodynamic description of Dvc_3 (Hildenborough) was not available at that time, the authors used the pK_a values of the homologous Dgc_3, confusing the interpretation of the data. Indeed, the $pK_a^{ox} = 5.3$ in Dvc_3 (Turner et al., 1994 and 1996) is lower than the $pK_a^{ox} = 6.3$ in Dgc_3 (Coletta et al., 1991) and the oxidation of Dvc_3 at pH 6.0 also involves an A to B transition. According to their model, biphasic kinetics would be expected at both pH values, which is in clear disagreement with the monophasic traces observed at pH 6.0.

It will be shown later in this thesis (section IV.2) that, according to our kinetic model, the amplitude of the fast phase is expected to depend mainly on the degree of residual oxidation of haem IV after the first reduction step takes place. Therefore, the relative amplitudes of the fast and slow phases and, ultimately, the biphasicity vs. monophasicity of the traces will depend upon physical factors that affect the difference between the redox potential of haem IV and the redox potentials of the other haems. Examples of these factors are the pH, because the redox-Bohr energies are different for each haem (Turner et al., 1994 and 1996), and the temperature, because the redox potential of haem IV is more sensitive to the temperature than those of the other haems (Bertrand et al., 1994). Since the difference between the fast and the slow rate constants is small in Dvc_3 it is possible that a monophasic signal could appear as the result of an increase in the amplitude of the fast phase.

The main objective of this kinetic study was the determination of the reduction rate constants of the individual haems in order to define their relative importance in the overall reduction process of Dgc_3 by different reducing agents and under different experimental conditions. Although considerable effort was involved in model development and data analysis in this thesis, our original objective was not fully achieved. There are some limitations intrinsic to the system which prevented the determination of accurate rate constants for all four haems. However, it was possible to demonstrate that, as predicted by electrostatics, among the four haems, haem IV has a distinct kinetic behaviour and works as the main entrance gate for electrons in the molecule. Haem IV has a rate constant that, depending on the reducing agent, is one to two orders of magnitude higher than the rate constants of the other three haems, being responsible for 40% to 70% of the total reduction.

It will be shown that, due to the redox properties of this cytochrome, particularly the existence of fast intramolecular electron exchange between the four haems, this kind of kinetic analysis cannot be dissociated from an accurate thermodynamic description of the system. The kinetic studies presented in this chapter are therefore strongly coupled to the thermodynamic modelling presented in the previous chapter. Although complementary information is obtained from thermodynamic and kinetic studies, these two aspects are strongly correlated in Dgc_3 which can be referred to as a 'thermodynamically controlled' system (Palmer and Olson, 1980). The major difficulty in the determination of the rate constants of the individual haems is precisely related to thermodynamics. It will be shown in the kinetic model section (III.3) that it is not possible to define individual rate constants for thermodynamically coupled haems. For Dgc_3, the determination of accurate individual rate constants is restricted to haem IV. This haem is the first haem to be reduced , at pH 9.6, and has a redox potential sufficiently

different from the redox potentials of haems I, II and III to reach a high percentage of reduction (75%) while the other haems remain almost completely oxidised (with percentages of reduction below 10%, cf. Figure III.11 below).

III.2 Materials and Methods

III.2.1 General aspects of stopped-flow spectrophotometry

A brief introduction to the stopped-flow technique is presented here to help the comprehension of the anaerobicity tests and results described below.

The stopped-flow spectrophotometer is essentially a UV-visible spectrophotometer coupled to a sample handling unit (Figure III.1) designed to carry out rapid mixing of the reagents, enabling the study of reactions that occur in the millisecond and second time scales.

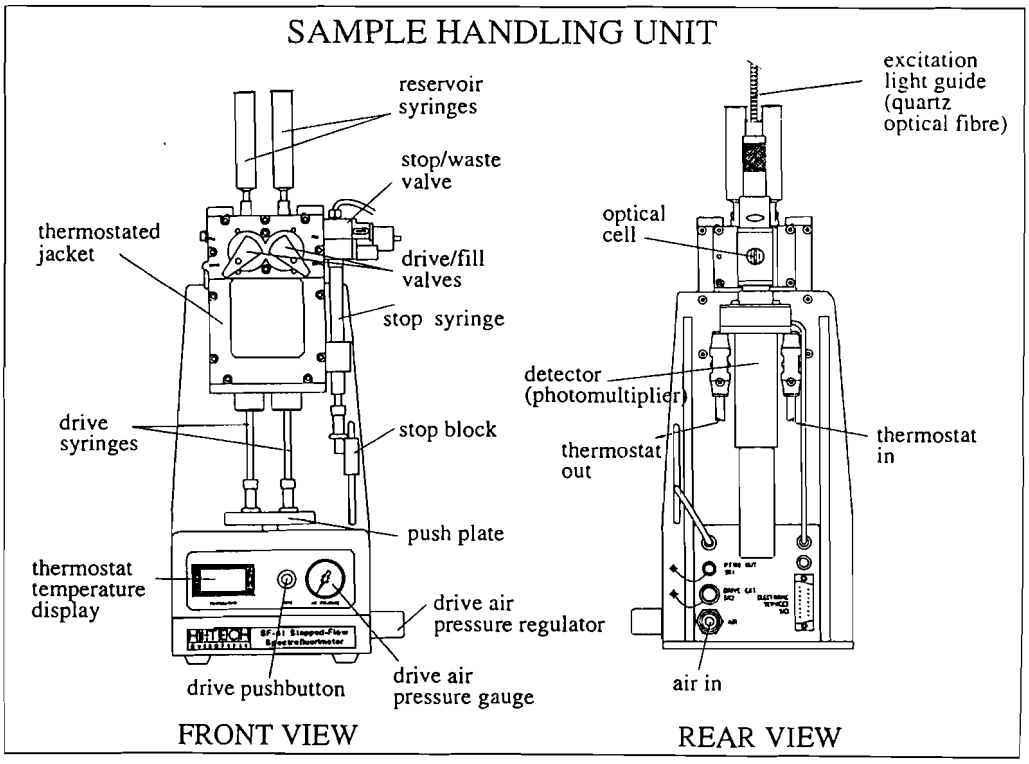

Figure III.1. Sample handling unit of the stopped-flow apparatus. Front and rear views. (Picture adapted from SF-61 Hi-Tech Scientific Users guide).

Both absorbance and fluorescence detection can be employed to follow the reactions by optical changes. The two reagents are held in the drive syringes, a common drive push plate is used to drive the syringes rapidly, displacing the reagents and causing them to mix rapidly in the mixing chamber that precedes the observation cell. The flowing reaction mix displaces the

aged solution (from previous runs) from the mixing chamber, observation cell and tubing until flow is stopped by a stop syringe, used to set the driven volume (stop volume). The aged solution flows through the tip of the stop syringe until the piston is stopped by a rigid stop block, causing rapid deceleration of the solutions and triggering the data acquisition system (Figure III.2). Because the solution takes a finite time to flow from the mixer to the observation point, the mixed solution is already of a certain age and has consequently reacted to a certain extent when the acquisition of the data starts. The age of the solution at the instant of stopping is defined as the deadtime. Since the process of mixing is not instantaneous, a short deadtime is not necessarily a good thing. In fact, if the mixing time exceeds the deadtime the reagents are still being mixed in the observation cell when data collection starts. For very fast reactions, at the limit of measurability, this results in a sigmoidal shape of the trace. The stopped-flow apparatus is designed such that the mixing time is smaller than the deadtime, but not much smaller, and problems of mixing can arise for viscous solutions.

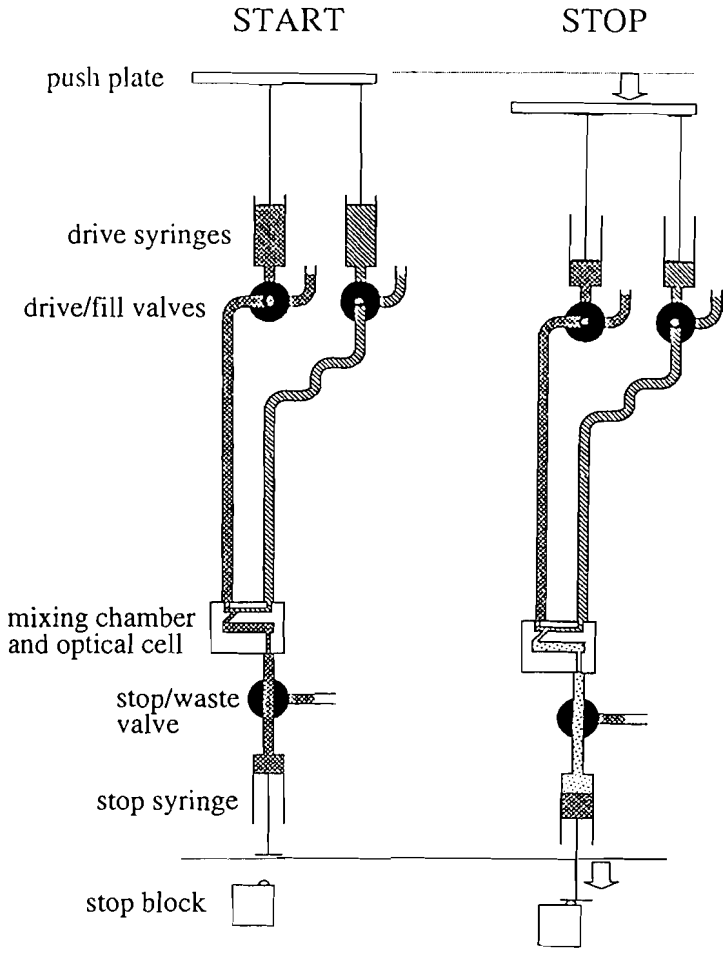

Figure III.2. Sample handling flow circuit diagram. Stock reagent solutions are stored in the reservoirs (not shown). Before the shot, the reagents are transferred to the drive syringes with the fill/drive valves in the fill position. START: with both fill/drive and stop/waste valves in the drive position the flow starts when the drive plate pushes the pistons of the drive syringes. The reagents are injected into the cell/mixer displacing the old solution. STOP: when the piston of the stop syringe hits the stop block the flow stops and data acquisition starts. The stop syringe has to be emptied before the next shot with the stop/waste valve in the waste position. (Picture adapted from Hi-Tech Scientific PQ/SF-53 Technical Manual.)

The complete stopped-flow apparatus includes a spectrophotometer unit, a sample handling unit, a data acquisition system (PC computer) and a thermostating system. The monochromatic light emitted by the optical assembly of the spectrophotometer unit is conducted to the sample handling unit by a quartz optical fibre. In absorbance measurements, a photomultiplier detects the light transmitted through the sample whereas in fluorescence measurements the photomultiplier captures the light emitted by the sample at 90° relative to the incident light, in either case the signal is sent to the data acquisition system. The temperature of the reagents in the drive syringes is kept constant by the thermostating bath connected to the sample handling unit.

III.2.2 Solving experimental problems for running experiments under strict anaerobic conditions

Running stopped-flow experiments under strict anaerobic conditions represented a difficult experimental problem that had to be dealt with in order to run the kinetic experiments in the absence of sodium dithionite, reported in section III.5. In our laboratory the first attempts were made using the sample handling unit SHU-53SF from Hi-Tech Scientific Instruments with a thermostating bath containing 0.1 M sodium dithionite (Hi-Tech Scientific PQ/SF-53 Technical Manual, Chapter 12 Anaerobic kit). Due to the high corrosive properties of this reducing agent, after several weeks the unit was corroded inside and this procedure had to be abandoned. By that time, the same company had developed a new sample handling unit (SHU-61) which, they claimed, was totally anaerobic due to the stainless steel coating of the Teflon tubing. An experiment had to be devised in our laboratory to test the anaerobic capacities of SHU-61. The description of the experimental procedure of the test developed and the analysis of the results obtained will be presented in this section, together with our conclusions concerning the deficiencies found in the anaerobic capacities of the sample handling unit SHU-61 from Hi-Tech Scientific.

III.2.2.1 Did you buy an anaerobic stopped-flow apparatus? How to make a test

A partially reduced methyl viologen solution (MeV) was used to monitor the oxygen ingress rate into the stopped-flow apparatus. Since MeV is blue in the reduced form and colourless

when oxidised, it is possible to calculate the number of moles of oxygen responsible for the measured oxidation by the decrease in optical density (OD) measured after a certain time relative to the reference OD value measured at time zero, provided that the extinction coefficient of methyl viologen and the stoichiometry of the reaction between molecular oxygen and methyl viologen are known.

To prevent oxidation of the partially reduced MeV samples by oxygen that is already inside the system, before the experiment all the stopped-flow components that make contact with the sample solutions (reservoir, drive and stop syringes, mixing chamber and Teflon tubing) were soaked with a 5 mM sodium dithionite solution for at least 15 hours, in order to eliminate the oxygen trapped in the Teflon. Also, to avoid external oxidation of the samples, the reservoir and drive syringes used were made of glass.

Sample preparation: Both reservoir syringes were filled with a degassed 40 μM methyl viologen solution prepared in glycine buffer pH 9.6. The MeV solutions were then partially reduced by adding through the tip of each syringe, a few microliters of a concentrated sodium dithionite solution prepared in the same buffer. Note that it is important not to leave excess dithionite in the sample because it will interfere with the oxygen ingress measurement.

Experimental conditions: Absorbance measurements were made at λ= 601nm, the wavelength at which MeV has the maximum absorption coefficient in the visible (ε_{601} = 13600 $M^{-1}cm^{-1}$, Mayhew 1978). In our experiments a spectral slit width of 0.5 nm and a pathlength of 1 cm were used. Since both drive syringes contained a partially reduced MeV solution no reaction was observed and each acquired trace was therefore a baseline with an OD corresponding to the oxidation status of the MeV solutions. The stop volume used depends on the type of experiment as explained below.

III.2.2.2. Determination of the oxygen ingress rate

Procedure: Since the objective of this experiment was to test the anaerobic capacities of the stopped-flow apparatus under normal working conditions, the stop volume suggested in the instrument manual (ca. 200 μl) was used. After flushing the mixing chamber and the whole circuit with the partially reduced MeV solution, the drive syringes were filled and 3 shots were discarded to assure that the observation cell placed after the mixing chamber was full of fresh sample. For each data point, one reference shot was acquired for time zero and, after a

certain time delay, one 'trigger' and one shot were acquired. The data points presented in Figure III.3 were obtained by changing the time delay from 1 to 16 min. Note that by pushing the trigger button without injecting new sample in the system, the trace acquired (here called 'trigger') corresponds to the old sample, after ageing for a certain time in the observation cell. The same procedure (refill drive syringes, discard 3 shots, acquire 1 reference shot, wait for the chosen time delay and acquire 1 trigger and 1 shot) was used for every time delay.

Results: The decrease in absorbance (ΔOD) with respect to the reference value taken at time zero was calculated for every time delay and plotted against time (Figure III.3). The oxygen ingress rate was calculated from the slope of the curve divided by 4 times the extinction coefficient of MeV. This calculation takes into account the fact that molecular oxygen is a 4 electron acceptor while MeV is a one electron donor.

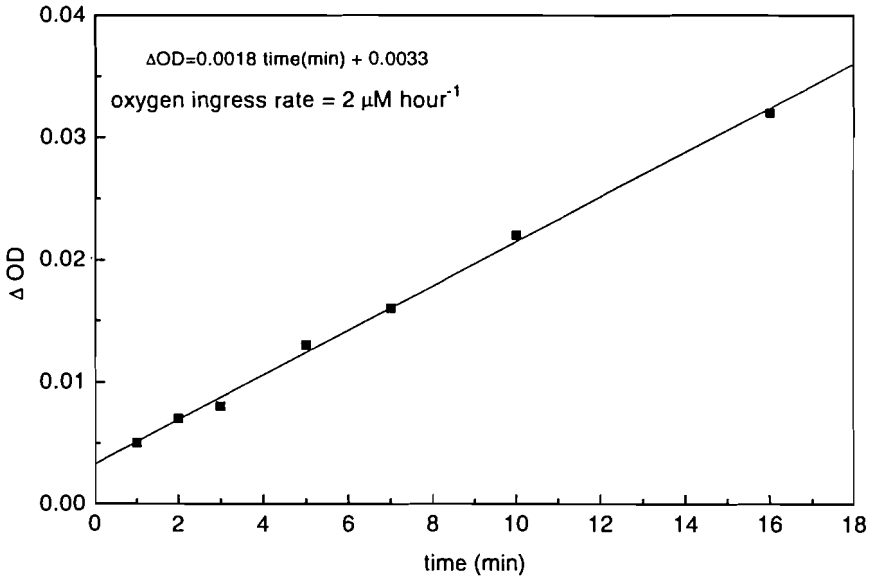

Figure III.3. Determination of the oxygen ingress rate. The decrease in absorbance (ΔOD) with respect to the reference value taken at time zero was measured for different time delays. The oxygen ingress rate was calculated from the slope of the curve taking in consideration the extinction coefficient of methyl viologen and the stoichiometry of the reaction with molecular oxygen.

III.2.2.3. Trying to localise the oxygen entrance point

Since there was oxygen leakage into the system, other experiments were performed with the objective of localising the oxygen ingress point. In these experiments, a smaller stop volume was used and a series of consecutive shots was acquired after a fixed time delay. With this procedure it was possible to probe the circuit connecting the drive syringes to the observation cell looking for areas of higher oxidation of the MeV solutions. The smaller the stop volume used, the more accurate the localisation of the oxygen entrance points was.

Procedure: After washing the sample handling unit with the partially reduced MeV sample the drive syringes were filled and the necessary number of shots was discarded to ensure complete substitution of the old sample inside the tubing and mixing chamber. The drive syringes were then refilled and a reference shot (t= 0) was acquired. After a time delay of 10 minutes a 'trigger' followed by the number of shots necessary to empty the drive syringes was recorded.

Results: During our tests this experiment was performed repeatedly with the sample handling unit under different conditions. In experiment A the sample handling unit was tested under normal working conditions and severe oxidation of the samples was observed. Tests B and C were performed with either nitrogen or argon flushing through the observation cell assembly, thermostat chamber (losing the thermostating capacity), bottom of drive syringes and fittings for the reservoir syringes. The absorbance measured for each shot relative to the reference absorbance taken before the time delay as a function of the total waste volume obtained for experiments A, B and C is represented in Figure III.4. Both the reference and the 'trigger' signal recorded after 10 min are plotted at volume zero. The 'trigger' signal always corresponded to a relative OD of 1, showing that no oxidation occurred inside the quartz observation cell.

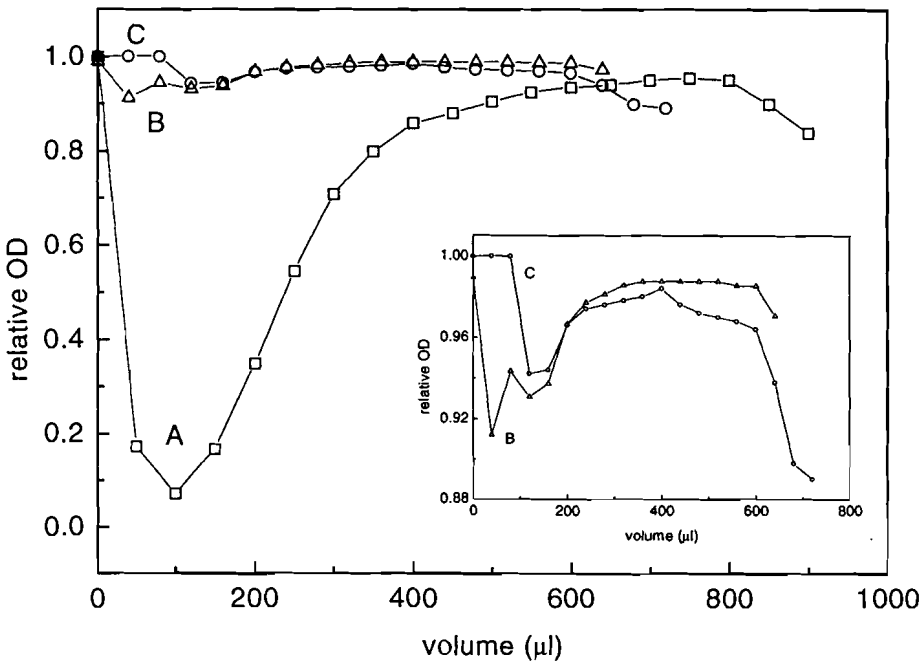

Figure III.4. Localisation of the oxygen ingress points of the sample handling unit of the stopped-flow apparatus. The circuit connecting the drive syringes to the observation cell was probed for points of oxygen entrance by performing a series of consecutive shots, with a very small stop volume, acquired after a fixed time delay. Tests A, B and C were performed under different working conditions: (A) normal working conditions, (B) with nitrogen or argon flushing through the system, (C) the same as in B but after two or three days of consecutive experiments keeping the system permanently under argon. INSERT: expanded scale to show that one point of oxygen entrance present in experiment B was eliminated in experiment C.

The comparison between the three curves showed that the main oxygen ingress point in curve A, located about 50 µl from the observation cell, was drastically reduced in curve B and completely eliminated in curve C. Since the volume of the quartz cell (mixing chamber and observation path) is ca. 75 µl, the main oxygen entrance during normal working conditions was probably situated at the Teflon junction between the tubing and the quartz cell. We believe that some oxygen trapped in the Teflon fittings was responsible for the oxidation still observed in test B. Between tests B and C two or three consecutive days of experiments, keeping argon flushing through the system the whole time, led to the complete elimination of this oxidation point, probably due to oxygen consumption by the reduced MeV samples. In curve B it is possible to distinguish this entrance point from another located about 120-160 µl from the observation cell, which is also present in curve C. The drive/fill valves are probably responsible for this other oxygen entrance point. The decrease in OD registered in the last shots of every experiment (situated at volumes larger than 500 µl) corresponds to oxidation of the sample solutions near the pistons of the drive syringes.

III.2.2.4 Measuring volumes

A different (aerobic) experiment was also performed in order to measure the volume of the tubing connecting the valves (fill/drive) with the observation cell. This experiment was also important to choose the stop volume to use in common experiments, in order to guarantee substitution of the old sample by the fresh one in the mixing chamber and observation cell.

Procedure: Again, a small stop volume (25 µl) was used in this experiment. After washing the stopped-flow circuits with water, both drive syringes were filled with an oxidised dye and **without discarding anything**, shots were acquired until a steady absorbance value was achieved.

Results: The plot of the relative OD versus total waste volume is shown in Figure III.5. Since no colour was registered before 100 µl, this corresponds to the volume of the tubing connecting the valves with the observation cell. From the picture is also evident that the stop volume to use with this sample handling unit cannot be less than 200 µl. For this stop volume, at least two shots must be discarded between different experiments, in order to prevent contamination of the samples.

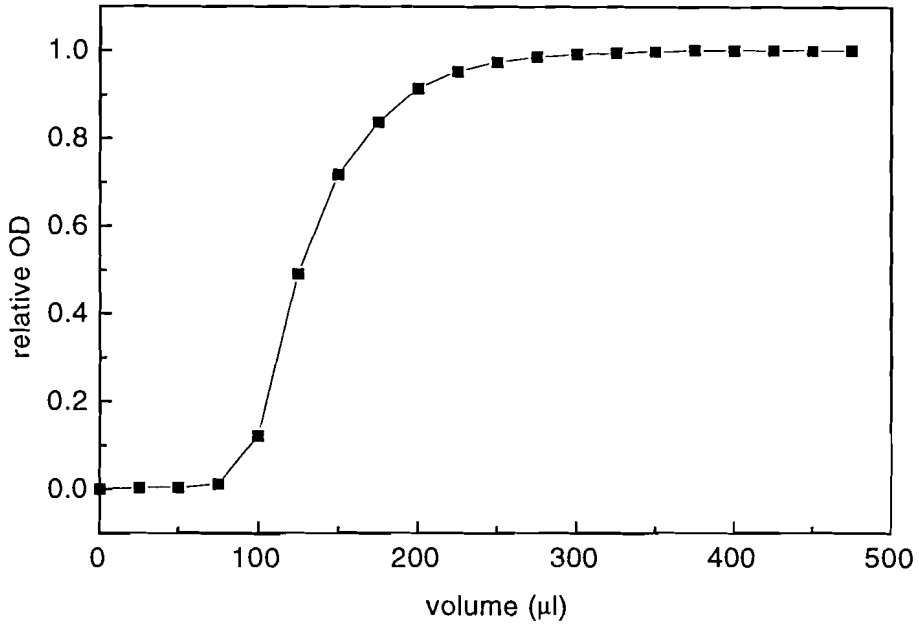

Figure III.5. Measurement of the volume of the tubing connecting the fill/drive valves to the observation cell. A coloured solution was used to measure the volume between the drive/fill valves and the observation cell. This volume is approximately 100 µl because no colour was observed for smaller volumes. This experiment also shows that a stop volume of at least 200 µl has to be used in order to guarantee substitution of the old sample by the fresh one in the mixing chamber and observation cell.

III.2.2.5 Conclusions

The tests performed with the SHU-61 from Hi-Tech Scientific Instruments demonstrated that there were serious problems of oxygen leakage into the system at the level of the Teflon fittings connecting the tubing to the quartz cell. This oxygen ingress point could be decreased by a continuous flux of nitrogen or argon through the observation cell assembly and thermostat chamber but, even under these circumstances, it would take several days to be eliminated completely. During that time it would be advisable to leave a dilute sodium dithionite solution inside the stopped-flow tubing, in order to consume all the oxygen trapped in the Teflon. The major disadvantage of this procedure would be the loss of the thermostating capacity, because the thermostat chamber would be full of nitrogen instead of water. Also, large quantities of nitrogen or argon would have to be used to keep an artificial anaerobic environment close to the leakage points, which is very expensive. Moreover, since we did not succeed in eliminating the oxidation of the test samples near the bottom of the drive syringes, the last shot of each refilled syringe should always be discarded, leading to considerable waste of material.

Considering the above arguments we reached the conclusion that, the only way to work under strict anaerobic conditions using the sample handling unit SHU-61 from Hi-Tech was to place it inside an anaerobic chamber. In this way, once the oxygen trapped in the Teflon has been removed, there are no further problems with contamination because the atmosphere of the chamber is free of oxygen.

Implementation of this protocol may save a couple of years to those wanting to perform stopped-flow experiments under strict anaerobic conditions.

III.2.3 Stopped-flow experiments on the reduction of cytochrome c_3 from *Desulfovibrio gigas* by sodium dithionite

The cytochrome c_3 was prepared as described in Louro et al., 1998b.

Rapid mixing kinetic experiments were carried out on a Gibson-Durrum stopped-flow instrument equipped with a 2 cm pathlength observation cell and connected to a digital system for the data collection and analysis (OnLIneSystem,USA). The signals acquired at λ= 552 nm were normalised in order to display the total oxidised fraction. Experiments were performed at a 0.25 M final buffer concentration (tris-maleate between pH 5.0 and 8.5 and glycine between pH 8.5 and 10.0), unless otherwise stated. All protein and buffer solutions were carefully degassed and the rapid-mixing instrument was exhaustively washed with degassed buffer in order to have a fully O_2-free environment. Solid sodium dithionite (Merck AG, FRG) was added to the degassed buffer to give the final desired concentration. The buffer system used for the reducing agent was the same as that in which the protein solution was dissolved except for the pH-dependence studies, in which, in view of the instability of sodium dithionite at pHs below 6.5, was initially dissolved in a low ionic strength degassed buffer ($\approx$1 mM glycine pH 8.2) whereas the protein solution was at the desired final pH in a higher concentrated buffer ($\approx$0.25 M); the final pH was measured after the mixing, this value being referred as the actual pH of the reaction.

In order to perform stopped-flow experiments in which the initial protein solution was already partially reduced, sodium dithionite solution was added to the desired amount. The degree of reduction was calibrated from the difference in absorbance at the α–peak at λ= 552 nm.

The experiments to study the dependence of the observed rate constants on the dithionite concentration were carried out at 25 °C, inside an anaerobic chamber with HI-TECH Scientific stopped-flow apparatus. Sodium dithionite solutions from 10 μM to 2 mM were prepared inside the anaerobic chamber in carefully degassed 0.25 M glycine buffer pH 9.6 by dilution of a stock solution standardised against potassium ferricyanide. The kinetic traces were fitted to a double exponential using the fitting routines of IS-1 Rapid Kinetics Software Suite from HI-TECH Scientific. The fast and slow observed rate constants obtained from the fittings were then represented as a function of the square root of the dithionite concentration after mixing.

The kinetic simulations were carried out using a FORTRAN program specially written for this purpose. The calculations were made according to the kinetic model presented in section III.3 and its particular adaptation to the stopped-flow studies with sodium dithionite (section III.4.1). The program calculates rate constants for the macroscopic electron transfer steps from the microscopic parameters using equations 14a-d from section III.3 with the optimised thermodynamic parameters for the fully reduced and deprotonated form of Dgc_3: e_1= -339 mV, e_2= -293 mV, e_3= -269 mV, e_4= -212 mV, I_{12}= 0 mV, I_{13}= +25 mV, I_{14}= -24 mV, I_{23}= -40 mV, I_{24}= +35 mV, I_{34}= +17 mV, I_{1H}= +62 mV, I_{2H}= +33 mV, I_{3H}= +33 mV, I_{4H}= +10 mV and g_B= -505 meV, (Louro et al., 1998b); e_i represents the microscopic redox potential of haem i when haems jkl are reduced, note that this redox potential is equivalent to the energy g_i (in meV) necessary to oxidise haem i under the same conditions; I_{ij}, represents the redox interacting potential between haems i and j and I_{iH} is the redox-Bohr interacting potential between haem i and proton H, these interacting potentials are equivalent to g_{ij} and g_{iH}, respectively the redox and redox-Bohr interacting energies (in meV); g_B is the ionisation energy of the fully reduced form which corresponds to a pK_a^{red} of 8.6. According to the adopted definitions (Turner et al.,1994 and 1996), positive cooperativities correspond to negative values for the interacting potentials.

The integrated form of the rate equations presented in appendix C was then used to calculate the time dependence of the populations of the redox stages from the pseudo-first order macroscopic rate constants, k_a', k_b', k_c' and k_d'. At any given time the total oxidised fraction was calculated from the populations of the stages through equation (16) of section III.4.1 and, in order to optimise the rate constants for the individual haems, the simulated curve computed for a given set of rate constants was compared with the kinetic data. The best set of parameters was obtained using the Marquardt method to fit simultaneously all the traces

acquired in the pH dependence study. All points were equally weighted and standard errors were computed with an assumed error of 0.1 for the oxidised fraction.

It is important to remark that the macroscopic rate constants k_a', k_b', k_c' and k_d', are pseudo-first order rate constants and therefore include the concentration of reducing agent. In the reaction of sodium dithionite with cytochrome c_3, the actual reducing agent is the dissociated species SO_2^-, the program calculates its concentration from the concentration of sodium dithionite used in the experiment and the equilibrium constant for the dissociation of $S_2O_4^{2-}$ to SO_2^- (see Results and Discussion section III.4.2).

III.2.4 Stopped-flow experiments on the interaction between cytochrome c_3, FMN and flavodoxin from *Desulfovibrio gigas*

Sample preparation - Cytochrome c_3 was purified as described in Louro et al., 1998b and flavodoxin from *Desulfovibrio gigas* was purified as previously described (Dubourdieu, 1970). Concentrated protein solutions were degassed by repeated cycles of vacuum and argon (grade N46 from Air Liquide), and transferred into an anaerobic chamber inside a closed container ful' of argon. The anaerobic chamber (MBraun MB150-GI) also had an argon atmosphere and was equipped with an oxygen analyser. To avoid the rapid reoxidation of the low potential cytochrome or of the reduced samples of flavodoxin in the presence of molecular oxygen, both sample preparation and experiments took place inside the anaerobic chamber, where the oxygen level was kept below 0.5 ppm. Reduced cytochrome c_3 samples were prepared outside the anaerobic chamber by flushing with hydrogen a degassed concentrated cytochrome solution containing catalytic amounts of hydrogenase. The reduced sample was kept under hydrogen pressure and subsequently transferred to the anaerobic chamber inside a closed bottle containing argon. Reduced flavodoxin samples were prepared inside the anaerobic chamber by addition of a concentrated solution of sodium dithionite, the excess being subsequently removed by two consecutive passages in a gel filtration column (Pharmacia PD-10), previously equilibrated with degassed buffer. Glycine/NaOH 0.25 M pH 9.6 was used as buffer in all the experiments reported here. It was always prepared inside the anaerobic chamber, using solid glycine and sodium hydroxide and carefully degassed deionised water (Millipore). Both oxidised and reduced protein solutions were obtained by dilution of the concentrated stock solutions to the desired concentrations with degassed buffer. After the experiments, the visible spectra of the samples were recorded in a SHIMADZU

UV 3100 spectrophotometer and the concentrations were determined using the following extinction coefficients: ε_{552}^{red}= 120 000 $M^{-1}cm^{-1}$ for the α-peak at λ= 552 nm in the reduced form of c_3, ε_{456}^{ox}= 10 200 $M^{-1}cm^{-1}$ for the peak at λ= 456 nm in the oxidised form of flavodoxin and ε_{445}^{ox}= 12 500 $M^{-1}cm^{-1}$ for the peak at λ= 445 nm in the oxidised form of FMN. All the concentrations referred to in the text correspond to final concentrations after mixing. Sodium dithionite solutions where prepared from solid material in degassed buffer. All reagents used were analytical grade.

Stopped-flow equipment - The kinetic experiments were carried out in a HI-TECH Scientific stopped-flow apparatus adapted to work inside an anaerobic chamber. The spectrophotometer unit (SU-40) was placed outside the anaerobic chamber and was connected by a quartz excitation light guide to the sample handling unit (SF-61) inside the anaerobic chamber. A spectral slit width of 0.5 nm was used for the excitation light. The detector used was the photomultiplier PM-60e from HI-TECH. All measurements were carried out in the absorbance mode with a 10 mm pathlength. The output signal was fed into a PC computer equiped with an appropriate software for data acquisition, IS-1 Rapid Kinetics Software Suite from HI-TECH Scientific. A thermostating bath (Haake G with Haake D8) was used to keep the temperature of the driving syringes and mixing chamber at 25 (±0.5) °C.

Data analysis - Traces with time scales ranging from 20 millisecond to 300 second were recorded at three different wavelengths, 433, 552 and 620 nm, to monitor the kinetic behaviour of the different species involved. At λ= 433 nm it is possible to follow the disappearance of oxidised flavins with a small optical contribution from cytochrome c_3, since there is pseudo-isosbestic point for the cytochrome at this wavelength. At λ= 552 nm both reduced cytochrome c_3 and the semiquinone form of the flavodoxin contribute to the observed signal, whereas at λ= 620 nm only the semiquinone signal is detectable, with an extinction coefficient similar to that at λ= 552 nm (see Figure III.6). Thus, in order to follow the cytochrome reduction without any optical contribution from flavodoxin, the signals recorded at λ= 620 nm were subtracted in the appropriate way from the signals at λ= 552 nm. Each trace at λ= 552 nm was then normalised in order to obtain the cytochrome reduced fraction $Y=(OD-OD^{ox})/(OD^{red}-OD^{ox})$. For each cytochrome concentration, the reference values for OD^{ox} and OD^{red} were obtained from the optical density at time zero and infinity, respectively, obtained in parallel experiments in which the same sample of oxidised cytochrome was reduced by excess sodium dithionite.

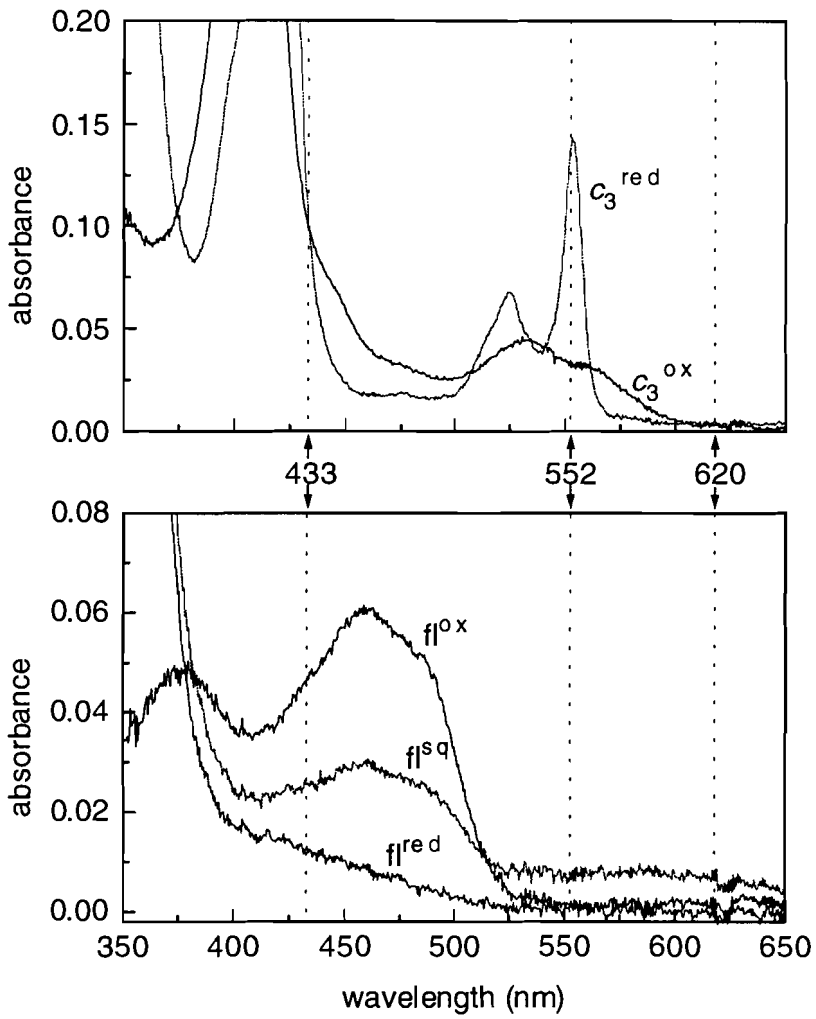

Figure III.6. Visible spectra from cytochrome c_3 and flavodoxin from *D. gigas* at different oxidation states. The top panel shows the spectra of fully oxidised (c_3^{ox}) and fully reduced (c_3^{red}) cytochrome c_3 and the bottom panel shows the spectra of flavodoxin in the oxidised flavoquinone form (fl^{ox}), in the half-reduced semiquinone form (fl^{sq}) and in the fully reduced hydroquinone form (fl^{red}). The observation wavelengths used in the stopped-flow experiments are indicated by dotted lines. The reduction of flavodoxin can be monitored at λ= 433 nm without significant optical interference from the cytochrome. Semiquinone formation and disappearance can be followed at λ= 620 nm. The reduction of the cytochrome is best monitored at λ= 552 nm and the optical contribution from the semiquinone at this wavelength can be subtracted using the signal at λ= 620 nm.

Simulations were made with a FORTRAN computer program specially written for the kinetic model previously described. The program includes different routines for the integration of the system of differential equations and the fitting of the individual rate constants, always assuming fast internal equilibration of electrons. The integration is done by the fourth order Runge-Kutta method with adaptive step size and the fitting procedures were made using the Marquardt method, using FORTRAN routines adapted from Press et al., 1989. The thermodynamic parameters used in the calculations involving cytochrome c_3 were those reported in the previous section (III.2.3). The macroscopic redox potentials used for flavodoxin were $E_{sq/red}$= -440 mV and $E_{ox/sq}$= -260 mV for the semiquinone/hydroquinone and oxidised/semiquinone pairs, respectively (Costa, 1989).

III.3 Kinetic model

Since four electrons are needed to achieve full reduction of Dgc_3 and the reducing agents used can only give one electron at a time, for each electron transfer event, the complete reaction scheme (Scheme I) must take into account at least the following steps: (1) complex formation; (2) electron transfer within the complex; and, (3) complex dissociation, in order to allow another molecule of electron donor to interact with the same molecule of cytochrome.

$$c_i^{ox} + A^{red} \underset{k^i_{-1}}{\overset{k^i_{+1}}{\rightleftharpoons}} [c_i^{ox} - A^{red}] \underset{k^i_{-2}}{\overset{k^i_{+2}}{\rightleftharpoons}} [c_i^{red} - A^{ox}] \underset{k^i_{-3}}{\overset{k^i_{+3}}{\rightleftharpoons}} c_i^{red} + A^{ox} \qquad \text{(Scheme I)}$$

In Scheme I, c_i^{ox} is a cytochrome molecule with haem i oxidised and c_i^{red} the same molecule with haem i already reduced; A^{red} and A^{ox} correspond to the electron donor in the reduced and oxidised forms, respectively. The complexes that result from the association of the two redox partners are represented in brackets. The bimolecular rate constant for the association process between oxidised (or partially oxidised) cytochrome and the reducing agent is k^i_{+1}, k^i_{-1} being the rate constant for the dissociation of the same complex before electron transfer takes place; k^i_{+2} and k^i_{-2} are the electron exchange rate constants directly to and from haem i, respectively; k^i_{+3} is the corresponding unimolecular dissociation rate constant; and k^i_{-3} is the bimolecular association rate constant between reduced (or partially reduced) cytochrome and the oxidised electron donor.

This complete model is rather complicated and involves a large number of parameters. At least six rate constants are required for each of the four haems, for the reactions both of the protonated and the deprotonated forms of the cytochrome, giving a total of 48 rate constants, which are impossible to define under our experimental conditions. However, since the experiments were performed at very high ionic strength, on the basis of previous reported results for the homologous cytochrome c_3 from *D. vulgaris* (Capeillère-Blandin et al. 1986 ; De Francesco et al. 1994), the first simplification which can be introduced is the collisional approximation (Scheme II):

$$c_i^{ox} + A^{red} \underset{k_{-i}}{\overset{k_{+i}}{\rightleftharpoons}} c_i^{red} + A^{ox} \qquad \text{(Scheme II)}$$

In this simplified scheme, the rate constants, k_{+i} and k_{-i}, refer to the rate of reduction and the rate of oxidation of each particular haem i by the reducing or oxidising agent A. For each individual haem, these rate constants are composite parameters which include information on complex formation and on the electron transfer process within the complex. Since it does not include an intermediate complex formation, this simplified model can neither account for saturation kinetics nor for a lag phase in the reduction process. Nonetheless, this approximation seems appropriate for simulating the data acquired under the experimental conditions used in the present work (see Sections III.4 and III.5).

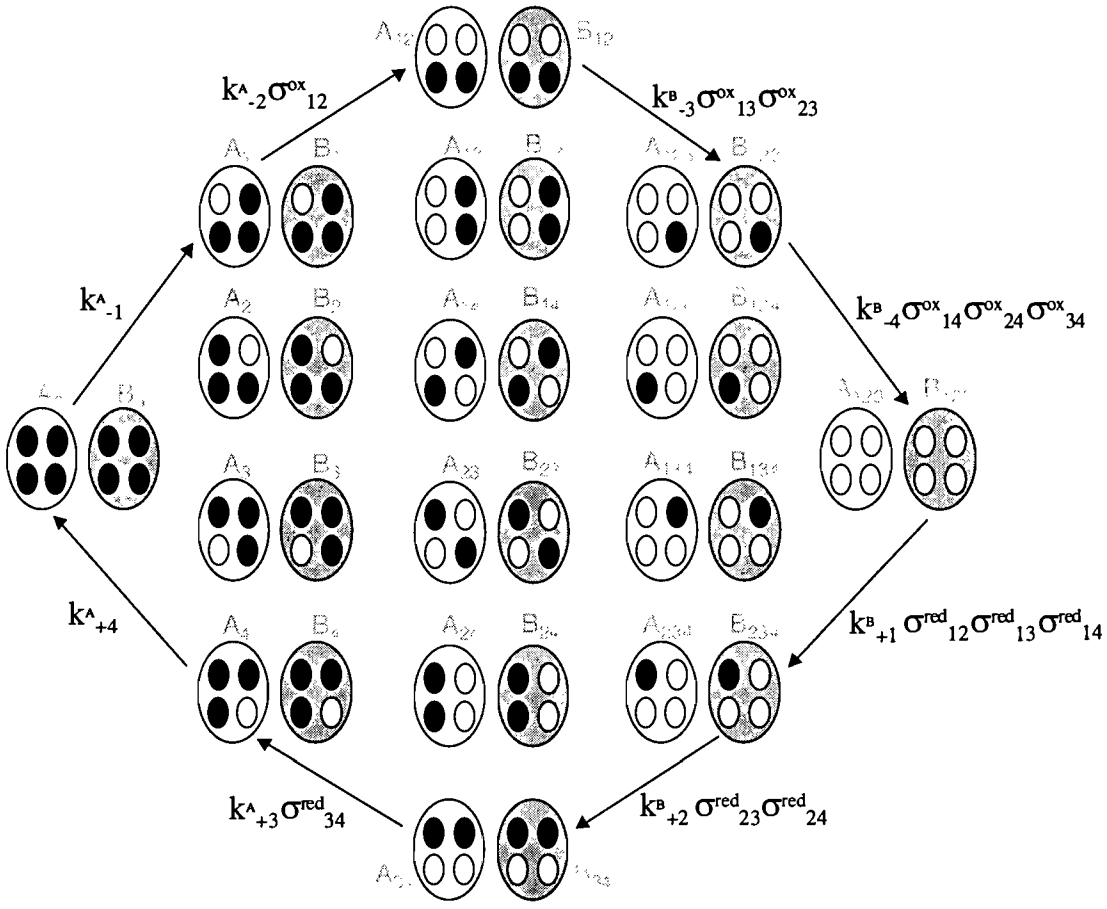

Figure III.7. Definition of the rate constants involved in the electron transfer reactions between the 32 microstates or the five oxidation stages and the electron donor or the electron acceptor. Protonated microstates are designated by A and deprotonated ones by B. The numbers in subscript indicate the haems which are oxidised in each microstate. The redox stages are numbered according to the number of oxidised haems in the microstates that belong to each stage. Rate constants of the reductive pathway are indicated by a subscript with a plus sign and the number of the haem which is being reduced, whereas those of the oxidative pathway have a subscript with a minus sign and the number of the haem which is being oxidised. The superscripts A and B indicate the protonation state of the microstates involved in the electron transfer step. Sigma factors of the reductive pathway have 'red' as a superscript whereas those of the oxidative pathway have 'ox' (see text for details on the significance of these factors). For the sake of simplicity only a few of the possible electron transfer steps are represented in the picture. Also, the electron donor or electron acceptor are not represented.

Figure III.7 shows only some of the possible electron transfer steps between the 32 microstates of cytochrome c_3 and the electron donor or electron acceptor. Since the rate constants for the individual haems are microscopic rather than macroscopic parameters, their determination depends upon an approach based on the microscopic populations. Microscopic reversibility is assumed for all electron transfer steps in this model. Instantaneous internal equilibration between the microstates in each stage is also assumed, because the rate for intramolecular electron exchange is much faster than that for the bimolecular reaction between cytochrome c_3 and the electron donor, at least in the concentration range used. The evidence for this comes from NMR data, which show that the intramolecular exchange rate for the electrons is faster than 10^5 s^{-1} for Dgc_3 (Santos et al., 1984a), and that the exchange rate for protons is diffusion controlled, as shown for the homologous Dvc_3 (Turner et al., 1996), whereas the faster observed reduction rates measured in the current work are of the order of 10^3 s^{-1}.

NMR studies also indicated that the second order rate constant for intermolecular electron exchange between cytochrome c_3 molecules belonging to different redox stages is of the order of 10^4 $M^{-1}s^{-1}$ (Santos, 1984a). Since, for the experimental conditions used in this work, the observed rate constants of the electron transfer reactions between Dgc_3 and the exogenous electron donor/acceptor are at least ten times higher than those expected for this process, all intermolecular electron transfer reactions were neglected in the present kinetic model.

The immediate consequence of fast intramolecular electron exchange is the appearance of thermodynamic equilibrium within each redox stage. Under these conditions, the complicated kinetic system comprising 32 microstates collapses into 5 macroscopic redox stages related to each other by four direct and four inverse macroscopic rate constants (see Figure III.7). The rate equations for this simple model are listed below (equations (1a-e)):

$$\frac{d[\text{stage IV}]}{dt} = -k_d[\text{stage IV}][A^{red}] + k_{-d}[\text{stage III}][A^{ox}] \quad (1a)$$

$$\frac{d[\text{stage III}]}{dt} = k_d[\text{stage IV}][A^{red}] + k_{-c}[\text{stage II}][A^{ox}] - k_{-d}[\text{stage III}][A^{ox}] - k_c[\text{stage III}][A^{red}] \quad (1b)$$

$$\frac{d[\text{stage II}]}{dt} = k_c[\text{stage III}][A^{red}] + k_{-b}[\text{stage I}][A^{ox}] - k_{-c}[\text{stage II}][A^{ox}] - k_b[\text{stage II}][A^{red}] \quad (1c)$$

$$\frac{d[\text{stage I}]}{dt} = k_b[\text{stage II}][A^{red}] + k_{-a}[\text{stage 0}][A^{ox}] - k_{-b}[\text{stage I}][A^{ox}] - k_a[\text{stage I}][A^{red}] \quad (1d)$$

$$\frac{d[\text{stage 0}]}{dt} = k_a[\text{stage I}][A^{red}] - k_{-a}[\text{stage 0}][A^{ox}] \quad (1e)$$

The time dependence of the total reduced haem is then obtained from the sum of all stages weighted according to the number of reduced haems. Since the ratios between forward and reverse rate constants are equal to the macroscopic equilibrium constants, the total reduced haem can be expressed in terms of the time dependent concentrations of the five stages and reducing agent, four macroscopic rate constants, k_a, k_b, k_c and k_d, for the electron transfer steps between stages 0 to IV, and four macroscopic equilibrium constants K_I, K_{II}, K_{III} and K_{IV}, defined for the equilibria between stages 0 to IV (equation (2)).

$$\frac{d[\text{total red haem}]}{dt} = \left([A^{red}][\text{stage I}] - \frac{[A^{ox}][\text{stage 0}]}{K_I}\right)k_a + \left([A^{red}][\text{stage II}] - \frac{[A^{ox}][\text{stage I}]}{K_{II}}\right)k_b + \left([A^{red}][\text{stageIII}] - \frac{[A^{ox}][\text{stage II}]}{K_{III}}\right)k_c + \left([A^{red}][\text{stage IV}] - \frac{[A^{ox}][\text{stage III}]}{K_{IV}}\right)k_d \quad (2)$$

However, in order to get information on the kinetic behaviour of individual haems, it is necessary to establish a relationship between the macroscopic rate constants and the rate constants for the individual haems. This relationship can be obtained by defining the rate equations for the 32 microstates, grouping them together in stages, defining the rate equation for the total reduced haem and finally comparing it with equation (2). In this process, it is assumed that all electron transfer reactions that lead to the reduction or oxidation of any particular microstate are independent.

To give an example, the differential equation that describes the time evolution of a deprotonated microstate c_i^B with haem i oxidised and haems j, k and l already reduced, must include as positive terms all the processes that lead to the formation of c_i^B and as negative terms all the processes that lead to its consumption (equation (3)). Formation of c_i^B can occur either by c_{ij}^B, c_{ik}^B and c_{il}^B being reduced by A^{red} with rate constants k^B_{+j}, k^B_{+k} and k^B_{+l} respectively, or by oxidation of c_0^B by A^{ox}, with a rate constant k^B_{-i}. Consumption of c_i^B can occur either by reduction with A^{red} with the rate constant k^B_{+i} or by oxidation with A^{ox} with

rate constants, k^B_{-j}, k^B_{-k} and k^B_{-l} (see Figure III.7). Thus, the differential equation can be written:

$$\frac{d[c_i^B]}{dt} = [A^{red}]\left(\sum_{jkl} k^B_{+j}\sigma_{ij}^{red}[c_{ij}^B] - k^B_{+i}[c_i^B]\right) - [A^{ox}]\left([c_i^B]\sum_{jkl} k^B_{-j}\sigma_{ij}^{ox} - k^B_{-i}[c_0^B]\right) \quad (3)$$

where the sigma factors σ_{ij}^{red} and σ_{ij}^{ox} are related to the redox interacting potentials as explained below.

Because of the fast internal equilibration, the concentration of any microstate can be expressed as a fixed fraction of the total concentration of the stage it belongs to. Therefore, the rate equation of c_i^B, a deprotonated microstate from stage I can be expressed as

$$\frac{d[c_i^B]}{dt} = \frac{[c_i^B]}{\sum_{stagel}([c_i^A]+[c_i^B])}\frac{d[\text{stage I}]}{dt} = \chi_i^B\frac{d[\text{stage I}]}{dt} \quad (4)$$

where the constant χ_i^B represents the fractional population of microstate c_i^B which is solely defined by the thermodynamic parameters. The substitution of the concentrations of microstates by the fractional populations and time dependent concentrations of stages in equation (3) leads to equation (5)

$$\begin{aligned}\frac{d[c_i^B]}{dt} = {} & [A^{red}]\left([\text{stage II}]\sum_{jkl} k^B_{+j}\sigma_{ij}^{red}\chi_{ij}^B - [\text{stage I}]k^B_{+i}\chi_i^B\right) \\ & -[A^{ox}]\left([\text{stage I}]\chi_i^B\sum_{jkl} k^B_{-j}\sigma_{ij}^{ox} - [\text{stage 0}]k^B_{-i}\chi_0^B\right)\end{aligned} \quad (5)$$

To reduce the number of parameters in this equation we can invoke microreversibility to correlate the direct and inverse rate constants. Microscopic reversibility at infinite time implies that (cf. Figure III.7)

$$\begin{aligned}[c_i^B]_\infty[A^{red}]_\infty k^B_{+i} &= [c_0^B]_\infty[A^{ox}]_\infty k^B_{-i} \\ [\text{stage I}]_\infty[A^{red}]_\infty k^B_{+i}\chi_i^B &= [\text{stage 0}]_\infty[A^{ox}]_\infty k^B_{-i}\chi_0^B\end{aligned} \quad (6a)$$

$$\chi_0^B k^B_{-i} = \frac{1}{K_I}k^B_{+i}\chi_i^B, \quad (6b)$$

and

$$\begin{aligned}
&\left[c_{ij}^{B}\right]_{\infty}\left[A^{red}\right]_{\infty}k_{+j}^{B}\sigma_{ij}^{red} = \left[c_{i}^{B}\right]_{\infty}\left[A^{ox}\right]_{\infty}k_{-j}^{B}\sigma_{ij}^{ox} \\
&\left[\text{stage II}\right]_{\infty}\left[A^{red}\right]_{\infty}k_{+j}^{B}\sigma_{ij}^{red}\chi_{ij}^{B} = \left[\text{stage I}\right]_{\infty}\left[A^{ox}\right]_{\infty}k_{-j}^{B}\sigma_{ij}^{ox}\chi_{i}^{B}
\end{aligned} \tag{6c}$$

$$\chi_{i}^{B}k_{-j}^{B}\sigma_{ij}^{ox} = \frac{1}{K_{II}}k_{+j}^{B}\sigma_{ij}^{red}\chi_{ij}^{B} \tag{6d}$$

where K_I and K_{II} are the macroscopic equilibrium constants defined between stages 0 and I, and stages I and II, respectively. Expansion of the sums and substitution in equation (5) leads to equation (7) where the rate equation for microstate c_i^B is expressed as a function of the time dependent concentrations of each stage and of the reducing agent, macroscopic equilibrium constants, sigma factors, fractional populations and reduction rate constants for the individual haems.

$$\begin{aligned}
\frac{d\left[c_{i}^{B}\right]}{dt} = &\left(\left[A^{red}\right]_{\text{stage II}} - \frac{\left[A^{ox}\right]\left[\text{stage I}\right]}{K_{II}}\right)\sum_{jkl}k_{+j}^{B}\sigma_{ij}^{red}\chi_{ij}^{B} \\
&-\left(\left[A^{red}\right]_{\text{stage I}} - \frac{\left[A^{ox}\right]\left[\text{stage 0}\right]}{K_{I}}\right)k_{+i}^{B}\chi_{i}^{B}
\end{aligned} \tag{7}$$

The extension from equation (7) to the sum of all microstates belonging to stage I (protonated and deprotonated forms of c_i, c_j, c_k and c_l) given in equation (8) is straightforward.

$$\begin{aligned}
\sum_{stagel}\frac{d\left(\left[c_{i}^{A}\right]+\left[c_{i}^{B}\right]\right)}{dt} = &\left(\left[A^{red}\right]_{\text{stage II}} - \frac{\left[A^{ox}\right]\left[\text{stage I}\right]}{K_{II}}\right)\begin{pmatrix}
\sum_{jkl}k_{+j}^{A}\sigma_{ij}^{red}\chi_{ij}^{A} + \sum_{jkl}k_{+j}^{B}\sigma_{ij}^{red}\chi_{ij}^{B} \\
+\sum_{ikl}k_{+i}^{A}\sigma_{ij}^{red}\chi_{ij}^{A} + \sum_{ikl}k_{+i}^{B}\sigma_{ij}^{red}\chi_{ij}^{B} \\
+\sum_{ijl}k_{+i}^{A}\sigma_{ik}^{red}\chi_{ik}^{A} + \sum_{ijl}k_{+i}^{B}\sigma_{ik}^{red}\chi_{ik}^{B} \\
+\sum_{ijk}k_{+i}^{A}\sigma_{il}^{red}\chi_{il}^{A} + \sum_{ijk}k_{+i}^{B}\sigma_{il}^{red}\chi_{il}^{B}
\end{pmatrix} \\
&-\left(\left[A^{red}\right]_{\text{stage I}} - \frac{\left[A^{ox}\right]\left[\text{stage 0}\right]}{K_{I}}\right)\begin{pmatrix}
k_{+i}^{A}\chi_{i}^{A} + k_{+i}^{B}\chi_{i}^{B} \\
+k_{+j}^{A}\chi_{j}^{A} + k_{+j}^{B}\chi_{j}^{B} \\
+k_{+k}^{A}\chi_{k}^{A} + k_{+k}^{B}\chi_{k}^{B} \\
+k_{+l}^{A}\chi_{l}^{A} + k_{+l}^{B}\chi_{l}^{B}
\end{pmatrix}
\end{aligned} \tag{8}$$

The differential equation for the total reduced haem is then calculated from the sum of all microstates, with each microstate weighted by the number of reduced haems (equation (9)):

$$\frac{d[\text{total red haem}]}{dt} = 4\sum_{stage0}\frac{d\left(\left[c_0^A\right]+\left[c_0^B\right]\right)}{dt} + 3\sum_{stageI}\frac{d\left(\left[c_i^A\right]+\left[c_i^B\right]\right)}{dt} + 2\sum_{stageII}\frac{d\left(\left[c_{ij}^A\right]+\left[c_{ij}^B\right]\right)}{dt} + \sum_{stageIII}\frac{d\left(\left[c_{ijk}^A\right]+\left[c_{ijk}^B\right]\right)}{dt} \quad (9)$$

Note that, when the total reduced haem is calculated, the second negative term in equation (8), will cancel out with a symmetric term coming from $d([c_0^A]+[c_0^B])/dt$.

This example was included here to show how the pattern observed in equation (2) also emerges from the description based on the 32 microstates, making it possible to establish a relationship between the macroscopic rate constants of equation (2) and the microscopic rate constants for the individual haems.

The number of parameters is significantly reduced by adopting the collisional model, since only two rates (k_{+i} and k_{-i}) are considered for each of the four haems in a given protonation state. By assuming microscopic reversibility, the equilibrium constant establishes a relationship between the forward and reverse rates (equation (10)), further reducing the number of parameters from 16 to eight reduction rate constants, one for each of the four haems for the protonated and deprotonated forms of the cytochrome.

$$k_{-i} = k_{+i}\exp\left(\frac{(E_A^0 - e_i)F}{RT}\right) \quad (10)$$

In equation (10) E^0_A is the midpoint redox potential of the reducing agent A, and e_i is the microscopic redox potential of haem i when all the other haems are reduced. Note that the product $(E^0_A - e_i)F$ is the ΔG^0 for the electron transfer reaction. However, due to the redox interacting potentials, the redox potential of haem i changes according to the haems which are already oxidised, i.e. the redox potential of haem i when haem j is oxidised, is given by $e_i^j = e_i + I_{ij}$. This change in the redox potential of the haems implies a change in the driving force, ΔG^0, for the electron transfer reaction and, therefore, the rate constant for a particular haem can change along the reduction process. This effect is accounted for by the introduction of sigma factors for the reductive (σ_{ij}^{red}) and the oxidative (σ_{ij}^{ox}) pathways. For example, if haems j and k are still oxidised, k_{-i} the rate constant for the oxidation of haem i, must be multiplied by $\sigma_{ij}^{ox}\,\sigma_{ik}^{ox}$ and k_{+i}, the rate constant for the reduction of the same haem must be multiplied by $\sigma_{ij}^{red}\,\sigma_{ik}^{red}$ (see Figure III.7). These sigma factors enabled us to establish the

relation between rate constants in different redox states. The mathematical expression that relates σ_{ij}^{red} with the redox interacting potential, I_{ij}, was derived from the Marcus equation for long range electron transfer (Marcus and Sutin, 1985) assuming that only the driving force, ΔG^0, changes during the reduction process (equation (11)).

$$\sigma_{ij}^{red} = \exp\left[\frac{I_{ij}F}{2RT}\left(1+\frac{\Delta G^0}{\lambda}+\frac{I_{ij}}{2\lambda}\right)\right] \qquad (11)$$

Note that, if ΔG^0 and I_{ij} are small relative to the reorganisation energy λ, the second and third terms inside the parenthesis will be much smaller than one, and the redox sigma factors will be given by equation (12):

$$\sigma_{ij}^{red} = \exp\left(\frac{I_{ij}F}{2RT}\right) \qquad (12)$$

thus, depending exclusively on the redox interacting potentials. Since, for the reactions studied with the only exception of the dithionite case, ΔG^0 is smaller than 0.3 eV and I_{ij} smaller than 0.04 eV, and the value of the reorganisation energy for this particular case is in the range 1–1.3 eV (P. L. Dutton, personal communication), this seems a reasonable approximation. In fact, ΔG^0 is small with respect to λ in most biological electron transfer reactions (Davidson, V.L., 1996). It follows that the sigma factors for the reductive and oxidative pathways are related to one another by $\sigma_{ij}^{red} = 1/\sigma_{ij}^{ox}$, such that the change in the equilibrium constant is equally distributed between the direct and inverse electron transfer reactions.

On the same theoretical basis, another set of sigma factors (σ_{iH}) enabled us to further reduce the number of parameters of the kinetic model by establishing a relationship between the rate constants for the protonated (A) and deprotonated (B) forms. According to the thermodynamic model presented in section II.3.3, the pH dependence of the redox potentials can be accounted for by the redox-Bohr interacting potentials (I_{iH}) defined between haem i and proton H. Again, assuming that the modifications caused by the pH in the rate constants for the individual haems depend uniquely on the change in the driving force for the electron transfer reaction, the sigma factors for the reduction pathway are related to the redox-Bohr interacting potentials through equation (13), derived from the Marcus equation.

$$\sigma_{iH}^{red} = \exp\left[\frac{-I_{iH}\,F}{2RT}\left(1+\frac{\Delta G^0}{\lambda}-\frac{I_{iH}}{2\lambda}\right)\right] \approx \exp\left(\frac{-I_{iH}\,F}{2RT}\right) \qquad (13)$$

Since the largest redox-Bohr energy is ca. 0.07 eV, i.e. much smaller than the reorganisation energy, the simplification considered above for the definition of redox sigma factors (σ_{ij}) is also valid for those of the protons (σ_{iH}), and the simplified expression for the definition of proton sigma factors was therefore used in the present model.

However, it should be noted that the assumption of rate constants depending exclusively on the change in ΔG^0 is more restrictive for the case of protons. Protonation of some aminoacid residues may cause structural changes that may affect the reorganisation energy, whereas the intramolecular electron transfer is sufficiently fast to minimise structural differences between the electronic microstates of any give stage. Also, the modification of charges at the surface of the protein, can affect complex formation and change the electron transfer rate by a mechanism independent of ΔG^0.

The introduction of proton sigma factors reduces the number of parameters from eight to four rate constants, one for each haem in the reference protonation state. Because most of the electron transfer reactions presented in this study were carried out at high pH, we decided to take the deprotonated state as the reference state. The individual rate constants in the protonated and deprotonated forms are therefore related by $k_{+i}^{A} = k_{+i}^{B}\,\sigma_{iH}$. Note that, according to the approximations made, this relationship is totally defined by the thermodynamic parameters (see equation (13)).

The critical result of introducing the sigma factors approximation is that the macroscopic rate constants k_a, k_b, k_c and k_d can now be related to the microscopic rates for the individual haems in the deprotonated form, k_{+i}, through sums of the relevant products of sigma factors and fractional populations, i.e. ultimately through the thermodynamic parameters (equations 14a-d).

$$k_a = \begin{bmatrix} \left(k_{+1}\chi_1^B + k_{+2}\chi_2^B + k_{+3}\chi_3^B + k_{+4}\chi_4^B\right) \\ +\left(k_{+1}\sigma_{1H}\chi_1^A + k_{+2}\sigma_{2H}\chi_2^A + k_{+3}\sigma_{3H}\chi_3^A + k_{+4}\sigma_{4H}\chi_4^A\right) \end{bmatrix} \quad (14a)$$

$$k_b = \begin{bmatrix} k_{+1}\left(\sigma_{12}\chi_{12}^B + \sigma_{13}\chi_{13}^B + \sigma_{14}\chi_{14}^B\right) + k_{+1}\sigma_{1H}\left(\sigma_{12}\chi_{12}^A + \sigma_{13}\chi_{13}^A + \sigma_{14}\chi_{14}^A\right) \\ +k_{+2}\left(\sigma_{12}\chi_{12}^B + \sigma_{23}\chi_{23}^B + \sigma_{24}\chi_{24}^B\right) + k_{+2}\sigma_{2H}\left(\sigma_{12}\chi_{12}^A + \sigma_{23}\chi_{23}^A + \sigma_{24}\chi_{24}^A\right) \\ +k_{+3}\left(\sigma_{13}\chi_{13}^B + \sigma_{23}\chi_{23}^B + \sigma_{34}\chi_{34}^B\right) + k_{+3}\sigma_{3H}\left(\sigma_{13}\chi_{13}^A + \sigma_{23}\chi_{23}^A + \sigma_{34}\chi_{34}^A\right) \\ +k_{+4}\left(\sigma_{14}\chi_{14}^B + \sigma_{24}\chi_{24}^B + \sigma_{34}\chi_{34}^B\right) + k_{+4}\sigma_{4H}\left(\sigma_{14}\chi_{14}^A + \sigma_{24}\chi_{24}^A + \sigma_{34}\chi_{34}^A\right) \end{bmatrix} \quad (14b)$$

$$k_c = \begin{bmatrix} k_{+1}\left(\sigma_{12}\sigma_{13}\chi_{123}^B + \sigma_{12}\sigma_{14}\chi_{124}^B + \sigma_{13}\sigma_{14}\chi_{134}^B\right) + k_{+1}\sigma_{1H}\left(\sigma_{12}\sigma_{13}\chi_{123}^A + \sigma_{12}\sigma_{14}\chi_{124}^A + \sigma_{13}\sigma_{14}\chi_{134}^A\right) \\ +k_{+2}\left(\sigma_{12}\sigma_{23}\chi_{123}^B + \sigma_{12}\sigma_{24}\chi_{124}^B + \sigma_{23}\sigma_{24}\chi_{234}^B\right) + k_{+2}\sigma_{2H}\left(\sigma_{12}\sigma_{23}\chi_{123}^A + \sigma_{12}\sigma_{24}\chi_{124}^A + \sigma_{23}\sigma_{24}\chi_{234}^A\right) \\ +k_{+3}\left(\sigma_{13}\sigma_{23}\chi_{123}^B + \sigma_{13}\sigma_{34}\chi_{134}^B + \sigma_{23}\sigma_{34}\chi_{234}^B\right) + k_{+3}\sigma_{3H}\left(\sigma_{13}\sigma_{23}\chi_{123}^A + \sigma_{13}\sigma_{34}\chi_{134}^A + \sigma_{23}\sigma_{34}\chi_{234}^A\right) \\ +k_{+4}\left(\sigma_{14}\sigma_{24}\chi_{124}^B + \sigma_{14}\sigma_{34}\chi_{134}^B + \sigma_{24}\sigma_{34}\chi_{234}^B\right) + k_{+4}\sigma_{4H}\left(\sigma_{14}\sigma_{24}\chi_{124}^A + \sigma_{14}\sigma_{34}\chi_{134}^A + \sigma_{24}\sigma_{34}\chi_{234}^A\right) \end{bmatrix} \quad (14c)$$

$$k_d = \begin{bmatrix} k_{+1}\sigma_{12}\sigma_{13}\sigma_{14}\left(\chi_{1234}^B + \sigma_{1H}\chi_{1234}^A\right) \\ +k_{+2}\sigma_{12}\sigma_{23}\sigma_{24}\left(\chi_{1234}^B + \sigma_{2H}\chi_{1234}^A\right) \\ +k_{+3}\sigma_{13}\sigma_{23}\sigma_{34}\left(\chi_{1234}^B + \sigma_{3H}\chi_{1234}^A\right) \\ +k_{+4}\sigma_{14}\sigma_{24}\sigma_{34}\left(\chi_{1234}^B + \sigma_{4H}\chi_{1234}^A\right) \end{bmatrix} \quad (14d)$$

All sigma factors in equations 14a-d were defined for the reduction pathway, the superscript 'red' was omitted in order to simplify the mathematical expressions. Also omitted was the superscript 'B' from all individual rate constants. Since the haem-haem interacting potentials (I_{ij}) do not depend upon the pH, the redox sigma factors are also pH independent. However, the fractional populations of protonated, χ_i^A, χ_{ij}^A, χ_{ijk}^A, and deprotonated, χ_i^B, χ_{ij}^B, χ_{ijk}^B, microstates are pH dependent. For pH values below pK_a^{ox} the protonated forms predominate and χ_i^A, χ_{ij}^A, $\chi_{ijk}^A > \chi_i^B$, χ_{ij}^B, χ_{ijk}^B whereas the opposite is observed for pH values above pK_a^{red}.

The significance of the factors weighting each rate constant in the different redox stages is easily understood. For a given stage, the rate constant of haem i, k_{+i}, is multiplied by the sum of all fractional population terms of that particular stage, having i as subscript. The rate constant is therefore weighted by the thermodynamic probability of finding cytochrome molecules with haem i still oxidised. The redox sigmas (σ_{ij}) establish the relationship between the rate constant of haem i in the reference state, when all the other haems are already

reduced, and the rate constant of the same haem when some of the other haems are still oxidised. The proton sigma (σ_{iH}) converts the rate constant of haem i for the deprotonated (B) form into the rate constant of the same haem for the protonated (A) one.

Equation (2) shows that a maximum of four composite rate constants can be extracted from the kinetic data and equations 14a-d show that only the rate constants for thermodynamically distinct haems can be defined. If the four haems were all thermodynamically separated, only one of them would change its oxidation state in each step and the fractional population terms would be such that four independent equations would be obtained, making it possible the determination of the microscopic rate constants from the composite macroscopic parameters. On the other hand, if the four haems had equal thermodynamic parameters, they would all change their oxidation state by the same amount in all steps. Their fractional populations and their sigma factors would be equal and the factors affecting each individual rate constant would be exactly the same in all four equations, making it impossible to distinguish between the individual rate constants, because the solution would be indeterminate.

It should be noted that even for thermodynamically separated haems the accurate determination of all four individual rate constants is not necessarily possible. The largest rate constant has to be that of the haem which is reduced first and the rate constants for the remaining haems have to decrease according to their order of reduction. Otherwise, due to the fast internal equilibration of the electrons, a smaller number of rate constants, compared to the number of haems, would be determined.

In order to find the individual reduction rate constants, simulated curves must be compared to the experimental data. These simulated curves are generated by numerical integration of the set of differential equations, starting from the populations at time zero, calculated for the starting solution potential and pH. It should be noted that the set of differential equations includes both the rate equations for cytochrome c_3 and for the reducing agent since, with the exception of the dithionite case discussed in section III.4.1, the concentration of reducing agent also changes with time, under the experimental conditions used in the present work. The case of dithionite is also exceptional insofar as the reactions are effectively irreversible and, therefore, integrated forms of the rate equations can be used for the simulations, as described in section III.4.1.

III.4 Kinetic studies of the reduction of cytochrome c_3 by sodium dithionite

III.4.1 Application of the kinetic model

The reduction of cytochrome c_3 from *D. gigas* by sodium dithionite was followed by stopped-flow spectrophotometry. These experiments were performed at different pH values in order to study the pH dependence of the reduction process. The experimental data were analysed with a kinetic model adapted from that described in section III.3. The principal alterations introduced here are related to the different experimental conditions used in this study. The concentration of reducing agent is always in large excess over the concentration of haems, thus, the pseudo-first order approximation is applicable. Also, it was not necessary to assume microscopic reversibility because the redox potential of sodium dithionite is sufficiently negative for the reverse electron transfer reactions to be neglected. Under these conditions, full reduction of cytochrome c_3 is always observed.

The redox sigma factors previously defined (σ_{ij}) are used to correlate the rate constants of individual haems in different stages and the proton sigma factors (σ_{iH}) are used to establish the relationship between the rate constants in different protonation states. It should be pointed out that, for the dithionite case, the approximation of sigma factors in terms of the Marcus theory is weaker because the difference in redox potentials between cytochrome c_3 and sodium dithionite is larger (see equations 11 and 13 of section III.3). However, the ΔG^0 is still smaller than the reorganisation energy λ, and it is assumed that the approximation is good enough for the determination of qualitative individual rate constants for the haems. According to this kinetic model, only one set of four rate constants is independent either for the protonated or deprotonated protein, and the other is fixed by the proton sigma factors. Therefore, the simulation of the pH dependence of the kinetic traces relies exclusively on the assumption of proton sigma factors, the redox-Bohr energies, and the ionisation energy of the fully reduced molecule, which determines the fractional populations of the acid (A) and basic (B) forms. The general shape of the fitted curves obtained indeed confirms that the approximation of sigma factors from Marcus theory is acceptable, even for the dithionite case (see Figure III.12 of section III.4.2).

Given the assumptions of irreversible reactions under pseudo-first order conditions, fast internal equilibration of electrons inside the cytochrome molecule (Santos et al., 1984a) and a diffusion limited exchange rate for protons (Turner et al., 1996), the overall reaction scheme reduces to a simple model of four consecutive reactions with four pH dependent pseudo-first

order rate constants k_a', k_b', k_c' and k_d' (Scheme III). These composite rate constants correspond to the previously defined k_a, k_b, k_c and k_d (cf. Figure III.7 and equations14a-d of section III.3) multiplied by the concentration of reducing agent [A^{red}], which is now constant.

$$\text{Stage IV(ox)} \xrightarrow{k_d'} \text{Stage III} \xrightarrow{k_c'} \text{Stage II} \xrightarrow{k_b'} \text{Stage I} \xrightarrow{k_a'} \text{Stage 0 (red)} \qquad \textbf{(Scheme III)}$$

(Step IV) (Step III) (Step II) (Step I)

The rate equations for this model are very simple (equations 15a-e) and have an analytical solution.

$$\frac{d[\text{stage IV}]}{dt} = -k_d'[\text{stage IV}] \tag{15a}$$

$$\frac{d[\text{stage III}]}{dt} = k_d'[\text{stage IV}] - k_c'[\text{stage III}] \tag{15b}$$

$$\frac{d[\text{stage II}]}{dt} = k_c'[\text{stage III}] - k_b'[\text{stage II}] \tag{15c}$$

$$\frac{d[\text{stage I}]}{dt} = k_b'[\text{stage II}] - k_a'[\text{stage I}] \tag{15d}$$

$$\frac{d[\text{stage 0}]}{dt} = k_a'[\text{stage I}] \tag{15e}$$

The integrated form of these rate equations that was used to calculated the time dependence of the populations of the stages and generate the simulated kinetic curves from the macroscopic parameters k_a', k_b', k_c' and k_d' is presented in appendix C. Since in some experiments the cytochrome was already partially reduced at time zero, it was necessary to take that into consideration for the definition of the boundary conditions. The population of any stage that comes from the previous stage is indistinguishable from the population of that stage that is already present at time zero, hence the extension of the integrated equations for the simpler model to account for partial reduction at time zero is straightforward (see Appendix C).

Having calculated the populations of the redox stages as a function of time, the total oxidised fraction is then given by equation (16).

$$\text{oxidised fraction} = \frac{(4[\text{Stage IV}] + 3[\text{Stage III}] + 2[\text{Stage II}] + [\text{Stage I}])}{4([\text{Stage IV}] + [\text{Stage III}] + [\text{Stage II}] + [\text{Stage I}] + [\text{Stage 0}])} \quad (16)$$

It is important to stress again that the pseudo-first order rate constants k_a', k_b', k_c' and k_d' are not the rate constants for the individual haems. Following the same procedure adopted in section III.3 it can be shown that these composite parameters are related to the individual rate constants, k_{+1}, k_{+2}, k_{+3}, and k_{+4}, defined for the deprotonated form of the cytochrome, through equations 14a-d of section III.3, multiplied by the concentration of reducing agent.

III.4.2 Results and Discussion

Figure III.8 reports the progress curves for the reduction of cytochrome c_3 from *D. gigas* at two extreme pH values.

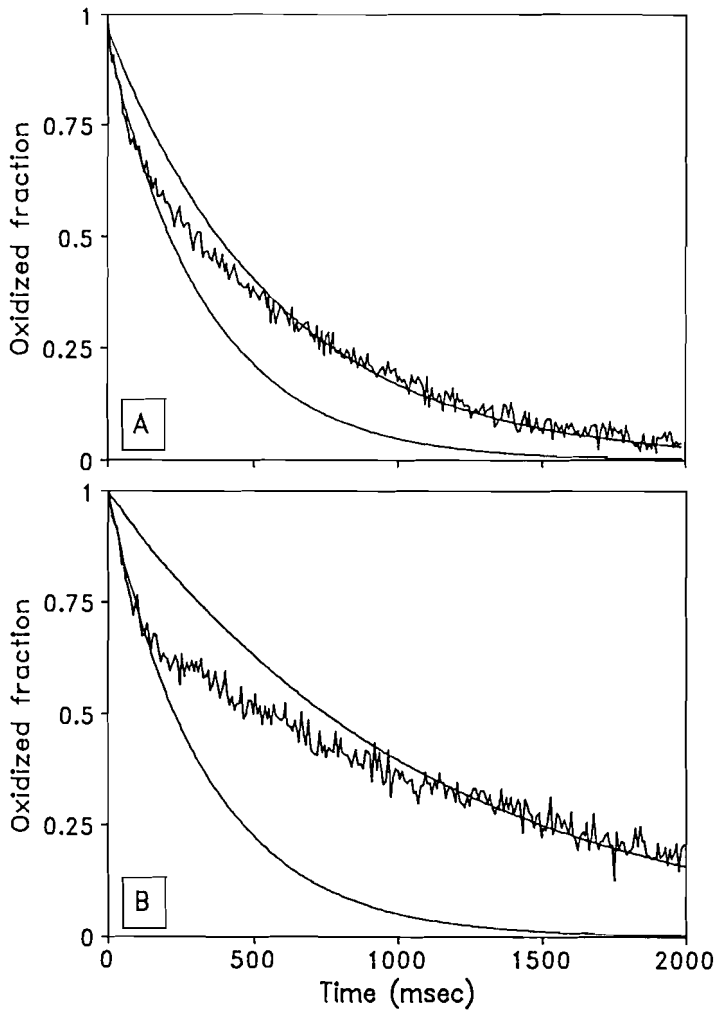

Figure III.8. Progress curves for the reduction of Dgc_3 by sodium dithionite at different pH values. The kinetic process has a biphasic character which increases with increasing pH. (A) pH 5.85, (B) pH 9.95. The two lines represented in each panel correspond to monoexponentials and show that the overall process cannot be simulated by a single exponential. T= 20 °C, [$Na_2S_2O_4$]= 100μM after mixing. Buffers: 0.25 M glycine pH 9.95 and 0.25 M tris/maleate pH 5.85.

It appears clear that the kinetic process has a biphasic character and that pH affects the features of the reaction, the biphasicity being greater at high pH. The rate constants of the two exponential processes are both dependent upon the square-root of the concentration of sodium dithionite (Figure III.9).

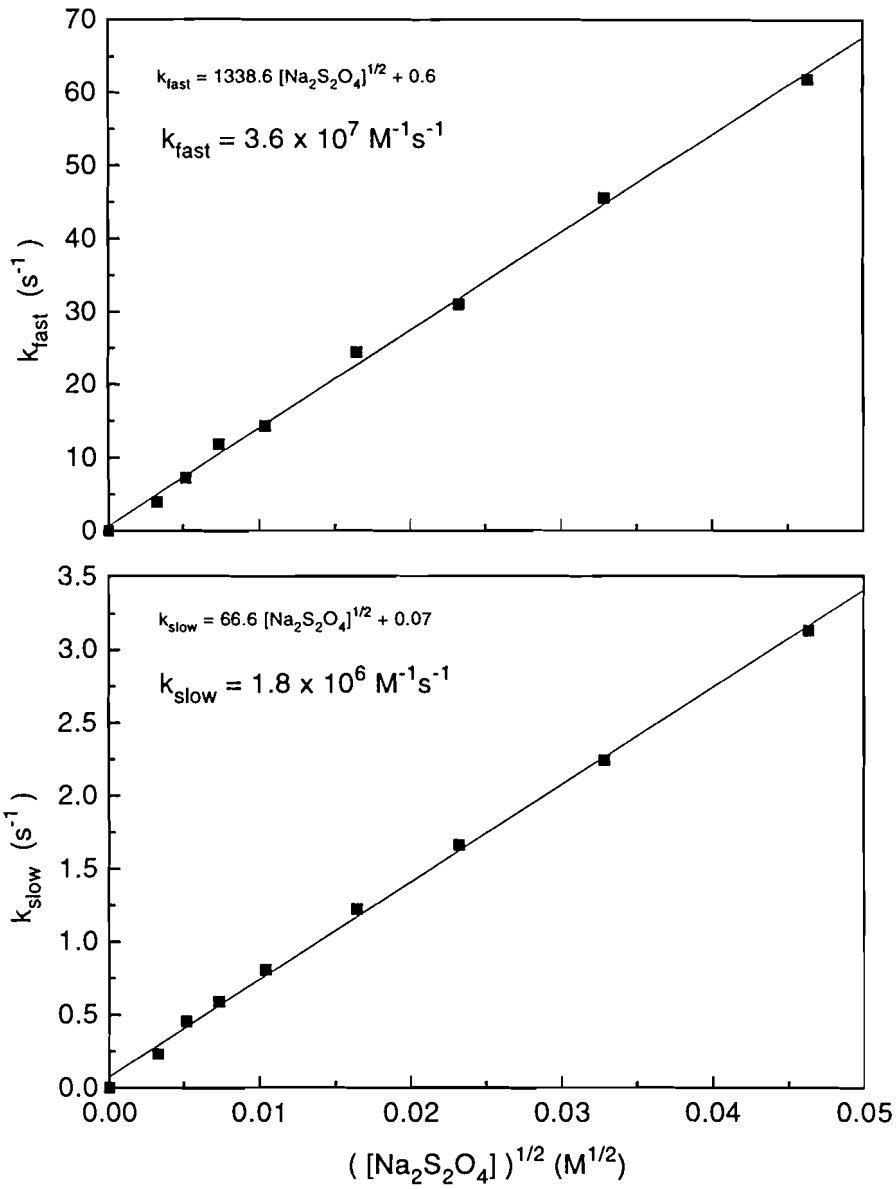

Figure III.9. Dependence of the second order rate constants on the square-root of the sodium dithionite concentration. TOP: The pseudo first order rate constants of the fast process are represented as a function of the square-root of the sodium dithionite concentration. BOTTOM: Equivalent representation for the pseudo first order rate constants of the slow process. Both fast and slow rate constants display a linear dependence on the square-root of the sodium dithionite concentration, showing that both processes refer to bimolecular reactions where the actual reductant is the species SO_2^- (Lambeth and Palmer, 1973).

This finding indicates that (i) both processes refer to bimolecular reactions, and (ii) the actual reducing agent is SO_2^-, the dissociated form of sodium dithionite, according to the work of Lambeth and Palmer, 1973. For the kinetic studies using sodium dithionite, the concentration of reducing agent, $[A^{red}]$ is therefore given by $[A^{red}] = \sqrt{K_d \times [Na_2S_2O_4]}$ where

K_d=1.4×10^{-9} M is the equilibrium constant for the reaction $S_2O_4^{2-} \leftrightharpoons 2\ SO_2^-$ (Lambeth and Palmer, 1973) and [$Na_2S_2O_4$] is the concentration of sodium dithionite after mixing the reagents in the stopped-flow apparatus.

The amplitude of the fast phase, which amounts to approximately 20-30% (somewhat depending on the pH value and buffer conditions) of the total optical density change for the reduction process, indicates that the first reduction step is faster and that it is dominated by the reduction rate of one of the four haems. This is further supported by the observation at pH 9.6 that, for a solution in which 34% of the haems are reduced at equilibrium, the reaction with sodium dithionite does not display any fast phase (Figure III.10).

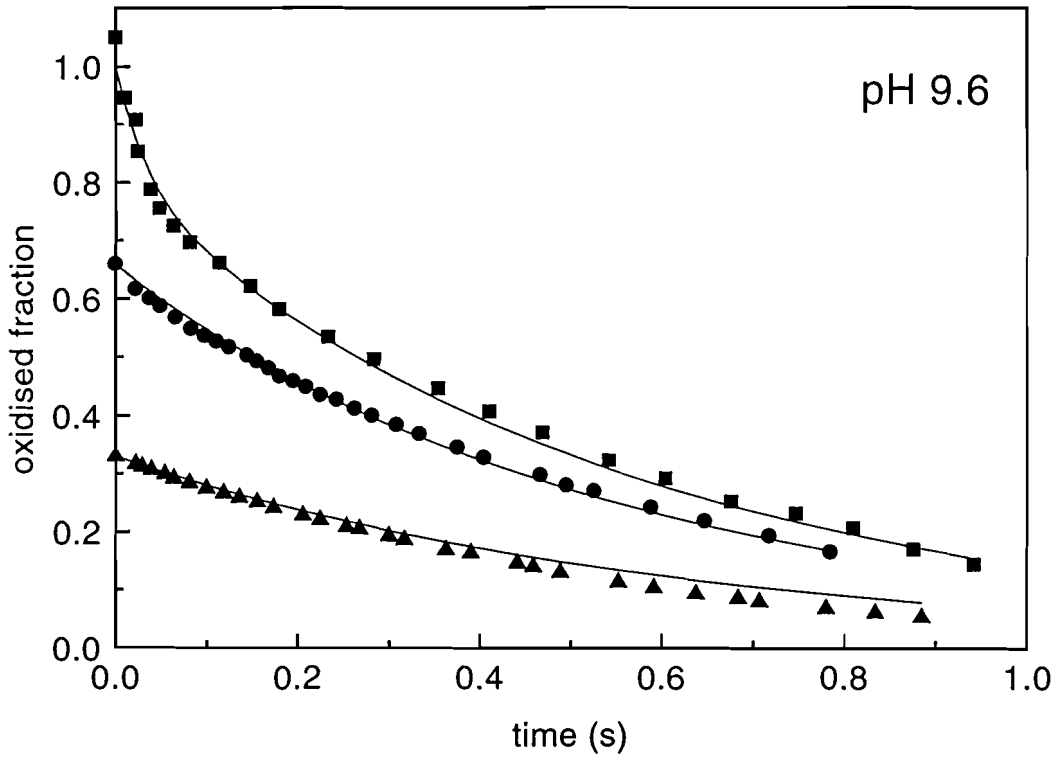

Figure III.10. Progress curves for the reduction of Dgc$_3$ by sodium dithionite, starting at different degrees of protein reduction. (■) fully oxidised protein, (●) 34% reduced protein and (▲) 67% reduced protein were mixed with sodium dithionite. The disappearance of the fast phase in the reactions between dithionite and partially reduced cytochrome samples indicates that haem IV is responsible for the initial fast phase of the reduction. [$Na_2S_2O_4$]= 550 μM after mixing. Buffer: 0.25 M glycine pH 9.6. T= 20 °C. Computer simulated curves using the kinetic model described in the text with the following rate constants are also shown: $k_{+1}= k_{+2}= k_{+3}= 1.8 \times 10^6\ M^{-1}s^{-1}$, $k_{+4}= 1.7 \times 10^7\ M^{-1}s^{-1}$.

The distribution of populations at equilibrium (Figure III.11) indeed shows that for 34% of global reduction, the haem with less negative redox potential (i.e., haem IV) is already 92% reduced, indicating that this haem is likely to be responsible for the initial fast phase of the reduction dynamics.

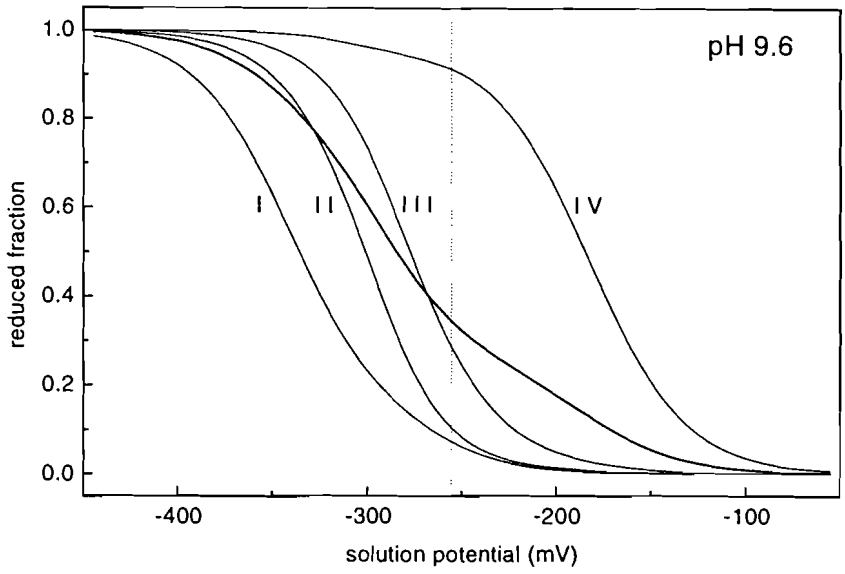

Figure III.11. Haem populations at equilibrium at pH 9.6. Thin lines correspond to the equilibrium populations of the individual haems. Roman numbers are used to identify the haems according to sequence numbering. The overall reduced fraction is represented by a thick line. The distribution of populations shows that for 34% of global reduction (dotted line) haem IV is already 92% reduced.

The kinetic model described was used to fit the pH dependence of the stopped-flow data, with four independent parameters, i.e. the four individual rate constants. The general shape of the traces and its pH dependence is reproduced by the simulations, validating the assumptions made in the kinetic model, the proton sigma factor approximation in particular (Figure III.12).

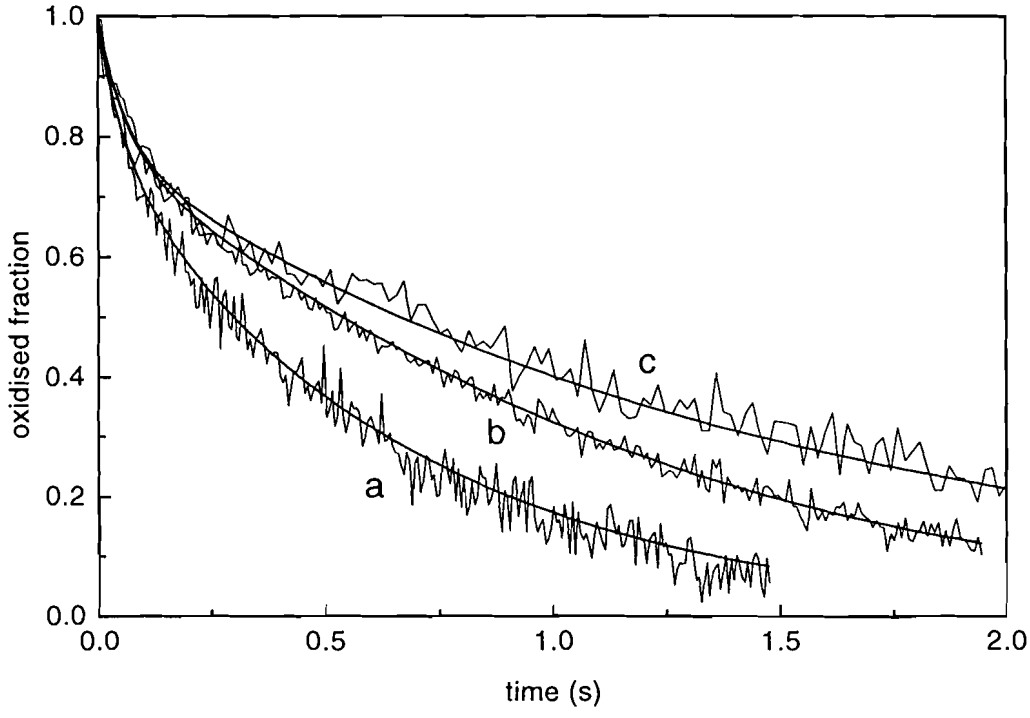

Figure III.12. pH dependence of the reduction kinetics of Dgc_3 with sodium dithionite. Progress curves for the reduction of Dgc_3 at different pH values are represented: (a) pH 5.5, (b) pH 7.4, (c) pH 9.6. The simulation of the reduction process using the kinetic model described in the text with rate constants $k_{+1}= k_{+2}= k_{+3}= 1.4 \times 10^6\ M^{-1}s^{-1}$ and $k_{+4}= 2.5 \times 10^7\ M^{-1}s^{-1}$ for the deprotonated form of Dgc_3, is also shown. $[Na_2S_2O_4]=$ 100 µM after mixing. Buffers: 0.25 M glycine pH 9.6 and 0.25 M tris/maleate pH 7.4 and 5.5. T= 20 °C.

However, the rate constants obtained in this fitting for the individual haems are not well defined, and display a high covariance. Also, with the exception of the rate constant for haem IV, the standard errors and the values of the parameters are of the same order of magnitude (Table III.2). This indicates that the data are not sufficient to define accurately four independent parameters and a kinetic model with a smaller number of parameters should be used. Since the fitting obtained with the minimum number of parameters, a single independent rate constant, is clearly unsatisfactory (cf. rmsd values in table III.2), a kinetic model starting with two independent parameters was developed. The rate constant for haem IV was taken as one of them because it was the only rate constant reasonably well defined in the first place. With two parameters it is possible to choose either to fix the rate constants of two of the haems at zero and adjust the rates constants of haem IV and another haem, or to establish a relationship between the rate constants of haems I, II and III. The result of the fit assuming different rate constants for haems I and IV while setting the rate constants for haems II and III to zero or with equal rate constants for haems I-III, fixed either for the basic or the acidic forms, is presented in table III.2 together with the result of the fit with one and with four independent parameters.

Table III.2. Rate constants for the reduction of individual haems by sodium dithionite. Comparison between models with a different number of parameters. Comparison between the rate constants ($M^{-1}s^{-1}$) and respective standard errors obtained from the fit of the pH dependent stopped-flow data considering kinetic models either with a different number of parameters (N) or a different definition of the parameters. The root mean square deviation (rmsd) of each fit is also shown

N	Observations	Haem I k_{+1}	Haem II k_{+2}	Haem III k_{+3}	Haem IV k_{+4}	rmsd
4	k_{+1}, k_{+2}, k_{+3}, k_{+4}	$1.9\pm6.3\times10^{5}$	$4.2\pm2.1\times10^{6}$	$1.5\pm1.1\times10^{6}$	$2.7\pm0.4\times10^{7}$	0.0259
2	$k_{+1}=k_{+2}=k_{+3}$, k_{+4} (B)	$1.4\pm0.1\times10^{6}$	$1.4\pm0.1\times10^{6}$	$1.4\pm0.1\times10^{6}$	$2.5\pm0.3\times10^{7}$	0.0266
2	$k_{+1}=k_{+2}=k_{+3}$, k_{+4} (A)	$3.4\pm0.2\times10^{6}$	$3.4\pm0.2\times10^{6}$	$3.4\pm0.2\times10^{6}$	$3.0\pm0.3\times10^{7}$	0.0262
2	k_{+1}, $k_{+2}=k_{+3}=0$, k_{+4}	$2.3\pm0.2\times10^{6}$	0	0	$2.7\pm0.3\times10^{7}$	0.0292
1	$k_{+1}=k_{+2}=k_{+3}=0$, k_{+4}	0	0	0	$8.8\pm0.1\times10^{7}$	0.0413

Taking the basic form as the reference state and the rate constant for haem IV as one of the parameters, the option with equal rate constants for the remaining haems was chosen for the

dithionite case. Since all haems in cytochrome c_3 are well exposed to the solvent and dithionite is a small inorganic molecule, there was no reason *a priori* to make a distinction between haems I, II and III. The rmsd values show that the quality of the fit with two independent parameters, either k_{+1} and k_{+4} with $k_{+2}=k_{+3}=0$ or $k_{+1}=k_{+2}=k_{+3}$ and a different k_{+4}, is very similar to that obtained with four parameters. Since the number of adjustable parameters in the model was decreased to two, the values for the rate constants obtained from this fit are reasonably well defined, with standard errors around 10%. The standard errors obtained for the fitted parameters provide a useful test of how well the solution is defined but, of course, they give no indication of the sensitivity of the parameters to the choice of model or the reproducibility of the experimental data. It is therefore instructive to compare the rate constants obtained by setting the values of haems I-III equal either in the acidic form or in the basic form for the pH dependence studies to probe the symmetry of the parameters with respect to the model assumptions, as well as the parameters obtained from different series of experiments (Figures III.10 and III.12) to investigate how sensitive are the parameters to the variability of the experimental data. The different sets of values obtained for the rate constants are presented in table III.3.

Table III.3. Rate constants for the reduction of the haems in the protonated and deprotonated forms of Dgc_3 by sodium dithionite. The values of the rate constants ($M^{-1}s^{-1}$) represent the best fit of the pH dependent data obtained by the Marquardt method assuming equal rate constants for haems I-III either for the deprotonated form of the cytochrome (HI-HIII fixed in the B form) or for the protonated form of the cytochrome (HI-HIII fixed in the A form). The values presented in the last row were obtained using a different data set at pH 9.6 and fixing the rate constants for the basic form.

Observations		Haem I k_{+1}	Haem II k_{+2}	Haem III k_{+3}	Haem IV k_{+4}
pH dependent data of Figure III.12. Rate constants for HI-HIII fixed in the B form.	Basic form (B)	1.4×10^6	1.4×10^6	1.4×10^6	2.5×10^7
	Acidic form (A)	4.4×10^6	2.5×10^6	2.6×10^6	3.0×10^7
pH dependent data of Figure III.12. Rate constants for HI-HIII fixed in the A form.	Basic form (B)	1.1×10^6	1.9×10^6	1.8×10^6	2.5×10^7
	Acidic form (A)	3.4×10^6	3.4×10^6	3.4×10^6	3.0×10^7
Data of Figure III.10 at pH 9.6.	Basic form (B)	1.8×10^6	1.8×10^6	1.8×10^6	1.7×10^7

Note that although the rate constants for haems I, II and III are taken to be equal for one of the forms of the cytochrome (either the basic or the acidic one), they are different for the other one because they are defined by the proton sigma factors which are different for each haem (see equation 13 of section III.3).

From table III.3 it can be seen that the rate constants calculated for haems I-III vary between $1.1x10^6$ and $1.9x10^6$ $M^{-1}s^{-1}$ in the basic form and $2.5x10^6$ and $4.4x10^6$ $M^{-1}s^{-1}$ in the acidic form. The range found for haem IV is from $1.7x10^7$ to $2.5x10^7$ $M^{-1}s^{-1}$ in the basic form and $3.0x10^7$ $M^{-1}s^{-1}$ in the acidic form. Thus, although the rate constants for haems I-III are not very well defined, it is apparent that they are approximately doubled at low pH whereas the rate constant of haem IV is slightly better defined and is less sensitive to pH. Moreover, the rate constant of haem IV for the deprotonated form is approximately one order of magnitude larger than the others, which agrees with the earlier expectations of finding one faster haem. This haem is responsible for the fast phase observed in the biphasic kinetic traces.

The higher rates of reduction observed at low pH are determined by the effect of the proton sigma factors on the rate constants of the individual haems. The rate constant most affected by a decrease in the pH value is that of haem I, because haem I has the higher redox-Bohr interacting potential (see Table II.4 of section II.3.3). On the other hand, the rate constant for haem IV is hardly affected. In fact, it is because the rate constants of haem IV and haems I-III are differently affected by the pH that the degree of biphasicity of the kinetic traces is different at high and low pH. The decreasingly biphasic appearance of the kinetic traces at lower pH values may therefore be attributed to the progressive increase in the rates for haems I-III.

The general shape of the kinetic traces at different pH values taken together is therefore easily understood. For the first 25% of reduction the curves are not strongly pH dependent because essentially only haem IV is being reduced and its rate constant is weakly pH dependent. After 25% reduction the kinetic traces spread (see Figure III.12) as the haems with more strongly pH dependent rate constants are being reduced.

The time evolution of the populations of the redox stages was calculated at an intermediate pH value for the solution with equal rate constants for haems I-III for the basic form and it is shown in Figure III.13.

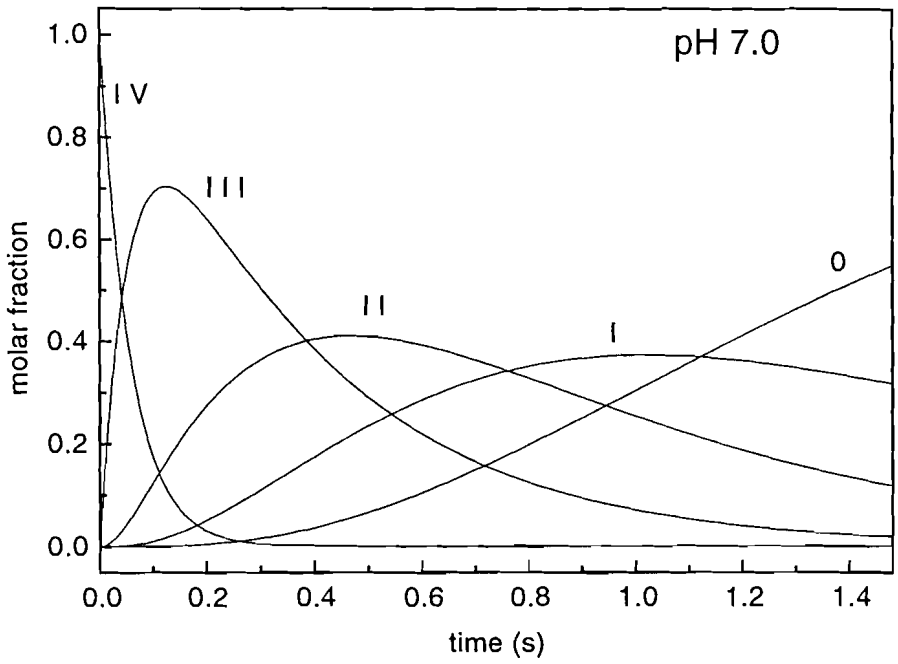

Figure III.13. Time evolution of the populations of the redox stages at pH 7.0. Roman numbers identify the redox stages according to the number of oxidised haems of the microstates that belong to each stage. The curves were calculated using the kinetic model described in the text with rate constants $k_{+1}= k_{+2}= k_{+3}= 1.4 \times 10^6$ $M^{-1}s^{-1}$ and $k_{+4}= 2.5 \times 10^7$ $M^{-1}s^{-1}$ for the deprotonated form of Dgc_3.

To compare the relative importance of the four haems in the reduction process of cytochrome c_3 from *D.gigas*, the fraction of electrons entering the molecule through each haem in each reduction step was calculated, again for the solution with equal rate constants for haems I-III for the basic form, and the result obtained for the two extreme pH values is presented in table III.4.

Table III.4. Fraction of electrons entering the cytochrome c_3 molecule through each haem in each reduction step at the two experimental extreme pH values. See Scheme III for the definition of the steps. The terms relative to each of the haems in equations 14 a-d of section III.3 were used to calculate these fractions for $k_{+1}=k_{+2}=k_{+3}=1.4\times10^6$ $M^{-1}s^{-1}$, $k_{+4}=2.5\times10^7$ $M^{-1}s^{-1}$. The total contribution for each haem is given by the sum of the respective fractions over the four steps divided by four.

Step	pH 5.5				pH 9.6			
	Haem I	Haem II	Haem III	Haem IV	Haem I	Haem II	Haem III	Haem IV
IV	0.070	0.037	0.045	0.847	0.031	0.028	0.032	0.910
III	0.445	0.103	0.131	0.321	0.399	0.135	0.192	0.274
II	0.363	0.216	0.104	0.316	0.324	0.282	0.100	0.294
I	0.582	0.171	0.069	0.178	0.736	0.125	0.051	0.087
Total	**0.365**	**0.132**	**0.087**	**0.416**	**0.372**	**0.142**	**0.094**	**0.391**

The contribution of each haem to the overall reduction process is also shown. These values indicate that the first reduction step (step IV) is dominated by haem IV. In the intermediate steps (steps III and II) electrons enter the molecule mainly through haems I and IV and haem I plays the major part in the last reduction step (step I). Although the rate constant for haem IV is larger than that for haem I, the percentage of electrons entering the molecule through each of them is similar, both contributing ca. 40% to the overall reduction process. Given the difference in the rate constants this result is only comprehensible in the context of the thermodynamic factors that weight each particular rate constant (equations 14a-d of section III.3). The values of these factors are presented in table III.5, again for the two extreme pH values.

Table III.5. Thermodynamic factors that weight the rate constants of each haem in each reduction step at two extreme pH values. The values correspond to the thermodynamic factors of equations 14 a-d of section III.3, calculated for pH 5.5 and 9.6, using the thermodynamic parameters reported in table II.4 of section II.3.3.

Step	pH 5.5				pH 9.6			
	Haem I	Haem II	Haem III	Haem IV	Haem I	Haem II	Haem III	Haem IV
IV	2.933	1.557	1.870	1.915	1.011	0.909	1.067	1.630
III	4.512	1.038	1.328	0.176	1.570	0.531	0.757	0.059
II	1.947	1.161	0.560	0.092	0.853	0.740	0.262	0.042
I	1.829	0.537	0.215	0.030	0.817	0.139	0.057	0.005

With the exception of step IV, the thermodynamic factors that affect haem IV are comparatively very small, whereas those affecting haem I are usually dominant. Therefore, if the rate constants for haems I-III are set equal, haem I gives a larger contribution to the overall reduction among these haems because the fraction of molecules with this haem oxidised and able to receive an electron from dithionite is larger during most of the reduction process. The importance of haem IV has a different origin. Because this haem becomes almost fully reduced (ca. 90%) in the first reduction step (step IV), the fraction of molecules which have this haem still oxidised and are able to receive an electron through it is very small during 75% of the reduction process. Thus, being at a disadvantage from the thermodynamic point of view, it is because its rate constant is higher than the others that haem IV plays such

an important role in the overall reduction of Dgc_3. It can be concluded that, in the reaction between Dgc_3 and sodium dithionite, haem IV has a distinct kinetic behaviour when compared to the other three haems in the molecule.

III.4.3. Conclusions

A qualitative description of the reduction pathway in the tetrahaem cytochrome c_3 from *D. gigas* is a prerequisite for a more detailed understanding of the redox function of this molecule. Obviously, the reaction with sodium dithionite investigated in this work cannot allow final conclusions to be drawn on the actual *in vivo* mechanism, but it represents a first insight into the different intramolecular relationships which regulate the electron uptake of the whole macromolecule. Furthermore, it is important to note that, although the present study was carried out with a non-physiological reducing agent, the faster haem to be reduced with sodium dithionite is haem IV, which, even though it is one of the less exposed to the solvent, is nearest to the lysine patch located on the surface of the protein (Matias et al., 1996). Computer graphics modelling studies have shown that this positive region is that used for the docking of flavodoxin in the homologous *D. vulgaris* proteins (Stewart et al., 1988); thus, the fact that a negatively charged reagent, such as sodium dithionite, was used allow us to draw some relevant qualitative conclusions.

It is worth remarking that the kinetic phenomenological behaviour observed for the reduction process by sodium dithionite in cytochrome c_3 from *D. gigas* (Catarino et al., 1991) differs from that observed for cytochrome c_3 from other sulphate-reducing bacteria (Favaudon et al, 1978 ; Tabushi et al., 1983 ; Capeillère-Blandin et al., 1986). Thus, although a biphasic time course has also been observed in these molecules, the relative amplitude of the fast phase was different, which has important effects on the whole observed kinetic pattern. This is hardly surprising, given the difference in the thermodynamic parameters of the haems observed for cytochrome c_3 molecules isolated from different *Desulfovibrio* species.

Moreover, in this thesis the kinetic treatment has been closely related to the thermodynamic information (cf. kinetic model section III.3), using a functional model which gives a better overall view of the system and allows an analysis of the reduction progress curves for each of the four haems (Figure III.14).

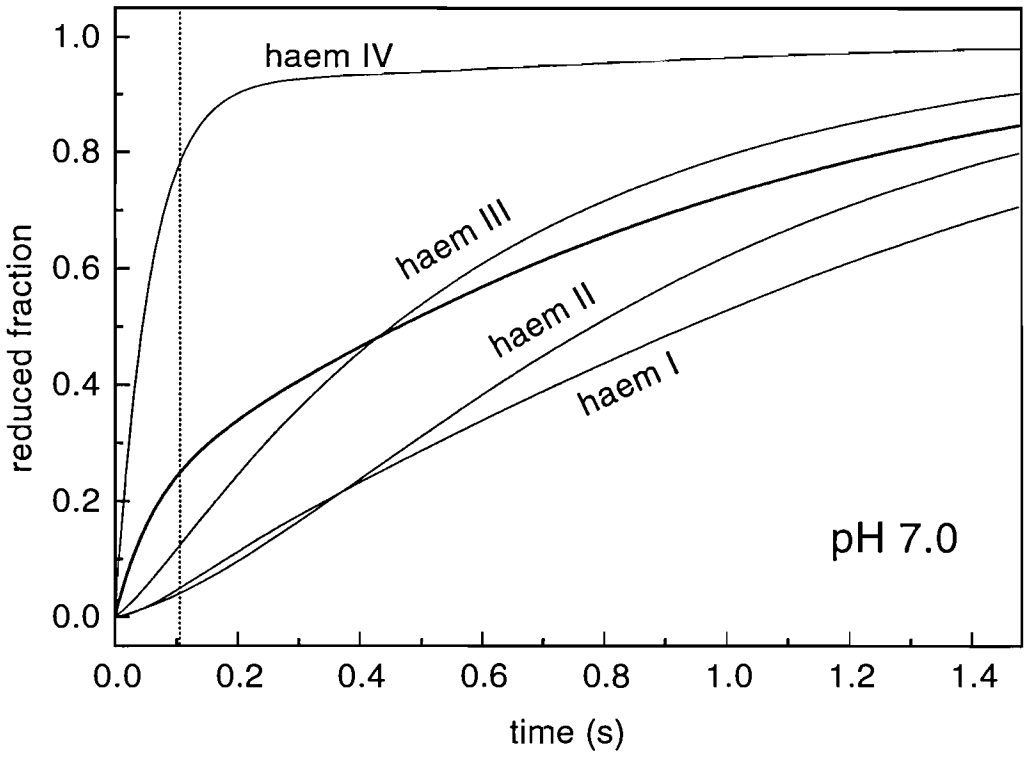

Figure III.14 Deconvolution of the overall reduction curve into the contributions from the individual haems at pH 7.0. The thick line represents the time evolution of the global reduced fraction of Dgc_3 and the thin lines represent the time evolution of the reduced fraction of each haem, numbered according to the sequence. The distribution of reduced haem populations that correspond to 25% of global reduction is indicated by a dotted line. The curves were calculated using the kinetic model described in the text with rate constants $k_{+1}= k_{+2}= k_{+3}= 1.4 \times 10^6$ $M^{-1}s^{-1}$ and $k_{+4}= 2.5 \times 10^7$ $M^{-1}s^{-1}$ for the deprotonated form of Dgc_3.

Limiting ourselves to thermodynamic considerations, we can only have a rough description of the actual function of the protein as an electron carrier, and a thorough kinetic investigation was necessary in order to formulate more realistic functional considerations. The satisfactory description of the general behaviour as a function of pH, with the thermodynamic and the kinetic model described above (sections II.3.3 and III.3, respectively) and the kinetic parameters determined in this section, together with the thermodynamic parameters reported in Table II.4 of section II.3.3, provides the necessary basis for a deeper understanding of the mechanism for the reduction pathway in cytochrome c_3 from *D. gigas*.

An important consequence of the fast intramolecular re-equilibration is that, after an initial fast observed reduction rate of haem IV, the interacting potentials are such that at about 90% reduction degree of this haem (for pH 7.0) the incoming electrons start to be drained from haem IV to haems II and III. Indeed, after this stage the population of molecules with haem IV reduced remains approximately constant while those of haems II and III attain about 60% of their total reduction, with a fairly fast observed reduction rate (Figure III.14).

It is particularly interesting that, as previously predicted (Xavier, A.V. 1986), the sizeable positive cooperativity between haems II and III, induces a strongly accentuated autocatalytic effect for the reduction progress curves of these two haems. This effect is nicely illustrated in figure III.14, where it is obvious that, as the population of molecules with haem III reduced increases, a sigmoidal shape for the progress curve of haem II reduction is clearly seen. The result is that the slopes of the two curves are quite similar for a large portion of the reduction process. Thus, the functional implication of the cooperativity between haems II and III is that a concerted two-electron transfer step can be performed by this molecule.

Another important observation is that, by virtue of the existence of a redox linked proton equilibrium between two forms A and B, there is a predominance of the B form in the oxidised state for pH values above pK_a^{ox} = 6.3, whereas the A form is predominant in the reduced state for pH values below pK_a^{red} = 8.5 (see section II.3, modelling of the thermodynamic properties). Therefore, for pH values within the range 6.3–8.5, during the reduction process the protein undergoes a B → A transition (see Figure II.15 of section II.3.) with important functional consequences especially in view of the thermodynamic and kinetic differences between the two forms. As a matter of fact, over the pH 7.0-8.0 range the B → A transition brings about a progressive acceleration of the transfer of electrons entering through haems IV and I and drained to haems II and III. Indeed, the proton sigma factors imply that the individual rate constants should be larger in the protonated form. Moreover, the relevant microscopic mid-point redox potentials of haems II and III become much closer to that of haem IV as the reduction process and the B→A transition is accomplished, favouring the intramolecular electron redistribution towards haems III and II.

Taking into consideration the fact that haem IV is always the fastest one to be reduced, it is tempting to speculate that this should be the haem involved in the interaction between cytochrome c_3 and the physiological electron donor proteins. However, such a hypothesis is far from being substantiated by the present data and it would require an accurate kinetic and thermodynamic investigation of the reaction with the physiological partners. Nevertheless, this is supported by studies which have shown that, in the proteins from *D. vulgaris*, the complex between cytochrome c_3 both with flavodoxin (Stewart et al 1988), as previously mentioned, and rubredoxin (Stewart et al 1989), involves an interaction between the acidic residues of these proteins and the lysine patch situated close to haem IV of cytochrome c_3.

III.5 Kinetic studies of the interaction between cytochrome c_3 and FMN or cytochrome c_3 and flavodoxin from *Desulfovibrio gigas*

III.5.1 Introduction

Flavodoxin isolated from *D. gigas* is a 16 kD protein containing one FMN cofactor per unit (Dubourdieu and LeGall, 1970). Two electrons are involved in the full reduction of the redox centre. In free FMN, one step of two electrons converts the oxidised form into the fully reduced one, with a midpoint redox potential of –290 mV. Bound to the protein, however, the intermediate redox state is stabilised and the reduction process is accomplished by two consecutive steps of one electron (Mayhew and Ludwig, 1975). The redox equilibria involved are represented in Scheme IV:

(Scheme IV)

$$\text{oxidised fl } (fl^{ox}) + 1e^- \overset{E_{ox/sq}}{\rightleftharpoons} \text{semiquinone fl } (fl^{sq}) + 1e^- \overset{E_{sq/red}}{\rightleftharpoons} \text{hydroquinone fl } (fl^{red})$$

where fl stands for flavodoxin, $E_{ox/sq}$, the midpoint redox potential for the oxidised/semiquinone couple is equal to –260 mV and $E_{sq/red}$ the midpoint redox potential for the semiquinone/hydroquinone couple is equal to –440 mV for *D. gigas* flavodoxin at pH 9.6 (Costa, 1989). It should be noted that, to be consistent with the microscopic analysis described for cytochrome c_3, the four microstates of flavodoxin should be considered here. However, since the difference in redox potentials for the two electron steps is close to 200 mV, the population of one of the four microstates is always negligible and, to simplify the analysis, it was ignored. Thus, the flavodoxin species referred above can be regarded as microstates and the midpoint redox potentials as microsopic parameters.

Although more flavodoxin is expressed in *D. gigas* grown under iron limitation, this protein is always present in the bacterial cytoplasm together with ferredoxin (Hatchikian and LeGall, 1970), unlike *Clostridium pastorianum* in which flavodoxin substitutes ferredoxin and is only expressed under iron limitation (Knight and Hardy, 1966). In *Desulfovibrio* spp. the flavodoxins have been suggested to be involved in the electron transport from hydrogenase to the sulfite-reducing system, using molecular hydrogen as the electron donor, or from the pyruvate phosphoroclastic system toward the sulfite-reducing system, using pyruvate as electron donor (Vervoort et al, 1994). *In vitro* cytochrome c_3 participates in the first of these reactions, by transferring electrons from hydrogenase to flavodoxin (Drake and Akagi 1977 ; Kim and Akagi, 1985). The formation of a complex between cytochrome c_3 and flavodoxin

may not be possible *in vivo*, because of the localisation of these proteins in different cellular compartments, cytochrome c_3 is in the periplasmic space whereas flavodoxin is in the cytoplasm (Bell et al., 1974 ; LeGall and Peck, 1987 ; LeGall et al., 1994). However, studies of complex formation between them, besides being good models for the study of electron transfer reactions between haems and flavin groups (Stewart et al., 1988 ; Palma et al., 1994), may still be physiologically relevant since they can mimic the interaction between flavodoxin and the hexadecahaem cytochrome c_3 which, showing some homology with tetrahaem cytochrome c_3, was proposed to be part of a transmembrane redox complex responsible for the coupling of the periplasmic oxidation of hydrogen to the cytoplasmic reduction of sulfite (Rossi et al, 1993). Moreover, the homology found recently between flavodoxin and the N-terminal domain of the 28 kD subunit of the nickel-iron *D. gigas* hydrogenase (Volbeda et al., 1995) conferred additional physiological relevance to these studies. The nickel-iron hydrogenase isolated from *D. gigas* is a periplasmic protein (Bell et al., 1974) and is the only hydrogenase so far shown to be present in this organism (LeGall et al., 1994). Cytochrome c_3 was first proposed to be redox partner of hydrogenase in 1968 (Yagi et al. 1968) and other studies have been published with experimental evidence supporting this idea since then (Louro et al., 1997a).

Further justification for the present studies is related to the fact that inter redox centre electron transfer is poorly understood and studies have to be performed and are being performed in many different systems, even synthetic ones, to improve the general knowledge about these reactions (Beratan et al., 1991 ; Moser et al., 1992 ; Robertson et al., 1994 ; Gray and Winkler, 1996).

The objective of the work reported in this section is the determination of the reduction rate constants for the individual haems in the tetrahaem cytochrome in electron transfer reactions with the hydroquinone and the semiquinone forms of flavodoxin. As explained in the kinetic model section, due to the very fast intramolecular electron exchange (Santos et al., 1984a), the kinetic analysis is intimately related to the thermodynamic description of the system. In this section all the thermodynamic calculations are made according to the model of five interacting centres previously described (section II.3.3), with the energy parameters determined by Louro et al., 1998b (presented in table II.4).

The analysis of similar kinetic data is usually based on the study of the dependence of the observed rate constants, which are obtained from fitting the overall kinetic curves with exponentials, on the concentration of reactants, in order to get information on the macroscopic

equilibrium binding constant and overall electron transfer rate. In this work this procedure was not followed because the experiments were carried out for similar concentrations of the two redox partners and therefore the pseudo-first order approximation is not applicable. Also, even under pseudo-first order conditions, the usual approach does not give information on the kinetic behaviour of the individual haems. The sum of four exponentials corresponds to a kinetic model in which the four haems react independently and simultaneously with the electron donor, without exchanging electrons between themselves. Because of the existence of fast equilibration of electrons inside the molecule, the observed rate constants obtained from this approach do not correspond to the true rate constants of the individual haems.

The experimental conditions were chosen in order to simplify the kinetic analysis and to allow the study of the very fast reaction between flavodoxin hydroquinone and oxidised cytochrome c_3. Small flavodoxin concentrations had to be used so that a reasonable change of the signal intensity is still observed after the deadtime of the apparatus. In fact, if a large excess of flavodoxin had been used, full reduction of the cytochrome would have taken place within the deadtime of the stopped-flow apparatus and no signal build up would have been observed. Thus, the kinetic studies were performed for various small flavodoxin-to-cytochrome concentration ratios and the minimum concentration of c_3 to be used was limited by the obtainable signal to noise ratio. The experimental curves thus acquired correspond to different levels of reduction, enhancing the resolution of the signal and helping the deconvolution of the full curves into the contributions from individual haems. Furthermore, these studies were carried out at high ionic strength, for which the collisional approximation seems reasonable (see kinetic model in section III.3) and at a pH value well above the pK_a^{red}, in order to simplify the analysis by reducing the system to the 16 deprotonated microstates (see section II.3).

The electron trafficking observed in the kinetic studies involving cytochrome c_3, flavodoxin, FMN and sodium dithionite presented in this section and in the previous one, as well as that observed in other published kinetic studies (De Francesco et al., 1994), is that expected from the analysis of the relative redox potentials of the intervening species (Figure III.15). Using sodium dithionite as reducing agent, full reduction of cytochrome c_3 and full reduction of flavodoxin is observed because the midpoint redox potential of dithionite is significantly lower than the midpoint potential of any of the redox centres in the proteins. For the cytochrome c_3/flavodoxin system the analysis is more complex because, although the semiquinone/hydroquinone couple has a redox potential well above the redox potential of any of the four haems in the cytochrome, the oxidised/semiquinone couple has a redox potential

close to that of the middle haems. According to these redox potentials, the hydroquinone form of flavodoxin can reduce the cytochrome fully, whereas the semiquinone form is only able to reduce it by ca. 50%. For the inverse reaction, the relative redox potentials show that reduced cytochrome c_3 is only able to reduce flavodoxin up to the semiquinone level (cf. left panel of Figure III.15).

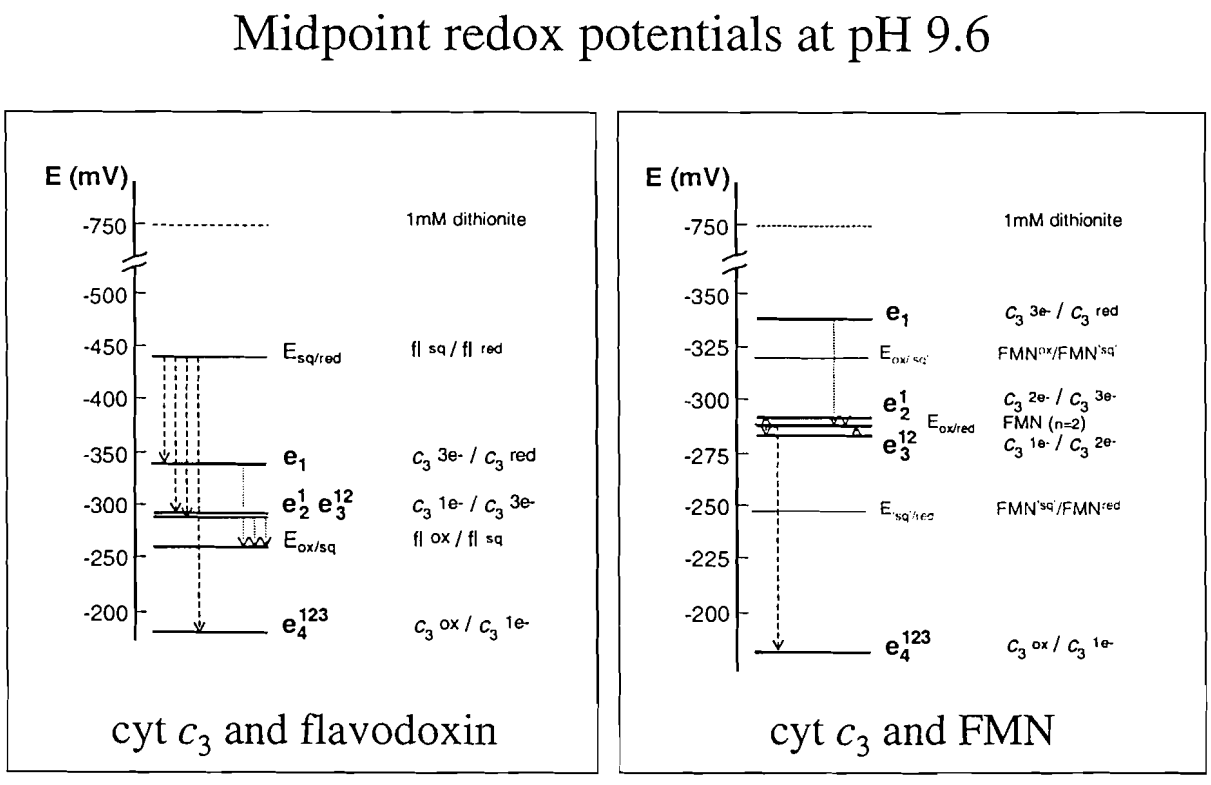

Figure III.15. Midpoint redox potentials of Dgc_3, flavodoxin from *D. gigas* and FMN at pH=9.6. LEFT PANEL: Most relevant redox potentials for the electron transfer reactions between Dgc_3 and flavodoxin. The dashed arrows represent electron transfer from the hydroquinone form of flavodoxin to oxidised or partially reduced cytochrome c_3, whereas the dotted arrows represent electron transfer from fully or partially reduced cytochrome c_3 to the oxidised form of flavodoxin. $E_{ox/sq}$ and $E_{sq/red}$ are the redox potentials of the oxidised/semiquinone and semiquinone/hydroquinone redox couples of flavodoxin, respectively. RIGHT PANEL: Most relevant redox potentials for the electron transfer reactions between Dgc_3 and FMN. The dashed arrows represent electron transfer from reduced FMN to oxidised or partially reduced cytochrome c_3, whereas the dotted arrows represent electron transfer from fully or partially reduced cytochrome c_3 to oxidised FMN. FMN is a two-electron system with $E_{ox/red}$ = -290 mV. The redox potentials for the oxidised/'semiquinone' ($E_{ox/sq}$) and 'semiquinone'/hydroquinone ($E_{sq/red}$) redox couples of FMN are also shown. Note that they appear in reverse order, indicating a strong positive cooperativity between the two electrons.
Only the potentials of the more significant redox populations of the cytochrome are represented in the picture: e_4^{123} is the redox potential of haem IV when the other three haems are still oxidised (i.e. it is the potential for the entry of the first electron in the molecule), e_3^{12} and e_2^1 are the redox potentials for the reduction of the two middle haems and e_1 is the redox potential for the reduction of haem I when the other three haems are already reduced (i.e. it is the potential for the entry of the last electron in the molecule).

The aim of the present work is to study the interaction between cytochrome c_3 from *D. gigas* and flavodoxin isolated from the same organism. Kinetic studies involving FMN, the protein

cofactor, are also presented here to compare the behaviour of the free redox centre with its behaviour inside the protein. Since this cofactor is not covalently attached to the apoprotein, there is always a certain amount of free FMN in equilibrium with the native flavodoxin, which can interfere with the kinetic studies. In order to be aware of the nature and extent of this interference it is necessary to perform kinetic studies with free FMN. Since most of the electron transfer studies between cytochrome c_3 and FMN were carried out for concentrations of the same order of magnitude of both redox partners, it is important to recall that the reduced free FMN molecule is a two electron donor with a redox potential around –290 mV (cf. right panel of Figure III.15), in order to understand the results obtained.

III.5.2 Results

To follow the electron transfer processes that take place between cytochrome c_3, FMN and flavodoxin, signals were acquired at different wavelengths (see Figure III.6). The reduction of the cytochrome is detected by an increase in absorbance at λ= 552 nm. However, the signal at this wavelength has a contribution of ca. 20 % from the semiquinone form of flavodoxin that has to be subtracted in order to obtain exclusively the optical change of the cytochrome. To follow the oxidation or reduction of flavodoxin, measurements are made at λ= 620 nm, a wavelength close to the maximum absorption for the semiquinone form of flavins, at which the cytochrome does not absorb. The reduction of oxidised FMN or flavodoxin can be observed by the decrease in absorbance at λ= 433 nm, a wavelength which corresponds to a pseudo isosbestic point for the cytochrome and is not far from the wavelength which has maximum absorption for oxidised flavins. Although the absorbance changes at this wavelength are small, this is not a true isosbestic point. In the initial stages of reduction, a small increase in absorbance is observed and, as reduction proceeds, this increase in absorbance is followed by a decrease of the same intensity. Comparable absorbance changes are detected in all cytochrome c_3 "isosbestic points", those of the α band displaying smaller intensity changes than those of the Soret band. At λ= 560 nm the absorbance changes follow the order described above whereas at λ= 413 nm and λ= 542 nm that order is reversed, in the sense that an initial decrease in absorbance is followed by a final increase. This apparently odd behaviour of the "isosbestic points" in cytochrome c_3 has already been described in the literature, where it has been attributed to the formation of a kinetic intermediate (Tabushi et al. 1983 ; Yagi, 1984) or to a conformational change triggered by reduction of haem IV

(Kazanskaya et al. 1996). In our opinion however, these absorbance changes may simply be the result of slightly different visible spectra of the four haems, particularly that of haem IV.

III.5.2.1 Reduction of FMN and flavodoxin by sodium dithionite

Stopped-flow kinetic studies of the reduction of flavodoxin from *D. gigas* by sodium dithionite are presented here and compared to the reduction of FMN, the protein cofactor alone. If the reduction is followed at λ= 433 nm, it is evident from the kinetic traces that the reduction of flavodoxin is much slower than the reduction of the cofactor alone: for the concentrations tested, the latter is completed in ca. 200 millisecond, whereas for flavodoxin the process takes about 300 second (see Figure III.16).

If the reduction process is followed at λ= 620 nm, FMN and flavodoxin display totally different behaviour. On the time scale for flavodoxin reduction, a bell-shaped signal is observed (Figure III.16A) indicating the formation and disappearance of a semiquinone form. It is also apparent from the figure that the signals recorded at λ= 620 nm and λ= 552 nm coincide, showing that the semiquinone band has similar extinction coefficients at these two wavelengths. On the time scale for FMN reduction, no signal is observable at λ= 620 nm (Figure III.16B), which is compatible with a simultaneous two-electron transfer going directly from the oxidised to the fully reduced form without formation of the intermediate semiquinone.

These results confirm that the protein moiety surrounding the FMN prosthetic group not only stabilises the intermediate semiquinone form by decreasing the midpoint redox potential of the couple fl^{sq}/fl^{red} (Curley et al., 1991 ; Stockman et al., 1994 ; Zhou and Swenson, 1996 ; Ludwig et al., 1997), but also displays a kinetic effect, slowing down the reaction with the negative reducing agent, possibly due to the presence of acidic residues close to the FMN group (Stewart et al., 1988 ; Watt et al., 1991 ; Helms and Swenson, 1992 ; Vervoort et al., 1994).

It is interesting to note that, in order to obtain a good simulation of the progress curve for flavodoxin reduction by sodium dithionite (Figure III.16A2), a comproportionation reaction (Dubourdieu et al., 1975 ; Mayhew and Ludwig, 1975) has to be considered in addition to the redox equilibria represented in Scheme IV. In this reaction, an oxidised flavodoxin molecule receives one electron from a fully reduced flavodoxin molecule, giving rise to two

semiquinone molecules. Since, independently of the presence of sodium dithionite, this process leads to a change in the concentrations of the three flavodoxin species, it was included in the differential equations defined for flavodoxin in the kinetic model.

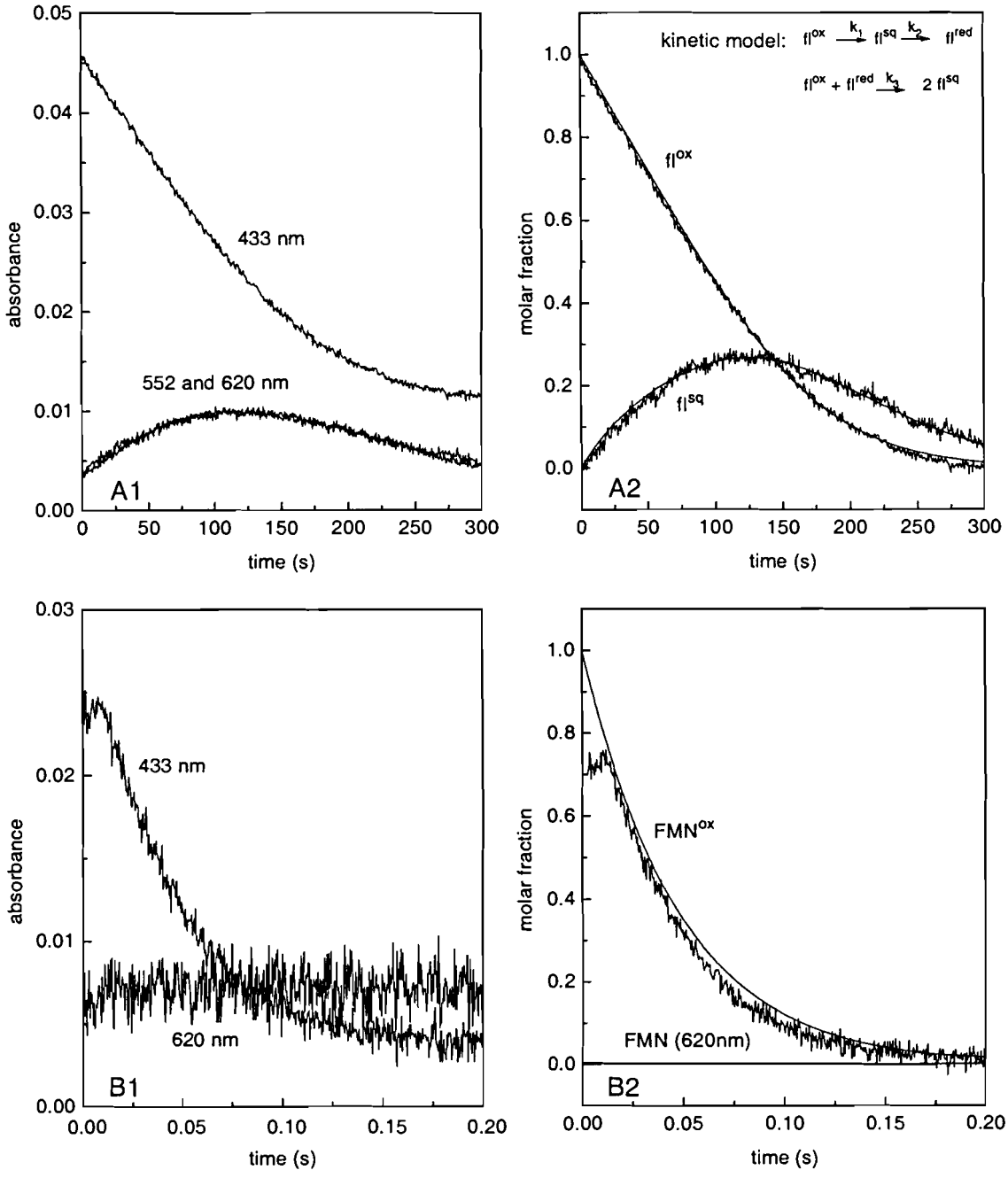

Figure III.16. Kinetics of reduction of flavodoxin from *D. gigas* and FMN by sodium dithionite. Flavodoxin and FMN react with sodium dithionite in different time scales and display different kinetic behaviour at 620 nm. (A1) Overall progress curves for the reduction of 5.9 μM flavodoxin by 500 μM sodium dithionite, followed at the wavelengths indicated in the picture. (A2) The same data after normalisation, together with computer simulated curves. The simulation of the time evolution of oxidised flavodoxin (fl^{ox}) and flavodoxin semiquinone (fl^{sq}) was made using the kinetic model indicated at the top with the following rate constants: k_1= 7×10^3 $M^{-1}s^{-1}$, k_2= 3×10^4 $M^{-1}s^{-1}$ and k_3= 3×10^3 $M^{-1}s^{-1}$. (B1) Overall progress curves for the reduction of 2.1 μM FMN by 125 μM sodium dithionite, followed at the wavelengths indicated in the picture. (B2) The same data after normalisation together with computer simulations. The simulation of the time evolution of oxidised FMN (FMN^{ox}) and FMN 'semiquinone' (FMN(620nm)) was made using the following rate constants: k_1= 5×10^7 $M^{-1}s^{-1}$, k_2= 1×10^{10} $M^{-1}s^{-1}$ and k_3= 0 $M^{-1}s^{-1}$. All experiments were performed at 25 °C in 0.25 M glycine buffer at pH 9.6.

The different kinetics of FMN and flavodoxin can be very useful in the determination of the amount of free FMN in a particular flavodoxin sample. The concentration of free FMN depends on the value of the binding constant, which changes with temperature, pH and ionic strength. However, since this cofactor is not covalently bound, its concentration can also depend on the age and history of the flavodoxin sample. For example, if a flavodoxin sample is lyophilised, a great quantity of the FMN dissociates from the protein and it is difficult to quantify it by visible spectroscopy since FMN and flavodoxin have very similar spectra. Nevertheless, this can be done easily by running a simple stopped-flow experiment against sodium dithionite. From the amplitudes of the fast and slow events recorded at λ= 433 nm the relative concentrations of free FMN and native flavodoxin can be calculated. Since it gives the concentrations of native flavodoxin and unbound FMN simultaneously, this method can be used for the determination of equilibrium binding constants under various experimental conditions.

III.5.2.2 Electron transfer between cytochrome c_3 and FMN

III.5.2.2.1 Oxidised c_3 vs. (FMN+dithionite)

The comparison between the reduction of cytochrome c_3 by sodium dithionite alone and by sodium dithionite in the presence of FMN (Figure III.17) shows that the signals are still biphasic in the presence of FMN, with slightly higher fast and slow rate constants. In the presence of FMN the fast rate constant increased ca. 10 times relative to dithionite alone, whereas the slow rate constant is only doubled. This result can be explained by the presence of two reducing agents competing for the reduction of the cytochrome, the larger increase observed for the fast rate constant is compatible with FMN being a more efficient electron donor for haem IV than for haem I (cf. section III.5.3.3), which is predictable from the relative redox potentials (Figure III.15, right panel).

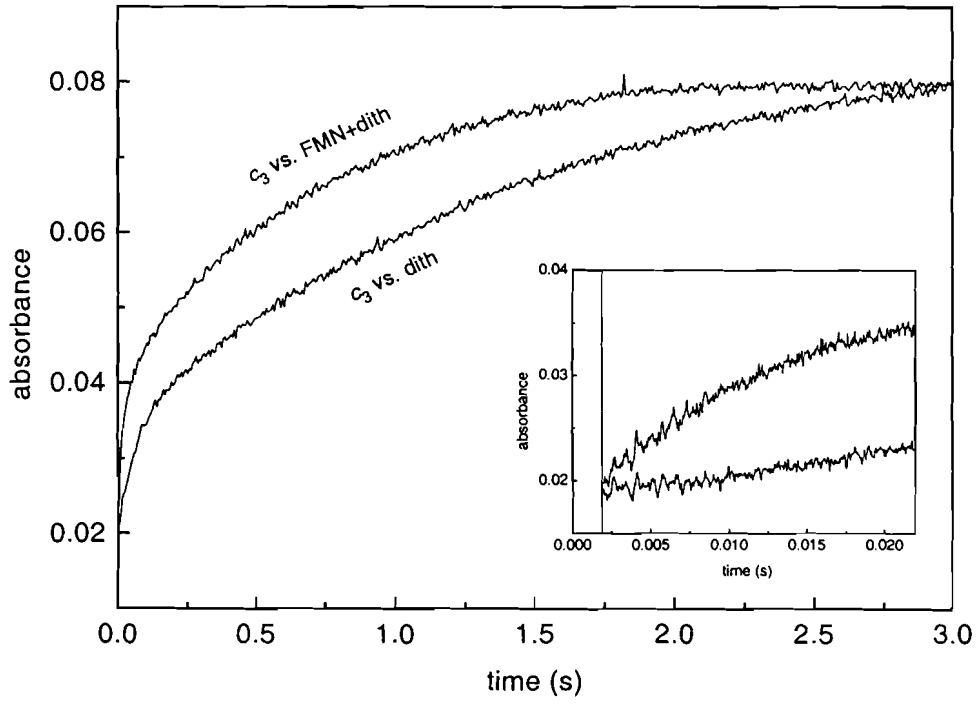

Figure III.17. Reduction of cytochrome c_3 by sodium dithionite alone and in the presence of FMN. Oxidised Dgc_3 was mixed with sodium dithionite in the stopped-flow apparatus and the absorbance at λ= 552 nm was recorded as a function of time (c_3 vs. dith). The same experiment was repeated after adding FMN to the syringe containing sodium dithionite (c_3 vs. (FMN+dith)). Concentrations after mixing: [Dgc_3]= 0.7 μM, [$Na_2S_2O_4$]= 125 μM, [FMN]= 2.1 μM. Buffer: 0.25 M glycine pH= 9.6. T= 25 °C. INSERT: Expanded time scale to show that the two progress curves are separated from the beginning. The deadtime of the stopped-flow apparatus is indicated by a vertical line.

III.5.2.2.2 Oxidised (c_3+FMN) vs. dithionite

However, a different effect is observed if FMN and cytochrome c_3 are present in the same syringe, thus both being oxidised at time zero. In this case, the reduction of cytochrome followed at λ= 552 nm shows a small initial lag phase with a reduction rate constant equal to that of the control experiment in which the cytochrome alone was mixed with sodium dithionite (Figure III.18A). FMN reduction by sodium dithionite takes place during the lag phase, after which an increase in the reduction rate of Dgc_3 is observed, since reduced FMN competes with dithionite for the reduction of the cytochrome.

The most intriguing feature of this experiment is the increase in the amplitude of the fast phase observed for increasing FMN concentrations (Figure III.18B). This effect is not present in c_3 vs. (FMN+dithionite) experiments in which the usual 25 % of fast phase is maintained. Also, the increase in the fast rate is not as pronounced as in the first case.

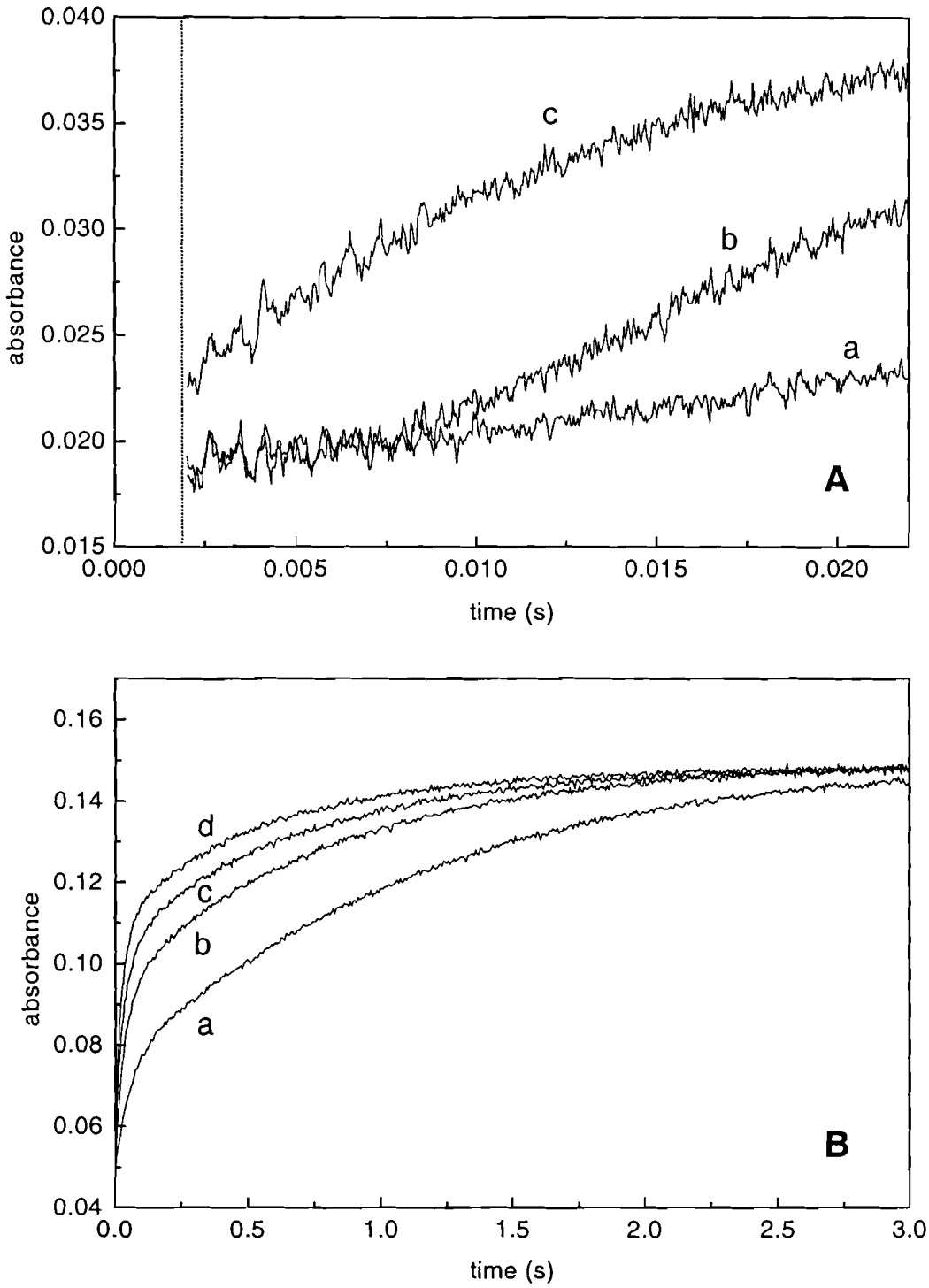

Figure III.18. Reduction of cytochrome c_3 by sodium dithionite in the presence of FMN. (A) The comparison between different kinds of experiments is shown for a short time scale: (a) cytochrome c_3 against sodium dithionite, (b) cytochrome c_3 plus oxidised FMN against sodium dithionite, (c) cytochrome c_3 against sodium dithionite plus reduced FMN. All signals were recorded at λ= 552 nm. The deadtime is indicated by a vertical line. Concentrations after mixing: [Dgc_3]= 0.7 μM, [$Na_2S_2O_4$]= 125 μM, [FMN]= 2.1 μM. (B) The reduction of Dgc_3 alone and in the presence of oxidised FMN are compared: (a) cytochrome c_3 against sodium dithionite, (b-d) The same experiment was performed with increasing amounts of FMN added to the syringe containing cytochrome c_3. All signals were recorded at λ= 552 nm. Concentrations after mixing: [Dgc_3]= 1.4 μM, [$Na_2S_2O_4$]= 250 μM, [FMN]= 1.2 μM (b), 2.3 μM (c) and 4.6 μM (d). All experiments were performed in 0.25 M glycine buffer pH= 9.6 at 25 °C.

III.5.2.2.3 Reduced c_3 vs. oxidised FMN

Experiments on the oxidation of reduced cytochrome c_3 by FMN were performed inside an anaerobic chamber. The cytochrome c_3 sample was reduced by hydrogen in the presence of catalytic amounts of hydrogenase and was mixed in the stopped-flow apparatus with an oxidised, but carefully degassed, FMN sample. For a constant cytochrome concentration, the percentage of oxidation observed increases with increasing concentrations of FMN up to a maximum of about 70 % for a 40 fold concentration excess of FMN (Figure III.19). The oxidation curves are biphasic and both rate constants increase with increasing FMN concentrations. On the basis of the redox potentials presented in Figure III.15 (right panel), full oxidation of c_3 is not expected, even for a large FMN excess, because the electron transfer from haem IV to FMN is highly unfavourable.

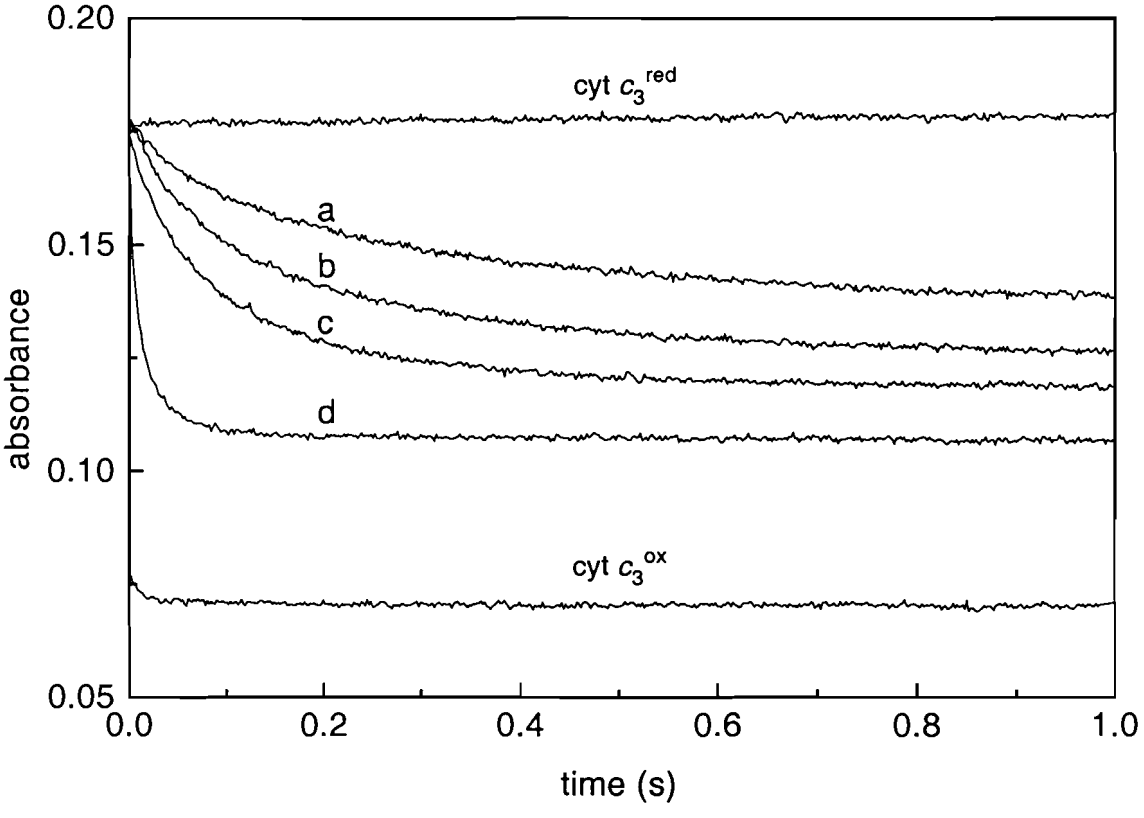

Figure III.19. Kinetics of oxidation of Dgc_3 by FMN. Cytochrome c_3 was reduced by hydrogen in the presence of catalytic amounts of hydrogenase and mixed in the stopped-flow under strict anaerobic conditions with different concentrations of oxidised FMN. Concentrations after mixing: [Dgc_3]= 1.5 μM; [FMN]= 1.5 μM (a), 3.1 μM (b), 5.7 μM (c) and 58 μM (d). The reference values for the absorbance of the reduced (cyt c_3^{red}) and oxidised (cyt c_3^{ox}) forms were obtained in the reaction of reduced cytochrome with sodium dithionite and potassium ferricianide, respectively. Buffer: 0.25 M glycine pH= 9.6. T= 25 °C. Absorbance measurements were made at λ= 552 nm.

III.5.2.3 Electron transfer between cytochrome c_3 and flavodoxin in the presence of excess sodium dithionite

III.5.2.3.1 Oxidised c_3 vs. (flavodoxin+dithionite)

The kinetics of reduction of cytochrome c_3 by fully reduced flavodoxin in the presence of a large excess of sodium dithionite are compared with the reduction of the cytochrome by dithionite alone. These results are presented in Figure III.20, where the biphasic character of the reaction with dithionite is evident. If reduced flavodoxin is in excess over cytochrome c_3, the cytochrome reduction rate is so dramatically increased that a significant part of the reaction occurs within the deadtime of the stopped-flow equipment (ca. 2 ms). However, if the reduced flavoprotein is not in excess, a very fast phase (essentially lost in the deadtime) is followed by a slower process that corresponds to the reduction of the cytochrome by dithionite alone (not shown).

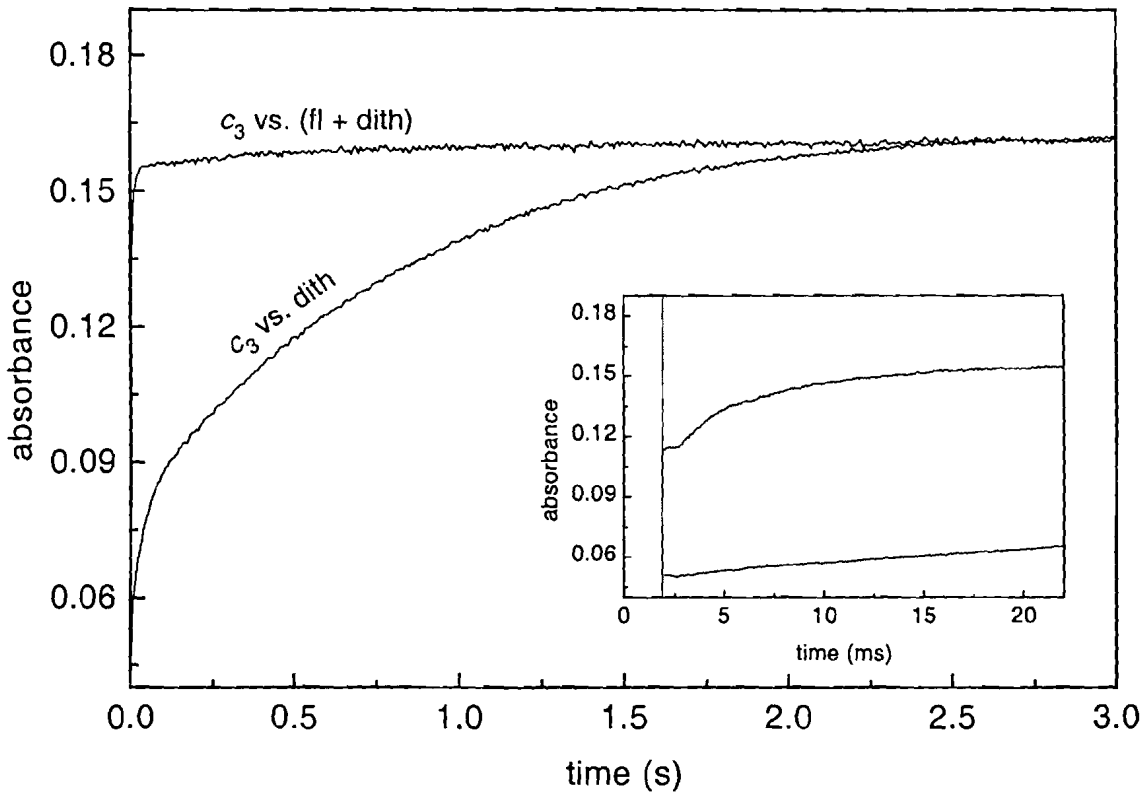

Figure III.20. Kinetics of reduction of Dgc_3 by sodium dithionite alone and in the presence of flavodoxin. Oxidised cytochrome c_3 was mixed with sodium dithionite in the stopped-flow apparatus and the absorbance at λ= 552 nm was recorded as a function of time (c_3 vs. dith). The same experiment was repeated after adding flavodoxin from *D.gigas* to the syringe containing sodium dithionite (c_3 vs. (fl+dith)). Absorbance measurements were made at λ= 552 nm and corrected for the optical contribution of flavodoxin semiquinone by subtraction of the corresponding signal at λ= 620 nm. Concentrations after mixing: [Dgc_3]= 1.3 μM; [$Na_2S_2O_4$]= 500 μM; [flavodoxin]= 5.2 μM. Buffer: 0.25 M glycine pH= 9.6. T= 25 °C. INSERT: The same experiment in a shorter time scale to show that part of the reaction is carried out within the deadtime of the stopped apparatus (indicated by a vertical line).

For a given flavodoxin-to-cytochrome concentration ratio, the amplitude of the very fast phase indicates that each reduced flavodoxin molecule transferred only one electron to the cytochrome in this phase. This result shows that the reduction of cytochrome c_3 by the hydroquinone form of flavodoxin is much faster than the reaction with sodium dithionite and that the semiquinone form of flavodoxin does not participate in the process if an excess of dithionite is present. Since the driving force for the reaction between oxidised c_3 and dithionite is larger than the driving force for the reaction between fully reduced flavodoxin and oxidised c_3 (cf. Figure III.15, left panel), for comparable concentrations of the reducing agent, the faster rate obtained in the presence of flavodoxin indicates that protein-protein recognition effects may have an important role in the electron transfer process even in a collisional mechanism.

III.5.2.3.2 Oxidised (c_3+flavodoxin) vs. dithionite

It is apparent from Figure III.21A that if flavodoxin is placed in the cytochrome syringe, thus being oxidised at time zero, the effect observed on the kinetics of cytochrome c_3 reduction by dithionite is exactly the opposite of that described above. After a fast phase similar to that observed with dithionite alone, the cytochrome reduction is slowed down in the presence of flavodoxin. This is interpreted as the result of electron transfer from cytochrome c_3 to oxidised flavodoxin, with subsequent formation of flavin semiquinone. It is evident from the corrected traces at λ= 552 nm that this process delays the complete reduction of the cytochrome until all flavodoxin is in the semiquinone form. On the other hand, the semiquinone formation is speeded up by electron transfer from the cytochrome, as is clear from the analysis of the traces at λ= 620 nm (Figure III.21B), showing the very slow reduction of flavodoxin by dithionite alone, compared to the much faster reduction in the presence of cytochrome c_3. The maximum transient amplitude of the semiquinone signal increases, possibly because the semiquinone is being formed at a faster rate, whereas its reduction rate is not significantly affected. It should be noted that cytochrome c_3 does not have the potential to reduce flavodoxin up to the hydroquinone form because the redox potential of the semiquinone/hydroquinone pair is more negative ($E_{sq/red}$= -440 mV) than the redox potential of any of the four haems in the cytochrome (cf. Figure III.15, left panel). Indeed, experiments on the reduction of oxidised flavodoxin by reduced c_3, in the absence of excess dithionite, show that the flavoprotein is only reduced to the semiquinone level (see next section, particularly Figure III.23, bottom panel).

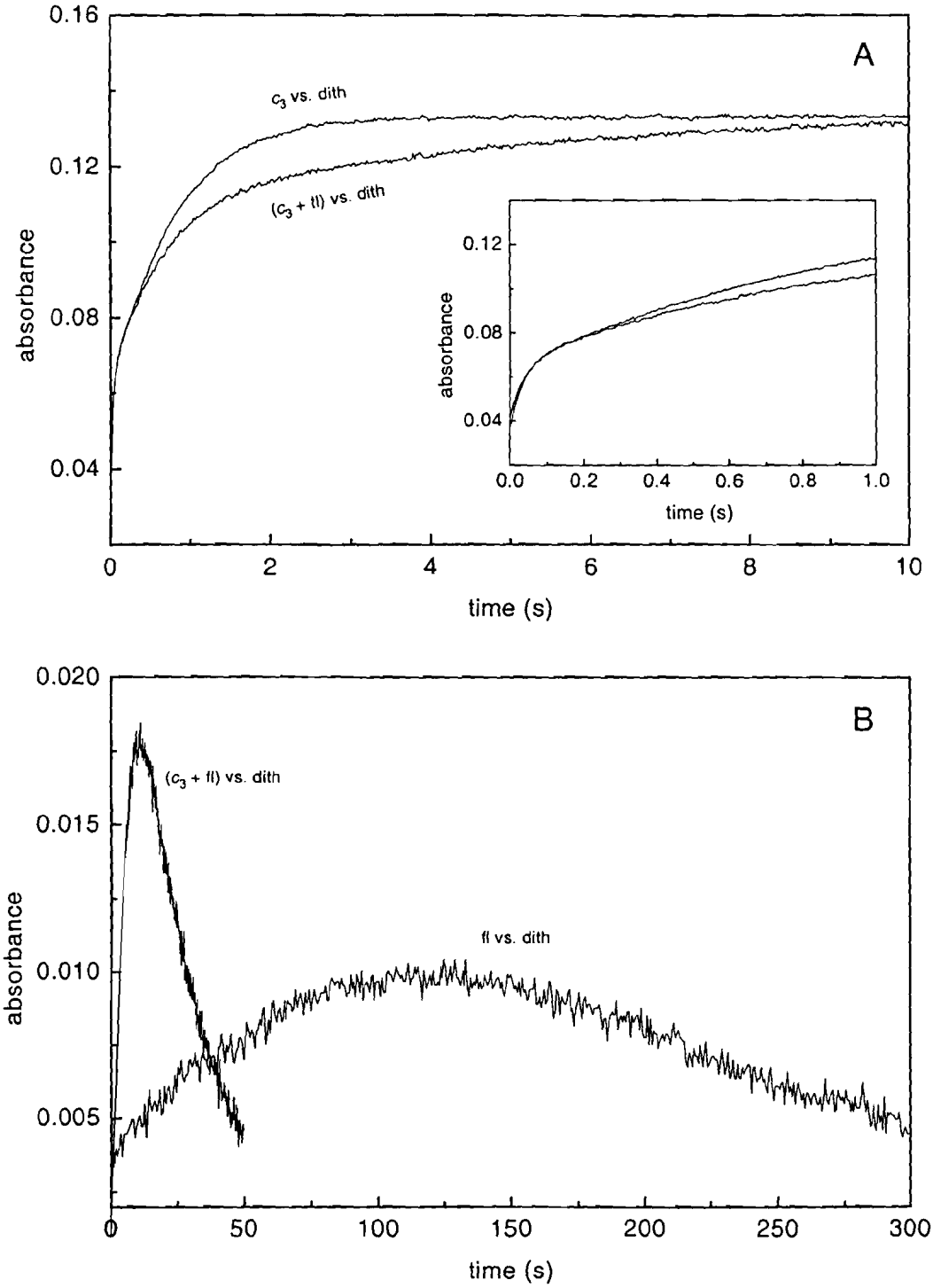

Figure III.21. Kinetics of reduction of Dgc_3 and flavodoxin alone and in the presence of each other by sodium dithionite. (A) The reduction of cytochrome c_3 is delayed in the presence of oxidised flavodoxin. The reduction of Dgc_3 by sodium dithionite was measured at λ= 552 nm (c_3 vs. dith). The experiment was repeated with flavodoxin from *D. gigas* added to the syringe containing cytochrome c_3 ((c_3+fl) vs. dith). Absorbance measurements were made at λ= 552 nm and corrected for the optical contribution of flavodoxin semiquinone by subtraction of the corresponding signal at λ= 620 nm. INSERT: The same experiment in a shorter time scale to show that the two curves are superimposed at the initial stages of reduction. (B) The reduction of flavodoxin is accelerated in the presence of cytochrome c_3. Kinetics of reduction of flavodoxin from *D. gigas* by sodium dithionite (fl vs. dith). The same experiment with cytochrome c_3 added to the syringe containing flavodoxin ((c_3+fl) vs. dith). Absorbance measurements were made at λ= 620 nm, a wavelength at which only the semiquinone form of flavodoxin contributes to the visible spectrum. Concentrations after mixing: [Dgc_3]= 1.1μM, [flavodoxin]= 5.9 μM, [$Na_2S_2O_4$]= 500 μM. Buffer: 0.25 M glycine pH= 9.6. T= 25 °C.

III.5.2.4 Electron transfer between cytochrome c_3 and flavodoxin in the absence of excess sodium dithionite

The electron transfer processes inferred from the two types of experiments described above, c_3 vs. (fl+dithionite) and (c_3+fl) vs. dithionite, were later confirmed by kinetic studies performed inside an anaerobic chamber, under strict anaerobic conditions. In the former studies a large excess of sodium dithionite was used in order to prevent reoxidation of the samples. To run stopped-flow experiments between oxidised cytochrome c_3 and fully reduced flavodoxin and between fully reduced cytochrome c_3 and oxidised flavodoxin in the absence of excess dithionite, strict anaerobic conditions were needed. In all the experiments performed the two initial species were mixed in concentrations of the same order of magnitude; the pseudo-first order approximation for the reducing species is therefore not valid under our experimental conditions.

III.5.2.4.1 Oxidised c_3 vs. reduced flavodoxin

If oxidised cytochrome c_3 is mixed with fully reduced flavodoxin in the stopped-flow apparatus, reduction of the cytochrome is immediately detected by the increase in absorbance at λ= 552 nm. Figure III.22 shows that, for different concentration ratios of the two proteins, a different extent of reduction of c_3 (top panels) and oxidation of flavodoxin (bottom panels) is observed. For each experiment, the amplitude of electron transfer observed is always in agreement with the differences in the redox potentials and the concentrations of the two proteins, indicating that the system evolves towards thermodynamic equilibrium.

It is also apparent from Figure III.22 (cf. left and right panels) that there are two different events taking place on different time scales. In the millisecond range, the very fast reduction of the cytochrome by the hydroquinone form of flavodoxin results in an increase of the absorbance at λ= 552 nm, which is mirrored by a simultaneous rapid semiquinone formation observed at λ= 620 nm. It should be noted that, since cytochrome c_3 is oxidised at time zero and flavodoxin is fully reduced, both signals should start at zero absorbance. However, this is not detectable because the deadtime of the stopped-flow apparatus does not allow the observation of the initial fast events. If the initial concentration of reduced flavodoxin is below four times the concentration of cytochrome, i.e. below the concentration of haems, further reduction of c_3 is achieved in the second time range. This slower process is the result

of electron transfer from the semiquinone form of flavodoxin, as observed by the decrease in the absorbance at λ= 620 nm.

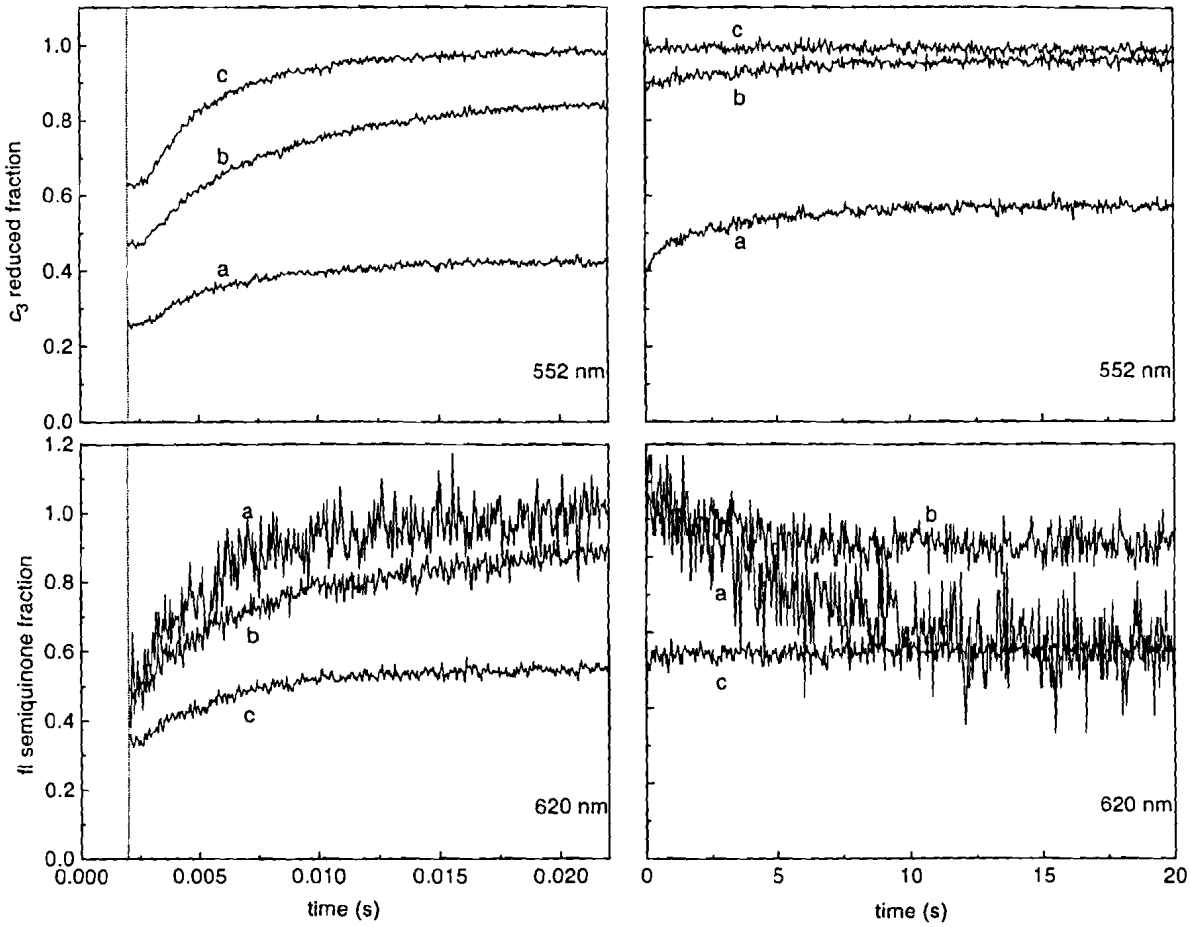

Figure III.22. Rapid and slow events in the reaction between oxidised cytochrome c_3 and reduced flavodoxin from *D. gigas*. LEFT PANELS: rapid events observed upon mixing oxidised cytochrome c_3 with different concentrations of reduced flavodoxin under strict anaerobic conditions. Rapid reduction of the cytochrome is observed (λ= 552 nm) with concomitant semiquinone formation (λ= 620 nm). The deadtime of the stopped-flow apparatus is indicated by a vertical line. RIGHT PANELS: slow events observed in the same experiment. For $[fl^{red}]/[c_3{}^{ox}]$ ratios below 4 (experiment a), further reduction of the cytochrome can be observed (λ= 552 nm) together with oxidation of semiquinone (λ= 620 nm). All signals were normalised in order to display the cytochrome reduced fraction (λ= 552 nm) and the flavodoxin semiquinone fraction (λ= 620 nm). The signals at λ= 552 nm were corrected for the semiquinone contribution. Concentrations after mixing: [Dgc_3]= 0.86 μM, [flavodoxin]= 1.4 μM (a), 3.3 μM (b) and 6.2 μM (c). Buffer: 0.25 M glycine pH= 9.6. T= 25 °C.

The comparison between these results and previously published kinetic data shows that, for similar concentrations of the two redox proteins, the time scale of the reduction of Dgc_3 by reduced flavodoxin (Figure III.22 left panels) is of the same order of magnitude as that of the reduction of Dmbc_3 by reduced ferredoxin I (Capeillère-Blandin et al., 1986). In both cases, part of the signal is lost in the deadtime of the apparatus and the part which is observed is monophasic. Also, both reactions are completed within ca. 20 ms. Therefore, similar second order rate constants are expected for the two reactions. Although the rate constant determined in this study for haem I is indeed similar to that measured by Capeillère-Blandin et al. (cf.

Table III.1), that of haem IV is almost two orders of magnitude higher. It should be noted that the reduction of haem IV takes place within the deadtime of the stopped-flow apparatus and the value of its rate constant is calculated from the application of the kinetic model, not from the rate constant of the observed monophasic trace. The rate constant of haem IV is too high to be determined by stopped-flow techniques and, in fact, the first 25% of the reaction was never observed in the stopped-flow the experiments. The observed monophasic signal has an amplitude of only 75% of the total optical density change and corresponds to the reduction of the three slower haems.

It is interesting to note that the rate constants measured by cyclic voltammetry for the reduction of Dgc_3 and Dmbc_3 by hydrogen in the presence of catalytic amounts of the hydrogenases isolated from the same organisms (Nivière et al., 1988 ; Haladjian et al., 1987) are of the same order of magnitude as those measured by stopped-flow techniques for the reduction of Dmbc_3 by ferredoxin I (Capeillère-Blandin et al., 1986) and for the slow part of the reaction between oxidised Dgc_3 and fully reduced flavodoxin (cf. Table III.1).

III.5.2.4.2 Reduced c_3 vs. oxidised flavodoxin

The oxidation of a reduced sample of cytochrome c_3 by different concentrations of oxidised flavodoxin is shown in Figure III.23. This process is much slower than the cytochrome reduction by the hydroquinone form of flavodoxin, occurring on the same time scale as reduction by the semiquinone (cf. Figure III.22).

The traces recorded at λ= 552 nm show partial oxidation of c_3, increasing with flavodoxin concentration, and have a biphasic character. However, since the fast phase is absent from the corresponding signals at λ= 620 nm, this phase is probably the result of electron transfer from cytochrome c_3 to free FMN. The maximum percentage of oxidation achieved in these experiments is close to 75 % for a flavodoxin-to-c_3 concentration ratio of 20 (not shown). It is apparent from the shape and amplitude of the traces acquired at λ= 620 nm that flavodoxin is reduced only to the semiquinone level, as expected from the redox potentials of both partners (cf. Figure III.15, left panel). The maximum 75 % oxidation observed is also consistent with the redox potentials presented, since electron transfer from haem IV to oxidised flavodoxin is highly unfavourable from the thermodynamic point of view.

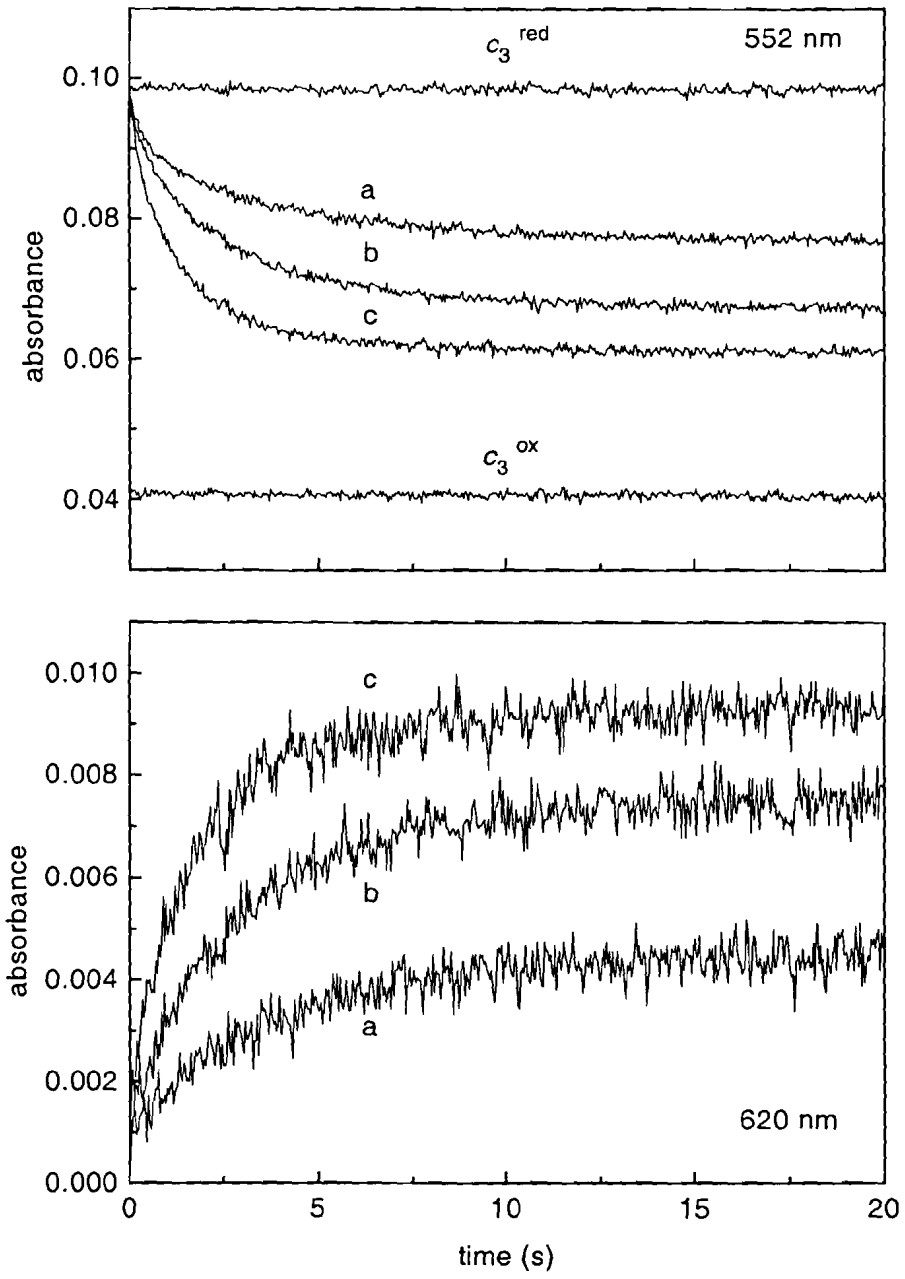

Figure III.23. Kinetics of oxidation of cytochrome c_3 by flavodoxin from *D.gigas*.
Cytochrome c_3 was reduced by hydrogen in the presence of catalytic amounts of hydrogenase and mixed with different concentrations of oxidised flavodoxin in the stopped-flow apparatus under strict anaerobic conditions. The oxidation of the cytochrome was monitored at λ= 552 nm (TOP PANEL), whereas the formation of flavodoxin semiquinone was monitored at λ= 620 nm (BOTTOM PANEL). The reference values for the absorbance of the reduced (c_3^{red}) and oxidised (c_3^{ox}) cytochrome were obtained from the reaction of reduced Dgc_3 with sodium dithionite and with potassium ferricyanide, respectively. The signals at λ= 552 nm were corrected for the semiquinone contribution. Concentrations after mixing: [Dgc_3]= 0.82 μM, [flavodoxin]= 1.1 μM (a), 2.9 μM (b) and 6.1 μM (c). Buffer: 0.25 M glycine pH= 9.6. T= 25 °C.

The results presented above, on the reoxidation of cytochrome c_3 by flavodoxin with both proteins isolated from *D. gigas*, are very similar to the results obtained by De Francesco et al., 1994, for the homologous *D. vulgaris* system at high ionic strength. In both cases the kinetics are biphasic and, although the two studies were performed at different pH values, 9.6 for

D. gigas and 7.5 for *D. vulgaris*, the second order rate constants obtained are of the same order of magnitude. Oxidised cytochrome c_3 and flavodoxin semiquinone are the result of the electron transfer process in both cases. However, while for *D. gigas* only 75 % oxidation is achieved, for *D. vulgaris* full reoxidation of the cytochrome is observed for a stoichiometry of 4 flavodoxin molecules per c_3 molecule. This difference is in agreement with the higher redox potential for the oxidised/semiquinone couple of *D. vulgaris* flavodoxin (-149 mV, Dubourdieu et al., 1975), which makes the electron transfer from any of the haems of Dvc_3 a thermodynamically favourable process, since all the midpoint redox potentials of this cytochrome are below –200 mV (cf. Table II.5 of section II.3.3).

III.5.3 Application of the kinetic model

In this section it will be shown that the simple collisional model described can simulate qualitatively most of the data presented in the results section. For the purpose of the model, it has been assumed that the reducing agent is able to give only one electron per encounter. Although the hydroquinone form of flavodoxin is able to give two electrons per encounter, it will be shown later that this is not the case in practice. This is because, as shown before, the electron transfer rate for the reaction with the hydroquinone form is three orders of magnitude faster than that with the semiquinone form and, since complex formation and dissociation are not rate limiting under our experimental conditions, it is faster to transfer two electrons from two hydroquinone molecules than two consecutive electrons from the same flavodoxin molecule. To define the differential equations of this system all of the processes that lead to cytochrome c_3 reduction or oxidation are considered independently, competing for the same sites with different rate constants. Thus, four reduction rate constants for the interaction of the deprotonated form of cytochrome c_3 with flavodoxin hydroquinone, plus four reduction rate constants for the interaction with flavodoxin semiquinone have to be defined.

Certain limitations of this study restrict our analysis to a qualitative level. These limitations concern essentially experimental problems and uncertainties in the relative redox potentials and concentrations. The relevant limiting factors will be discussed for each set of experimental data.

Since most of the observed traces have a biphasic character similar to those obtained in the kinetic studies with sodium dithionite, a kinetic model with only two independent parameters will be used for the preliminary analysis presented here. In this first approach, the rate

constants of haems I and IV were taken as the two kinetic parameters of the model, on the basis of the electron fluxes calculated for each individual haem in the reaction between Dgc_3 and dithionite (see Table III.4 of section III.4). In that section, it was shown that fittings of similar quality were obtained either taking only the rate constants of haems I and IV (the other two being zero) or equal rate constants for haems I-III and a different rate constant for haem IV. The second model was chosen for the analysis of the kinetic data with sodium dithionite because the reducing agent was a small inorganic molecule and, therefore, equally accessible to all the haems (section III.4). However, for the analysis of the kinetic studies presented in this section, the first model is used. Since the reducing agent is another protein, it is more likely that there will be preferential interactions with some of the haems than indiscriminate interaction with all of them.

For the sake of simplicity normalised data are be used in the simulations. Thus, in this section, reduced fraction rather than OD is represented as function of time.

III.5.3.1 Reaction with fully reduced flavodoxin

For the very fast electron transfer reaction from flavodoxin hydroquinone to cytochrome c_3, there are serious experimental problems due to the deadtime, mixing time and the small concentrations that had to be used in order to observe any reaction after the deadtime. In fact, a significant part of the reaction is lost in the deadtime, with a consequent loss of information about the rate for the first 25 % of the reduction. While the traces are clearly biphasic in the reaction with dithionite, with the fast phase corresponding to the first 25 % of reduction, this first 25 % is missing from the exponential fittings in the reaction with hydroquinone and thus the very fast observed traces are essentially monophasic. This does not mean that haem IV is no longer the faster haem to react with the hydroquinone, it simply means that the experimental curves lack information about the rate constant of this haem because it is too fast to be determined by stopped-flow techniques. In fact, simulations made with the collisional model presented here give a value of $3\times10^9\ M^{-1}s^{-1}$ for the rate constant of haem IV, indicating that this haem still reacts much faster than the others (Figure III.24).

In order to decrease the observed rates and increase the percentage of reaction observed after the deadtime, small concentrations of the two redox partners were used in these studies. Very noisy traces with amplitudes close to the detection limits are therefore obtained, even with the 10 mm pathlength used. A problem of imperfect mixing arises from the use of this pathlength,

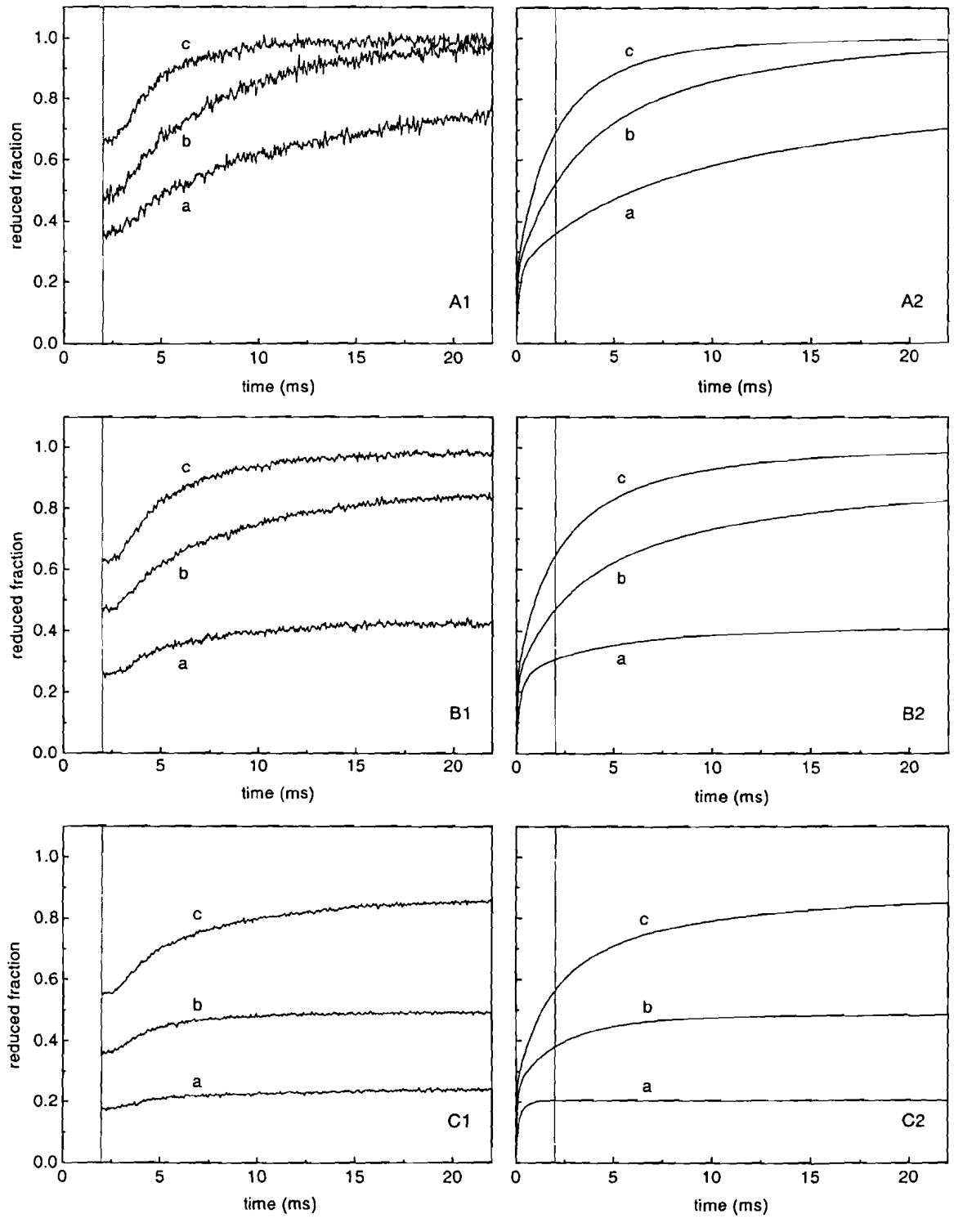

Figure III.24. Kinetics of reduction of Dgc_3 by the hydroquinone form of flavodoxin. Experimental data and simulations. Different traces correspond to different cytochrome to flavodoxin concentration ratios. LEFT PANELS: Experimental data acquired at λ= 552 nm and corrected for the optical contribution of the semiquinone. The traces were normalised in order to display the cytochrome reduced fraction as a function of time. RIGHT PANELS: Computer simulations using the collisional model described in the text with the following second order rate constants for the electron transfer process from fully reduced flavodoxin to haem i: k_{+1}= 5.0×10^7 $M^{-1}s^{-1}$, k_{+2}= k_{+3}= 0.0 $M^{-1}s^{-1}$, k_{+4}= 3.0×10^9 $M^{-1}s^{-1}$. Concentrations after mixing: [Dgc_3]= 0.39 μM (A1, A2), 0.86 μM (B1, B2) and 1.70 μM (C1, C2); [flavodoxin]= 1.4 μM (a), 3.3 μM (b) and 6.2 μM (c). Buffer: 0.25 M glycine pH= 9.6. T= 25 °C. The deadtime of the stopped-flow apparatus is indicated by a vertical line.

resulting in the sigmoidal shape of the traces during the first few millisecond. Indeed, since in the 10 mm pathlength the observation is made along the direction of the flow, the solution observed is not all of the same age. The solution which enters the cell is only 2-(2.25/2)= 0.875 ms old, whereas the solution leaving the cell is already 2+(2.25/2)= 3.125 ms old (see section 5.F of the SF-61 Hi-Tech Scientific Users guide). As the mixing time is not necessarily much smaller than the deadtime, there is no guarantee that the reagents are thoroughly mixed at 0.875 ms, especially for viscous protein solutions. In fact, it is apparent from the traces that the sigmoidal shape is more marked for the higher protein concentrations. Because the observed reaction progress is smaller than that expected for a perfect mixing, the simulated curves should pass above the sigmoidal part of the experimental traces, leaving only the final stages of reduction to be reliable for fitting, which is clearly insufficient for accurate quantitative analysis.

As mentioned before, the present analysis is based on restricting the number of haems involved in direct electron transfer with fully reduced flavodoxin. Since very fast monophasic signals were observed after the deadtime, the first attempt was made assuming the involvement of only one haem. However, the shape of the simulated curves did not match the shape of the experimental traces and two haems had to be considered. Therefore, the rate constants of haems I and IV were taken as the two kinetic parameters of the model, as discussed above. The result of the fit of the extended data set presented in Figure III 24 panels A to C is listed in table III.6.

Table III.6. Reduction rate constants for the electron transfer reactions between cytochrome c_3 and flavodoxin from *D. gigas*. For comparison, the reduction rate constants for the reactions with sodium dithionite and FMN are also presented. In this preliminary analysis only haems I and IV were considered to play a role in the interaction with the different redox partners. The parameters k_{+i} ($M^{-1}s^{-1}$) are the second order rate constant for the reduction of haem i, obtained from the application of the model to the observed experimental traces; fl^{sq} stands for flavodoxin semiquinone and fl^{red} for flavodoxin hydroquinone.

	k_{+1} ($M^{-1}s^{-1}$)	k_{+2} ($M^{-1}s^{-1}$)	k_{+3} ($M^{-1}s^{-1}$)	k_{+4} ($M^{-1}s^{-1}$)
Dithionite	2.4×10^6	0	0	2.2×10^7
FMN	3.0×10^5	0	0	3.0×10^7
	2.0×10^6	0	0	3.0×10^7
fl^{red}	5.0×10^7	0	0	3.0×10^9
fl^{sq}	2.2×10^4	0	0	2.2×10^5

It should be noted that, because of the severe experimental limitations described above, these rate constants can only be regarded as orders of magnitude. Nevertheless, the simulations show that the time evolution of the different species in these experiments can be simulated by the very simple collisional model. Since each reduced flavodoxin molecule gives only one electron in this very fast phase, more than one encounter with different flavodoxin molecules is needed to achieve more than 25% reduction and the general shape of the traces would be different if complex formation and dissociation steps were rate limiting.

The initial sigmoidal shape of the traces cannot be caused by complex formation being the rate limiting step because a significant part of the reduction of the cytochrome occurs within the deadtime of the apparatus and the reaction involves consecutive one-electron steps. In addition, if the lag phase arose from complex formation, it should decrease with increasing protein concentrations, which is not observed.

Besides the mixing problem already mentioned, it is apparent from Figure III.24 (curve a of panels C) that the observed slope after the fast phase in the experimental curve is not well simulated by the present model. This slope reflects the reduction of cytochrome c_3 by reduced free FMN, which is in equilibrium with the bound cofactor in flavodoxin (Dubourdieu, 1970). Since the current set of differential equations only takes into account interactions between cytochrome c_3 and flavodoxin, the FMN contribution does not show up in the simulated curves. The assignment of this slope to Dgc_3 reduction by free FMN is based on the results obtained from the kinetic studies between c_3 and FMN. The electron transfer rate observed in c_3 vs. (FMN+dith) experiments is of the same order of magnitude as that attributed to FMN in these experiments. Moreover, the amplitude of the signal is also compatible with the expected concentration of free FMN on the basis of the dissociation equilibrium constant for *D. gigas* flavodoxin, K_d= 0.0147 μM (Dubourdieu, 1970).

III.5.3.2 Reaction with flavodoxin semiquinone

For the cases of FMN and semiquinone, the limitations which prevent quantitative analysis of the data do not originate in the poor quality of the kinetic traces since the problems of deadtime and insufficient mixing are not relevant for these longer time scales. Now the problems are related to uncertainties in the relative redox potentials and concentrations. For partners which have similar redox potentials, the error in the final percentage of reduction associated with an uncertainty in the redox potentials is much larger, since the final

equilibrium mixture depends both on their initial concentrations and on their relative redox potentials. Under these circumstances, any small change in the relative redox potentials upon complex formation will be significant. Imprecise calculations of the relative concentrations of the redox partners, caused by poorly defined extinction coefficients, can also affect the final percentages of reduction. Given this perspective, the poor quality of some of the simulations of the data is easily understood, and the validity of the model should not be questioned until reliable values are found for the extinction coefficients and for the relative redox potentials in the complexes between Dgc_3 and FMN and Dgc_3 and flavodoxin.

It is shown in Figure III.25 that the collisional model developed in this thesis, with the rate constants reported in Table III.6 for flavodoxin semiquinone and dithionite, is able to simulate the time dependence of the different species involved in the electron transfer reaction between cytochrome c_3 and flavodoxin semiquinone. Information on the reduction of Dgc_3 by the semiquinone is taken from the simulations of the slow events in c_3 vs. fl^{red} experiments, for flavodoxin concentrations smaller than 4 times the cytochrome concentration (see Figure III.25 panels A). On the other hand, information on c_3 oxidation by semiquinone is taken from c_3^{red} vs. fl^{ox} (see Figure III.25 panels B and C) and (c_3+fl) vs. dithionite experiments (see Figure III.25 panels D and E). Note that, in the reaction between reduced Dgc_3 and oxidised flavodoxin, an initial fast phase is observed at λ= 552 nm but not at λ= 620 nm. This fast phase is probably the result of electron transfer from cytochrome c_3 to free FMN, which is faster than the equivalent reaction with flavodoxin semiquinone (cf. section III.5.3.3), and does not show up at λ= 620 nm because there is no semiquinone formation during FMN reduction (cf. Figure III.16).

Figure III.25. Kinetics of electron transfer reactions between Dgc_3 and flavodoxin semiquinone. Experimental data and simulations. Different panels correspond to different experiments that give information about the electron transfer processes which occur between cytochrome c_3 and flavodoxin semiquinone. LEFT PANELS: Experimental data acquired at the wavelengths indicated in the pictures. The traces at λ= 552 nm were corrected for the optical contribution of the semiquinone. All traces were normalised in order to display either the cytochrome reduced fraction (λ= 552 nm) or the semiquinone fraction (λ= 620 nm) as a function of time. RIGHT PANELS: Computer simulations using the collisional model described in the text with the following rate constants for the electron transfer reaction from flavodoxin semiquinone to haem i: k_{+1}= 2.2×10^4 $M^{-1}s^{-1}$, k_{+2}= k_{+3}= 0.0 $M^{-1}s^{-1}$, k_{+4}= 2.2×10^5 $M^{-1}s^{-1}$. PANELS A: Slow events in the reaction between reduced flavodoxin and oxidised cytochrome c_3. Concentrations after mixing [Dgc_3]= 5.6 μM and [flavodoxin]= 1.8 μM. PANELS B and C: Reaction between reduced cytochrome c_3 and oxidised flavodoxin. The oxidation of the cytochrome is monitored at λ= 552 nm and the reduction of flavodoxin to the semiquinone level is observed at λ= 620 nm. Concentrations after mixing: [Dgc_3]= 0.82 μM, [flavodoxin]= 1.1 μM (a), 2.9 μM (b) and 6.1 μM (c). PANELS D: Reduction of cytochrome c_3 alone (a) and in the presence of flavodoxin (b) by sodium dithionite. Concentrations after mixing: [Dgc_3]= 1.1 μM, [flavodoxin]= 5.9 μM, [$Na_2S_2O_4$]= 500 μM. PANELS E: Reduction of flavodoxin alone (a) and in the presence of cytochrome c_3 (b) by sodium dithionite. Concentrations after mixing: [Dgc_3]= 1.1 μM, [flavodoxin]= 5.9 μM, [$Na_2S_2O_4$]= 500 μM. All experiments were performed in 0.25 M glycine buffer at pH= 9.6. T= 25 °C.

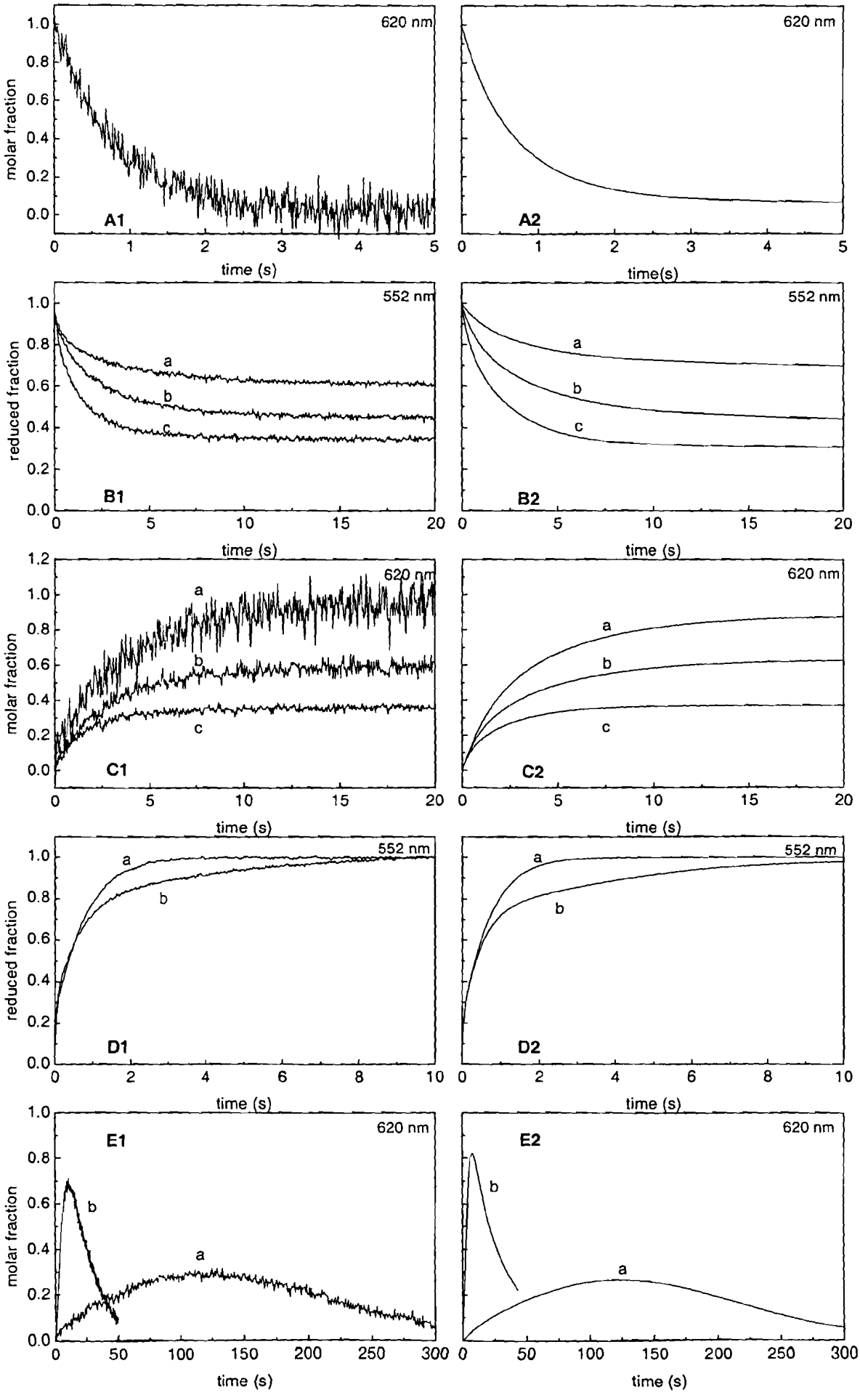
620 nm
molar fraction
A1
time (s)
620 nm
A2
time(s)
552 nm
reduced fraction
a
b
c
B1
time (s)
552 nm
a
b
c
B2
time (s)
620 nm
molar fraction
a
b
c
C1
time (s)
620 nm
a
b
c
C2
time (s)
552 nm
reduced fraction
a
b
D1
time (s)
552 nm
a
b
D2
time (s)
620 nm
molar fraction
E1
b
a
time (s)
620 nm
E2
b
a
time (s)

III.5.3.3 Reaction with FMN

The reaction between cytochrome c_3 and FMN occurs on an intermediate time scale, between the very fast reaction with hydroquinone and the slow reaction with semiquinone. The second order rate constants obtained in this preliminary analysis for the reduction of haems I and IV by FMN are close to those obtained for sodium dithionite (Table III.6). However, since on thermodynamic grounds FMN contributes mainly to the reduction of haem IV, the biphasic character of the overall progress curves is expected to increase in the presence of FMN. Although the concentrations of sodium dithionite (ca. 125 μM) and FMN (ca. 2 μM) are very different in the experiment presented in Figure III.17, the time scales of the traces are comparable because the actual electron donor in dithionite is the dissociated species SO_2^-, which is present in a much smaller concentration ($\sqrt{1.4\text{x}10^{-9}[dithionite]}$, according to Lambeth and Palmer, 1973). Considering that FMN is a two electron donor while SO_2^- can only give one electron, the rate constants for the transfer of one electron to haem IV are similar for FMN and SO_2^-. Therefore, the ten fold increase observed for k_{fast} in the experiments with FMN, reported in Figure III.17, can be explained by the presence of a five times more concentrated two-electron donor.

The application of the kinetic model to the FMN case presents a problem of stoichiometry. Since FMN is a two-electron donor and cytochrome c_3 is an acceptor of four consecutive electrons, the simulation of the FMN data should be made considering only two-electron steps with a midpoint redox potential of -290 mV (Clark, 1972). Under these conditions, the only populated stages would be stage zero (fully reduced molecule with four electrons), stage two (half reduced molecule with two electrons) and stage four (fully oxidised molecule) since intermolecular electron exchange is in fact slow for the concentrations used in these experiments. However, the final percentages of reduction can reach any value through the relative concentrations of stages zero, two, and four, just as they do if all five stages are accessible.

A simplified approach was followed, which consisted of considering two one-electron steps with a very high positive cooperativity between the redox potentials. Thus, for the reduction of FMN at pH = 9.6, two steps with n = 1 and redox potentials E_{1step} = -316 mV and E_{2step}= -250 mV were used. These latter values were calculated for pH = 9.6 from the redox potentials at pH = 7 reported in Mayhew and Ludwig, 1975, assuming a redox potential change of 30 mV per pH unit according to Clark, 1972. This later approach is simpler because it is compatible with the framework developed for the analysis of the flavodoxin data and,

although less accurate, we believe that it is adequate for the qualitative level of this work. Therefore, the simulation of the reduction and oxidation of Dgc_3 in the presence of FMN was performed using the same differential equations used for the reaction with flavodoxin but with the redox potentials given above and different reduction rate constants for the two steps, such that only a negligible amount of the intermediate semiquinone is formed. The simulations obtained with the collisional model for the reduction rate constants reported in Table III.6 are shown in Figure III.26. It can be seen that, although not perfect, the simulations are able to reproduce the time scale and general behaviour of the traces, both for the reduction and the oxidation pathways.

It should be noted that, although the time scales are comparable, the results obtained in (c_3+FMN) vs. dithionite experiments are qualitatively different from the results obtained for c_3 vs. (dithionite+FMN), since an increase in the percentage of the fast phase is observed in the first case but not in the second. This result is unexpected on the basis of our simple collisional model. In both cases, an increase in the reduction rate is observed, relative to the control experiment with sodium dithionite alone. This means that FMN is contributing to the reduction of c_3 in both cases. Therefore, in a (c_3+FMN) vs. dithionite experiment, FMN must itself be reduced by dithionite, before transferring the electrons to c_3. Apart from the observed lag phase (see FigureIII.18A), this experiment should be similar to the one starting with FMN already reduced. In fact, all the simulations show ca. 25 % of fast phase, in clear disagreement with the experimental data obtained for (c_3+FMN) vs. dithionite. One possible explanation for this result could be formation of a stable complex between cytochrome c_3 and oxidised FMN. In these experiments, there is enough time to allow complex formation before the electron transfer takes place, in clear contrast with what happens in c_3 vs. (FMN+dithionite) experiments. If the negatively charged phosphate group of FMN interacts with the cytochrome molecule preferentially in the vicinity of haem IV, which is not unreasonable due to the presence of the lysine patch, the redox potential of this haem might be affected, becoming more negative because of the presence of additional negative charges. Under these circumstances, the redox potential of haem IV would become closer to the redox potentials of the other haems, which could result in an increase of the amplitude of the fast phase.

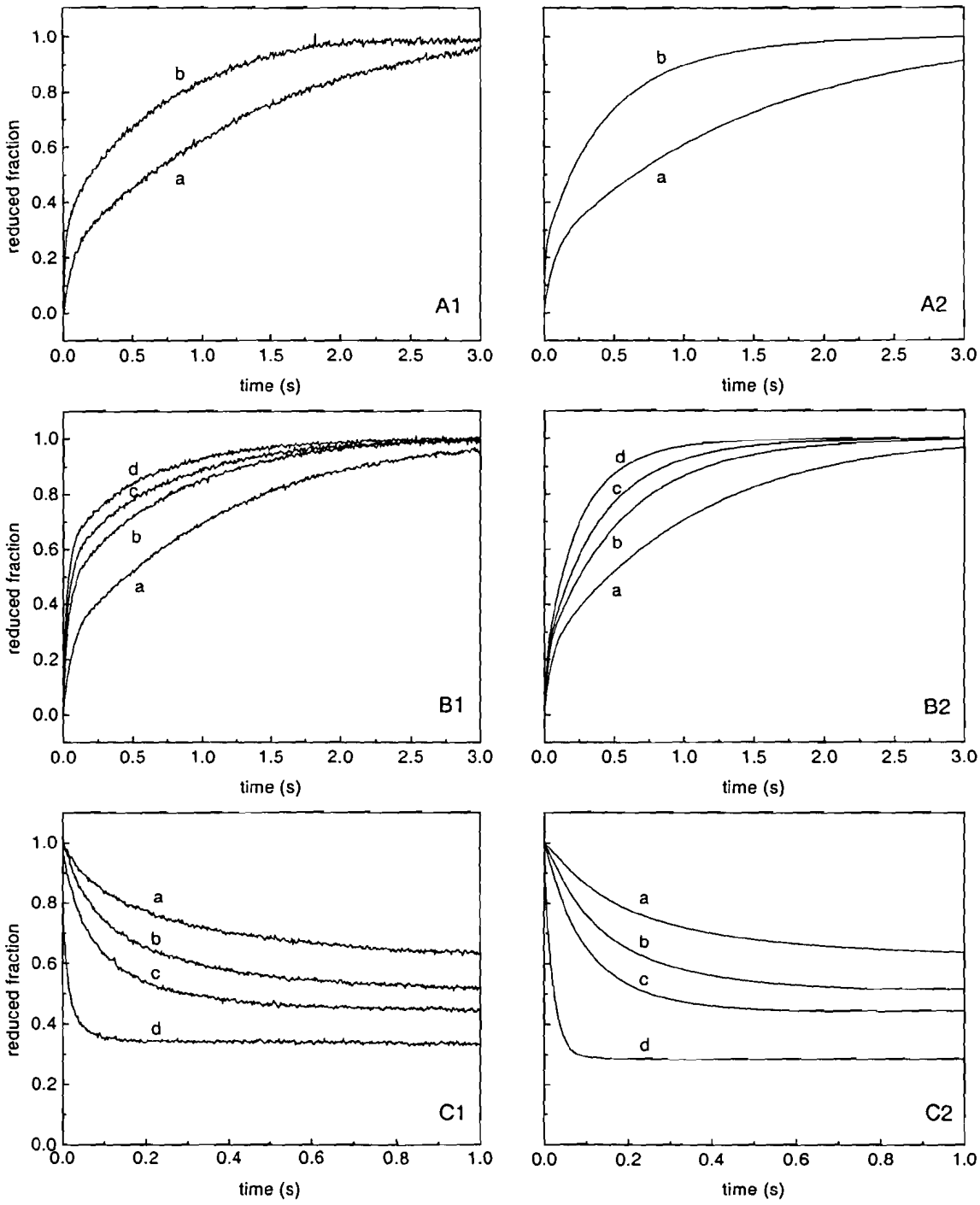

Figure III.26. Kinetics of reduction and oxidation of Dgc_3 in the presence of FMN. Experimental data and simulations. LEFT PANELS: experimental data acquired at λ= 552 nm and normalised in order to display the cytochrome reduced fraction as a function of time. Different experiments are represented in different panels. RIGHT PANELS: computer simulations using the collisional model described in the text with the following rate constants for the electron transfer from FMN^{red} to haem i: $k_{+1}= 3.0x10^5$ $M^{-1}s^{-1}$, $k_{+2}= k_{+3}= 0.0$ $M^{-1}s^{-1}$, $k_{+4}= 3.0x10^7$ $M^{-1}s^{-1}$ and from FMN^{sq} to haem i: $k_{+1}= 2.0x10^6$ $M^{-1}s^{-1}$, $k_{+2}= k_{+3}= 0.0$ $M^{-1}s^{-1}$, $k_{+4}= 3.0x10^7$ $M^{-1}s^{-1}$. PANELS A: Reduction of cytochrome c_3 by sodium dithionite alone (a) and with FMN added to the syringe containing sodium dithionite (b). Concentrations after mixing: [Dgc_3]= 0.7 μM, [FMN]= 2.1 μM, [$Na_2S_2O_4$]= 125 μM. PANELS B: Reduction of cytochrome c_3 by sodium dithionite (a) the same experiment was repeated with increasing amounts of oxidised FMN added to the syringe containing the cytochrome (b-d). Concentrations after mixing: [Dgc_3]= 1.4 μM, [$Na_2S_2O_4$]= 250 μM, [FMN]= 1.2 μM (b), 2.3 μM (c) and 4.6 μM (d). PANELS C: Reaction between reduced cytochrome c_3 and different concentrations of oxidised FMN under strict anaerobic conditions. Concentrations after mixing: [Dgc_3]= 1.5 μM, [FMN]= 1.5 μM (a), 3.1 μM (b), 5.7 μM (c) and 58 μM (d). All experiments were performed in 0.25 M glycine buffer at pH= 9.6. T= 25 °C.

III.5.4 Future developments

For the purpose of this thesis, I have restricted the analysis of the electron transfer data presented in this section to the qualitative level described above. The limitations to detailed quantitative analysis have been mentioned and other approaches have to be designed in order to overcome them. As part of this section on Future developments, some suggestions are made in this direction, but it should be stressed that any improvement beyond the qualitative level would be extremely time consuming both from the experimental and from the data analysis points of view. The additional information that might eventually be obtained from a more detailed analysis must be considered in the context of the amount of work involved in order to decide whether it would be worthwhile to extend these studies.

Even with experimental improvements, the determination of well defined rate constants for the four haems is restricted simply because some of the haems are thermodynamically linked. It was mentioned earlier that the system is always at internal equilibrium due to the very fast intramolecular exchange rate (Santos et al, 1984a), which means that only the rate constants for haems with significantly different thermodynamic parameters can be determined accurately (see kinetic model section III.3). The covariance matrix that results from a fitting procedure, without constraints on the number of haems involved, indeed shows that some of the rates are highly correlated. The highest covariance is found between the rate constants for haems II and III, as expected since these haems have the largest positive cooperativity between them (see Modelling of the thermodynamic properties, section II.3.3). Thus, the method cannot be used to discriminate between electrons entering the molecule through haem II or haem III. The covariances found between the rate constant of haem I and the rate constants for the middle haems (II and III) are smaller but not negligible. Since haem IV is the thermodynamically more separated haem in *D. gigas*, the lower covariances found are those involving haem IV. Thus, if a rate constant can be found for haem IV, it will be well defined, as was shown for the reaction between Dgc_3 and sodium dithionite (section III.4). The rate constants obtained for the other haems can never be well defined since different combinations of rate constants can generate very similar overall progress curves.

It should be stressed that the limitations found for an accurate determination of the rate constants of the individual haems are intrinsic to the system and cannot be overcome by any kind of improvements made in the analysis of the data. Since the rate constants for the individual haems would always be highly correlated, making it impossible to find unique

solutions. Therefore, the additional information obtained from a more detailed set of experiments seems unlikely to justify the investment of effort.

The main conclusion taken from the present work, which is that haem IV shows different kinetic behaviour, is well substantiated and, although more accurate values for the rate constants might eventually be obtained, the orders of magnitude reported here give a valuable insight into the kinetic behaviour of Dgc_3 in the electron transfer reactions with different redox partners.

III.5.4.1 Experimental progress

III.5.4.1.1 Improving the quality of the data

To proceed to a quantitative analysis of this complicated system it is necessary first to improve the quality of the data. For the very fast reaction with hydroquinone it is essential to avoid the mixing artefact in the beginning of the traces. To do so with the existing equipment, measurements have to be made using the 1.5 mm pathlength, i.e. across the direction of the flow. The consequent seven fold decrease in the signal cannot be compensated by an increase in the concentration of the reagents because the reaction would become even faster and more signal would be lost in the deadtime. An alternative to increasing the concentrations would be to acquire data in the more intense Soret band. There is no simple way of subtracting the optical contribution of the oxidised flavin at this wavelength (λ= 419 nm), however, since this contribution is only ca. 3 % (much smaller than the ca. 20 % at λ= 552 nm), it may be neglected. Also, the signal to noise ratio can be improved by averaging over a larger number of traces.

In addition to the mixing problem, there is the deadtime problem which cannot be overcome, because of the design of the stopped-flow apparatus. Thus, the deadtime has to be accurately determined to allow the correct positioning of the kinetic traces on a true reaction time scale and, although the very beginning will be missing, the fitting of these traces may be reliable.

As mentioned in the section on the application of the model, rigorous determination of the concentrations of the samples using good extinction coefficients and the determination of the redox potentials in the complexes would be essential to improving the analysis of the slower reactions with FMN and semiquinone. The first approach to the problem of redox potentials would be the performance of redox titrations, followed by visible spectroscopy, of the redox

partners alone and in the complex. If the results of the two titrations match, the complete analysis can be made using the present values, otherwise a more thorough investigation of the redox behaviour of both partners in the complex is needed.

III.5.4.1.2 Running experiments at different pH values

Both the thermodynamic (Coletta et al., 1991, Louro et al., 1998b) and the kinetic (Catarino et al., 1991) behaviour of Dgc_3 depend on the pH. Thus, since all the kinetic experiments with FMN and flavodoxin reported above were performed at pH = 9.6, a pH value above pK_a^{red}, the intrinsic rates for the reduction of the individual haems correspond to the deprotonated form (B) of the cytochrome. To have the complete description of this system, similar experiments have to be done at different pH values, some of them preferably below pK_a^{ox}. Note that, although it is not absolutely necessary to run experiments at a pH value below pK_a^{ox}, it is better to do so because the higher percentage of protonated cytochrome during the whole reduction process will allow a better definition of the limits of the rate constants for the A form. However, even if it is not possible to run experiments at such a low pH, provided that pH values between pK_a^{ox} and pK_a^{red} are included, the equilibrium between the A and B forms would provide sufficient information to test the sigma factor approximation used in the kinetic modelling of the pH dependence of the kinetic traces (see section III.3). The analysis of the pH dependence of the reaction between Dgc_3 and flavodoxin would follow the same strategy used for the data obtained for the reaction with sodium dithionite (section III.4.2). In that case, the same set of data was fitted by fixing either the rate constants for the protonated or for the deprotonated forms of the cytochrome in order to study the limits of variability of the rate constants determined. The rate constants of the other form are then calculated from the sigma factors, which are directly related to the redox-Bohr interacting potentials, according to the equations derived in the section on the kinetic model.

III.5.4.1.3 Running experiments at different ionic strengths

The influence of the ionic strength on the electron transfer between flavodoxin and Dgc_3 is another important factor that deserves further investigation. In principle, the dependence of the electron transfer rates on the ionic strength provides information on the type of interactions established between the two proteins upon complex formation. Several electron

transfer studies between flavodoxins and *c*-type cytochromes have been published and most of them include the investigation of ionic strength effects (Simondsen et al, 1982 ; Matthew et al., 1983 ; Tollin et al., 1984 ; Weber and Tollin 1985 ; Cheddar et al., 1986). With respect to cytochrome c_3, a strong influence of the ionic strength on the reaction between reduced Dvc_3 and flavodoxin isolated from the same organism has already been reported (De Francesco et al., 1994). If Dgc_3 behaves in a similar way, through formation of a more stable complex between the two redox partners, saturation kinetics are expected at low ionic strength. It has already been mentioned that, if this is the case, the simple collisional kinetic model would not be applicable and its extension to consider complex formation would enable us to obtain separate information on the binding constants and electron transfer rates.

III.5.4.1.4 Running experiments in the presence of calcium or phosphate ions.

Another interesting aspect that deserves investigation is the effect of the presence of different ions (particularly calcium and phosphate) on the electron transfer properties of Dgc_3. The X-ray structure of this protein revealed the unusual presence of a Ca^{2+} ion coordinated by six oxygen atoms, four from a protein loop near the N-terminus and two from each propionate of haem IV (Matias et al., 1996). Since haem IV is the main entrance gate for electrons in Dgc_3, it would be worth trying to remove this ion by chelating agents and study its effect on the kinetic properties.

It has been observed by NMR that the presence of phosphate changes the reoxidation pattern of Dgc_3 (Santos, 1984), indicating alterations in the thermodynamic parameters determined for this cytochrome. This effect is probably due to a specific interaction between this ion and the protein. There is preliminary evidence that the presence of phosphate affects the kinetics of reduction of Dgc_3 by sodium dithionite and that this effect depends on pH (unpublished results).

Regarding the interpretation of data collected under different experimental conditions, it should be noted that, since cytochrome c_3 is a thermodynamically controlled system, any modification of the kinetic properties has to be interpreted bearing in mind that changes in the thermodynamic parameters may have also occurred. Thus, under new experimental conditions, a complete thermodynamic analysis has to be made before drawing any conclusions from the new kinetic data.

III.5.4.2 Improvements in data analysis

The next step in data analysis is the quantitative description of the system by obtaining more accurate values for kinetic parameters from the fitting of the experimental results. This has to proceed through the above mentioned improvements in the quality of the data. However, if the use of higher quality data sets together with correct redox potentials and accurate concentration measurements does not improve the simulations, the validity of the restrictive hypothesis assumed for the derivation of the collisional model described in section III.3 would have to be questioned and more complex models may have to be developed.

To reduce the number of adjustable rate constants to four for each redox partner, microscopic reversibility was assumed by considering the ratio between the reduction rates (k_{+i}) and the oxidation rates (k_{-i}) equal the equilibrium constant (see kinetic model section III.3). This assumption is not necessarily valid for complex kinetic mechanisms (Denbigh, 1971). If this is the case, the fitting of eight independent rate constants, four reduction rate constants plus four oxidation rate constants per redox partner, would have to be considered.

Note that for the reaction with the hydroquinone neither the redox potential problem nor the equilibrium condition introduced into the calculation of the inverse rates are particularly relevant. Since the difference in the redox potentials between the haems in Dgc_3 and the semiquinone/hydroquinone couple of flavodoxin is large (cf. Figure III.15 left panel), the rate constant for the inverse reaction is negligible (see equation 10 of section III.3) and the final extent of cytochrome reduction depends solely on the relative concentrations of the two partners.

The simple collisional model may also collapse through formation of a kinetically detectable intermediate complex, which is more likely to happen under other experimental conditions, for instance in low ionic strength media. In this case the model would have to be extended in order to consider the formation of the intermediate complex. However, in both cases there would be extra information in the experimental data to support an increase in the number of parameters.

Finally, it should be stressed that, the derivation of the kinetic model in terms of the rate constants for the individual haems presented in this thesis relies on the sigma factor approximation (section III.3), because otherwise it would be impossible to correlate the rate constant of any haem in a given redox step with the rate constant of the same haem in a different redox step. If factors other than the driving force change during the reduction

process, or if the value of the driving force approaches the value of the reorganisation energy, the derivation of sigma factors in terms of the Marcus equation would not hold and the simple model presented in this work could not be used for the analysis of the kinetic data.

III.5.5 Conclusions

The conclusions taken from the present analysis of the data on the electron transfer reactions between cytochrome c_3 and flavodoxin from *D. gigas* are similar to those taken from previous studies in which sodium dithionite was used as reducing agent (Catarino et al., 1991). Under the experimental conditions used in this work, low concentrations and high ionic strength, a simple collisional model is able to simulate the general behaviour of the kinetic traces observed. The application of the model to the experimental data indicates that haem IV is working as the main electron entrance gate in the molecule. The major role played by haem IV in the reduction process either by sodium dithionite (Catarino et al., 1991) or by flavodoxin, can be easily rationalised. Indeed, although it is the second least exposed to the solvent (Matias et al., 1996), this haem is the nearest one to the lysine patch postulated as a docking site for the physiological partners (Stewart et al., 1988 ; Stewart et al., 1989 ; Dolla et al., 1991 ; Palma et al., 1994). Moreover, it displays the least negative redox potential and thus, according to the Marcus theory (Marcus and Sutin, 1985), has the largest driving force for the reduction process.

With flavodoxin semiquinone, FMN, and sodium dithionite, the intrinsic rate constant for the reduction of haem IV is only one order of magnitude faster than that of haem I, but with flavodoxin hydroquinone two orders of magnitude separate the rates for the reduction of these haems. Thus, the contribution of haem IV to the overall reduction is more important for flavodoxin hydroquinone than for the other cases. Indeed, in the reaction between oxidised Dgc_3 and flavodoxin hydroquinone, haem IV accounts for ca. 70 % of the total reduction, whereas, for instance for the dithionite case, only 40 % of the electrons enter the cytochrome molecule through this haem (see Table III.4 of section III.4).

It is worth mentioning that, because of the homology found between flavodoxin and domain II in the small subunit of the periplasmic hydrogenase (Volbeda et al., 1995), the electron transfer reaction between oxidised cytochrome c_3 and fully reduced flavodoxin is functionally more relevant than any of the others presented in this chapter. This reaction might mimic the reduction of the cytochrome by electrons coming from the splitting of molecular hydrogen

which is achieved by the periplasmic hydrogenase, the proposed physiological reaction, according to the hydrogen cycling mechanism (Odom and Peck, 1981). On this basis, the electron transfer studies with hydroquinone flavodoxin strengthen the view that haem IV is indeed the electron entrance gate in the cytochrome c_3 molecule.

IV CONCLUDING REMARKS

IV CONCLUDING REMARKS

IV.1 Thermodynamic properties of cytochromes c_3

Several models have been proposed for the analysis of the thermodynamic behaviour of cytochromes c_3. An overview of these models was presented in chronological order in this thesis, giving special emphasis to the modelling strategies and to the physical significance of the parameters defined in each case. Since cytochrome c_3 has four redox centres, the simpler models consider either four consecutive reversible electron transfer steps or four independent redox centres. However, since the existence of redox interactions among the haems was demonstrated by Santos et al., 1984a, more complex models have been developed in order to obtain information about the individual centres.

Santos et al., 1984a constructed a model with 16 microstates for the electron distribution between the four redox centres and, although 32 Nernst equations are necessary to relate these microstates, they showed that four microscopic redox potentials and six haem-haem interactions are sufficient to fully characterise the redox behaviour of the system at discrete pH values. The determination of the thermodynamic parameters of Dgc_3 at two different pH values showed that the microscopic redox potentials and, apparently, the haem-haem interactions were pH dependent, proving the existence of haem-proton interactions. The presence of haem-haem interactions was also observed in Dvc_3 (Miyazaki F) by Fan et al., 1990a. In this work the same model was used for the determination of the microscopic parameters of Dvc_3 (Miyazaki F) at a single pH value, thus obtaining no information about haem-proton interactions.

Following the pioneer work of Santos et al., 1984a and using the same data set, we proposed the first model which integrates the pH and the solution potential as variables of the system (Coletta et al, 1991). According to this model, the change in the thermodynamic parameters with the pH, particularly the haem-haem interactions, was the result of a pH-linked conformational change. Since the A/B model introduces new acid/base equilibria between the protonated and deprotonated conformations, the number of microstates increases to 32 and the number of parameters necessary to describe the thermodynamic properties of the system increases to 21 because each conformation is characterised by four microscopic redox potentials and six haem-haem interactions, and it is also necessary to define the equilibrium constant for the protonation of the reference state. It should be noted that, because of the assumptions of the model, the redox-Bohr and the haem-haem interactions are allowed to mix making it more difficult to associate positive haem-haem interactions with redox-linked

conformational changes. However, the positive cooperativity observed between haems II and III in Dgc_3 already pointed towards a redox-linked conformational change. Since this interaction was pH independent the proton could not be assisting the positive cooperativity between the haems. Although using a number of parameters larger than necessary, the A/B model showed for the first time that Dgc_3 couples proton and electron transfer in the physiological pH range.

Later, Turner et al., 1994 and 1996, showed that it was not necessary to invoke any change in the haem-haem interactions to explain the pH dependence of the haem methyl chemical shifts of Dvc_3 (Hildenborough) and proposed a model free of any structural assumptions. The model of five interacting centres does not imply any conformational changes *a priori* and uses only 15 parameters: the four haems and the ionisable centre are characterised by four microscopic redox potentials and by the pK_a of the fully reduced molecule and ten two-site interactions establish the relationships between the five centres. It has been demonstrated that this model uses the minimum number of parameters necessary to describe the complex network of cooperativities associated with the thermodynamic behaviour of different cytochrome c_3 molecules. Moreover, since in this model the haem-haem interactions are clearly separated from the redox-Bohr interactions and since it is not necessary to invoke three-site interactions to explain the properties of the system, it has been demonstrated that there are no major conformational changes associated either with pH or with redox potential. Therefore, the positive cooperativities observed between some of the haems are probably the result of localised movements.

It is interesting to note that, although different cytochromes are characterised by different parameters, some particular features are common to all of them; there is always a significant positive cooperativity between two of the haems and there are also positive cooperativities between the haems and an ionisable centre. The haems which display the unusual positive cooperativity are not the same in all cytochromes (cf. Table II.1) and, although for Dgc_3 and Dvc_3 they correspond to the middle haems with respect to oxidation order, this is not the case for Ddc_3 ATCC 27774. The ionisable group seems to be most closely associated with haem I for Dgc_3 and Dvc_3 whereas for Ddc_3 ATCC 27774 the group which ionises in the physiological pH region seems to be located in the vicinity of haem II. Since the architecture of the haem core is maintained in all cytochromes c_3 isolated so far and different haems play different roles in these molecules, there is no obvious relationship between the highly conserved structural arrangement of the haems and the network of cooperativities established among the five centres. It appears that these molecules have diverged in evolution while

retaining a common capability, which is the concerted transfer of two electrons coupled to the ionisation of an acid/base group. These properties result from the interplay of all cooperativities of the system. While negative cooperativities keep the redox potentials of the other two haems well separated, the positive cooperativity between two haems, assisted by the redox-Bohr cooperativities, forces the concerted two-electron step. Moreover, since the pK_a of the ionisable group increases along the reduction process as the result of haem-proton interactions (cf. Figure II.15), the acid/base centre becomes protonated when the pK_a becomes higher than the solution pH and coupling between electron and proton transfer is achieved.

It should be noted that these properties of cytochrome c_3 only became apparent after using thermodynamic models which take into account both pH and solution potential changes for the analysis of the available data. Indeed, this is the most important result of the thermodynamic modelling. By demonstrating that all cytochromes c_3 are able to perform a concerted two-electron step coupled to the uptake or release of protons, these models have shown that this protein has the ability to perform energy transduction (Louro et al., 1996a, and 1997b).

Both thermodynamic and kinetic control are essential to achieve energy transduction. On the one hand, it is necessary that the system displays the appropriate thermodynamic properties that lead to the coupling of electron and proton transfer and, on the other hand, the kinetic properties must drive the reactions in the correct direction.

It was shown that the kinetics of cytochrome c_3 are under thermodynamic control because there is fast intramolecular electron exchange in the stopped-flow time scale. Consequently, an accurate thermodynamic description of the redox and acid/base properties of the molecule is also essential for the analysis of the kinetic data. In this work, the model of five interacting centres was used for the simulation of the kinetic data of Dgc_3 and the results have shown that the kinetics do indeed assist the two-electron step through the acceleration of the electron transfer process that occurs when protonation takes place.

IV.2 Kinetic properties of cytochromes c_3

The electron transfer reactions between cytochrome c_3 from *Desulfovibrio gigas* and several electron donors and acceptors were studied using stopped-flow techniques coupled to visible spectroscopy. The results obtained were analysed in the framework of a kinetic model developed for this particular system with the objective of determining the rate constants for the individual haems. The complete kinetic scheme, which includes all possible electron transfer reactions between the 32 microstates, is reduced to a simple model of four consecutive electron transfer steps on the basis of the fast intramolecular electron exchange observed in this cytochrome. It is shown that the rate constants of the redox steps can be related to the rate constants of the individual haems through the thermodynamic parameters, provided that the approximation of using sigma factors is valid, i.e. that the rate constants for the individual haems are modulated along the reduction process by the haem-haem interacting potentials according the Marcus equation. Similarly, the pH dependence of the reduction of Dgc_3 by sodium dithionite is simulated assuming the validity of proton sigma factors. These factors determine the changes in the rate constants of the haems upon protonation which result from the redox-Bohr interacting potentials, again through application of the Marcus equation.

The application of the model to the stopped-flow data led to the determination of rate constants for the four haems. However, it was shown for the case of dithionite that these rate constants were not well defined because some of the haems are thermodynamically coupled. Therefore, a simpler model with only two parameters is used for the analysis of the data in this work. One of these parameters should be the rate constant of haem IV because it is well defined in Dgc_3, the second one is chosen to be either a rate constant which is the same for each of the other three haems or the rate constant of haem I.

The results show that haem IV has a kinetic behaviour which is distinct from the other three haems. In the reaction with sodium dithionite, the reduction rate constant of this haem is one order of magnitude faster than the rate constants of the other three. Since haem IV is the first to be reduced and a relatively large gap separates its redox potential from those of the other haems, a biphasic process is observed which consists of ca. 25 % of fast phase and ca. 75 % of slow phase. The computer simulation of the time evolution of the individual haems shows that, because of the redox interacting potentials, haem IV starts draining electrons to the other haems after attaining ca. 90 % of reduction, which makes it the entry gate for ca. 40 % of the total reduction process. It should be noted that the fast phase observed corresponds to the initial reduction of haem IV. After the first reduction step, although haem IV continues to

react ca. ten times faster than the other haems, only ca. 10% of the molecules have this haem still oxidised and able to receive an electron from sodium dithionite. Consequently, the rate of electrons entering the molecule through haem IV during the draining process is similar to the rate of electrons entering the molecule through the slower haems.

The importance of haem IV in the reduction process of Dgc_3 is even more marked in the reaction with fully reduced flavodoxin. Indeed, since two orders of magnitude separate the rate constant of haem IV from the rate constant of haem I in this reaction, the overall contribution of the faster haem rises to ca. 70 %.

The study of the pH dependence of the kinetics of reduction of Dgc_3 by sodium dithionite showed that the rates are faster in the acidic form, in accordance with the larger driving force for the electron transfer reaction. The biphasicity of the traces is lower at low pH because the increase in the rate constant of the slower haem I is larger than the increase in the rate constant of the faster haem IV. One interesting feature that emerges from the difference in rates between the basic and the acidic forms is that the reduction starts in the basic form and ends in the acidic one at physiological pH and, therefore, there is an acceleration of the reduction process. Consequently, the thermodynamic cooperativities which make the concerted transfer of two electrons possible are kinetically assisted by the increase in the reduction rate.

The different kinetic behaviour of haem IV can be related in structural terms to its proximity to a group of lysine residues. This positively charged region on the surface of the protein has been proposed to act as a docking site for the physiological partners (Stewart et al., 1988 ; Stewart et al., 1989 ; Dolla et al., 1991 ; Palma et al., 1994). A negatively charged electron donor, such as sodium dithionite, was therefore chosen for the initial kinetic studies. Later, a flavoprotein isolated from the same organism was used, working either as electron donor or electron acceptor depending on the experimental conditions. The sequence similarity found between flavodoxin and the N-terminal domain of the 28 kD subunit of the nickel-iron hydrogenase isolated from *D. gigas* (Volbeda et al., 1995) makes it a good model for the study of the interaction between cytochrome c_3 and hydrogenase, which is the actual electron donor *in vivo* (Yagi et al., 1968). The experimental results show that haem IV displays the highest reduction rate constant among the four haems, independently of either of the two reducing agents. However, the difference between the rate constant of haem IV and those of the other haems is more marked for the reaction between oxidised Dgc_3 and fully reduced flavodoxin. Since, among the reactions studied, this is the most similar to the actual electron

transfer reaction between cytochrome c_3 and hydrogenase, it strengthens the idea that the lysine patch is indeed the docking site for the physiological partners and that electrons enter the cytochrome molecule through the haem located in its vicinity. For Dgc_3, as well as for most of the cytochromes c_3, the haem nearest to the lysine patch is haem IV.

It is important to note that, despite the limitations raised to the accurate determination of the rate constants for the reduction of the four individual haems, the general conclusions of this work are well established and would not be significantly changed by any improvements in the quality of the data or by more sophisticated methods of analysis. Since either an inadequate experimental method or the specific properties of the system under study may lead to poorly determined rate constants for the individual haems, a brief discussion of the more relevant factors in different cases will be presented.

During the development of the kinetic model and the analysis of the data, indeterminate rate constants for the individual haems were frequently associated with the low resolution of the visible spectra for the discrimination of the four haems. At first sight it seems that accurate values for the individual rate constants could be obtained if it were possible to distinguish the individual haems by visible spectroscopy. In fact, the situation is more complicated. Due to the fast intramolecular electron exchange, the system is at thermodynamic equilibrium within every redox stage and, even if different signals could be assigned to the different haems, the time evolution of each of the signals would reflect the time evolution of the populations at equilibrium within the stages and not the rates for the entrance of the electrons into each separate haem. The conclusion is that the indeterminacy of the values of the rate constants of haems I-III in Dgc_3 is intrinsic to the system and does not derive from the experimental technique used to measure the rates.

Interestingly, the information which can be obtained from stopped-flow studies of this kind depends on the specific properties of each particular system. If intramolecular electron exchange were slow in cytochromes c_3, which is not the case, then the determination of individual rate constants would depend solely on the resolution of the visible spectra. The rate constants obtained from the simple analysis of the data with exponentials would be equal to the rate constants of the individual haems. However, it would be absolutely impossible to assign those individual rate constants to the haems in the structure unless each haem displayed a different visible spectra. It should be noted that this assignment would be impossible for haems with similar spectra even if they were thermodynamically uncoupled because the observed order of reduction of the haems in a stopped-flow experiment does not necessarily

follow the thermodynamic order.

Thus, on the one hand, the fast intramolecular electron exchange rate observed in cytochromes c_3 makes it impossible to find accurate values for the rate constants of thermodynamically coupled haems but, on the other hand, it enables the assignment of the rate constants to the haems in the structure, provided that a reliable thermodynamic description of the system is available. In this way, it was possible to demonstrate that haem IV is the main electron entrance gate in Dgc_3 and to determine the rate constant for the reduction of this haem in the reaction with different electron donors. This would have been impossible if the intramolecular electron exchange had been slow because the four haems in Dgc_3 are indistinguishable in the visible spectra.

Only the kinetic properties of cytochrome c_3 isolated from *Desulfovibrio gigas* were studied for this thesis. Other kinetic studies reported in the literature have been mentioned in section III.1. These studies involved cytochromes c_3 isolated from *Desulfovibrio vulgaris* Hildenborough and Miyazaki strains and *Desulfomicrobium baculatum* strain Norway 4 (formerly *Desulfovibrio desulfuricans* Norway and recently reclassified as *Desulfomicrobium norvegicum* by Genthner et al., 1997). Since the intramolecular electron exchange rate is also fast for these cytochromes, the kinetic model developed in this thesis can now be used as a basis for re-analysing the early kinetic data, provided that accurate thermodynamic parameters are known for each of these cytochromes.

The determination of the thermodynamic parameters of Dmbc_3 is not yet complete, which precludes the application of the new kinetic model. However, the thermodynamic parameters of Dvc_3 have already been published (Turner et al., 1996 and Salgueiro et al., 1997b for the Hildenborough and Miyazaki strains, respectively).

A quantitative analysis of the published kinetic data is beyond the scope of this work, but it is appropriate to comment briefly on some of the results reported in the literature for Dvc_3, particularly with respect to an apparent inconsistency in the biphasicity of the kinetic traces and the relative amplitudes of the fast and slow phases. Both monophasic and biphasic kinetic traces have been obtained for the reduction of Dvc_3 under different experimental conditions and, for the biphasic curves, the relative amplitudes of the fast and the slow phases vary from study to study (cf. Table III.1).

The biphasic nature of the kinetics of cytochrome c_3 has been interpreted in different ways. Capeillère-Blandin et al. 1986, related the difference in rates observed in the reduction of

Dmbc_3 by sodium dithionite to the existence of haems in fast and slow internal exchange of electrons. Favaudon et al, 1978 suggested that the four haems in Dvc_3 were in slow intramolecular equilibration of electrons and concluded that the haems were kinetically equivalent two by two. For the same cytochrome, De Francesco et al., 1994 proposed a model in which the biphasic character of the traces was originated by a two state conformational transition between acidic and basic forms. Schlereth et al., 1993 observed a conformational change associated with redox transitions in Dgc_3 and Dmbc_3 and suggested that these conformational changes might give rise to the biphasic reduction kinetics observed for various cytochromes c_3. The explanation proposed here is an extension of that given in Catarino et al., 1991, where the biphasicity of the traces was related to the existence of one haem reacting at a faster rate with the electron donor, in fast intramolecular electron exchange with the other slower haems. Depending on the separation between the redox potentials of the fast and slow haems, either monophasic or biphasic curves are observed and, for the biphasic ones, different percentages of fast phase are possible. It is also proposed here that the haem closest to the lysine patch, which is usually haem IV, works as the electron capture site on the reaction with negatively charged electron donors.

It is well known that the redox potential of each haem in Dvc_3 depends not only on the pH but also changes along the reduction process because of the redox interacting potentials (Turner et al., 1996). Consequently, the order of reduction and the separation between the redox potentials of the four haems is not obvious from the redox potentials determined for the fully reduced state only. However, for a particular pH value, the percentages of reduction for each of the haems at each intermediate stage can be calculated from the thermodynamic parameters. The values shown in Table IV.1 were calculated for the basic form at a pH value well above pK_a^{red} (7.5) and for the acid form at a pH value well below the pK_a^{ox} (5.4).

It is concluded from the table that the order of reduction of the haems in Dvc_3 is the same at high and low pH. Haem IV is reduced first, followed by haems I and II, and haem III is the last to be reduced. However, the percentage of reduction attained by each haem at each stage is pH dependent. At high pH, haem IV undergoes a higher percentage of reduction in the first step, i.e. the step from stage IV to stage III, than it does at low pH, and the same is true for haem III in stages II and I. Conversely, haem I is significantly more reduced in stage II at low pH than it is at high pH. Note that, in the basic form haems I, II, and III display similar percentages of reduction in stage II, whereas in the acidic form haem I is clearly more reduced than haems II and III.

Table IV.1. Percentages of reduction for each of the haems in Dvc_3 in each oxidation stage for the protonated and the deprotonated forms of the cytochrome. These values were calculated from the thermodynamic parameters reported by Turner et al., 1996, according to the thermodynamic model of five interacting centres described in section II.3.3. The haem which experiences the largest change in its reduction state in each step is marked with an asterisk. Shaded areas indicate the haems which have been significantly reduced in previous steps.

Acidic form	**Stage IV**	**Stage III**	**Stage II**	**Stage I**	**Stage 0**
Haem I	0	0.234	0.825 *	0.975	1
Haem II	0	0.053	0.334	0.941 *	1
Haem III	0	0.116	0.138	0.197	1 *
Haem IV	0	0.597 *	0.703	0.886	1
Basic form	**Stage IV**	**Stage III**	**Stage II**	**Stage I**	**Stage 0**
Haem I	0	0.027	0.408 *	0.836	1
Haem II	0	0.029	0.334	0.919 *	1
Haem III	0	0.102	0.380	0.307	1 *
Haem IV	0	0.842 *	0.878	0.938	1

Since haem IV of Dvc_3 is also located close to a lysine patch and has a comparable redox profile to that of Dgc_3, it is likely that this haem reacts faster than the other three haems with negatively charged electron donors. Thus, the relative amplitudes of the fast and slow phases are expected to depend mainly on the extent to which haem IV, which is the first haem to be reduced, transfers electrons to the other haems. If its redox potential is distinct from those of the other haems a high percentage of reduction is attained by this haem in the first reduction step, and a kinetic profile similar to that observed for Dgc_3 is anticipated. However, if a relatively low percentage of reduction is achieved, haem IV is able to drain electrons to the other haems and the amplitude of the fast phase is expected to increase because haem IV can continue to react rapidly during most of the reduction process. Therefore, the different percentages of reduction calculated for haem IV in the first reduction step (Table IV.1) indicate that the relative amplitudes of the fast and slow phases should be different at high and low pH. The larger difference between the degree of reduction of haem IV and those of the other haems at high pH should lead to a smaller amplitude of the fast phase while the electrons entering the molecule through the faster haem IV would be drained to the other haems at low pH, increasing the amplitude of the fast phase.

These predictions were based on thermodynamic parameters determined for Dvc_3 at room temperature, in low ionic strength media and in the absence of phosphate ions. However, it is

known that the redox potentials of the haems in cytochrome c_3 are sensitive, among other things, to these factors (Santos, 1984 ; Bertrand et al., 1994 and 1995.). Therefore, the separation between the redox potentials of haem IV and the other haems can be dependent not only on the pH but also on the temperature, ionic strength and on the presence of phosphate. These effects on the redox potentials are reflected in the modulation of the relative amplitudes of the fast and slow phases.

Moreover, it is apparent from the values of the rate constants reported in the literature (cf. Table III.1) that the difference between the fast and the slow rate constants is much smaller in Dvc_3 than in Dgc_3. The less marked biphasicity of the kinetic traces in Dvc_3 makes it easier to vary the phases and different relative amplitudes could easily be found under different experimental conditions.

In conclusion, the apparent discrepancies of the results of the kinetic studies with Dvc_3 reported in the literature (Favaudon et al., 1978 ; Tabushi et al., 1983 ; Capeillère-Blandin et al., 1986 ; De Francesco et al., 1994) can be understood in the framework of the kinetic model developed in this thesis together with the thermodynamic parameters determined for this cytochrome and their possible variation with experimental conditions.

There are no studies reported in the literature concerning the kinetic properties of cytochrome c_3 isolated from *Desulfovibrio desulfuricans* (ATCC 27774). NMR experiments show that the intramolecular electron exchange rate is also fast for this molecule and since the thermodynamic characterisation of this protein has been completed recently (Louro et al., 1998c), the kinetic model developed can be used to make some predictions. The parameters determined for this molecule indicate that haem III should be the first haem to be reduced, followed by haem IV with a redox potential ca. 100 mV more negative. Haems I and II have close redox potentials, more than 100 mV below haem IV. At physiological pH, these last haems should be reduced simultaneously. Assuming that haem IV is kinetically differentiated from the other haems because of the proximity of the lysine patch, the general kinetic behaviour of this cytochrome in the reaction with a negatively charged reducing agent can be anticipated. The electrons entering the molecule through the faster haem IV would be transferred internally to haem III until this haem is completely reduced and the reduction would proceed at a fast rate until haem IV is fully reduced. After, the large difference between the redox potential of haem IV and the redox potentials of the remaining haems I and II would not favour the uphill redistribution of electrons and the last 50 % of the reduction should occur at a slower rate. The electron transfer reaction between cytochrome c_3 from *D.*

desulfuricans (ATCC 27774) and sodium dithionite was followed by stopped-flow techniques coupled to visible spectroscopy in our laboratory. The preliminary results obtained showed that this is indeed the case. The biphasic kinetic traces observed display 54 % of fast phase and 46 % of slow phase (unpublished results), in agreement with the predictions based on the thermodynamic parameters and the kinetic model discussed in this thesis.

IV.3 Proposed model for energy transduction mediated by cytochrome c_3 in sulfate-reducing bacteria

One interesting consequence of the thermodynamic modelling has been the proposal of a new mechanism for energy transduction in sulfate-reducing bacteria, which involves a direct coupling between the periplasmic hydrogenase and cytochrome c_3 (Louro et al., 1997a,b).

According to the hydrogen cycling hypothesis the oxidation of molecular hydrogen by the periplasmic hydrogenase is a crucial step in the metabolism of these organisms because it is the only energy producing step when hydrogen is used as unique energy source. However, the hydrogen uptake activity of the periplasmic hydrogenase at physiological pH is only ca. 40% of its maximum activity, which seems inconsistent with the fundamental role suggested for this enzyme. Louro et al., 1997a showed that in the presence of cytochrome c_3 this value increases to values close to its maximum activity, demonstrating that coupling between the periplasmic hydrogenase and cytochrome c_3 is essential for the bioenergetic mechanism of these organisms.

One possible explanation for the decrease in the hydrogen uptake activity of hydrogenase with decreasing pH is that it becomes more difficult to release the protons that result from the reaction into the solution. Since cytochrome c_3 can directly accept both electrons and protons, the reaction becomes less sensitive to the pH of the solution and higher levels of activity are obtained at physiological pH. This work proposed that cytochrome c_3 accepts high energy electrons (low redox potential) and low energy protons (high pK_a) from hydrogenase and, after an energy transduction step, releases low energy electrons to the electron transfer complexes in the membrane and high energy protons either to the solution or, in a localised fashion, to the ATP synthase in the membrane. The basis for this mechanism is the effective gating of protons and electrons accomplished by cytochrome c_3 which imposes a cycle between a reduced form with a high affinity for protons and an oxidised form with a low affinity for protons because of the redox-Bohr effect. Note that, the order of the steps in this

cycle is not arbitrary and kinetic control may be crucial to guarantee the correct order of steps to achieve energy transduction. According to this scheme, the hydrogenase/cytochrome c_3 system performs energy transduction in the absence of a membrane confinement.

The kinetic studies with sodium dithionite showed that the electron transfer rate is faster in the protonated form of the cytochrome. Since, because of the thermodynamic parameters, at physiological pH the oxidised form is deprotonated whereas the reduced one is protonated, while reduction takes place there is an acceleration of the process, due to the coupled protonation of the molecule. On the one hand, this acceleration assists kinetically the concerted two-electron step and, on the other hand, it may provide the kinetic control necessary to avoid unproductive pathways in energy transduction.

REFERENCES

Akutsu, H., Hazzard, J.H., Bartsch, R.G. and Cusanovich, M.A. (1992) Reduction kinetics of the four hemes of cytochrome c_3 from *Desulfovibrio vulgaris* by flash photolysis, *Biochim. Biophys. Acta 1140*, 144-156.

Badziong, W. and Thauer, R.K. (1978) Growth yields and growth rates of *Desulfovibrio vulgaris* (Marburg) growing on hydrogen plus sulfate and hydrogen plus thiosulfate as the sole energy sources, *Arch. Microbiol. 117*, 209-214.

Badziong, W. and Thauer, R.K. (1980) Vectorial electron transport in *Desulfovibrio vulgaris* (Marburg) growing on hydrogen plus sulfate as sole energy source, *Arch. Microbiol. 125*, 167-174.

Badziong, W., Ditter, B. and Thauer, R.K. (1979) Acetate and carbon dioxide assimilation by *Desulfovibrio vulgaris* (Marburg), growing on hydrogen and sulfate as sole energy source, *Arch. Microbiol. 123*, 301-305.

Badziong, W., Thauer, R.K. and Zeikus, J.G. (1978) Isolation and characterization of *Desulfovibrio* growing on hydrogen plus sulfate as the sole energy source, *Arch. Microbiol. 116*, 41-49.

Barata, B.A.S., LeGall., J. and Moura, J.J.G. (1993) Aldehyde oxidoreductase activity in *Desulfovibrio gigas*: *in vitro* reconstitution of an electron-transfer chain from aldehydes to the production of molecular hydrogen, *Biochemistry 32*, 11559-11568.

Bell, G.R., Lee, J.P., Peck, H.D.Jr. and LeGall, J. (1978) Reactivity of *Desulfovibrio gigas* hydrogenase towards natural and artificial electron donors, *Biochimie* (Paris) *60*, 315-320.

Bell, G.R., LeGall, J. and Peck Jr., H.D. (1974) Evidence for the periplasmic location of hydrogenase in *Desulfovibrio gigas*, *J. Bacteriol. 120*, 994-997.

Benosman, H., Asso, M., Bertrand, P., Yagi, T. and Gayda, J.-P. (1989) EPR study of the redox interactions in cytochrome c_3 from *Desulfovibrio vulgaris* Miyazaki, *Eur. J. Biochem. 182*, 51-55.

Beratan, D.N. Betts, J.N. and Onuchic, J.N. (1991) Protein electron transfer rates set by the bridging secondary and tertiary structure, *Science 252*, 1285-1288.

Bertini, I., Gori-Savellini, G. and Luchinat, C. (1997) Are unit charges always negligible?, *JBIC 2*, 114-118.

Bertrand, P., Asso, M., Mbarki, O., Camensuli, P., More, C. and Guigliarelli, B. (1994) Individual redox characteristics and kinetic properties of the hemes in cytochromes c_3: New methods of investigation, *Biochimie 76*, 524-536.

Bertrand, P., Mbarki, O., Asso, M., Blanchard, L., Guerlesquin, F. and Tegoni, M. (1995) Control of the redox potential in *c*-type cytochromes: importance of the entropic contribution, *Biochemistry 343*, 11071-11079.

Bianco, P. and Haladjian (1981) Current-potential responses for a tetrahemic protein: a method of determining the individual half-wave potentials of cytochrome c_3 from *Desulfovibrio desulfuricans* strain Norway, *Electrochim. Acta 26*, 1001-1004.

Bianco, P. and Haladjian (1994) Recent progress in the electrochemistry of *c*-type cytochromes, *Biochimie 76*, 605-613.

Bruschi, M., Loutfi, M., Bianco, P. and Haladjian, J. (1984) Correlation studies between structural and redox properties of cytochromes c_3, *Biochem. Biophys. Res. Commun. 120*, 384-389.

Bryant, M.P., Campbell, L.L., Reddy, C.A. and Crabill, M.R. (1977) Growth of *Desulfovibrio* in lactate or ethanol media low in sulfate in association with H_2-utilizing methanogenic bacteria, *Appl. Environ. Microbiol. 33*, 1162-1169.

Brysch, K., Schneider, C., Fuchs, G. and Widdel, F. (1987) Lithoautotrophic growth of sulfate-reducing bacteria, and description of *Desulfobacterium autotrophicum* gen. nov., sp. nov. *Arch. Microbiol. 148*, 264-274.

Bühler, Dr.H. and Baumann, Dr.R. (1982) Calibration of pH electrodes, Ingold booklets (E-Th5) by Ingold, Dr.W., AG, CH-8902 Urdorf, Switzerland.

Bühler, Dr.H. and Galster, Dr.H. (1980) Redox measurement, principles and problems, Ingold booklets (E-Th2) by Ingold, Dr.W., Zürich, Switzerland.

Cambillau, C., Frey, M., Mosse, J., Guerlesquin, F. and Bruschi, M. (1988) Model of a complex between the tetraheme cytochrome c_3 and the ferredoxin I from *Desulfovibrio desulfuricans* Norway, *Proteins: Struct. Funct. Genet. 4*, 63-70.

Cammack, R., Fauque, G., Moura, J.J.G. and LeGall, J. (1984) ESR studies of cytochrome c_3 from *Desulfovibrio desulfuricans* strain Norway 4. Midpoint potentials of the four haems, and interactions with ferredoxin and colloidal sulphur, *Biochim. Biophys. Acta 784*, 68-74.

Campbell, L.L. and Postgate, J.R. (1965) Classification of the spore-forming sulfate-reducing bacteria, *Bacteriol. Rev. 29*, 359-363.

Campos, A.P.S. (1994), Caracterização espectroscópica de ferroproteínas envolvidas em processos biológicos fundamentais, *capítulo 7*, Tese de Doutoramento, Faculdade de Ciências e Tecnologia, Universidade Nova de Lisboa, Lisboa.

Capeillère-Blandin, C., Guerlesquin, F. and Bruschi, M. (1986) Rapid kinetic studies of the electron-exchange reaction between cytochrome c_3 and ferredoxin from *Desulfovibrio desulfuricans* Norway strain and their individual reactions with dithionite. *Biochim. Biophys. Acta 848*, 279-293.

Catarino, T., Coletta, M., LeGall, J. and Xavier, A.V. (1991) Kinetic study of the reduction mechanism for *Desulfovibrio gigas* cytochrome c_3, *Eur. J. Biochem. 202*, 1107-1113.

Cheddar, G., Meyer, T.E., Cusanovich, M.A., Stout, C.D. and Tollin, G. (1986) Electron transfer reactions between flavodoxin semiquinone and *c*-type cytochromes: comparisons between various flavodoxins, *Biochemistry 25*, 6502-6507.

Chen, L., LeGall, J., Fareleira, P., Santos, H. and Xavier, A.V. (1993a) Purification and characterization of an NADH-rubredoxin oxidoreductase involved in the utilization of oxygen by *Desulfovibrio gigas*, *Eur. J. Biochem. 216*, 443-448.

Chen, L., LeGall, J., Fareleira, P., Santos, H. and Xavier, A.V. (1995) Malate metabolism by *Desulfovibrio gigas* and its link to sulfate and fumarate reduction: purification of the malic enzyme and detection of $NAD(P)^+$ transhydrogenase activity, *Anaerobe 1*, 227-235.

Chen, L., Liu, M.Y., LeGall, J., Fareleira, P., Santos, H. and Xavier, A.V. (1993b) Rubredoxin oxidase, a new flavo-hemo-protein, is the site of oxygen reduction to water by the "strict anaerobe" *Desulfovibrio gigas*, *Biochem. Biophys. Res. Comm. 193*, 100-105.

Clark, W.M. (1972) Oxidation-reduction potentials of organic systems, *chapter 14*, Robert E. Krieger Publishing Company, Huntington, New York.

Coleman, M.L., Hedrick, D.B., Lovley, D.R., White, D.C. and Pye, K. (1993) Reduction of Fe(III) in sediments by sulphate-reducing bacteria, *Nature 361*, 436-438.

Coletta, M., Catarino, T., LeGall, J. and Xavier, A.V. (1991) A thermodynamic model for the cooperative functional properties of the tetraheme cytochrome c_3 from *Desulfovibrio gigas*, *Eur. J. Biochem. 202*, 1101-1106.

Costa, H.S. (1989) Determinação dos potenciais de oxidação-redução da flavodoxina de *Desulfovibrio gigas* em função do pH, Relatório de Estágio, Faculdade de Ciências e Tecnologia, Universidade Nova de Lisboa, Lisboa.

Coutinho, I.B. (1993) Estrutura e propriedades físico-químicas do citocroma c_3. Aplicação de RMN uni- e bidimensional à caracterização de proteínas multihémicas, *capítulo 4*, Tese de doutoramento, Faculdade de Ciências e Tecnologia, Universidade Nova de Lisboa, Lisboa.

Coutinho, I.B. and Xavier, A.V. (1994) Tetraheme cytochromes, *Methods Enzymol. 243*, 119-140.

Coutinho, I.B., Turner, D.L., LeGall, J. and Xavier, A.V. (1993) Characterization of the structure and redox behaviour of cytochrome c_3 from *Desulfovibrio baculatus* by ^{1}H-nuclear-magnetic-resonance spectroscopy, *Biochem. J. 294*, 899-908.

Coutinho, I.B., Turner, D.L., LeGall, J. and Xavier, A.V. (1995) NMR studies and redox titration of the tetraheme cytochrome c_3 from *Desulfomicrobium baculatum*. Identification of the low-potential heme, *Eur. J. Biochem. 230*, 1007-1013.

Creaser, I.I., Geue, R.J., Harrowfield, J.MacB., Herlt, A.J., Sargeson, A.M., Snow, M.R. and Springborg, J. (1982) Synthesis and reactivity of aza-capped encapsulated Co(III) ions, *J. Am. Chem. Soc. 104*, 6016-6025.

Curley, J.P., Carr, M.C., Mayhew, S.G. and Voordouw, G. (1991) Redox and flavin-binding properties of recombinant flavodoxin from *Desulfovibrio vulgaris* (Hildenborough), *Eur. J. Biochem. 202*, 1091-1100.

Czjzek, M., Payan, F., Guerlesquin, F. and Bruschi, M. and Haser, R. (1994) Crystal structure of cytochrome c_3 from *Desulfovibrio desulfuricans* Norway at 1.7 Å resolution, *J. Mol. Biol. 243*, 653-667.

Dalsgaard, T. and Bak, F. (1994) Nitrate reduction in a sulfate-reducing bacterium, *Desulfovibrio desulfuricans*, isolated from rice paddy soil: sulfide inhibition, kinetics and regulation, *Appl. Environ. Microbiol. 60*, 291-297.

Davidson, V.L. (1996) Unravelling the kinetic complexity of interprotein electron transfer reactions, *Biochemistry 35*, 14035-14039.

De Francesco, R., Edmondson, D.E., Moura, I., Moura, J.J.G. and LeGall, J. (1994) Kinetic studies on the electron-transfer reaction between cytochrome c_3 and flavodoxin from *Desulfovibrio vulgaris* strain Hildenborough, *Biochemistry 33*, 10386-10392.

Denbigh, K.G. (1971) 'The Principles of Chemical Equilibrium', *chapter 15*, 3rd ed., Cambridge University Press, Cambridge.

Der Vartanian, D.V., Xavier, A.V. and LeGall, J. (1978) EPR determination of the oxidation-reduction potentials of the hemes in cytochrome c_3 from *Desulfovibrio vulgaris*, *Biochimie (Paris) 60*, 321-325.

Dilling, W. and Cypionka, H. (1990) Aerobic respiration in sulfate-reducing bacteria, *FEMS Microbiol. Lett. 71*, 123-127.

Dolla, A., Leroy, G., Guerlesquin, F. and Bruschi, M. (1991) Identification of the site of interaction between cytochrome c_3 and ferredoxin using peptide mapping of the cross-linked complex, *Biochim. Biophys. Acta 1058*, 171-177.

Drake, H.L. and Akagi, J.M. (1977) Characterization of a novel thiosulfate-forming enzyme isolated from *Desulfovibrio vulgaris*, *J. Bacteriol. 132*, 132-138.

Dubourdieu, M. (1970) Contribution à l'étude Physicochimique des flavodoxines des bactéries sulfato-réductrices, *chapitres 2 et 4*, Thèse de Doctorat de Spécialité (Biochimie) Faculté des Sciences de Marseille, Marseille.

Dubourdieu, M. and LeGall, J. (1970) Chemical study of two flavodoxins extracted from sulfate reducing bacteria, *Biochem. Biophys. Res. Commun. 38*, 965-972.

Dubourdieu, M., LeGall, J. and Favaudon, V. (1975) Physicochemical properties of flavodoxin from *Desulfovibrio vulgaris*, *Biochim. Biophys. Acta 376*, 519-532.

Dutton, P.L. (1978) Redox potentiometry: determination of midpoint potentials of oxidation-reduction components of biological electron transfer systems, *Methods Enzymol. 54*, 411-435.

Fan, K., Akutsu, H., Kyogoku, Y. and Niki, K. (1990a) Estimation of microscopic redox potentials of a tetraheme protein, cytochrome c_3 of *Desulfovibrio vulgaris*, Miyazaki F, and partial assignments of heme groups, *Biochemistry 29*, 2257-2263.

Fan, K., Akutsu, H., Niki, K., Higuchi, N. and Kyogoku, Y. (1990b) Determination of the macroscopic formal potentials of cytochrome c_3 of *Desulfovibrio vulgaris*, Miyazaki F, through the combined use of ^{1}H NMR and an optically transparent thin-layer electrode cell, *J. Electroanal. Chem. 278*, 295-306.

Fareleira, P., LeGall, J., Xavier, A.V. and Santos, H. (1997) Pathways for utilization of carbon reserves in *Desulfovibrio gigas* under fermentative and respiratory conditions, *J. Bacteriol. 179*, 3972-3980.

Favaudon, V., Ferradini, C., Pucheault, J. Gilles, L. and LeGall, J. (1978) Kinetics of reduction of the cytochrome c_3 from *Desulfovibrio vulgaris*, *Biochem. Biophys. Res. Commun. 84*, 435-440.

Fude, L., Harris, B., Urrutia, M.M. and Beveridge, T.J. (1994) Reduction of Cr(VI) by a consortium of sulfate-reducing bacteria (SRB III), *Appl. Environ. Microbiol. 60*, 1525-1531.

Gayda, J.-P., Benosman, H., Bertrand, P., More, C. and Asso, M. (1988) EPR determination of interaction redox potentials in a multiheme cytochrome: cytochrome c_3 from *Desulfovibrio desulfuricans* Norway, *Eur. J. Biochem. 177*, 199-206.

Gayda, J.-P., Bertrand, P., More, C., Guerlesquin, F. and Bruschi, M. (1985) EPR potentiometric titration of c_3-type cytochromes, *Biochim. Biophys. Acta 829*, 262-267.

Gayda, J.-P., Yagi, T., Benosman, H. and Bertrand, P. (1987) EPR redox study of cytochrome c_3 from *Desulfovibrio vulgaris* Miyazaki, *FEBS Lett. 217*, 57-61.

Genthner, B.R.S., Friedman, S.D. and Devereux, R. (1997) Reclassification of *Desulfovibrio desulfuricans* Norway 4 as *Desulfomicrobium norvegicum* comb. nov. and confirmation of *Desulfomicrobium escambiense* (corrig., formerly "*escambium*") as a new species in the genus *Desulfomicrobium*, *International Journal of Systematic Bacteriology 47*, 889-892.

Gray, H.B. and Winkler, J.R. (1996) Electron transfer in proteins, *Annu. Rev. Biochem. 65*, 537-561.

Guigliarelli, B., Bertrand, P., More, C., Haser, R. and Gayda, J.P. (1990) Single-crystal electron paramagnetic resonance study of cytochrome c_3 from *Desulfovibrio desulfuricans* Norway strain: assignment of the heme midpoint potentials, *J. Mol. Biol. 216*, 161-166.

Gunner, M.R., Alexov, E., Torres, E. and Lipovaca, S. (1997) The importance of the protein in controlling the electrochemistry of heme metalloproteins: methods of calculation and analysis, *JBIC 2*, 126-134.

Haladjian, J., Bianco, P., Guerlesquin, F. and Bruschi, M. (1987) Electrochemical study of the electron exchange between cytochrome c_3 and hydrogenase from *Desulfovibrio desulfuricans* Norway, *Biochem. Biophys. Res. Commun. 147*, 1289-1294.

Hansen, T.A. (1993) Carbon metabolism of sulfate-reducing bacteria, pp. 21-40. In Odom, J.M. and Singleton, R.Jr. (ed.), *The sulfate-reducing bacteria: contemporary perspectives*. Springer-Verlag, New York.

Hansen, T.A. (1994) Metabolism of sulfate-reducing prokaryotes, *Antonie van Leeuwenhoek 66*, 165-185.

Hatchikian, E. C. and LeGall, J. (1970) Étude du métabolisme des acides dicarboxyliques et du pyruvate chez les bactéries sulfato-réductrices. II - Transport des electrons; accepteurs finaux, *Ann. Inst. Pasteur 118*, 288-301.

Helms, L.R. and Swenson, R.P. (1992) The primary structures of the flavodoxins from two strains of *Desulfovibrio gigas*. Cloning and nucleotide sequence of the structural genes, *Biochim. Biophys. Acta 1131*, 325-328.

Hensgens, C.M.H., Vonck, J., van Beeumen, J., van Bruggen, E.F.J., Hansen, T.A. (1993) Purification and characterization of an oxygen-labile, NAD-dependent alcohol dehydrogenase from *Desulfovibrio gigas*, *J. Bacteriol. 175*, 2859-2863.

Higuchi, Y., Kusunoki, M., Matsuura, Y., Yasuoka, N. and Kakudo, M. (1984) Refined structure of cytochrome c_3 at 1.8 Å resolution, *J. Mol. Biol. 172*, 109-139.

Ishimoto, M., Koyama, J. and Nagai, Y. (1954) A cytochrome and a green pigment of sulfate-reducing bacteria, *Bull. Chem. Soc. Japan 27*, 564-565.

Kazanskaya, I., Lexa, D., Bruschi, M. and Chottard, G. (1996) Electron transfer in tetrahemic cytochromes c_3: spectroelectrochemical evidence for a conformational change triggered by heme IV reduction, *Biochemistry 35*, 13411-13418.

Kim, J.-H. and Akagi, J.M. (1985) Characterization of a trithionate reductase system from *Desulfovibrio vulgaris*, *J. Bacteriol. 163*, 472-475.

Kissinger, C. (1989) PhD Thesis, Washington University, St. Louis, Missouri.

Knight, E. and Hardy, R.W.F. (1966) Isolation and characteristics of flavodoxin from nitrogen-fixing *Clostridium pastorianum*, *J. Biol. Chem 241*, 2752-2756.

Lambeth, D.O. and Palmer, G. (1973) The kinetics and mechanism of reduction of electron transfer proteins and other compounds of biological interest by dithionite, *J. Biol. Chem 248*, 6095-6103.

LeGall, J. and Fauque, G. (1988) Dissimilatory reduction of sulfur compounds, pp. 587-639. In Zehnder, A.J.B. (ed.) *Biology of anaerobic microorganisms*. John Wiley, New York.

LeGall, J. and Peck Jr., H.D. (1987) Amino-terminal amino acid sequences of electron transfer proteins from Gram-negative bacteria as indicators of their cellular localization: the sulfate-reducing bacteria, *FEMS Microb. Rev. 46*, 35-40.

LeGall, J., Payne, W.J., Chen, L., Liu, M.Y. and Xavier, A.V. (1994) Localization and specificity of cytochromes and other electron transfer proteins from sulfate-reducing bacteria, *Biochimie 76*, 655-665.

Liu, C.-L., and Peck, H.D.Jr. (1981) Comparative bioenergetics of sulfate reduction in *Desulfovibrio* and *Desulfotomaculum* spp., *J. Bacteriol. 145*, 966-973.

Liu, C.-L., Hart, N. and Peck, H.D.Jr. (1982) Inorganic pyrophosphate: energy source for sulfate-reducing bacteria of the genus *Desulfotomaculum*, *Science 217*, 363-364.

Louro, R.O., Brennan, L., Correia, I., Coutinho, I.B., Turner, D.L. and Xavier, A.V. (1998a) (manuscript in preparation)

Louro, R.O., Catarino, T., LeGall, J. and Xavier, A.V. (1997a) Redox-Bohr effect in electron/proton energy transduction: cytochrome c_3 coupled to hydrogenase works as a 'proton thruster' in *Desulfovibrio vulgaris*, *JBIC 2*, 488-491.

Louro, R.O., Catarino, T., Piçarra-Pereira, M.A., Pacheco, I., LeGall, J., Turner, D.L. and Xavier, A.V. (1998b) Functional and mechanistic studies of cytochrome c_3 from *Desulfovibrio gigas* – The thermodynamics of a 'Proton-Thruster', (manuscript in preparation).

Louro, R.O., Catarino, T., Salgueiro, C.A., LeGall, J. and Xavier, A.V. (1996a) Redox-Bohr effect in the tetrahaem cytochrome c_3 from *Desulfovibrio vulgaris*: a model for energy transduction mechanisms, *JBIC 1*, 34-38.

Louro, R.O., Catarino, T., Salgueiro, C.A., LeGall, J., Turner, D.L. and Xavier, A.V. (1997b) Molecular basis for energy transduction: mechanisms of cooperativity in multihaem cytochromes. In Canters, G.W. and Vijgenboom, E. (eds.), *Biological electron transfer chains: genetics, composition and mode of operation*. NATO ASI series, Kluwer Academic Publishers, *in press*.

Louro, R.O., Catarino, T., Turner, D.L., LeGall, J. and Xavier, A.V. (1998c) (manuscript in preparation)

Louro, R.O., Pacheco, I., Turner, D.L., LeGall, J. and Xavier, A.V. (1996b) Structural and functional characterization of cytochrome c_3 from *D. desulfuricans* ATCC 27774 by ^{1}H-NMR, *FEBS Lett. 390*, 59-62.

Lovley, D.R. and Phillips, E.J.P. (1994) Reduction of chromate by *Desulfovibrio vulgaris* and its c_3 cytochrome, *Appl. Environ. Microbiol. 60*, 726-728.

Lovley, D.R., Widman, P.K., Woodward, J.C. and Phillips, E.J.P. (1993) Reduction of uranium by cytochrome c_3 of *Desulfovibrio vulgaris*, *Appl. Environ. Microbiol. 59*, 3572-3576.

Ludwig, M.L., Pattridge, K.A., Metzger, A.L. and Dixon, M.M. (1997) Control of oxidation-reduction potentials in flavodoxin from *Clostridium beijerinckii*: the role of conformation changes, *Biochemistry 36*, 1259-1280.

Magro, V., Pieulle, L., Forget, N., Guigliarelli, B., Petillot, Y. and Hatchikian, E.C. (1997) Further characterization of the two tetraheme cytochromes c_3 from *Desulfovibrio africanus*: nucleotide sequences, EPR spectroscopy and biological activity, *Biochim. Biophys. Acta 1342*, 149-163.

Marcus, R.A. and Sutin, N. (1985) Electron transfers in chemistry and biology, *Biochim. Biophys. Acta 811*, 265-322.

Matias, P.M., Frazão, C., Morais, J., Coll, M. and Carrondo, M.A. (1993) Structure analysis of cytochrome c_3 from *Desulfovibrio vulgaris* Hildenborough at 1.9 Å resolution, *J. Mol. Biol. 234*, 680-699.

Matias, P.M., Morais, J., Coelho, R., Carrondo, M.A., Wilson, K., Dauter, Z. and Sieker, L. (1996) Cytochrome c_3 from *Desulfovibrio gigas*: crystal structure at 1.8 Å resolution and evidence for a specific calcium-binding site, *Protein Science 5*, 1342-1354.

Matthew, J.B., Weber, P.C., Salemme, F.R. and Richards, F.M. (1983) Electrostatic orientation during electron transfer between flavodoxin and cytochrome *c*, *Nature 301*, 169-171.

Mauk, A.G. and Moore, G.R. (1997) Control of metalloprotein redox potentials: what does site-directed mutagenesis of hemoproteins tell us?, *JBIC 2*, 119-125.

Mayhew, S.G. (1978) The redox potential of dithionite and SO_2^- from equilibrium reactions with flavodoxins, methyl viologen and hydrogen plus hydrogenase. *Eur. J. Biochem. 85*, 535-547.

Mayhew, S.G. and Ludwig, M.L. (1975) Flavodoxin and electron-transferring flavoproteins, pp. 57-118. In Boyer, P.D., (ed.) *The Enzymes*, vol. 12, 3rd ed. Academic Press, New York.

Messias, A.C., Kastrau, D.H.W., Costa, H.S., LeGall, J., Turner, D.L., Santos, H. and Xavier, A.V. (1998) Solution structure of *Desulfovibrio vulgaris* (Hildenborough) ferrocytochrome c_3: structural basis for functional cooperativity. (*submitted to J. Mol. Biol.*)

Mitchell, G.J., Jones, J.G. and Cole, J.A. (1986) Distribution and regulation of nitrate and nitrite reduction by *Desulfovibrio* and *Desulfotomaculum* species, *Arch. Microbiol. 144*, 35-40.

Moore, G.R. and Pettigrew, G.H. (1990) 'Cytochromes *c*: evolutionary, structural and physicochemical aspects' Springer, Berlin, Heidelberg, New York.

Moore, G.R., Pettigrew, G.W., Pitt, R.C. and Williams, R.J.P. (1980) pH dependence of the redox potential of *Pseudomonas aeruginosa* cytochrome *c*-551, *Biochim. Biophys. Acta 590*, 261-271.

Morais, J., Palma, P.N., Frazão, C., Caldeira, J., LeGall, J., Moura, I., Moura., J.J.G. and Carrondo, M.A. (1995) Structure of the tetraheme cytochrome from *Desulfovibrio desulfuricans* ATCC 27774: X-ray diffraction and electron paramagnetic resonance studies, *Biochemistry 34*, 12830-12841.

Moreno, C., Campos, A., Teixeira, M., LeGall, J., Montenegro, M.I., Moura, I., Dijk, C.van and Moura, J.J.G. (1991) Simulation of the electrochemical behavior of multi-redox systems. Current potential studies on multiheme cytochromes, *Eur. J. Biochem. 202*, 385-393.

Moser, C.C., Keske, J.M., Warncke, K., Faird, R.S. and Dutton, P.L. (1992) Nature of biological electron transfer, *Nature 355*, 796-802.

Moura, I., Teixeira, M., Huynh, B.H., LeGall, J. and Moura, J.J.G. (1988) Assignment of individual heme EPR signals of *Desulfovibrio baculatus* (strain 9974) tetraheme cytochrome c_3. A redox equilibria study, *Eur. J. Biochem. 176*, 365-369.

Moura, J.J.G., Santos, H., Moura, I., LeGall, J., Moore, G.R., Williams, R.J.P. and Xavier, A.V. (1982) NMR redox studies of *Desulfovibrio vulgaris* cytochrome c_3. Electron transfer mechanisms, *Eur. J. Biochem. 127*, 151-155.

Niki, K., Kobayashi, Y. and Matsuda, H. (1984) Determination of macroscopic standard potentials of a molecule with a reversible *n*-consecutive one-electron transfer process. Application to a tetra-heme protein: cytochrome c_3, *J. Electroanal. Chem. 178*, 333-341.

Nivière, V., Hatchikian, E.C., Bianco, P. and Haladjian, J. (1988) Kinetic studies of electron transfer between hydrogenase and cytochrome c_3 from *Desulfovibrio gigas*. Electrochemical properties of cytochrome c_3, *Biochim. Biophys. Acta 935*, 34-40.

Odom, J.M. (1993) Industrial and environmental activities of sulfate-reducing bacteria, pp. 189-210. In Odom, J.M. and Singleton, R.Jr. (ed.), *The sulfate-reducing bacteria: contemporary perspectives*. Springer-Verlag, New York.

Odom, J.M. and Peck, H.D.Jr. (1981) Hydrogen cycling as a general mechanism for energy coupling in the sulfate-reducing bacteria, *Desulfovibrio* sp., *FEMS Microbiol. Lett. 12*, 47-50.

Palma, P.N., Moura, I., LeGall, J., Van Beeumen, J., Wampler, J.E. and Moura, J.J.G. (1994) Evidence for a ternary complex formed between flavodoxin and cytochrome c_3: H-NMR and molecular modeling studies, *Biochemistry 33*, 6394-6407.

Palmer, G. and Olson, J.S. (1980) Concepts and approaches to the understanding of electron transfer processes in enzymes containing multiple redox centers, pp.187-220. In Michael Coughlan (ed.), *Molybdenum and molybdenum-containing enzymes*, Pergamon Press, New York.

Papa, S., Guerrieri, F. and Izzo, G. (1979) Redox-Bohr effects in the cytochrome system of mitochondria, *FEBS Lett. 105*, 213-216.

Park, J.-S., Kano, K., Niki, K. and Akutsu, H. (1991) Full assignment of heme redox potentials of cytochrome c_3 of *D. vulgaris* Miyazaki F by ^{1}H-NMR, *FEBS Lett. 285*, 149-151.

Park, J.-S., Ohmura, T., Kano, K., Sagara, T., Niki, K., Kyogoku, Y. and Akutsu, H.(1996) Regulation of the redox order of four haems by pH in cytochrome c_3 from *D. vulgaris* Miyazaki F, *Biochim. Biophys. Acta 1293*, 45-54.

Peck, H.D.Jr. (1993) Bioenergetic strategies of the sulfate-reducing bacteria, pp. 41-76. In Odom, J.M. and Singleton, R.Jr. (ed.), *The sulfate-reducing bacteria: contemporary perspectives*. Springer-Verlag, New York.

Pereira, I.A.C., Teixeira, M. and Xavier, A.V. (1998) Hemeproteins in anaerobes, *Structure and bonding 91*, 65-89.

Piçarra-Pereira, M.A., Turner, D.L., LeGall, J. and Xavier, A.V. (1993) Structural studies on *Desulfovibrio gigas* cytochrome c_3 by two-dimensional ^{1}H-nuclear-magnetic-resonance spectroscopy, *Biochem. J. 294*, 909-915.

Porras, A.G. and Palmer, G. (1982) The room temperature potentiometry of xanthine oxidase. pH-dependent redox behavior of the flavin, molybdenum and iron-sulfur centers, *J. Biol. Chem. 257*, 11617-11626.

Postgate, J.R. (1952) Growth of sulphate reducing bacteria in sulphate-free media, *Research* (London) *5*, 189-190.

Postgate, J.R. (1954) Presence of cytochrome in an obligate anaerobe, *Biochemical J. 56*, xi-xii.

Postgate, J.R. (1984) *The sulfate-reducing bacteria*, Cambridge University Press, Cambridge.

Postgate, J.R. and Campbell, L.L. (1966) Classification of *Desulfovibrio* species, the nonsporulating sulfate-reducing bacteria, *Bacteriol. Rev. 30*, 732-738.

Press, W.H., Flannery, B.P., Teukolsky, S.A. and Vetterling, W.T. (1989) Numerical Recipes. The Art of Scientific Computing (FORTRAN Version), *Chapters. 14 and 15*, Cambridge University Press, Cambridge.

Prince, R.C., Linkletter, S.J.G. and Dutton, P.L. (1981) The thermodynamic properties of some commonly used oxidation-reduction mediators, inhibitors and dyes, as determined by polarography, *Biochim. Biophys. Acta 635*, 132-148.

Robertson, D.E., Farid, R.S., Moser, C.C., Urbauer, J.L., Mulholland, S.E., Pidikiti, R., Lear, J.D., Wand, A.J., DeGrado, W.F. and Dutton, P.L. (1994) Design and synthesis of multi-haem proteins, *Nature 368*, 425-432.

Rossi, M., Pollock, B.R., Reij, M.W., Keon, R.G., Fu, R. and Woordouw, G. (1993) The *hmc* operon of *Desulfovibrio vulgaris* subsp. *vulgaris* Hildenborough encodes a potential transmembrane redox protein complex, *J. Bacteriol. 175*, 4699-4711.

Rueter, P., Rabus, R., Wilkes, H., Aeckersberg, F., Rainey, F.A., Jannasch, H.W. and Widdel, F. (1994) Anaerobic oxidation of hydrocarbons in crude oil by new types of sulphate-reducing bacteria, *Nature 372*, 455-458.

Salgueiro, C.A., Turner, D.L. and Xavier, A.V. (1997a) Use of paramagnetic NMR probes for structural analysis in cytochrome c_3 from *Desulfovibrio vulgaris*, *Eur. J. Biochem. 244*, 721-734.

Salgueiro, C.A., Turner, D.L., LeGall, J. and Xavier, A.V. (1997b) Reevaluation of the redox and redox-Bohr cooperativity in tetrahaem *Desulfovibrio vulgaris* (Miyazaki) cytochrome c_3, *JBIC 2*, 343-349.

Salgueiro, C.A., Turner, D.L., Santos, H., LeGall, J. and Xavier, A.V. (1992) Assignment of the redox potentials to the four haems in *Desulfovibrio vulgaris* cytochrome c_3 by 2D-NMR, *FEBS Lett. 314*, 155-158.

Santos, H., (1984) Relação estrutura-função em citocromos multihémicos: caracterização por RMN dos mecanismos de transferência electrónica em citocromos c_3 de bactérias redutoras de sulfato, *capítulos 4 e 5*, Tese de doutoramento, Faculdade de Ciências e Tecnologia, Universidade Nova de Lisboa, Lisboa.

Santos, H., Moura, J.J.G., Moura, I., LeGall, J. and Xavier, A.V. (1984a) NMR studies of electron transfer mechanisms in a protein with interacting redox centres: *Desulfovibrio gigas* cytochrome c_3, *Eur. J. Biochem. 141*, 283-296.

Santos, H., Turner, D.L. and Xavier, A.V. (1984b) Two-dimensional NMR studies of electron transfer in cytochrome c_3, *J. Magn. Reson. 59*, 177-180.

Saraiva, L.M., Salgueiro, C.A., LeGall, J., van Dongen, W.M.A.M. and Xavier, A.V. (1996) Site-directed mutagenesis of a phenylalanine residue strictly conserved in cytochromes c_3, *JBIC 1*, 542-550.

Schlereth, D.D., Fernández, V.M. and Mäntele, W. (1993) Protein conformational changes in tetraheme cytochromes detected by FTIR spectroelectrochemistry: *Desulfovibrio desulfuricans* Norway 4 and *Desulfovibrio gigas* cytochromes c_3, *Biochemistry 32*, 9199-9208.

Seitz, H.-J. and Cypionka, H. (1986) Chemolithotrophic growth of *Desulfovibrio desulfuricans* with hydrogen coupled to ammonification of nitrate or nitrite, *Arch. Microbiol. 146*, 63-67.

Simondsen, R.P., Weber, P.C., Salemme, F.R. and Tollin, G. (1982) Transient kinetics of electron transfer reactions of flavodoxin: ionic strength dependence of semiquinone oxidation by cytochrome *c*, ferricyanide, and ferric ethylenediaminetetraacetic acid and computer modeling of reaction complexes, *Biochemistry 21*, 6366-6375.

Singleton, R.Jr. (1993) The sulfate-reducing bacteria: an overview, pp. 1-20. In Odom, J.M. and Singleton, R.Jr. (ed.), *The sulfate-reducing bacteria: contemporary perspectives.* Springer-Verlag, New York.

Sokol, W.F., Evans, D.H., Niki, T. and Yagi, T. (1980) Reversible voltammetric response for a molecule containing four non-equivalent redox sites with application to cytochrome c_3 of *Desulfovibrio vulgaris*, strain Miyazaki, *J. Electroanal. Chem. 108*, 107-115.

Stellwagen, E. (1978) Haem exposure as the determinate of oxidation-reduction potential of haem proteins, *Nature 275*, 73-74.

Stewart, D.E., LeGall, J., Moura, I., Moura, J.J.G., Peck, H.D.Jr., Xavier, A.V., Weiner, P.K. and Wampler, J.E. (1988) A hypothetical model of the flavodoxin-tetraheme cytochrome c_3 complex of sulfate-reducing bacteria, *Biochemistry 27*, 2444-2450.

Stewart, D.E., LeGall, J., Moura, I., Moura, J.J.G., Peck, H.D.Jr., Xavier, A.V., Weiner, P.K. and Wampler, J.E. (1989) Electron transport in sulfate-reducing bacteria. Molecular modeling and NMR studies of the rubredoxin-tetraheme-cytochrome-c_3 complex, *Eur. J. Biochem. 185*, 695-700.

Stockman, B.J., Richardson, T.E. and Swenson, R.P. (1994) Structural changes caused by site-directed mutagenesis of tyrosine-98 in *Desulfovibrio vulgaris* flavodoxin delineated by ^{1}H and ^{15}N NMR spectroscopy: implications for redox potential modulation, *Biochemistry 33*, 15298-15308.

Tabushi, I., Nishiya, T., Shimomura, M., Kunitake, T., Inokuchi, H. and Yagi, T. (1984) Cytochrome c_3 modified artificial liposome. Structure, electron transport, and pH gradient generation, *J. Am. Chem. Soc. 106*, 219-226.

Tabushi, I., Nishiya, T., Yagi, T. and Inokuchi, H. (1983) Kinetic study on the successive four-step reduction of cyt c_3, *J. Biochem. 94*, 1375-1385.

Tollin, G, Cheddar, G., Watkins, J.A., Meyer, T.E. and Cusanovich, M.A. (1984) Electron transfer between flavodoxin semiquinone and *c*-type cytochromes: correlations between electrostatically corrected rate constants, redox potentials and surface topologies, *Biochemistry 23*, 6345-6349.

Turner, D.L., Salgueiro, C.A., Catarino, T., LeGall, J. and Xavier, A.V. (1994) Homotropic and heterotropic cooperativity in the tetrahaem cytochrome c_3 from *Desulfovibrio vulgaris*, *Biochim. Biophys. Acta 1187*, 232-235.

Turner, D.L., Salgueiro, C.A., Catarino, T., LeGall, J. and Xavier, A.V. (1996) NMR studies of cooperativity in the tetrahaem cytochrome c_3 from *Desulfovibrio vulgaris*, *Eur. J. Biochem. 241*, 723-731.

Turner, N., Barata, B., Bray, R.C., Deistung, J., LeGall, J. and Moura, J.J.G. (1987) The molybdenum iron-sulphur protein from *Desulfovibrio gigas* as a form of aldehyde oxidase, *Biochem. J. 243*, 755-761.

Van Leeuwen, J.W., Van Dijk, C., Grande, H.J. and Veeger, C. (1982) A pulse-radiolysis study of cytochrome c_3. Kinetics of the reduction of cytochrome c_3 by methyl viologen radicals and the characterisation of the redox properties of cytochrome c_3 from *Desulfovibrio vulgaris* (Hildenborough), *Eur. J. Biochem. 127*, 631-637.

Vervoort, J., Heering, D., Peelen, S. and Berkel, W. (1994) Flavodoxins, *Methods Enzymol. 243*, 188-203.

Volbeda, A., Charon, M.-H., Piras, C., Hatchikian, E. C., Frey, M. and Fontecilla-Camps, J.C. (1995) Crystal structure of the nickel-iron hydrogenase from *Desulfovibrio gigas*, *Nature 373*, 580-587.

Voordouw, G. (1995) The genus *Desulfovibrio*: the centennial, *Appl. Environ. Microbiol. 61*, 2813-2819.

Wang, D.L., Stankovich, M.T., Eng, L.H. and Neujahr, H.Y. (1991) Redox properties of cytochrome c_3 from *Desulfovibrio desulfuricans* NCIMB 8372, *J. Electroanal. Chem. 318*, 291-307.

Watt, W., Tulinsky, A., Swenson, R.P. and Watenpaugh, K.D. (1991) Comparison of the crystal structures of a flavodoxin in its three oxidation states at cryogenic temperatures, *J. Mol. Biol. 218*, 195-208.

Weber, P.C. and Tollin, G. (1985) Electrostatic interactions during electron transfer reactions between *c*-type cytochromes and flavodoxin, *J. Biol. Chem 260*, 5568-5573.

Widdel, F. (1988) Microbiology and ecology of sulfate- and sulfur-reducing bacteria, pp. 469-585. In Zehnder, A.J.B. (ed.) *Biology of anaerobic microorganisms*. John Wiley, New York.

Widdel, F. and Hansen, T.A. (1991) The dissimilatory sulfate- and sulfur- reducing bacteria, pp.583-624. In Balows, A., Trüper, H.G., Dworkin, M., Harder, W. and Schleifer, K.-H. (eds.) *The prokaryotes*, 2nd ed., vol. I. Springer-Verlag, New York.

Wilson, G.S. (1978) Determination of oxidation-reduction potentials, *Methods Enzymol. 54*, 396-410.

Wüthrich, K. (1986) NMR of proteins and nucleic acids, John Wiley & Sons, New York.

Xavier, A.V. (1986) Energy transduction coupling mechanisms in multiredox centre proteins, *J.Inorg.Biochem. 28*, 239-243.

Xavier, A.V. and Moura, J.J.G. (1978) NMR studies of electron carrier proteins from sulphate reducing bacteria, *Biochimie 60*, 327-338.

Xavier, A.V., Moura, J.J.G., LeGall, J. and Der Vartanian, D.V. (1979) Oxidation-reduction potentials of the hemes in cytochrome c_3 from *Desulfovibrio gigas* in the presence and absence of ferredoxin by EPR spectroscopy, *Biochimie (Paris) 61*, 689-695.

Yagi, T. (1984) Spectral and kinetic abnormality during the reduction of cytochrome c_3 catalysed by hydrogenase with hydrogen, *Biochim. Biophys. Acta 767*, 288-294.

Yagi, T., Honya, M. and Tamiya, N. (1968) Purification and properties of hydrogenases of different origins, *Biochim. Biophys. Acta 153*, 699-705.

Zhou, H.-X. (1997) Control of reduction potential by protein matrix: lesson from a spherical protein model, *JBIC 2*, 109-113.

Zhou, Z. and Swenson, R.P. (1996) Evaluation of the electrostatic effect of the 5'-phosphate of the flavin mononucleotide cofactor on the oxidation-reduction potentials of the flavodoxin from *Desulfovibrio vulgaris* (Hildenborough), *Biochemistry 35*, 12443-12454.

APPENDICES

Appendix A: Sequential model

Appendix B: Individual model

Appendix C: Integrated rate equations

APPENDIX A: 'SEQUENTIAL MODEL'.

CALCULATION OF THE GLOBAL OXIDISED FRACTION FOR A MODEL OF FOUR CONSECUTIVE REVERSIBLE REDOX STEPS.

$$\text{Stage 0} \underset{}{\overset{E_I}{\rightleftharpoons}} \text{Stage I} \overset{E_{II}}{\rightleftharpoons} \text{Stage II} \overset{E_{III}}{\rightleftharpoons} \text{Stage III} \overset{E_{IV}}{\rightleftharpoons} \text{Stage IV}$$

(fully reduced) (fully oxidised)

The global oxidised fraction is given by the weighted average of the populations of the stages, according to the number of oxidised haems haems in each stage.

$$\text{oxidised fraction} = \frac{4[stage\,IV]+3[stage\,III]+2[stage\,II]+[stage\,I]}{4([stage\,IV]+[stage\,III]+[stage\,II]+[stage\,I]+[stage\,0])} \quad (1)$$

The populations of consecutive stages are related to one another by the Nernst equation:

$$E = E_I + \frac{RT}{F}\ln\frac{[stage\,I]}{[stage\,0]} \rightarrow [stage\,I] = [stage\,0]\exp\left(\frac{(E - E_I)F}{RT}\right) \quad (2)$$

$$E = E_{II} + \frac{RT}{F}\ln\frac{[stage\,II]}{[stage\,I]} \rightarrow [stage\,II] = [stage\,I]\exp\left(\frac{(E - E_{II})F}{RT}\right)$$

$$E = E_{III} + \frac{RT}{F}\ln\frac{[stage\,III]}{[stage\,II]} \rightarrow [stage\,III] = [stage\,II]\exp\left(\frac{(E - E_{III})F}{RT}\right)$$

$$E = E_{IV} + \frac{RT}{F}\ln\frac{[stage\,IV]}{[stage\,III]} \rightarrow [stage\,IV] = [stage\,III]\exp\left(\frac{(E - E_{IV})F}{RT}\right)$$

It is possible to express the population of each stage as a function of the population of the fully reduced state ([*stage* 0]), the solution potential (E), and the macroscopic redox potentials (E_I, E_{II}, E_{III} and E_{IV}):

$$[stage\,II] = [stage\,0]\exp\left(\frac{(E - E_I)F}{RT}\right)\exp\left(\frac{(E - E_{II})F}{RT}\right)$$

$$[stage\,II] = [stage\,0]\exp\left(\frac{(2E - E_I - E_{II})F}{RT}\right) \quad (3)$$

Similarly,

$$[stage\ III] = [stage\ 0]\exp\left(\frac{(3E - E_I - E_{II} - E_{III})F}{RT}\right) \quad (4)$$

$$[stage\ IV] = [stage\ 0]\exp\left(\frac{(4E - E_I - E_{II} - E_{III} - E_{IV})F}{RT}\right) \quad (5)$$

Substitution of equations (2-5) in equation (1) gives the complete expression of the oxidised fraction as a function of the solution potential and the macroscopic redox potentials. Note that the oxidised fraction does not depend on the population of stage 0 because the term [*stage* 0] cancels. If the following definitions are used,

$$X = \exp\left(\frac{E\,F}{RT}\right)$$

$$K_I = \exp\left(\frac{-E_I\,F}{RT}\right)$$

$$K_{II} = \exp\left(\frac{-(E_I + E_{II})\,F}{RT}\right)$$

$$K_{III} = \exp\left(\frac{-(E_I + E_{II} + E_{III})\,F}{RT}\right)$$

$$K_{IV} = \exp\left(\frac{-(E_I + E_{II} + E_{III} + E_{IV})\,F}{RT}\right)$$

The expression of the oxidised fraction can be written:

$$\text{oxidised fraction} = \frac{4K_{IV}X^4 + 3K_{III}X^3 + 2K_{II}X^2 + K_I X}{4\left(K_{IV}X^4 + K_{III}X^3 + K_{II}X^2 + K_I X + 1\right)}$$

Note that, since the reduced fraction is given by the weighted average of the populations of the stages according to the number of reduced haems in each stage, the full expression of the reduced fraction is:

$$\text{reduced fraction} = \frac{4 + 3K_I X + 2K_{II}X^2 + K_{III}X^3}{4\left(1 + K_I X + K_{II}X^2 + K_{III}X^3 + K_{IV}X^4\right)}$$

APPENDIX B: 'INDIVIDUAL MODEL'.

CALCULATION OF THE GLOBAL OXIDISED FRACTION FOR A SYSTEM WITH FOUR INDEPENDENT REDOX CENTRES.

$$C_1^{ox} + 1\,e^- \overset{e_1}{\rightleftharpoons} C_1^{red}$$

$$C_2^{ox} + 1\,e^- \overset{e_2}{\rightleftharpoons} C_2^{red}$$

$$C_3^{ox} + 1\,e^- \overset{e_3}{\rightleftharpoons} C_3^{red}$$

$$C_4^{ox} + 1\,e^- \overset{e_4}{\rightleftharpoons} C_4^{red}$$

In this case, the global oxidised fraction is simply given by the sum of the oxidised fractions of the individual centres, divided by 4:

$$\text{oxidised fraction} = \frac{1}{4}\left(\frac{[C_1^{ox}]}{[C_1^{ox}] + [C_1^{red}]} + \frac{[C_2^{ox}]}{[C_2^{ox}] + [C_2^{red}]} + \frac{[C_3^{ox}]}{[C_3^{ox}] + [C_3^{red}]} + \frac{[C_4^{ox}]}{[C_4^{ox}] + [C_4^{red}]} \right) \qquad (1)$$

The oxidised and reduced populations of each centre (C_i) are related to each other by the Nernst equation:

$$E = e_i + \frac{RT}{F} \ln \frac{[C_i^{ox}]}{[C_i^{red}]} \quad \rightarrow \quad [C_i^{ox}] = [C_i^{red}] \exp\left(\frac{(E - e_i)F}{RT} \right) \qquad (2)$$

In the case of the four haems of cytochrome c_3, the concentration of the four redox centres is equal, because they belong to the same molecule. Therefore, molar fractions can be used instead of concentrations, in order to simplify the expressions. Under these circumstances, $[C_i^{ox}] + [C_i^{red}] = 1$.

It follows that, the expression of the oxidised fraction as a function of the solution potential (E) and the midpoint redox potential (e_i) is, for each redox centre:

$$[C_i^{ox}] = \frac{\exp\left(\frac{(E - e_i)F}{RT}\right)}{1 + \exp\left(\frac{(E - e_i)F}{RT}\right)} \quad (3)$$

Since $[C_i^{ox}] + [C_i^{red}] = 1$, substitution of equation (3) in equation (1) gives the expression for the global oxidised fraction as a function of the solution potential and the midpoint redox potentials of the four independent centres:

$$\text{oxidised fraction} = \frac{1}{4}\left(\frac{\exp\left(\frac{(E - e_1)F}{RT}\right)}{1 + \exp\left(\frac{(E - e_1)F}{RT}\right)} + \frac{\exp\left(\frac{(E - e_2)F}{RT}\right)}{1 + \exp\left(\frac{(E - e_2)F}{RT}\right)} + \frac{\exp\left(\frac{(E - e_3)F}{RT}\right)}{1 + \exp\left(\frac{(E - e_3)F}{RT}\right)} + \frac{\exp\left(\frac{(E - e_4)F}{RT}\right)}{1 + \exp\left(\frac{(E - e_4)F}{RT}\right)} \right)$$

If the following definitions are used,

$$X = \exp\left(\frac{E\,F}{RT}\right)$$

$$\beta_i = \exp\left(\frac{-e_i\,F}{RT}\right)$$

The expression of the global oxidised fraction can be simplified to:

$$\text{oxidised fraction} = \frac{1}{4}\left(\frac{\beta_1 X}{\beta_1 X + 1} + \frac{\beta_2 X}{\beta_2 X + 1} + \frac{\beta_3 X}{\beta_3 X + 1} + \frac{\beta_4 X}{\beta_4 X + 1} \right)$$

Note that, since for each of the four centres the reduced fraction is equal to one minus the oxidised fraction, the overall expression for the reduced fraction is:

$$\text{reduced fraction} = \frac{1}{4}\left(\frac{1}{\beta_1 X + 1} + \frac{1}{\beta_2 X + 1} + \frac{1}{\beta_3 X + 1} + \frac{1}{\beta_4 X + 1} \right)$$

APPENDIX C: INTEGRATED RATE EQUATIONS FOR A REACTION MECHANISM WITH FOUR CONSECUTIVE FIRST-ORDER STEPS

$$\text{Stage IV} \xrightarrow{k_d'} \text{Stage III} \xrightarrow{k_c'} \text{Stage II} \xrightarrow{k_b'} \text{Stage I} \xrightarrow{k_a'} \text{Stage 0}$$

(fully oxidised) (fully reduced)

The pseudo first-order reaction scheme IV→III→II→I→0 for the reduction process, leads to rate equations which are easily integrated. Expressions for the case of pure stage IV existing at time zero have been published previously (Tabushi et al., 1983).

The integrated rate equations for an arbitrary starting point corresponding to a partially reduced state are given here.

In practice, the populations of the different stages at time zero, in an equilibrated mixture of partially reduced cytochrome c_3, are calculated from the thermodynamic parameters.

$$[\text{Stage IV}] = [\text{Stage IV}]_0 \exp(-k_d' t)$$

$$[\text{Stage III}] = [\text{Stage IV}]_0 \left[\frac{k_d'}{k_c' - k_d'} \exp(-k_d' t) + \frac{k_d'}{k_d' - k_c'} \exp(-k_c' t) \right] + [\text{Stage III}]_0 \exp(-k_c' t)$$

$$[\text{Stage II}] = [\text{Stage IV}]_0 \left[\frac{k_d' k_c'}{(k_c' - k_d')(k_b' - k_d')} \exp(-k_d' t) + \frac{k_d' k_c'}{(k_d' - k_c')(k_b' - k_c')} \exp(-k_c' t) + \frac{k_d' k_c'}{(k_d' - k_b')(k_c' - k_b')} \exp(-k_b' t) \right] + [\text{Stage III}]_0 \left[\frac{k_c'}{k_b' - k_c'} \exp(-k_c' t) + \frac{k_c'}{k_c' - k_b'} \exp(-k_b' t) \right] + [\text{Stage II}]_0 \exp(-k_b' t)$$

$$[\text{Stage I}] = [\text{Stage IV}]_0 \left[\begin{array}{l} \dfrac{k_d' k_c' k_b'}{(k_c' - k_d')(k_b' - k_d')(k_a' - k_d')} \exp(-k_d' t) + \dfrac{k_d' k_c' k_b'}{(k_d' - k_c')(k_b' - k_c')(k_a' - k_c')} \exp(-k_c' t) \\ + \dfrac{k_d' k_c' k_b'}{(k_d' - k_b')(k_c' - k_b')(k_a' - k_b')} \exp(-k_b' t) + \dfrac{k_d' k_c' k_b'}{(k_d' - k_a')(k_c' - k_a')(k_b' - k_a')} \exp(-k_a' t) \end{array} \right]$$

$$+ [\text{Stage III}]_0 \left[\begin{array}{l} \dfrac{k_c' k_b'}{(k_b' - k_c')(k_a' - k_c')} \exp(-k_c' t) + \dfrac{k_c' k_b'}{(k_c' - k_b')(k_a' - k_b')} \exp(-k_b' t) \\ + \dfrac{k_c' k_b'}{(k_c' - k_a')(k_b' - k_a')} \exp(-k_a' t) \end{array} \right]$$

$$+ [\text{Stage II}]_0 \left[\frac{k_b'}{k_a' - k_b'} \exp(-k_b' t) + \frac{k_b'}{k_b' - k_a'} \exp(-k_a' t) \right]$$

$$+ [\text{Stage I}]_0 \exp(-k_a' t)$$

$$[\text{Stage 0}] = [\text{Stage IV}]_0 \left[\begin{array}{l} 1 - \dfrac{k_c' k_b' k_a'}{(k_c' - k_d')(k_b' - k_d')(k_a' - k_d')} \exp(-k_d' t) - \dfrac{k_d' k_b' k_a'}{(k_d' - k_c')(k_b' - k_c')(k_a' - k_c')} \exp(-k_c' t) \\ - \dfrac{k_d' k_c' k_a'}{(k_d' - k_b')(k_c' - k_b')(k_a' - k_b')} \exp(-k_b' t) - \dfrac{k_d' k_c' k_b'}{(k_d' - k_a')(k_c' - k_a')(k_b' - k_a')} \exp(-k_a' t) \end{array} \right]$$

$$+ [\text{Stage III}]_0 \left[\begin{array}{l} 1 - \dfrac{k_b' k_a'}{(k_b' - k_c')(k_a' - k_c')} \exp(-k_c' t) - \dfrac{k_c' k_a'}{(k_c' - k_b')(k_a' - k_b')} \exp(-k_b' t) \\ - \dfrac{k_c' k_b'}{(k_c' - k_a')(k_b' - k_a')} \exp(-k_a' t) \end{array} \right]$$

$$+ [\text{Stage II}]_0 \left[1 - \frac{k_a'}{k_a' - k_b'} \exp(-k_b' t) - \frac{k_b'}{k_b' - k_a'} \exp(-k_a' t) \right]$$

$$+ [\text{Stage I}]_0 \left[1 - \exp(-k_a' t) \right]$$

$$+ [\text{Stage 0}]_0$$